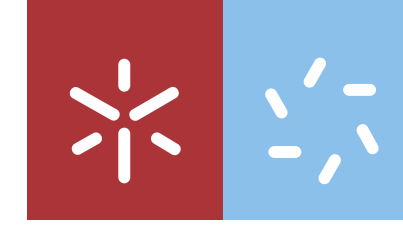




**Rational design and synthesis of novel
selective PI3K inhibitors for cancer therapy**

Vitor Lobo

UMinho | 2022

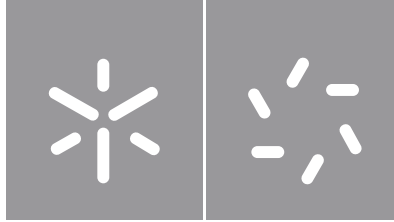


Universidade do Minho
Escola de Ciências

Vitor Daniel Pereira Lobo

**Rational design and synthesis of novel
selective PI3K inhibitors for cancer therapy**

fevereiro de 2022



Universidade do Minho

Escola de Ciências

Vitor Daniel Pereira Lobo

**Rational design and synthesis of novel
selective PI3K inhibitors for cancer therapy**

Dissertação de Mestrado
Mestrado em Química Medicinal

Trabalho efetuado sob a orientação da
Professora Doutora Maria Alice Gonçalves Carvalho
e da
Doutora Tarsila Gabriel Castro

DIREITOS DE AUTOR E CONDIÇÕES DE UTILIZAÇÃO DO TRABALHO POR TERCEIROS

Este é um trabalho académico que pode ser utilizado por terceiros desde que respeitadas as regras e boas práticas internacionalmente aceites, no que concerne aos direitos de autor e direitos conexos.

Assim, o presente trabalho pode ser utilizado nos termos previstos na licença abaixo indicada.

Caso o utilizador necessite de permissão para poder fazer um uso do trabalho em condições não previstas no licenciamento indicado, deverá contactar o autor, através do RepositóriUM da Universidade do Minho.



Atribuição-NãoComercial-SemDerivações
CC BY-NC-ND

<https://creativecommons.org/licenses/by-nc-nd/4.0/>

ACKNOWLEDGEMENTS

This work is the result of an enormous effort and dedication, which certainly resulted in a personal growth. I am sure that without the presence and support of many people, finishing this thesis would have been much more difficult.

First of all, I want to leave a special recognition to my supervisors, Doctor Alice Carvalho and Doctor Tarsila Castro for all the support, motivation, sharing of knowledge and extreme patience. I would also like to thank them for always being available to answer any questions and for trusting in my choices since I proposed the dissertation topic.

I want to take the opportunity to thank the Centre of Chemistry from University of Minho. Also, the access to computing resources funded by the Project “Search-ON2: Revitalization of HPC infrastructure of UMinho” (NORTE-07-0162-FEDER-000086), co-founded by the North Portugal Regional Operational Programme (ON.2–O Novo Norte), under the National Strategic Reference Framework (NSRF), through the European Regional Development Fund (ERDF), is gratefully acknowledge.

To Doctor Elisa Pinto, for her unquestionable professionalism and flexibility in providing the NMR spectrums.

To my colleagues of LAB15, for all the companionship, help and moments of fun, especially Miguel, André, Sofias, Daniela, Mariana, Diogo and Ananda. However, I am positive that the time spent in the lab would not have been the same without the presence of Joana, the best desk neighbour I could have ever asked for.

To my “Esties”, Tisco and Tias, Alexandra and Andreia, Márcia, Guilherme, Letícia, David, Cátia, Rita and Diana, friends from Paradise, and my best friend, Leandro for the constant support.

Finally, I leave a huge thank you to my mother, sister and nephews, to whom I dedicate this thesis. Thank you for the love and pride that you have for me, and for always believing in my value.

STATEMENT OF INTEGRITY

I hereby declare having conducted this academic work with integrity. I confirm that I have not used plagiarism or any form of undue use of information or falsification of results along the process leading to its elaboration.

I further declare that I have fully acknowledged the Code of Ethical Conduct of the University of Minho.

RESUMO

A via da fosfatidilinositol-3 quinase (PI3K) é uma das cascatas de sinalização patogénica mais frequentemente ativada numa grande variedade de cancros. Nos últimos 15 anos tem havido um crescimento na procura de inibidores seletivos das 4 isoformas da classe I da PI3K, uma vez que demonstram melhor especificidade e reduzida toxicidade em relação aos inibidores existentes. Dada a similaridade estrutural entre alguns compostos reportados como inibidores seletivos de PI3K, e compostos sintetizados e testados pelo grupo de investigação, a possibilidade destes últimos poderem ser ativos nestes tipos de recetores foi considerada.

Foi construída uma biblioteca virtual contendo 661 ligandos que se submeteu a um *screening* virtual nas 4 isoformas da classe I da PI3K. No *screening* foram identificados 68 ligandos selectivos, 60 para PI3K α e 8 para PI3K γ . A análise estatística dos resultados permitiu estabelecer correlações entre os dados de afinidade e algumas propriedades fisico-químicas dos ligandos. Também foram investigados os locais de ligação estabelecidos pelos ligandos seletivos no centro ativo das isoformas alfa e gama da PI3K.

Com o objetivo de sintetizar uma amostra dos ligandos submetidos ao *screening* virtual, foi estabelecida uma via sintética extensa a partir de reagentes comerciais, que se dividiu em duas partes: síntese de reagentes de partida e síntese de produtos finais. A síntese de reagentes de partida contemplou a preparação de derivados de 2-(3-aminofenil)-purina (**1-23**) através de uma abordagem sintética já reportada. A síntese de produtos finais ocorreu por reação dos compostos **1-23** com agentes acilantes seguida de reação com nucleófilos. Foram sintetizados uma série de diferentes amidas, ureias e carbamatos usando diferentes metodologias. De um modo geral, as abordagens sintéticas seguidas foram eficientes, contudo, em alguns casos há necessidade de algum trabalho futuro, para otimizar algumas das vias sintéticas.

Palavras-chave: Cancro, isoformas da PI3K, inibidores seletivos, *screening* virtual.

ABSTRACT

The phosphatidylinositol-3 kinase (PI3K) pathway is one of the most frequently activated pathogenic signalling cascades in a wide variety of cancers. In the last 15 years there has been an increase in the search for selective inhibitors of the 4 class I isoforms of PI3K, as they demonstrate better specificity and reduced toxicity in comparison to existing inhibitors. Given the structural similarity between some compounds reported as selective PI3K inhibitors, and those synthesised and tested by the research group, the possibility that these may be active on these receptors was considered.

A virtual library containing 661 ligands was constructed and subjected to a virtual screening on the 4 class I isoforms of PI3K. In the screening, 68 selective ligands were identified, 60 for PI3K α and 8 for PI3K γ . Statistical analysis of the results allowed the establishment of correlations between the affinity data and some of the physicochemical properties of the ligands. The binding sites established by the selective ligands in the active centre of the alpha and gamma isoforms of PI3K were also investigated.

In order to synthesize a sample of the ligands submitted to virtual screening, an extensive synthetic route was established from commercial reagents and was divided into two parts: synthesis of starting reagents and synthesis of final products. The synthesis of starting reagents contemplated the preparation of 2-(3-aminophenyl)-purine derivatives (**1-23**) through an already reported synthetic approach. The synthesis of final products occurred by reaction of compounds **1-23** with acylation agents, followed by reaction with nucleophiles. A new series of different amides, ureas and carbamates were synthesised using different methodologies. Overall, the synthetic approaches followed were efficient, however, in some cases there is a need for some future work to optimise some of the synthetic routes.

Keywords: Cancer, PI3K isoforms, selective inhibitors, virtual screening.

LIST OF CONTENTS

Chapter 1 - Introduction	1
1.1. The Cancer Burden	2
1.2. Targeted therapy	3
1.2.1. The RAS Gene Mutation	6
1.3. An overview of the PI3K/AKT/mTOR pathway	10
1.3.1. PI3K signalling in human cancer.....	15
1.3.2. Different classes of PI3K inhibitors.....	16
1.3.3. Selective targeting of class I PI3K isoforms	19
1.3.3.1. PI3K α selective inhibitors	21
1.3.3.2. PI3K β selective inhibitors.....	22
1.3.3.3. PI3K γ selective inhibitors	23
1.3.3.4. PI3K δ selective inhibitors.....	24
1.4. Computational Chemistry in drug development	26
1.4.1. Quantum chemical approaches in protein-ligand binding energy	28
1.5. Objectives	30
Chapter 2 - Virtual Screening - Results and Discussion	32
2.1. Molecular targets	33
2.2. Ligands' design	37
2.3. Virtual Screening	38
2.3.1. Evaluation of ligand selectivity.....	39
2.3.2. Correlation between the variation of $\Delta G_{\text{binding}}$ and ligand properties	51
2.3.3. Analysis of P-L interactions in PI3K α and PI3K γ	57
Chapter 3 - Chemical Synthesis - Results and Discussion	63
3.1. Synthesis of starting reagents	65
3.1.1. Synthesis of 5-amino-4-amidino-imidazoles (28).....	65
3.1.2. Characterization of 5-amino-4-amidino-imidazoles (28).....	66
3.1.2.1. Physical and analytical characterization	66
3.1.2.2. Infra-red spectroscopy (IR) characterization.....	66
3.1.2.3. ^1H and ^{13}C NMR spectroscopy characterization	67
3.1.3. Synthesis of the purine derivatives (29) and (1-23)	70
3.1.3.1. Synthesis of 2-(3-nitrophenyl)-purine derivatives (29).....	70
3.1.3.2. Acylation of 9-(amino-aryl) purine derivatives.....	71
3.1.3.3. Reduction of 2-(3-nitrophenyl)-purine derivatives (29)	75
3.1.4. Characterization of the purine derivatives (29) and (1-23).....	78

3.1.4.1. Physical and analytical characterization	78
3.1.4.2. Infra-red spectroscopy (IR) characterization.....	79
3.1.4.3. ¹ H and ¹³ C-NMR spectroscopy characterization	80
3.2. Synthesis of final products	94
3.2.1. Acylation of 2-(3-aminophenyl)-purine derivatives.....	96
3.2.2. One-pot synthesis of ureas from 2-(3-aminophenyl)-purine derivatives	97
3.2.3. Reaction of the acylated 2-(3-aminophenyl)-purine derivatives with nitrogen nucleophiles	100
3.2.4. Attempts towards the reduction of azides.....	107
3.2.5. Characterization of final compounds	110
3.2.5.1. Physical and analytical characterization	110
3.2.5.2. Infra-red spectroscopy (IR) characterization.....	112
3.2.5.3. ¹ H-NMR spectroscopy characterization	115
3.2.5.4. ¹³ C-NMR spectroscopy characterization.....	124
Chapter 4 - Conclusions and Future Perspectives	138
Chapter 5 - Methods.....	144
5.1. Virtual Screening.....	145
5.1.1. Targets Preparation	145
5.1.2. Ligand Preparation	147
5.1.3. Virtual Screening	149
5.2. PCA analysis.....	150
5.3. Chemical Synthesis – General techniques.....	151
5.3.1. Starting reagents	151
5.3.1.1. General procedure for the synthesis of 5-amino-4-amidino-imidazoles (28).....	151
5.3.1.2. General procedure for the synthesis of 2-(3-nitrophenyl)purine derivatives (29a-h).....	152
5.3.1.3. Acylation of 4-(2-(3-nitrophenyl)-9-(aniline)-9H-purin-6-yl)morpholine derivatives (29e-f).....	154
5.3.1.4. General procedure for the reduction of 2-(3-nitrophenyl)-purine derivatives (29).....	158
5.3.2. Final Products	161
5.3.2.1. General procedure for the acylation of 2-(3-aminophenyl)-purine derivatives.....	161
5.3.2.2. General procedure for the one pot synthesis of ureas from 2-(3-aminophenyl)-purine derivatives ..	164
5.3.2.3. Reaction of the acylated 2-(3-aminophenyl)-purine derivatives with nitrogen nucleophiles	167
Chapter 6 - References.....	172
Appendix.....	179

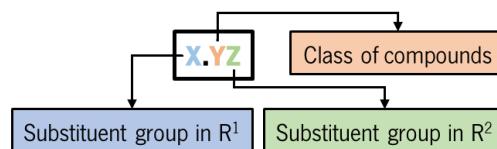
LIST OF ABBREVIATIONS

$\Delta G_{\text{binding}}$	Free Energy of Binding
ADT	Auto Dock Tools
AKT	Serine/threonine kinase B
CDI	1,1'-Carbonyldiimidazole
CDK	Cyclin-dependent kinases
CLL/SLL	Chronic lymphocytic leukemia/ small lymphocytic lymphoma
CSC	Cancer stem cells
DFT	Density-functional theory
DMAP	4-(dimethylamino) pyridine
DMSO	Dimethyl sulfoxide
EGFR	Epidermal Growth Factor Receptor
FF	Force Field
FL	Follicular lymphoma
HBA	Hydrogen Bond Accepting
HBD	Hydrogen Bond Donor
HMBC	Heteronuclear Multiple-Bond Correlation
HMQC	Heteronuclear Multiple-Quantum Correlation
HRAS	Harvey rat sarcoma viral oncogene homolog
IR	Infra-Red
KRAS	Kirsten rat sarcoma viral oncogene homolog
LogP	Partition Coefficient
m.p.	Melting point
MAPK	Mitogen-activated protein kinase
MDR	Multidrug-Resistant
MIBK	Methyl isobutyl ketone
MM	Molecular Mechanics
mTOR	Mechanistic target of rapamycin
Mw	Molecular weight
NMR	Nuclear Magnetic Resonance
NRAS	Neuroblastoma RAS viral oncogene homolog
NSCLS	Non-small cell lung cancer

PCA	Principal component analysis
PD	Pharmacodynamics
PDB	Protein Data Bank
PDGFR	Platelet-derived growth factor receptor
PH	Pleckstrin homology
PI3K	Phosphatidylinositol 3-kinase
PIP2	Phosphatidylinositol 4,5-bisphosphate
PIP3	Phosphatidylinositol 3,4,5-trisphosphate
PK	Pharmacokinetics
PL	Protein-Ligand
ppm	Parts per million
PtdIns	Phosphatidylinositols
PTEN	Phosphatase and tensin homolog
QC	Quantum Chemistry
QM	Quantum Mechanics
RAF	Rapidly Accelerated Fibrosarcoma
Rf	Refractivity
RMSD	Root-mean-square deviation
RTK	Receptor tyrosine kinases
SF	Scoring Function
TGF	Transforming growth factor
TIL	Tumor-infiltrating lymphocytes
TLC	Thin Layer Chromatography
TME	Tumor microenvironment
TNF	Tumor necrosis factor
TP53	Tumour protein 53
UV	Ultraviolet
VEGF	Vascular endothelial growth factor
VS	Virtual Screening

EXPLANATORY SHEET FOR THE NUMERATION OF COMPOUNDS

The final compounds of this work were specifically numbered in order to facilitate the presented *in silico* assays. According to this numeration (**X.YZ**), **X** represents a number that identifies the substituent group R¹, which varies between **1** and **23**. Then, **Y** represents the 11 classes of compounds discussed. Finally, **Z** represents a character that identifies the substituent group R² (**a-e**), for each class of final products (**1-9**). All remaining non-final compounds addressed were numbered sequentially starting at **24**, or by the same system with a different group R² (**f-h**).



Substituent group in R ¹								
Class of compounds								
Substituent group in R ²								

Chapter 1

INTRODUCTION

1.1. The Cancer Burden

Cancers are a result of a progressive accumulation of driver gene mutations that successively increase cell proliferation. These mutations may be inherited, induced by environmental factors, or result from DNA replication errors [1]. As a result, cancer is acknowledged as a disease responsible for the uncontrolled growth and spread of anomalous cells [2]. There are different types of cancer once it is a variational disease due to the dependence on the tissue where it is formed, being this variety one of the major challenges for its specific diagnosis, followed by the treatment efficacy [3].

Cancer is currently one of the leading causes of death in the world, where the cancer burden is gradually rising [4]. Estimates for 2020 pointed to 19.3 million new cases of cancer and 10.0 million cancer deaths worldwide, and it is predicted that by 2040, the number of new cancer cases per year will likely rise to 29.5 million and the number of cancer-related deaths to 16.4 million [5], [6]. Although preventing cancer continues to be one of the most promising strategies for minimizing these values of incidence and mortality, the frequently late-stage symptoms, and therefore the late diagnosis of this disease continues to restrict therapy options. This happens because the most common adult epithelial cancers represent the late stage in the course of all cancer development. Once cancer becomes invasive, it has the potential to disseminate to other tissues, remaining metastasis a major cause of cancer-related mortality and a central focus of research [4], [7], [8].

There are many types of cancer treatments depending on the tissue and advancement of the disease, however, most of these treatments are rather limited and can only be applied in specific situations. Surgery, for example, can be applied efficiently as a local treatment for solid tumours that are not metastasized. Radiotherapy is another example of cancer treatment that uses high doses of radiation to kill cancer cells and shrink tumours, having the consequence of not only killing and slowing the growth of cancer cells but also affecting nearby healthy cells, which can cause drastic side effects. The same happens with hormone therapy and immunotherapy where the treatment acts not only against cancer but also affects healthy cells and other tissues in the body. Chemotherapy is the most used treatment for the majority of cancer types being also commonly combined with other treatments. This therapy kills fast-growing cancer cells but once it is not selective, it also kills or slows the growth of healthy cells that grow and divide rapidly [9].

Despite the huge efforts towards the discovery of novel chemotherapeutic strategies for the treatment of different types of cancer, the disease continues to be a major concern worldwide.

Consequently, there is an urgent need to explore newer and selective classes of therapeutics against cancer cells. The regulation of the cell division and apoptotic pathways associated with cell death are known as important and strategic keys for comprehending the regulation processes of these abnormal cells. Therefore, the identification of cell-cycle regulators and apoptotic activators to combat cancer cells represent an attractive and promising strategy for the discovery and development of potential antitumor agents [2]. A great amount of information about genes and proteins and their roles in the making of cancer cells was discovered in the last few decades, being the role of mutated genes in cancer cells of most importance in the development of a newer and promising strategy for treating cancer, denominated targeted therapy [3].

1.2. Targeted therapy

Targeted therapy is a type of cancer treatment that uses drugs or other substances that target specific biologic molecules (molecular targets), such as proteins that control how cancer cells grow, divide, and spread. As researchers learn more about the DNA changes and proteins that drive cancer, they can design new promising treatments that target these proteins. One of the advantages of molecular targeted therapy is its ability to deliver drugs effectively with high specificity while being less toxic compared to conventional chemotherapy [9], [10].

The identification of ideal targets is essential for the successful development of molecular targeted cancer therapies. One of the bases of cancer occurrence is dictated by the alteration of the genetic profile which leads to mutation or changes in proteins and receptors that promote cell survival and proliferation. These 2 specific genetic alterations that can distinguish cancer cells from normal cells can be used as molecular targets in the development of molecular targeted drugs. By understanding the physiology and characteristic of specific molecular targets in cancer, researchers can identify potential molecular strategies to inhibit tumour growth and progression. Cancer markers can be determined using genome sequencing which enables the comparison of the genes and proteins expression of normal and malignant cells to identify changes in their expressions, which is important when identifying molecular targets for drug development [10].

A lot of progress in sequencing thousands of cancer genomes and advances in cancer biology have uncovered many drivers of tumorigenesis. The RAS, TP53 (p53) and MYC are among the most frequently altered driver genes in cancer [10]. Thus, RAS being the most frequently mutated oncogene, MYC the most frequently amplified gene and TP53, the most frequently mutated tumour suppressor gene

and overall, the most mutated gene in cancer. Theoretically, these are highly attractive targets for cancer treatment. However, all three respective proteins lack a readily identifiable accessible deep pocket into which potential low molecular weight drugs can bind with high affinity [10], [11]. Also, aside from RAS, which exhibits weak intrinsic catalytic activity (GTPase), neither p53 nor MYC possess enzyme activity. For this reason, these macromolecules cannot be targeted. Finally, all three proteins are located intracellularly, that is, RAS on the inner layer of the cell membrane and both p53 and MYC in the nucleus [11]. Consequently, they cannot be easily reached with high molecular weight drugs [11]. Many of these drivers are associated with different signalling pathways in cancer, which include different kinases that have provided druggable targets yielding significant clinical benefits over the past few decades [12]. These proteins play a significant role in regulating signalling pathways that modulate many physiological functions such as cell growth, proliferation, migration, and angiogenesis. Dysregulation of these protein kinases may cause abnormal cell growth, turning them into promising targets. These include growth factors, signalling molecules, cell-cycle proteins, modulators of apoptosis and molecules that promote angiogenesis, among many others [10], [12].

Once cancer cell proliferation and metastasis are highly dependent on the formation of tumour vessels for nutrient and oxygen supply, targeting angiogenesis promoters to inhibit the growth of blood vessels in the microenvironment of the tumour is considered an attractive alternative [13]. Also, there is the notion that therapy directed against the supporting host tissue rather than the tumour itself will be less prone to resistance, once the genetic plasticity of the cancer is not reflected in the stroma [10]. A few examples of these promoters are vascular endothelial growth factor (VEGF), basic fibroblast growth factor (bFGF), angiogenin, transforming growth factor (TGF)- α , TGF- β , tumour necrosis factor (TNF)- α , platelet-derived endothelial growth factor (PDGFR), granulocyte colony-stimulating factors, placental growth factors, interleukin-8, hepatocyte growth factor, matrix metalloproteinases (MMPs), integrin, and epidermal growth factors [10], [13].

Many novel promising agents have been experimentally designed and developed and are increasingly entering clinical trials evaluation. However, the frequently observed alterations in the drug targets have posed a big challenge to a successful cancer treatment. In recent years, great progress has been made in targeted therapy discovery [13]. Notably, many new drugs are designed primarily based on specific genetic backgrounds. The main challenge of targeted therapy today is the identification of particular cancer mutations which affect the efficacy of targeted therapies as well as the identification of a specific group of patients most likely or unlikely to respond to certain targeted therapies. Several novel

targets, including the programmed death-1/programmed death-ligand 1 (PD1/PDL1) and cyclin-dependent kinases 4 and 6 (CDK4/6), have been validated, with several new targeted drugs being approved [14]. Some newly approved drugs are directly designed to deal with some known activating mutations, such as the T790M mutation in epidermal growth factor receptor (EGFR), which is a prevalent target in several human cancers, such as lung, breast, colorectal, thyroid, and melanoma cancer. Since the elucidation of the role of cyclin-dependent kinases (CDKs) in cell-cycle regulation, these proteins have been also extensively explored as potential drug targets, such as other different kinases in the PI3K/Akt/mTOR pathway (Figure 1a) [13], [14].

One of the key mechanisms and major challenges in molecular targeted therapy is the induction of apoptosis in tumour cells. However, disabling of the apoptosis process plays an important role in promoting tumorigenesis, leading to treatment resistance in many tumour types, what is already current in modern chemotherapy (Figure 1b) [10], [12].

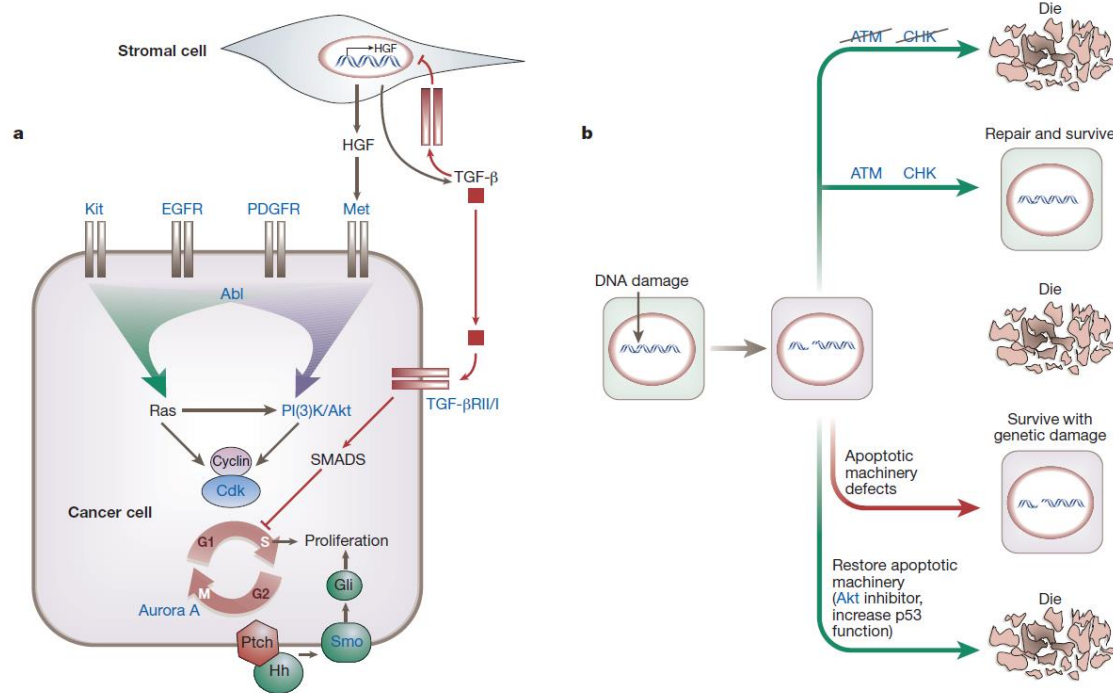


Figure 1 Cancer pathways and targeted therapy. **a)** Multiple signalling pathways upregulated in cancer cells owing to specific alterations in oncogenes or tumour suppressors that stimulate tumour-cell proliferation, often by promoting G1–S cell-cycle progression. Signals from the tumour microenvironment, including stromal fibroblasts, can positively or negatively shape cancer-cell proliferation. The Inhibition of growth-promoting pathways by therapy tailored to the specific genetic alterations found in cancer offers a new therapeutic approach; **b)** Classical chemotherapy and radiotherapy eliminate cancer cells by inducing DNA damage and subsequent apoptosis. DNA-damage-response pathways promote repair and survival. Defects in the apoptotic machinery can allow cancer cells to survive DNA damage, which may lead to the acquisition of further mutations. Inhibition of DNA-damage-response pathways or restoration of defective apoptosis pathways may render cancer cells more susceptible to DNA-damaging agents and provide potential avenues for more efficient and tumour-specific future therapies in the future [13].

1.2.1. The RAS Gene Mutation

Rat sarcoma (RAS) genes have the distinct honour of being the first mutated genes identified in human cancer, ushering the era of molecular targeted anticancer drug discovery. The RAS protein is a membrane-bound protein with inherent GTPase activity and is activated by numerous extracellular stimuli, cycling between an inactive (GDP-bound) and active (GTP-bound) conformations, therefore acting as a molecular switch [15], [16]. RAS activation causes a conformational change that allows engagement with more than 20 different proteins from 10 effector families. When bound to GTP, it activates intracellular signalling pathways with specific proteins and lipids, critical for cell proliferation and angiogenesis [17].

There are three RAS oncogene products (KRAS, NRAS and HRAS). These present a high sequence homology and are the most intensively studied proteins because of their mutation in approximately 30% of human cancers. These proteins act as binary molecular switches that interact with a large number of catalytically distinct downstream effectors such as RAF, PI3K and Ral guanine nucleotide dissociation stimulator (RALGDS). These effectors, which are activated by their interaction with RAS, in turn, regulate cytoplasmic signalling, leading to gene expression and cell cycle progression [12], [15], [18].

Mutations of RAS that render the protein constitutively active are widely observed in cancer. However, there are distinctive patterns in the mutation frequencies associated with each type of cancer. As RAS proteins activate signalling networks controlling cell proliferation, differentiation and survival, mutated RAS, being constitutively activated and persistently turned “on”, enhances downstream signalling leading to tumorigenesis [17]. Oncogenic RAS mutations also lead to gain-of-function missense mutations with almost all detected in patients clustering in three hot spots at codons 12, 13 and 61 [17]. The frequency of mutated hot spots in RAS proteins also varies depending on the tissue of origin. For example, mutations affecting Q61 in NRAS are more frequent in melanoma (85% of NRAS mutations), whereas mutations in G12 in KRAS are more common in lung cancers, colorectal carcinomas (CRC) and pancreatic cancers (50%, 78% and 97% of KRAS mutations), respectively [19].

Kirsten rat sarcoma (KRAS) viral gene and neuroblastoma rat sarcoma viral oncogene (NRAS) control the fate of cells through the cell cycle by retransmitting extracellular signals to the nucleus. Activation of these mutated genes causes constant signalling and promotion of survival genes regardless of the blockage of EGFR. Many targeted therapy drugs target the EGFR pathway, and the absence of wild-type KRAS and NRAS genes have been found to turn the therapy ineffective. A preclinical study using

siRNA to target KRAS has shown encouraging results in lung and pancreatic cancers which significantly decreased KRAS level and inhibited tumour growth [10].

Genetic and biochemical studies have shown that RAS signalling mediated by KRAS plays a crucial role in tumour initiation, progression and drug resistance. Its mutation is the major event in pancreatic cancer, with over 90% of patients harbouring somatic oncogenic point mutations in KRAS, and in colorectal cancer with about 40 % [20]. These patients have an overall low survival rate with a poor response towards standard therapies including the combination of targeted therapy and standard chemotherapy drugs [20], [21]. New technologies and insights into signalling pathways that KRAS control have allowed researchers to develop novel therapies by blocking KRAS processing, or by identifying targets that KRAS cancers depend on for survival [22].

Several agents have been developed for treating tumours with RAS mutations, including direct and indirect approaches (Figure 2).

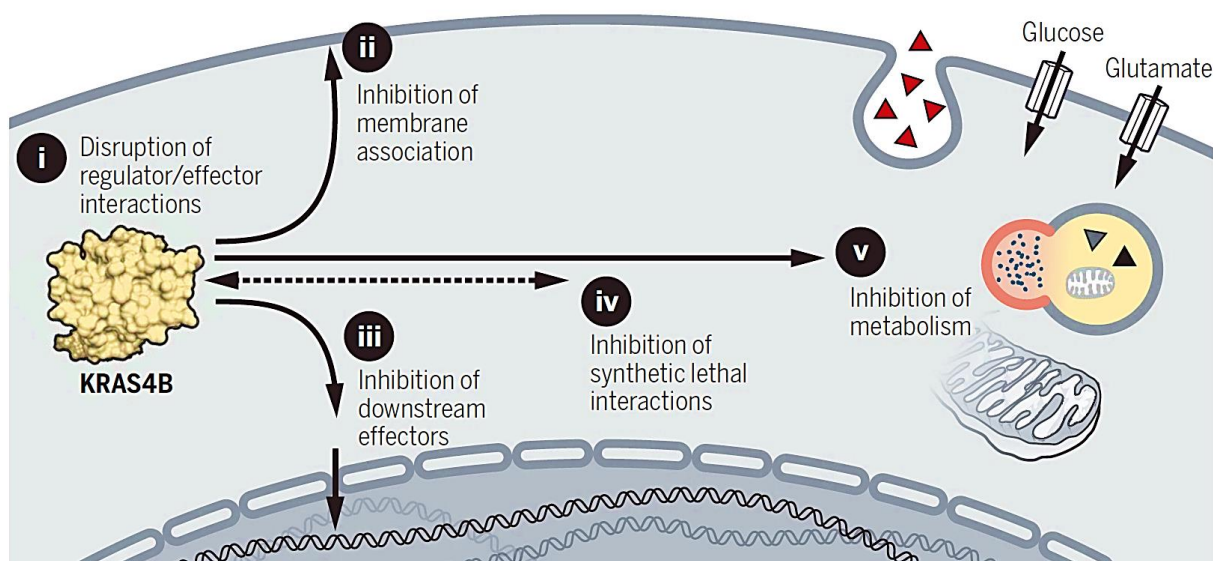


Figure 2 Five general strategies for anti-RAS drug development. (i) Molecules that directly bind RAS and disrupt its interaction with guanine nucleotide exchange factors or with effectors such as the RAF serine/threonine kinases. Also shown are four indirect approaches that target (ii) proteins modulating RAS spatial organization and association with the plasma membrane (e.g., farnesyltransferase and PDE d), (iii) RAS effector signalling (e.g., RAF and PI3K), (iv) synthetic lethal interactors of mutant RAS, and (v) RAS regulated metabolic processes in cancer cells [18].

Several of these new therapeutic agents are showing promising clinical effects and many more are being developed [23]. The latest advances in the understanding of RAS biology have led to new opportunities for direct targeting of RAS or to target key RAS effectors and vulnerabilities. While these new agents and approaches have already shown promising results in preclinical and clinical studies, the

complexity of RAS signalling and the potential for robust adaptive feedback continue to present substantial challenges [19], [24].

Direct inhibition of RAS proteins (Figure 2 i) has proved difficult since RAS proteins have been considered weak drug targets as a result of a perceived lack of drug-binding pockets other than the nucleotide-binding pocket and to the picomolar binding affinity of GTP for RAS, thus rendering GTP-competitive inhibitors ineffective [19]. Several compounds interact with KRAS at an important interaction site, preventing the formation of active KRAS-GTP. Although a few of these molecules exhibited low (micromolar) *in vitro* affinity, they inhibited cancer cell growth in cell-based assays, being still unclear whether this effect was due to antagonism of KRAS function or to off-target activities. Among the molecules that directly bind RAS, the most provocative class comprises those designed to recognize the specific RAS mutation G12C. These initial G12C inhibitors (AMG510, MRTX849, JNJ-74699157, and LY3499446) had limited cellular activity, but later refinement and development led to the compound ARS-853 with the same mechanism of action and with improved biochemical and cellular activities. This compound strongly inhibited the proliferation of cancer cells with RAS G12C mutations [15], [18].

Targeting RAS plasma membrane localization (Figure 2 ii) is an indirect approach that consists of RAS oncogenic activity depending on the RAS association with the inner face of the plasma membrane, and the subsequent identification of the posttranslational modifications that modulated this association [15]. The RAS isoforms are synthesized initially as cytosolic, inactive proteins. The RAS C-terminal CAAX (C, cysteine; AA, aliphatic amino acid; X, terminal amino acid) tetrapeptide sends signals for a series of posttranslational modifications. The first is the farnesyltransferase-catalysed covalent addition of a farnesyl fraction to the cysteine residue of the CAAX motif. The second, which occurs at the cytosolic surface of the endoplasmic reticulum, is the proteolytic removal of the last three amino acids by RAS converting enzyme 1 (RCE1). Finally, isoprenylcysteine carboxyl methyltransferase (ICMT) facilitates methyl transfer to the C-terminal amino acid to negate the negative charge and prevent plasma membrane repulsion. Therefore, all these CAAX-signaled modifications contribute to RAS association with the plasma membrane. Given the essential role of the farnesyl lipid modification for all subsequent posttranslational modifications and RAS oncogenic activity, farnesyltransferase inhibitors were developed and demonstrated to potently block HRAS-driven growth of cancer cells [18].

The second indirect approach is the blockade of downstream effector signalling (Figure 2 iii). This is one of the most attractive and popular anti-RAS strategies, even with at least 11 catalytically diverse downstream effector families. The two more attractive effectors are the RAF-MEK-ERK mitogen-activated

protein kinase (MAPK) cascade and the PI3K-AKT-mTOR pathway [12]. Mutations in genes encoding components of each pathway are known to drive human cancer development, and their gene products are druggable protein kinases. Numerous inhibitors against each component of both the RAF-MEK-ERK and PI3K-AKT-mTOR effector pathways have been developed and are under clinical evaluation [18].

The RAS/RAF/MEK/ERK (MAPK) signalling cascade is responsible for fundamental cell functions such as cell growth, survival and differentiation. The MAPK pathway also integrates signals from complex intracellular networks in performing cellular functions [25]. Monotherapy with MAPK inhibitors has been associated with very limited improvement of outcomes in clinical trials for patients with RAS-mutant cancers, with only some activity in patients with NRAS-mutant melanoma but little effect in those with KRAS-mutant cancers [19]. Resistance to this pathway inhibitors can be mediated by PI3K/AKT/mTOR activation [18]. This signalling pathway is involved in various vital functions, including cell proliferation, survival, metastasis, metabolism, and angiogenesis. Thus, many diseases, especially cancer, arise as a result of dysregulation or mutation of the PI3K/AKT/mTOR pathway. About 30-50% of human tumours are likely due to the activated PI3K/AKT/mTOR pathway. Inhibiting this pathway leads to cellular death and cancer control, while its pathological activation can develop cancer either due to point mutations of PI3K genes or inactivation of tumour suppressor gene phosphatase and tensin homologue gene (PTEN) [16], [26].

Besides the current development of drugs that block the MAPK and PI3K downstream pathways, new efforts are still underway to exploit previously unrecognized vulnerabilities in RAS, such as altered metabolic networks or novel pathways identified through synthetic lethal screens and of harnessing the immune system [22]. This leads to the third indirect approach for targeting mutant RAS which is based on the concept of synthetic lethality (Figure 2 iv). Synthetic lethal interaction is associated with mutant RAS genes whose functions are essential in RAS-mutant but not wild-type RAS cells. The identification of synthetic lethal ligands of mutant RAS was reported including several protein kinases such as STK33 and TBK1. However, subsequent studies failed to validate a strong functional linkage of these hits with mutant RAS [18].

At last, cancers harbouring mutations in KRAS and other RAS-driven cancers are highly dependent on the upregulation of metabolic processes to sustain oncogenic cell growth. In recent years RAS-dependent metabolic processes have been identified as potentially actionable vulnerabilities in RAS-mutant cancers [19]. Mutant RAS has been linked to increased glucose metabolism (Figure 2 v) and the diversion of glucose metabolites into nucleotide and lipid biosynthetic pathways. In fact, RAS can drive

increased glucose uptake by up-regulating the expression of the glucose transporter GLUT1. KRAS also up-regulates glycolytic enzymes to enhance the conversion of pyruvate to lactate [18].

In addition to altering cellular metabolism, RAS mutations can also influence the tumour microenvironment (TME) and the immune response. The presence of a mutation in KRAS or the activation of RAF/MEK/ERK can result in an immunosuppressive TME and reduce the number of tumour-infiltrating lymphocytes (TILs). The role of mutant RAS in regulating the interaction between the tumour and the immune system is complex but can potentially be exploited as a viable antitumor therapy. Harnessing the immune system to target RAS-mutant cancers has shown promising results in both preclinical and clinic models [19].

1.3. An overview of the PI3K/AKT/mTOR pathway

The PI3K/AKT/mTOR signalling pathway regulates multiple cellular processes involved in various vital functions, including cell proliferation, survival, metastasis, metabolism and angiogenesis [27]. Phosphoinositide 3-kinases (PI3Ks) have been known as widely expressed lipid kinases that act as signal transducers downstream of cell-surface receptors [28]. Compared with other signalling pathways, the components of the PI3K/AKT/mTOR signalling pathway are rather complicated. The regulatory mechanisms and biological functions of this signalling pathway are important in many human diseases, including ischaemic brain injury, neurodegenerative diseases, chronic allergy and inflammation, diabetes, systemic lupus erythematosus, atherosclerosis, cardiovascular disease and cancer, which arise as a result of the dysregulation or mutation of this pathway [26], [29], [30].

The PI3K/AKT/mTOR signalling pathway (Figure 3) consists of two parts: phosphatidylinositol 3-kinase (PI3K) and its downstream macromolecule serine/threonine-protein kinase B (PKB; also known as AKT). The PI3K/AKT/mTOR pathway is stimulated by RTK and cytokine receptor activation. Tyrosine residues are then phosphorylated and provide anchor sites for PI3K translocation to the membrane [29]. Phosphorylated lipids are produced at cellular membranes during signalling events and contribute to the recruitment and activation of various signalling components [31]. In mammals, PI3Ks belong to the lipid kinases family which phosphorylates the hydroxyl moiety of the inositol ring, yielding products of which the most characterized is phosphatidylinositol-3,4,5-trisphosphate (PIP3), the second messenger that activates AKT or other cellular messengers such as the mammalian target of rapamycin (mTOR) [26], [32].

The enzyme activity to phosphorylate the 3-hydroxyl group of membrane phosphatidylinositols (PtdIns) interconnects a group of at least eight proteins that differ in expression, regulation, structure, and substrate specificity within the family of PI3Ks [33]. Many important physiological processes including cell division, metabolism and motility are regulated by PIP3, which is generated by the phosphorylation of the 3' hydroxyl group on the inositol head group of phosphatidylinositol-4,5-bisphosphate (PIP2). This lipid is produced in response to external stimuli by the action of kinases called class I phosphoinositide-3 kinases (PI3Ks). PIP3 is sensed by many downstream effectors which in turn results in their recruitment to the membrane and the activation of their downstream targets. One of the most well-studied PIP3 effectors is the protein kinase AKT, which recognizes PIP3 through its pleckstrin homology (PH) domain, which in turn relieves an autoinhibitory interaction between the PH and kinase domains. AKT phosphorylates numerous targets including mTOR complex1 activating protein TSC2, glycogen synthase kinase 3 β (GSK3 β) and FOXO family transcription factors, which control cellular processes associated with growth, survival, and metabolism. Other PIP3 effectors include Guanine Nucleotide Exchange factors, GTPase activating proteins and cytoskeletal proteins which regulate movement and structural integrity [34].

The PI3K/AKT/mTOR signal transduction pathway is controlled by many factors, including the tumour suppressor PTEN, that catalyses the reaction opposite of PIP3 generation by converting PIP3 in PIP2 (Figure 3). PTEN downregulates the PI3K/AKT/mTOR pathway to suppress cell proliferation and interfere with cellular metabolism, and inhibition of PTEN activity activates AKT and downstream pathways. PTEN plays an important role in regulating glucose homeostasis by modulating AKT activity [29]. As the main molecule downstream of the PI3K signalling pathway, the serine/threonine-protein kinase AKT comprises three subtypes, AKT1, AKT2 and AKT3, which are encoded by PKB α , PKB β and PKB γ , respectively. The specific tissue expression patterns of the different AKT subtypes suggest their key roles in the maintenance of physiological functions in different tissues or organs [29]. Finally, mTOR, a serine/threonine-protein kinase, is a member of the PI3K-associated kinase protein family that participates in sensing nutritional signals and regulating cell growth and proliferation. The mTOR includes mTOR complex 1 (mTORC1) and mTOR complex 2 (mTORC2). mTORC1, which is composed of mTOR, Raptor and mLST8, mainly regulates cell growth and energy metabolism and is sensitive to rapamycin [29]. mTORC2, which is composed of mTOR, Rictor, Sin1 and mLST1, is mainly involved in the reconstruction of the cytoskeleton and cell survival and is not sensitive to rapamycin.

While mTORC1 is a downstream molecule of AKT and is activated by phosphorylated AKT, mTORC2 fully activates AKT by phosphorylating a serine residue. The AKT/TSC1–TSC2 signalling pathway can also regulate mTOR activity as well as cell growth and proliferation. TSC2 has GTPase activity and inhibits the small GTPase Rheb, which is necessary for mTORC1 activation. Following phosphorylation of TSC2 by AKT, TSC2 loses its ability to inhibit mTORC1 and activate mTOR. Also, TSC2 can be directly

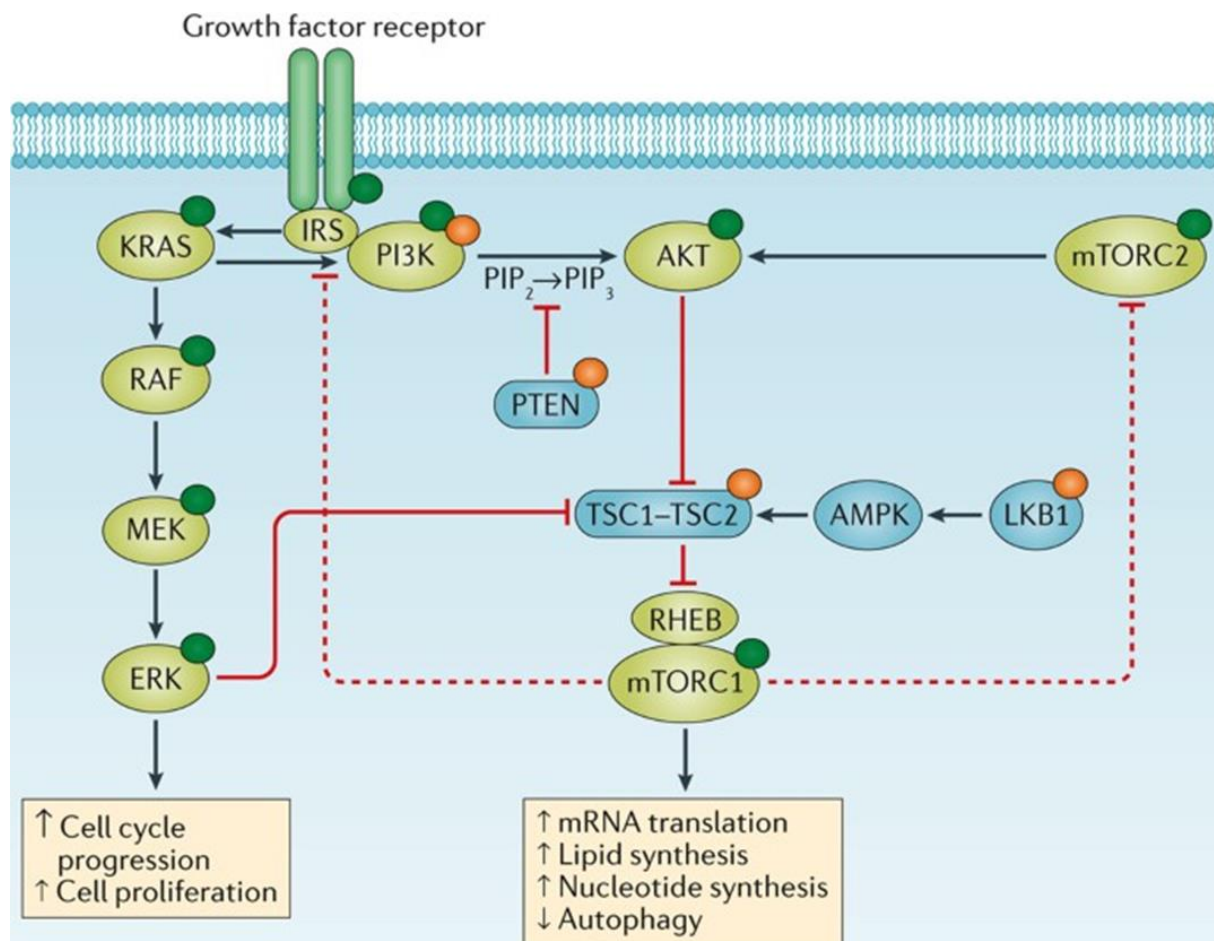


Figure 3 PI3K/AKT/mTOR signalling pathway [32]. The class I PI3K proteins are recruited to the plasma membrane by adaptor proteins, such as insulin receptor substrate (IRS) family members, that interact with these activated cell-surface receptors, leading to phosphorylation of PIP_2 to PIP_3 , a second messenger that activates the AKT kinases, which are able to phosphorylate tuberous sclerosis protein 1 (TSC1) and TSC2, and thereby dissociate the TSC1–TSC2 complex. This complex negatively regulates the activity of mTOR therefore, AKT results in the activation of mTORC1 and ultimately in increased protein and lipid synthesis and decreased autophagy, which supports cell growth and proliferation. Notably, mTORC1 is involved in a negative feedback loop that serves to prevent the over activation of AKT (dashed red lines). The PI3K/AKT/mTOR pathway can be upregulated by activating molecular alterations in the PI3K subunits, AKT, and mTOR (depicted by green circles) or by loss-of-function alterations in the PI3K regulatory subunits, PTEN, TSC1, TSC2, and LKB1 (depicted by orange circles). In parallel, activation of the growth factor receptor tyrosine kinases and G protein-coupled receptors induces KRAS/RAF/MEK/ERK signalling, and ERK activation can further contribute to mTORC1 activation through dissociation of the TSC1–TSC2 complex. KRAS can also reinforce the activation of PI3K. Notably, the KRAS/RAF/MEK/ERK pathway can also be activated constitutively by gain-of-function alterations in the component kinases or cell-surface receptors (green circles) [32].

activated by AMPK phosphorylation, and AKT can completely inhibit TSC2 and activate mTOR by inhibiting AMPK [29].

Human cells express three different classes of PI3K enzymes [30], [33]. These consist of eight PI3K isoforms, divided into three classes based on structural, catalytic and regulatory properties [35]. They are subdivided into three major classes (I, II and III) based on their structural homology, coding genes, distinct structures, regulation and substrate specificity [28] (Figure 4). Among these kinases, the most widely studied are class I PI3Ks, which can be activated directly by cell surface receptors [29]. It is now becoming clear that PI3K isoforms are subject to differential regulation and may play distinct roles within the cell. There are three catalytic subunits of class II PI3Ks (PI3K-C2 α , β , γ) [26]. These were shown to be associated with several receptors, such as EGFR or PDGFR and were found to be induced by chemokines, cytokines, and insulin [33]. On the other hand, the 2 Class III subunits form a constitutive heterodimer that is found in discrete multiprotein complexes, having vital roles in autophagy, endocytosis, phagocytosis and intracellular trafficking. The structural difference between the 3 main classes of the PI3K family can be summarized as shown in Figure 4 [26], [35]. Like class I, class III isoforms are heterodimers with a catalytic and regulatory subunit [30], [36]. Although classes II and III characterisation has lagged behind that of the class I PI3Ks, they have received increased attention in recent years, allowing new details of their roles to come to light [35], [37].

There are four members of the class I PI3Ks, which act upstream of this pathway, converting PIP2 into PIP3 [38], [39]. This class is subdivided into class IA (PI3K α , β and δ isoforms) and class IB (PI3K γ isoform) [40]. The regulation of PI3K activity is driven by the interplay between signals arising from upstream activating stimuli and the interpretation of these signals by the PI3K catalytic and regulatory components. This diversity in the ability of various PI3K isoforms to differentially sense signalling inputs is key to their broad and crucial physiological roles [34].

Class IA PI3Ks are activated by a variety of cell surface receptors, such as receptor tyrosine kinases (RTKs), G protein-coupled receptors (GPCRs) and the small G protein Ras, while class IB PI3K, which consist of only one subunit PI3K γ , is activated via the direct binding of p110 γ to the G $\beta\gamma$ subunit of G protein-coupled receptors (GPCRs) [28], [33], [37]. The p110 catalytic subunit has five well characterized domains; an N-terminal Adaptor Binding Domain (ABD), a Ras Binding Domain (RBD), a C2 domain, a helical domain, and a catalytic domain which is homologous to that of other lipid kinases (Figure 4) [34]. These different p110 isoforms have very distinct expression patterns in human cells and

tissues, as p110 α and p110 β are ubiquitously expressed in all cells, while p110 δ and p110 γ are primarily expressed in hemopoietic cells and a few select tissues such as neurons and the heart and play major roles in immune responses and inflammations. Each catalytic isoform forms a dimer with a regulatory subunit that modulates the activity and subcellular localization of the complex [28], [30], as demonstrated in Figure 4, right panel.

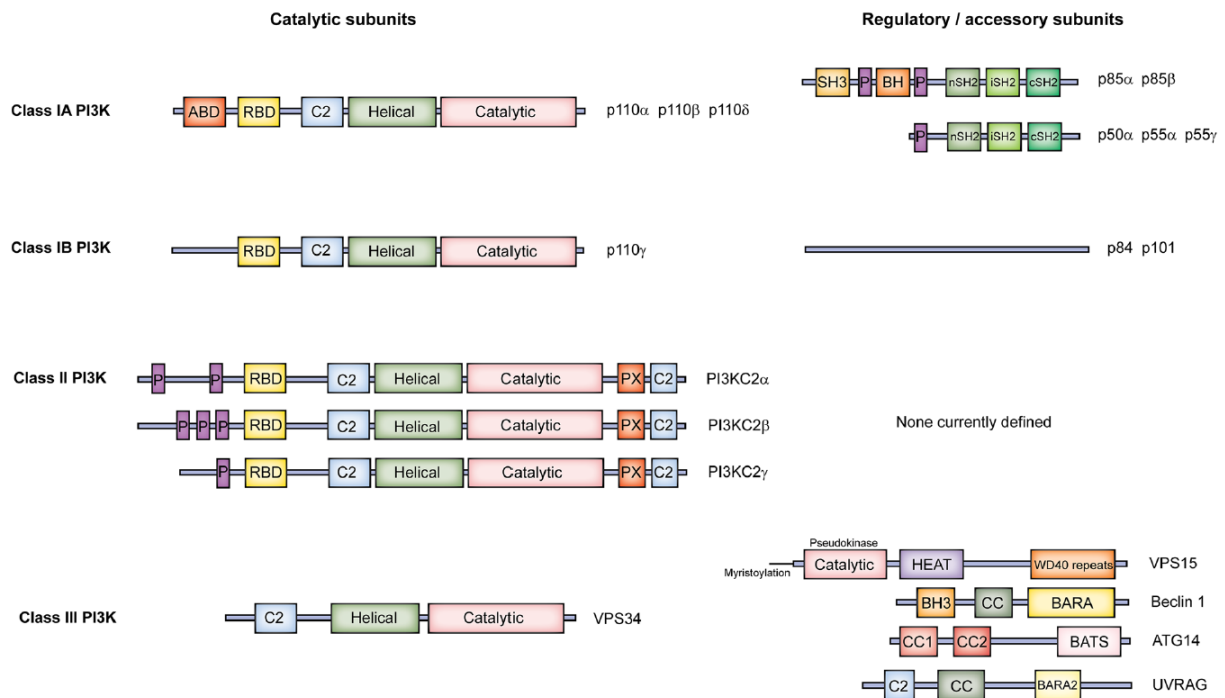


Figure 4 Domain organisation of the PI3Ks. Class I, II and III PI3K catalytic subunits share a core region consisting of a C2 domain, helical domain and kinase domain, but differ in other regions of the protein. While the domain structure of the Class IA regulatory subunits is well defined, the Class IB regulatory subunits have no clearly-defined domain structure, while no regulatory subunits have been reported for the Class II PI3Ks. The Class III PI3K, VPS34, associates with a range of accessory proteins to form at least two distinct complexes [35].

The class IA catalytic isoforms (p110 α , p110 β , and p110 δ) interact with a p85-binding domain (p85-BD) that binds to a RAS-binding domain (RBD) [34]. On the other hand, class IB PI3Ks are heterodimers consisting of the p101/p84 regulatory subunit and the p110 γ catalytic subunit [29]. The p85 regulatory subunits have an important role in the stabilization of the catalytic subunit, inhibition of basal lipid kinase activity and activation of downstream RTKs. All five p85 family proteins contain two Src homology domains (nSH2 and cSH2) separated by a coiled-coil inter-SH2 domain (iSH2) (Figure 4) [26]. The p85 α and p85 β isoforms additionally have an amino-terminal SH3 and breakpoint cluster homology (BH) domains [26], [34].

1.3.1. PI3K signalling in human cancer

One of the most common events in human cancer is the activation of the PI3K/AKT/mTOR signalling pathway, generally described as a consequence of genetic alterations of pathway members, such as point mutations of PI3K genes or inactivation of PTEN, having a critical role in driving tumour initiation and progression [26], [41]. The PI3K catalytic subunit is one of the most highly mutated/amplified in several cancer types and that has prompted the advancement of inhibitors of several segments of this pathway, including the PI3K, AKT and mTOR kinases, and rapamycin analogues that hinder mTORC1 [26], [38], [40]. PI3K is allosterically activated by RAS, and many tyrosine kinases that activate PI3Ks are themselves the target of mutations or amplification in cancer [31], [33].

Cancer cells frequently contain elevated amounts of PIP3 due to increased activity of oncogenic signalling proteins residing upstream of PI3K. PIK3CA and PTEN were found to be respectively, the second and third most highly mutated genes in human cancers [30]. Activation of class I PI3Ks occurs through multiple upstream pathways that couple a broad range of cell surface receptors to specific PI3K isoforms [30]. This activation converts PIP2 in PIP3 that directly binds to the pleckstrin homology (PH) domain of AKT to cause the activation of serine-threonine kinase AKT, which then moves from the cytoplasm to the cell membrane [42]. AKT activation regulates GSK3 (glycogen synthesis kinase 3) and blocks FOXO mediated transcription of CDK inhibitor, p27 which in turn promotes cell cycle progression. AKT also promotes cell growth through phosphorylation of mTOR1 which leads to protein translation, in addition to up-regulation of hypoxia-inducible factor 1a (HIF-1a) that promotes angiogenesis through transcribing VEGF. Insulin receptor substrate (IRS) and PI3K are negatively regulated via phosphorylation of S6K, leading to a feedback loop. Thus, inhibition of mTORC1 can activate upstream proteins like PI3K and Akt [43].

The PI3K/AKT pathway is a key link that synergizes many of the targets involved in incorporating the modulation of apoptosis, cell growth, and cellular metabolism that are associated with the mechanism of multiple drug resistance (MDR) in a variety of cancers [42]. The MDR phenotype often accompanies activation of the PI3K/AKT pathway, which renders a survival signal to withstand cytotoxic anticancer drugs and enhances cancer stem cell (CSC) characteristics. Activated AKT directly activates mTORC1 via the phosphorylation of mTOR. The phosphorylation of tuberous sclerosis complex 2 (TSC2) by AKT reduces TSC1 and TSC2, which activates mTORC1. When TSC2 was inactivated by AKT, Rheb-GTP stimulated mTORC1 activity and subsequently phosphorylated eukaryotic translation initiation factor

4E-binding protein 1 (4EBP1), which leads to angiogenesis or cell cycle progression [41]. However, activation of the PI3K/AKT pathway alone is not responsible for MDR in many cases, and synergistic transduction with up or downstream targets is required [42]. The PI3K/AKT/mTOR pathway is also affected by miRNAs that act as negative transcriptional regulators of target genes with different potential roles in tumorigenesis and behaviour. These generally cause mutations in PIK3CA, PTEN and AKT, and eventually lead to MDR [26], [41].

All these mechanisms highlight how understanding PI3K-dependent and AKT-independent signalling mechanisms, that drive cancer progression, are crucial for the development of novel and more effective approaches for targeting the PI3K pathway for therapeutic benefit in cancer [41].

1.3.2. Different classes of PI3K inhibitors

PI3K has become an important anticancer drug target, and there is a very high interest in the pharmaceutical development of PI3K inhibitors. Numerous of these inhibitors have exhibited good results in solid tumours in preclinical studies [29]. The inhibitors of this pathway are therefore considered a fruitful strategy to combat cancer, being mainly divided according to selectivity into three generic classes: pan-PI3K inhibitors, selective isoform PI3K inhibitors and dual PI3K/mTOR inhibitors (Figure 5) [26], [44], [45].

Pan-PI3K inhibitors are ATP-competitive inhibitors that target all four isoforms of class I PI3Ks. This leads to many unfavourable side effects as a result of the unselective blockage of PI3K. These inhibitors are used in cases of PTEN inactivation or aberrant upstream PI3K signalling due to their effective blockage of the PI3K pathway [26]. Some Pan-PI3K inhibitors (Figure 6) include pictilisib, which demonstrated a favourable safety profile with advanced solid tumour or non-squamous nonsmall cell lung cancer (NSCLC) in a phase I clinical trial and completed phase II clinical studies in patients with breast cancer; buparlisib, which completed phase III clinical trials for patients with advanced-stage breast cancer; and copanlisib, already approved for the treatment of relapsed follicular lymphoma [26], [32], [44].

The development of specific PI3K isoform inhibitors is currently designed to achieve the same goal as pan-PI3K inhibitors but without the adverse effects. This may offer a therapeutic benefit in a broad range of clinical settings not only for cancer but also inflammatory and immunological diseases [46], [47]. Their therapeutic window is however restricted due to the selectivity towards mutant isoforms. Selective inhibitors are considered a new strategy to combat certain types of cancer depending on which isoform

is amplified or mutated in this type of cancer. They can be classified accordingly to the class I PI3K isoform they inhibit and will be further presented and discussed [26].

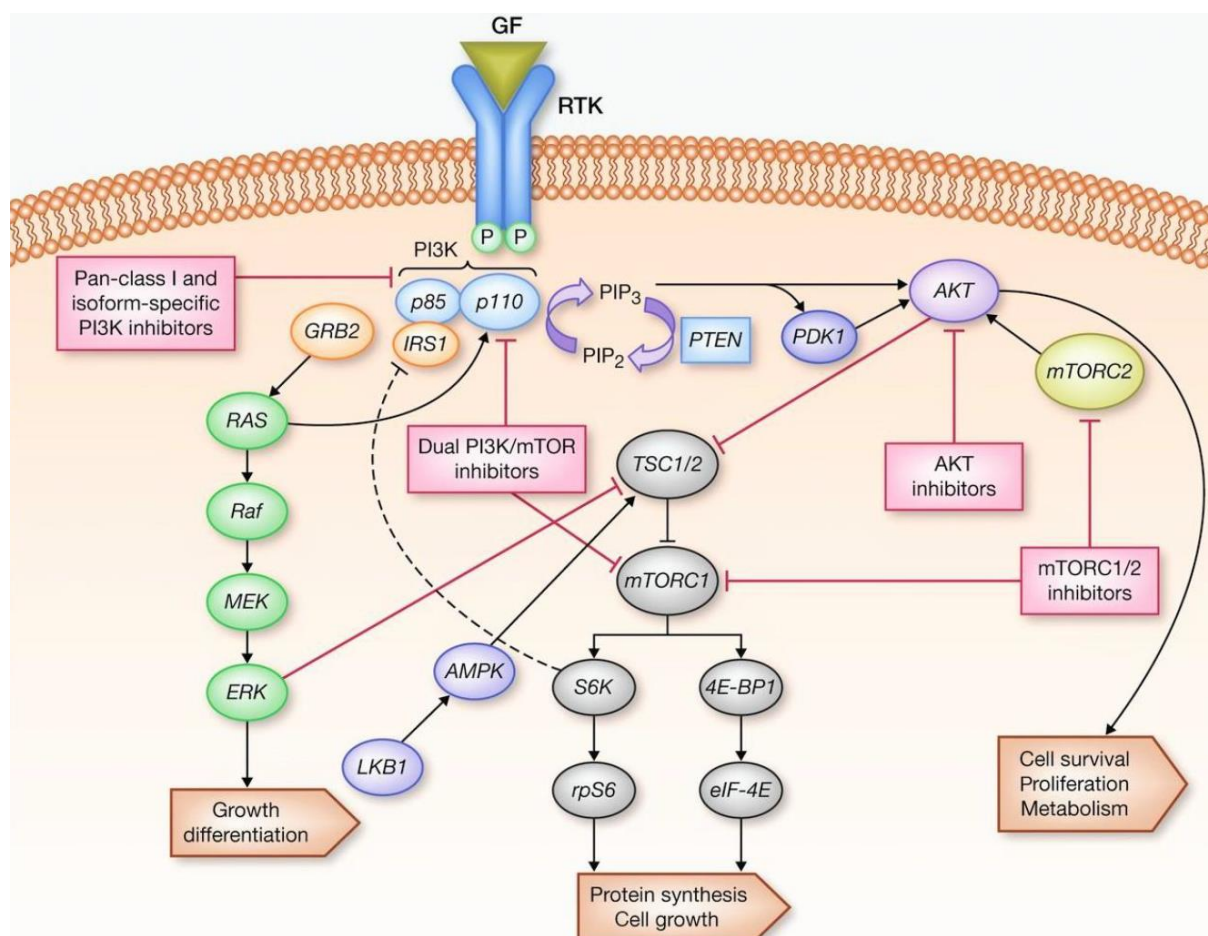


Figure 5 Overview of the PI3K/AKT/mTOR pathway, drug targets and classes of inhibitors. Activating nodes (PI3K, AKT, PDK1, mTORC1 and mTORC2) and negative regulators (PTEN, TSC complex) are highlighted. Interaction with RAS and LKB1/AMPK pathways is also displayed [45].

Sometimes researchers seek to design dual PI3K/mTOR inhibitors as they gather the advantage of having better efficacy and overcoming the resistance problem [27]. Some PI3K inhibitors show mTOR inhibitory activity due to their binding to the catalytic domain of mTOR, which shares a high degree of similarity with the p110 catalytic subunit of the class I PI3Ks. However, despite the advantages of dual inhibitors, designing selective PI3K inhibitors also avoid toxicity that may arise from mTOR kinase inhibitory activity, making that strategy a more appealing one [32]. Among PI3K/mTOR dual inhibitors, there are a few agents in clinical trials such as gedatolisib, with ongoing phase I/II clinical studies in patients with advanced-stage NSCLC or breast cancer; and LY3023414, with ongoing phase II clinical studies for a diversity of cancers (Figure 6) [26], [27], [32].

Besides the above-mentioned inhibitors, PI3K/AKT/mTOR signalling pathway inhibitors also include AKT and mTOR inhibitors (Figures 5 and 6). Malignancies bearing AKT mutations or gene amplifications are the logical targets for the development of AKT directed compounds. Nevertheless, it has been noted that AKT inhibition can lead to the activation of other PI3K molecules [32]. In addition, the minimal activity of AKT inhibitors has been shown in tumours with PIK3CA mutations. MK-2206 is a popular and potent oral allosteric inhibitor of all AKT isoforms with antitumor activity in preclinical models [26], [32], [48].

Additionally, there are two types of mTOR inhibitors, those that inhibit the activity of mTORC1, and ATP-competitive mTOR inhibitors that affect the activity of both mTORC1 and mTORC2 [36]. The two rapamycin analogues currently used are everolimus, which is licensed for breast, renal and pancreatic neuroendocrine tumours, and temsirolimus, which is licensed for high-risk renal carcinoma and mantle cell lymphoma [32], [36], [48]. Nevertheless, AKT and mTOR inhibitors still show limited clinical efficacy. That is why the recent knowledge regarding the divergent roles of PI3K isoforms in different types of cancer, isoform-selective PI3K inhibitors remain the most attractive for precise cancer therapy [48], [49].

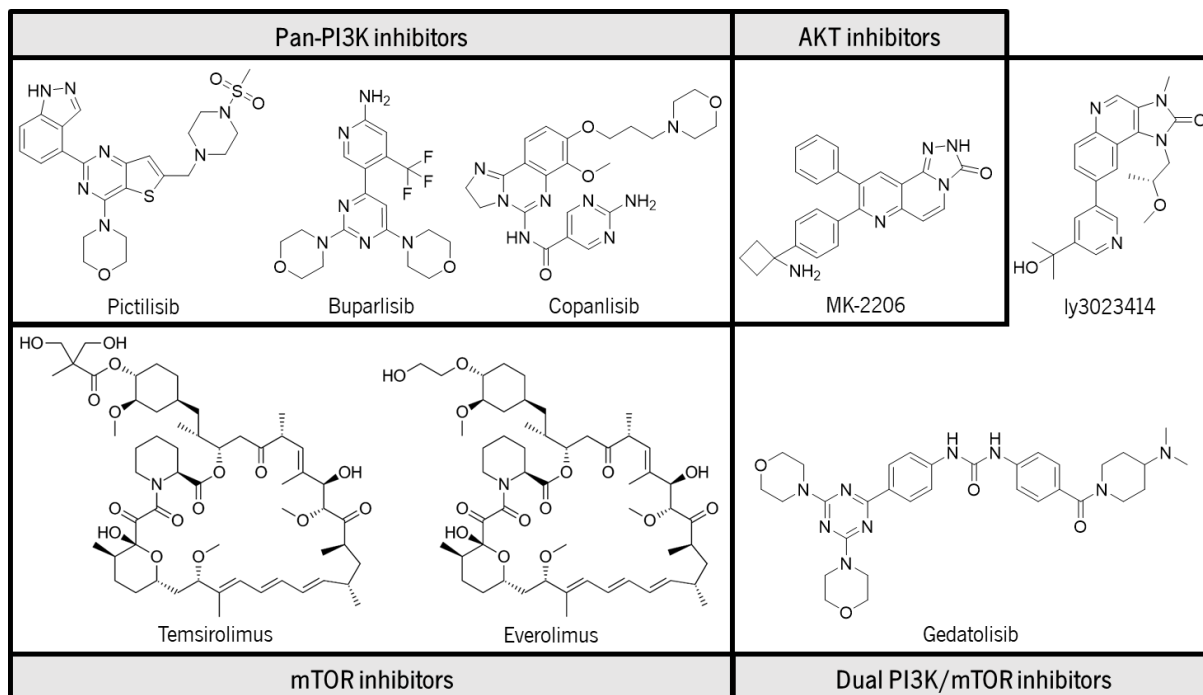


Figure 6 Examples of chemical structures of 4 different classes of inhibitors: Pan-PI3K inhibitors; Dual PI3K/mTOR inhibitors; AKT inhibitors and mTOR inhibitors.

1.3.3. Selective targeting of class I PI3K isoforms

The effort to develop isoform-specific PI3K inhibitors, together with novel therapeutic strategies aims for a more favourable safety inhibitory profile by reducing the toxicity and side-effects of current inhibitors [27], [44]. Thus, an understanding of the molecular details of these four regulatory subunits can shed light on targeted therapy [34].

Figure 7 shows the sequence alignment of residues for the 4 class I PI3K isoforms. Given the high degree of similarity that exists between the amino acid sequence forming the ATP-binding pockets of the four class I PI3Ks, it was expected that isoform-selective PI3K inhibitors would be difficult to obtain [37], [50]. Class I PI3Ks ATP binding sites are highly homologous, differing only in a few residues, which are divided into two regions [50]. Non-conserved residues in the two regions are highlighted in red in Figure 7 and can confer selectivity due to the chemical and conformational differences of these regions among the four isoforms. Of all these, the residues detached within rectangles are the ones reported to be the most common residues that interact with selective inhibitors. Thus, they can define specific interactions, allowing inhibitor specificity [50]. Although the divergent roles of each isoform in different signalling contexts, tissues and types of diseases have been extensively studied, continuous efforts are needed to explore the precise functions among PI3K isoforms to implement precise targeting [49].

	772	774	778	780	800	802	836	848	850	851	852	853	854	855	859	922	930	932	933
PI3Kα	M	S	P	W	I	K	Y	I	V	V	R	N	S	H	Q	M	F	I	D
PI3Kβ	M	S	P	W	I	K	Y	I	V	V	S	T	S	E	D	M	F	I	D
PI3Kγ	M	S	P	W	I	K	Y	I	V	V	K	D	A	T	K	M	F	I	D
PI3Kδ	M	S	P	W	I	K	Y	I	V	V	L	R	S	D	N	M	F	I	D

Figure 7 Binding pocket insights into PI3K isoforms. Sequence alignment indicates the conserved and variable residues in each PI3K isoform [50].

The **PI3K α** and **β** isoforms are broadly expressed and regulate a wide range of physiological processes, including cell growth, proliferation, differentiation, motility, survival, and intracellular trafficking [28], [51]. The **PI3K α** isoform is the predominant catalytic isoform involved in glucose homeostasis regulation and vasculogenesis [37]. On the other hand, the **PI3K β** isoform plays a secondary role in insulin signalling. It can also activate platelets, leading to the development of thrombotic diseases [51].

The γ and δ isoforms are especially expressed in leukocytes and control different aspects of immune responses. The effects of PI3K inhibition on different lymphocyte subsets are normally involved in the development of autoimmune toxic effects [37]. Because of their immunomodulatory role, recent preclinical studies supported the combination of some **PI3K δ** isoform inhibitors with immune checkpoint blockers [34]. Moreover, **PI3K γ** is involved in blood pressure homeostasis by regulating particularly myogenic tone [37]. It also plays an important role in inflammation, tumour immune environment, and cardiovascular disease [34]. Loss-of-function and gain-of-function mutations in the **PI3K δ** isoform have revealed that this enzyme can substantially impact immune responses to infectious agents and their products [52]. Multiple PI3K inhibitors have entered the clinic targeting a variety of blood cancers, with numerous clinical trials also ongoing for solid tumours [34].

According to their preferential distribution and activity, in addition to shared adverse effects, inhibition of the **PI3K α** isoform may be associated with hyperglycemia; inhibition of **PI3K β** isoform, with anaemia; inhibition of **PI3K γ** , with hypertension; and blockade of **PI3K δ** , with immunomodulation, leading to skin eruption, liver dysfunction, pneumonitis, pyrexia, and hematologic toxic effects [28].

Dual PI3K isoform inhibitors have a broader effect than inhibition of either single isoform alone. However, the challenge, in this case, is the difficulty of controlling the balance activity between the two isoforms, still taking into consideration all the other requirements for being a drug. Any undesired inhibition of either isoform causes mechanism-based side effects, which will be a potential issue [26], [49]. Figure 8 shows the chemical structures of known dual and triple PI3K isoform inhibitors. Duvelisib, also known as IPI-145, is the most important dual PI3K γ/δ inhibitor. The FDA approved drug is currently being used in the treatment of patients with relapsed/refractory chronic lymphocytic leukaemia/small lymphocytic lymphoma (CLL/SLL) or relapsed/refractory follicular lymphoma (FL). Tenzalisib is a member of the next generation, oral, selective, PI3K γ/δ inhibitor for PI3K γ and PI3K δ , respectively. It has an apoptotic and anti-proliferative activity as well as modulating the tumour microenvironment resulting in a significant reduction of angiogenesis in preclinical models [26].

Other dual or triple isoform-selective inhibitors, represented in figure 8, have also been discovered for cancer treatment such as BAY80-6946 (PI3K α /PI3K δ), AZD8186 (PI3K β /PI3K δ) and GDC0032 (PI3K α /PI3K γ /PI3K δ). Their divergent selectivity profiles fit well with the complexity of human tumours, and this advantage provides an optimal therapeutic strategy for precise therapy [36], [49].

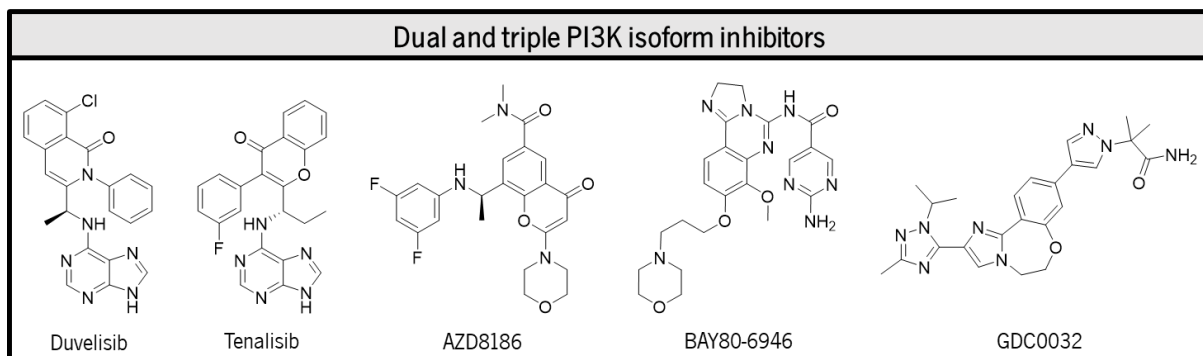


Figure 9 Chemical structure of known dual PI3K γ/δ , α/δ , β/δ isoform inhibitors: duvelisib, tenalisisb, AZD8186 and BAY80-6946; and the triple PI3K $\alpha/\gamma/\delta$, isoform inhibitor GDC0032.

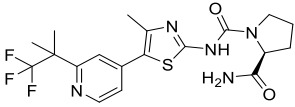
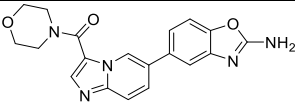
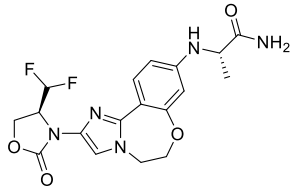
1.3.3.1. PI3K α selective inhibitors

Activating mutations in p110 α are frequent in malignant tumours, with the gene encoding p110 α , PIK3CA, being the 2nd most frequent oncogene in human cancer [34]. This oncogene encodes the respective mutated kinase at a cumulative frequency of 15% across all cancer types making it one of the most commonly mutated kinases in the human genome [37]. Gene PIK3CA mutations occur in all domains of p110 α specifically the helical and kinase domains. Kinase mutations increase the interaction between p110 α with membranes [36]. The importance and high frequency of PIK3CA mutation in solid tumours have attracted attention towards the development of PI3K α -selective inhibitors [34].

PI3K p110 α specific inhibitors are effective in PIK3CA mutations. One of these specific inhibitors is BYL719, also known as Alpelisib (Table 1), which is a promising FDA approved inhibitor that possesses optimal PI3K α selectivity, potency and pharmacokinetic properties [36]. The PI3K α inhibitor treatment results in G1 phase arrest without killing cells in vitro, which is consistent with the lack of tumour regression in clinical trials. Sporadic studies have indicated the induction of apoptosis by BYL719, but this effect appears to be dependent on cell types. Recent preclinical studies have found that the growth of HER2- or KRAS-driven solid tumours highly relies on PI3K α , and the inhibition of this isoform is sufficient to halt tumour growth to an extent similar to that of blocking all class I isoforms, underscoring PI3K α as a promising target in these types of tumours [37]. Moreover, PI3K α is important for angiogenesis in solid tumours, which may suffer from a deficient blood supply upon inhibition of this isoform. The function of PI3K α in cell metabolism regulation has been also observed to promote cancer cell survival. In addition, decreased glucose consumption is considered a positive sign in predicting the antitumor effect of these inhibitors [49].

There are a few other examples of selective PI3K α inhibitors undergoing clinical trials for a diversity of cancers, such as TAK-117, also known as serabelisib, INK-117 or MLN-117 and GDC-0077, also known as inavolisib. These inhibitors are represented in Table 1 as well as their current stages of development.

Table 1 Examples of selective isoform PI3K α inhibitors that are approved for clinical use or are under clinical development.

Drug structure & name	Stage of clinical development
 <p>Alpelisib, BYL719</p>	<p>Approved by the FDA for PIK3CA-mutated, HR+, HER2-advanced breast cancer and ongoing clinical trials as monotherapy for head and neck squamous cell carcinoma [49], [53].</p>
 <p>TAK-117, serabelisib, INK-117 or MLN-117</p>	<p>Undergoing a phase II combinatory study with an oral mTOR inhibitor in triple-negative breast cancer. Another phase II combinatory study also evaluated the efficacy and safety of this drug in the treatment of metastatic clear-cell renal cell carcinoma patients [53].</p>
 <p>GDC-0077 or inavolisib</p>	<p>Currently undergoing several clinical trials singly and in combination with other drugs for the treatment of breast cancer [50].</p>

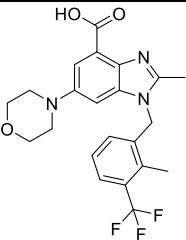
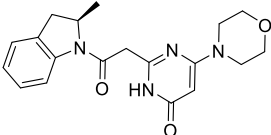
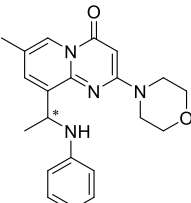
1.3.3.2. PI3K β selective inhibitors

PI3K β is another ubiquitously expressed class I PI3K. The knockout of PIK3CB avoids tumour formation in PTEN-null prostate cancer mouse models. PTEN loss or mutation is detected in a considerable fraction of tumours (20-75%), including gliomas, breast, colon, lung, endometrial and prostate cancers [36], [49]. Hence, PI3K β has been recognized as a therapeutic target in this subset of solid tumours [26].

TGX221 (Table 2), a PI3K β -selective inhibitor has been used as a template for further optimization. It was the first PI3K β inhibitor with selectivity towards this isoform. TGX-221 exists as 2 enantiomers, being the (R)-enantiomer much more potent against the p110 β -isoform [26]. The TGX221 analogue SAR260301 (Table 2) has been developed for the treatment of solid tumours. PI3K β inhibitors have been shown to selectively inhibit the growth of tumour cells deficient in PTEN, which prompted a new clinical trial to investigate the efficacy of the PI3K β -selective inhibitor GSK2636771 (Table 2) in patients with PTEN-null advanced solid tumours [49]. However, targeting PI3K β in PTEN-deficient tumours may be compromised by tumour heterogeneity, coexisting genetic alterations and micro-

environmental factors. Moreover, the prolonged treatment of PTEN-deficient tumour cells with a PI3K β inhibitor may also shift isoform dependency from PI3K β to PI3K α [49]. GSK2636771 is a p110 β selective inhibitor studied in PTEN-deficient tumours. It is considered to help avoid several toxicities found in other treatments. This specific p110 inhibition is also being studied in combination with androgen receptor antagonists for the treatment of prostate cancer [36].

Table 2 Examples of selective isoform PI3K β inhibitors that are approved for clinical use or are under clinical development.

Drug structure & name	Stage of clinical development
 <p>GSK2636771</p>	<p>Undergoing phase I combinatory study with Enzalutamide in male patients with CRPC. In another phase Ib/IIa, a dose-finding study is evaluating the safety, efficacy and clinical activity of GSK2636771 with Paclitaxel in patients with a higher grade of gastric adenocarcinoma. NCI is also currently testing GSK2636771 in cancer patients with a PTEN alteration [53].</p>
 <p>SAR260301</p>	<p>Phase I study completed demonstrated acceptable safety in patients with advanced solid tumours; no further development due to the rapid clearance of the compound, which did not allow a sustained pathway inhibition [32], [54].</p>
 <p>TGX-221</p>	<p>Undergoing phase II clinical trials for the treatment of recurrent or persistent endometrial cancer [53].</p>

1.3.3.3. PI3K γ selective inhibitors

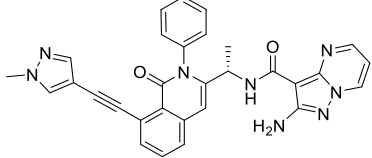
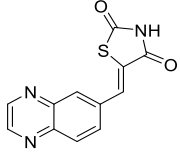
Unlike the ubiquitously expressed PI3K α and PI3K β , PI3K γ is preferentially expressed in the hematopoietic system, specifically in leukocytes. It is a key regulator in cellular migration, thus, a variety of diseases related to an influx of inflammatory effector cells inhibitor could be treated by inhibiting this PI3K isoform, including inflammation, respiratory and metabolic disorders, and cancer [26].

Moreover, PI3K γ plays an important and well-established role in regulating the differentiation and activation of myeloid-lineage immune cells, such as myeloid-derived suppressor cells (MDSCs) and macrophages [36]. In the treatment of solid tumours, functional inhibition of PI3K γ in the tumour microenvironment (TME) may likewise have the potential to safely modulate the efficacy of immune-activating agents and influence disease progression. A high degree of tumour infiltration by MDSCs has

been correlated with immune evasion and poor prognosis in human cancers and serves as a negative predictive marker for single-agent immunotherapy regimens [36]. Consequently, PI3K γ is an attractive and promising target for combination therapies to reverse immune evasion associated with chronic inflammation of the TME [55]. In addition, it was recently found that in pancreatic ductal adenocarcinoma, KRASG12R is impaired in driving macropinocytosis because of the activation of a key effector, p110 α . However, overexpression of PI3K γ in this cancer compensates for this deficiency, providing one basis for the prevalence of this otherwise rare KRAS mutant in pancreatic but not other cancers [56].

In this regard, the restricted expression pattern of PI3K γ can alleviate the risk of undesirable side effects when inhibiting PI3K γ , which has motivated the development of PI3K γ -specific inhibitors. With the validation of PI3K γ as a promising drug target for the treatment of inflammatory disease and, possibly, leukaemia and pancreatic ductal adenocarcinoma, some PI3K γ -selective inhibitors have been discovered, but only a few of them have advanced to clinical trials [26], [49], [57]. Examples include eganelisib, also known as IPI-549, and AS605240 (Table 3).

Table 3 Examples of selective isoform PI3K γ inhibitors that are approved for clinical use or are under clinical development.

Drug structure	Stage of clinical development
 <p>IPI-549 or eganelisib</p>	<p>A phase I study is evaluating the safety, efficacy, PK and PD of eganelisib in combination with a selective dual adenosine receptor, A2aR/A2bR antagonist, plus pegylated liposomal doxorubicin (PLD) in patients with triple-negative breast cancer or gynaecological tumours [53].</p>
 <p>AS605240</p>	<p>Undergoing a phase I combinatory treatment with paclitaxel that may improve the outcome of claudin-low breast cancer by standard chemotherapy, especially for the patients who cannot tolerate the full dose of paclitaxel [58].</p>

1.3.3.4. PI3K δ selective inhibitors

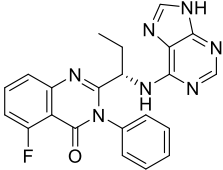
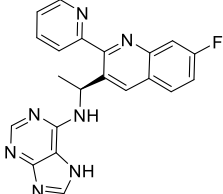
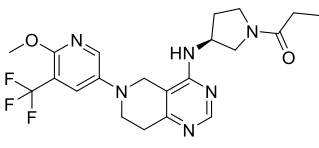
PI3K δ is the primary PI3K isoform in leukocytes that mediates signals from RTKs and immunoreceptor tyrosine-based activation motif (ITAM)-containing proteins because of its high enrichment in these cells. Pharmacological inactivation of PI3K δ reveals its importance for the function of T cells, B cells, mast cells and neutrophils. Hyper-activated PI3K signalling is a common event in leukaemia specimens and cultured cells [36]. Hence, targeting PI3K δ may be beneficial both for autoimmune diseases and cancer.

Although oncogenic mutations or overexpression of PIK3CD have not been found in chronic lymphocytic leukaemia (CLL) tumour cells in primary patient samples, increased PI3K activity has been observed, which is highly dependent on the PI3K δ isoform. PI3K δ inhibitors attenuate survival signals by blocking constitutive PI3K signalling including phosphorylation of AKT and ERK1/2. High concentrations and long-term treatment are required for PI3K δ inhibitors to induce apoptosis *in vitro*, suggesting that the induction of apoptosis is unlikely the direct mechanism to exert anti-cancer activity [52]. Thus, PI3K δ inhibitors may display dual mechanisms to directly decrease tumour cell survival and to reduce survival signals in the microenvironment [49].

Loss-of-function and gain-of-function mutations in the PI3K δ isoform have revealed that this enzyme can substantially impact immune responses to infectious agents and their products. Moreover, studies indicate that inhibition of the PI3K pathway could potentially be effective in limiting the growth of certain microbes via modulation of the immune system [52].

Idelalisib, also known as CAL-101 (Table 4), was the first orally potent and selective PI3K δ inhibitor. It represented the pioneer structure for other selective PI3K δ inhibitors, just as AMG319 and leniolisib (Table 4) [26].

Table 4 Examples of selective isoform PI3K γ inhibitors that are approved for clinical use or are under clinical development.

Drug structure & name	Stage of clinical development
 <p data-bbox="279 1422 502 1451">Idelalisib or CAL-101</p>	<p data-bbox="619 1265 1374 1435">Approved by FDA for patients with relapsed chronic lymphocytic leukaemia and indolent lymphoma [49]. Tested in a phase Ib study trial with BCL201 (selective BH3-mimetic inhibitor of BCL-2) in patients with follicular lymphoma and mantle cell lymphoma and undergoing combinatory studies with other drugs [53].</p>
 <p data-bbox="279 1664 502 1693">AMG319</p>	<p data-bbox="619 1512 1374 1646">Tested in patients with R/R lymphoid malignancies to evaluate its tolerability, safety and pharmacokinetic profile [53]. Currently undergoing a phase II study in patients with head and neck squamous cell carcinoma [32].</p>
 <p data-bbox="231 1854 550 1883">Leniolisib</p>	<p data-bbox="619 1713 1374 1877">Tested in phase II/III trials for senescent T cells lymphadenopathy and immunodeficiency (APDS/PASLI) derived from activated PI3K syndrome/ p110-activating mutation [53]. Also tested in patients with primary Sjögren's syndrome (PSS) in phase II trials [53].</p>

1.4. Computational Chemistry in drug development

For many years, both the identification and optimization of novel drug lead compounds were accomplished within the drug discovery process by the experimental high-throughput screening of large chemical libraries, turning the drug discovery into a costly and time-consuming technique. However, for the last 25 years, theoretical developments, enhanced computational algorithms, faster computing resources, and improved visualization tools enabled the use of computational methods to model and visualize protein-ligand (PL) interactions, to calculate binding free energy ($\Delta G_{\text{binding}}$) at different degrees of accuracy, and to screen, *in silico*, chemical libraries using ligand and structure-based approaches [59].

Today, computational chemistry is well established as a valuable tool in any drug lead discovery work, aimed at saving time, effort, resources, and reducing costs [59]. The central quantity in PL association is the binding free energy, a property of enormous relevance in the pharmaceutical industry, and no effort is too great to accurately estimate it in a computationally efficient way, which depends on several factors, such as the energy model of the system; the accounting for protein flexibility; the presence of water molecules within the binding site and the solvation model [60].

A fundamental hypothesis in classical drug design is that the successful action of a drug in the human body depends on the molecular interactions between the ligand and the active site of a target macromolecule. The strength of this interaction is influenced by the spatial arrangement of the ligand atoms and its atomic interactions with the biological residues [61]. Thus, docking plays an important role in predicting the orientation of the ligand when it is bound to a protein receptor or enzyme using shape and electrostatic interactions to quantify it. The AutoDock energy function (Equation 1) is a weighted sum of terms representing van der Waals (vdW), hydrogen bond (hbond), electrostatic (elec), torsions (tor) and desolvation contributions (sol), which are calculated between pairs of atoms (i,j). The sum of all these interactions is approximated by a docking score, which represents the binding energy (ΔG) [62], [63].

$$\Delta G = \Delta G_{vdW} \sum_{i,j} \left(\frac{A_{i,j}}{r_{i,j}^{12}} - \frac{B_{i,j}}{r_{i,j}^6} \right) + \Delta G_{hbond} \sum_{i,j} E(t) \left(\frac{C_{i,j}}{r_{i,j}^{12}} - \frac{D_{i,j}}{r_{i,j}^6} + E_{hbond} \right) + \Delta G_{elec} \sum_{i,j} \left(\frac{q_i q_j}{\epsilon r_{i,j} \cdot r_{i,j}} \right) + \Delta G_{tor} N_{tor} + \Delta G_{sol} \sum_{i,j} (S_i V_j + S_j V_i) e^{\left(\frac{-r_{i,j}^2}{2\sigma^2} \right)}$$

Equation 1

Broadly, generating a receptor-ligand structure *in silico* involves two main components: docking and scoring. Docking requires the prediction of the preferred orientation of the ligand to the receptor upon

binding. Scoring, on the other hand, details the atomic interactions between protein and ligand [64]. This usually means force field-based molecular mechanical level treatment with some auxiliary scoring components to rank the generated poses. Scoring functions (SFs) can be divided into three categories: empirical, knowledge-based, and force-field-based. Among these, force field-based scoring uses energy functions as the main component [60]. However, this energy function is primarily based on force field and thus cannot take into account quantum effects [64]–[66]. It is generally agreed that common docking software can provide reasonably good accuracy for identifying the most important binding poses. Scoring on the other hand is still a major problem because the accurate ranking of binding affinities turns out to be a very difficult task for the commonly used “scoring functions”. Such scoring functions treat the interactions of ligands and proteins at a rather low theoretical level so that increasing the theoretical and computational effort seems to be a promising way to improve on the scoring problem [66].

High throughput docking of small molecule ligands into high-resolution protein structures has become a standard component of computational approaches in drug discovery. In typical pharmaceutical applications, the receptor structure is kept fixed, while the optimal location and conformation of the ligand (which is allowed to remain flexible) are sought using a variety of sampling algorithms. Examples are fast shape matching, genetic algorithms, simulated annealing, and Monte Carlo simulations [64].

Several software packages, including FlexX, DOCK, GOLD, GLIDE and AutoDock, are now widely used in the pharmaceutical industry and are capable of screening libraries of ligands consisting of millions of compounds [67]. Although strategies in the ligand placement differ one from another, these programs are broadly categorized as ranging from incremental construction approaches, such as FlexX to shape-based algorithms, genetic algorithms (GOLD), systematic search techniques (Glide, Schrödinger, Portland, OR 97201), and Monte Carlo simulations (LigandFit) [60]. Among these programs, AutoDock Vina, GOLD, and MOE-Dock predicted top-ranking poses with the best scores. These docking programs can predict experimental poses with root-mean-squared deviations (RMSDs) averaging from 1.5 to 2 Å. However, flexible receptor docking, especially backbone flexibility in receptors, still presents a major challenge for the available docking methods [68]. Nevertheless, the true potential of this technique is revealed when used in a high-throughput fashion to screen up to millions of molecules, aiming to generate a sub-library rich in potential binders, thus imposing a structural filter on a given chemical library to prioritize compounds for synthesis [60].

It should be highlighted that one of the main advantages of docking is that *in silico* generated poses usually serve as the starting point for *in silico* ligand optimization, using for example molecular

dynamics-based calculation of binding free energies, such as Molecular Mechanics-Poisson Boltzmann Surface Area (MM-PBSA) and MM-Generalized Born Surface Area (MMGBSA) methods [59]. In the last 10 years, there have been continuous efforts to enhance scoring functions by incorporating some type of quantum mechanical (QM) based calculations, especially deriving system-specific charges, such as the QM-polarized ligand docking approach [60], [69].

1.4.1. Quantum chemical approaches in protein-ligand binding energy

A challenge to virtual screening (VS) approaches is the development of a method that can not only accurately predict real binding affinities but is also fast enough to screen libraries of many thousands of molecules. A common approach is to first make use of fast but simplified SFs to obtain initial 'good' binders, followed by the use of more sophisticated methods than empirical force field approaches, such as free-energy perturbation, the linear-response approximation, and a combination of the molecular mechanical energies with the Poisson–Boltzmann continuum solvent approaches for estimation of binding affinities. However, these methods are still affected by deficient FF calculations [61].

For the past 20 years, a remarkable advance in theoretical and algorithmic developments was seen, for the calculation of binding affinities, ranging from fast estimates, to be used in high-throughput docking and scoring, to much slower, yet more accurate calculations using free energy perturbation or thermodynamic integration, via molecular dynamics simulations, well-suited to guide chemical synthesis for hit-to-lead optimization. Most docking developments have been mainly rooted in molecular mechanics (MM) force fields (FF) [61]. However, to better characterize protein-ligand interactions, at least in some cases, the use of a QM description would be necessary. The QM formulation is theoretically exact, as in principle, it accounts for all contributions to the energy (including terms or effects usually missing in FFs, such as electronic polarization, charge transfer, halogen bonding, and covalent-bond formation). Moreover, the QM framework is general across the chemical space so that all elements and interactions can be considered equally, thus avoiding MM parameterizations. The development of fast yet accurate docking scoring functions still constitutes an area of active research [59], [60].

Quantum chemistry (QC) and its latest applications of explicit quantum mechanics (QM) calculations to structure-based drug design in the context of lead identification and optimization is becoming more and more important in the study of PL interactions [60]. The last 10 years have seen a

remarkable interest in the development and application of QM-based methods in the field of drug discovery. This was triggered by the interest in modelling biomolecular systems more accurately, and allowed by the unprecedented growth of computational power [60]. Essentially, QM provides the conceptual framework for understanding chemistry and the theoretical foundation for computational methods that model the electronic structure of chemical compounds. These are divided into three types of approaches: *ab initio*, density functional theory (DFT) and semiempirical [70].

Firstly, QC *ab initio* methods provide a convergent path to the exact solution of the Schrödinger equation and can therefore give 'the right answer for the right reason', but they are costly and thus restricted to relatively small molecules [70]. On the other hand, density functional theory has become the workhorse of computational chemistry because of its favourable price/performance ratio, allowing for fairly accurate calculations on medium-size molecules, but there is no systematic path of improvement despite the first-principles character of DFT [70]. Finally, QC semiempirical methods are the simplest variant of electronic structure theory, involving integral approximations and parameterizations that limit their accuracy but make them very efficient so that large molecules can be modelled realistically. These methods start from an *ab initio* or first principles formalism and then introduce rather drastic assumptions to speed up the calculations by neglecting many of the less important terms in the underlying equations. To compensate for the errors caused by these approximations, empirical parameters are incorporated into the formalism and calibrated against reliable experimental or theoretical reference data [70].

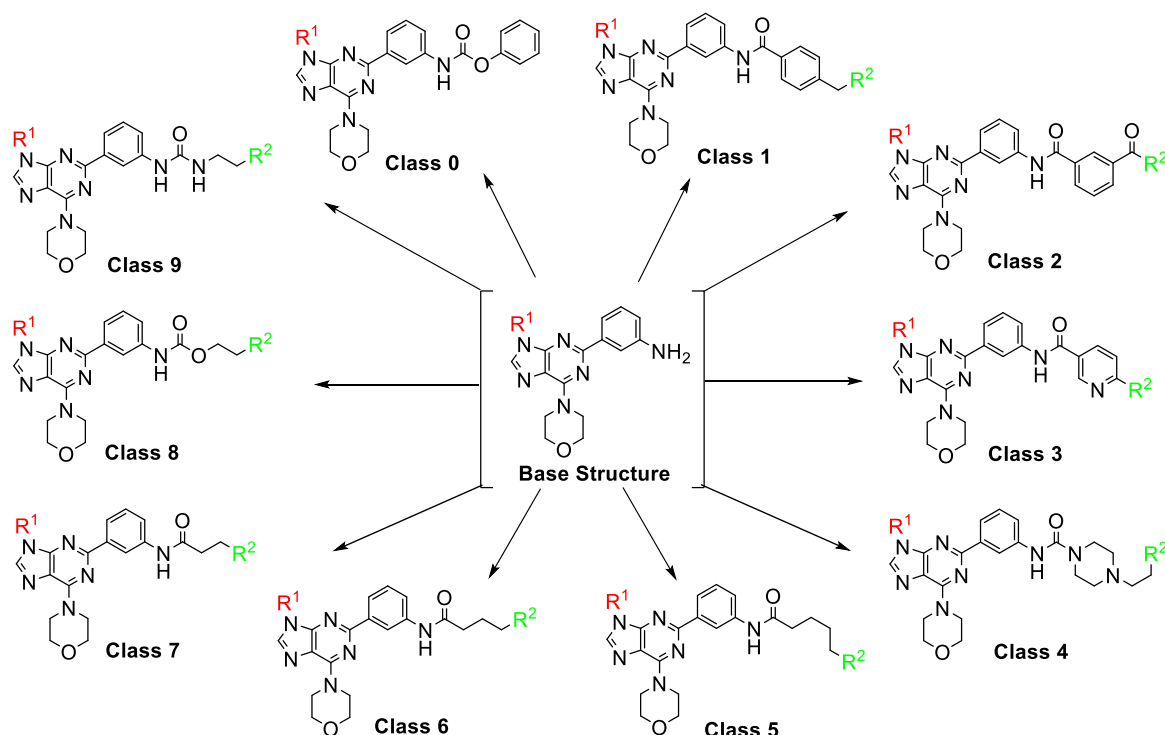
Hybrid quantum mechanical/molecular mechanical (QM/MM) methods have become a standard tool for the description of large molecular systems, in which QM level calculations are needed for parts of the system. A typical example would be an enzyme, as it is a large biomolecule where only a small region of it is involved in catalytic activities. All QM/MM methods are developed to treat quantum mechanically the part of the system that undergoes the most important electronic changes during a reaction or upon binding a substrate and the rest of the system by molecular mechanics. Various QC theories, such as Hartree–Fock, DFT or semiempirical methods, have been combined with force fields such as AMBER, CHARMM, GROMOS or OPLS to be used [64].

Overall, the results obtained using QM approaches are very encouraging, but still different sources of errors that should be addressed to improve the accuracy and predictability of these methods, as these remain system-dependent, needing further validation and benchmarking. Also, despite the progress in computational speed, there is a need for optimized codes, as most QM applications for drug discovery cannot still be used industrially [70]. Furthermore, conformational sampling and protein flexibility require

a lot of computing time, so that in most high-throughput approaches, only local energy minimization is performed, or even no minimization at all. Finally, solvation contribution, especially in charges systems and entropic considerations, is usually omitted in many of these types of calculations. Despite these limitations, it is clear that reliable QM methods for biomolecular systems would be a tremendous step forward toward predictive binding free energy calculations [60].

1.5. Objectives

Recently, in our research group, compounds with the base structure shown in scheme 1, were synthesized and tested *in vitro* against HCT116 cell line. Among all the tested compounds, some were identified as promising drugs due to their remarkable anticancer activity. In the literature, compounds with a similar structure to the ones synthesized and tested by our research group are reported to show biological activity in PI3K [26]. Considering the similarity of the structures published and the ones synthesized, we considered the hypothesis that our compounds could also be active in this type of receptors.



Scheme 1 Chemical structure of the 11 classes of compounds in study and the base structure they derive from.

This work aims, through computational chemistry and molecular modelling techniques, specifically molecular docking, to design and synthesize selective inhibitors for the class I isoforms of

PI3K, incorporating the identified base structure. Eleven classes of compounds were designed, where 9 of them intrinsically vary the substituent groups present at C₂ and N₉ positions of the molecule (R¹ and R²). A total of 661 compounds were designed, and affinity for the 4 isoforms of the target under study was evaluated through molecular docking assays. Some of the designed compounds were also synthesized to be subsequently *in vitro* tested in cancer cell lines and to assess a possible correlation between the docking affinity results of the different molecules studied and the results of their *in vitro* biological activity. A series of physicochemical properties for the designed inhibitors will be considered to relate molecular descriptors to the binding affinity and activity, giving, at last, an ideal pharmacophore for each PI3K isoform.

Chapter 2

Virtual Screening
RESULTS AND DISCUSSION

Introduction

In this chapter, the results of the virtual screening of 661 compounds designed are presented for the 4 class I PI3K isoforms.

In the first part of this chapter (**2.1.**), the biological targets under study are presented and discussed as well as their structural differences. Secondly, the ligands under study are presented (**2.2.**). These ligands are divided into 11 classes according to their chemical structures and physicochemical properties. Finally, the binding affinity results for the 4 isoforms of PI3K are presented (**2.3.**). Also in this subchapter, a correlation is attempted between the binding affinity results for each isoform and one or more physicochemical properties of the respective ligands.

2.1. Molecular targets

The difficulty in discovering selective inhibitors for the PI3K class I isoforms essentially resides in the structural similarities between these 4 isoforms. As mentioned in the introductory chapter (**1.3.3.**), there is a high degree of similarity between the amino acid sequences representing the active ATP binding site of these isoforms. Despite this factor, there are a few variations in a fragment of the amino acidic sequence, representing a segment of the active centre. Despite being a highly difficult process, through these variations it becomes possible to develop selective inhibitors between the 4 isoforms.

The Protein Data Bank (PDB) database was accessed from which 8 proteins were chosen, 2 for each isoform (Table 1 from Appendix). The choices of the receptors were based globally by their resolution, year of publication and publisher, and expression organism. Considering the size of the ligands designed in **2.2.**, one additional criterion had to be considered when choosing the receptors (Table 1 in the appendix). Given the limiting characteristic of docking, in which the receptor is taken as a rigid structure, it is important that the cavity containing the active site has a conformation with dimensions able to accommodate the designed ligands, thus cavities containing similar molecules in size/volume were considered.

After targets selection, an alignment of the structures was performed, which confirmed the conservation of the active site in all 4 PI3K isoforms. Figure 10 shows the alignment of the tertiary structures of the 4 chosen receptors, presented in different colours. In it, it is possible to observe an optimal overlap of the different secondary structures. Similarly, the ligands of the crystallographic

structures appear in the same spatial position, also overlaid, which confirms the high conservation of the active centre for all 4 receptors.

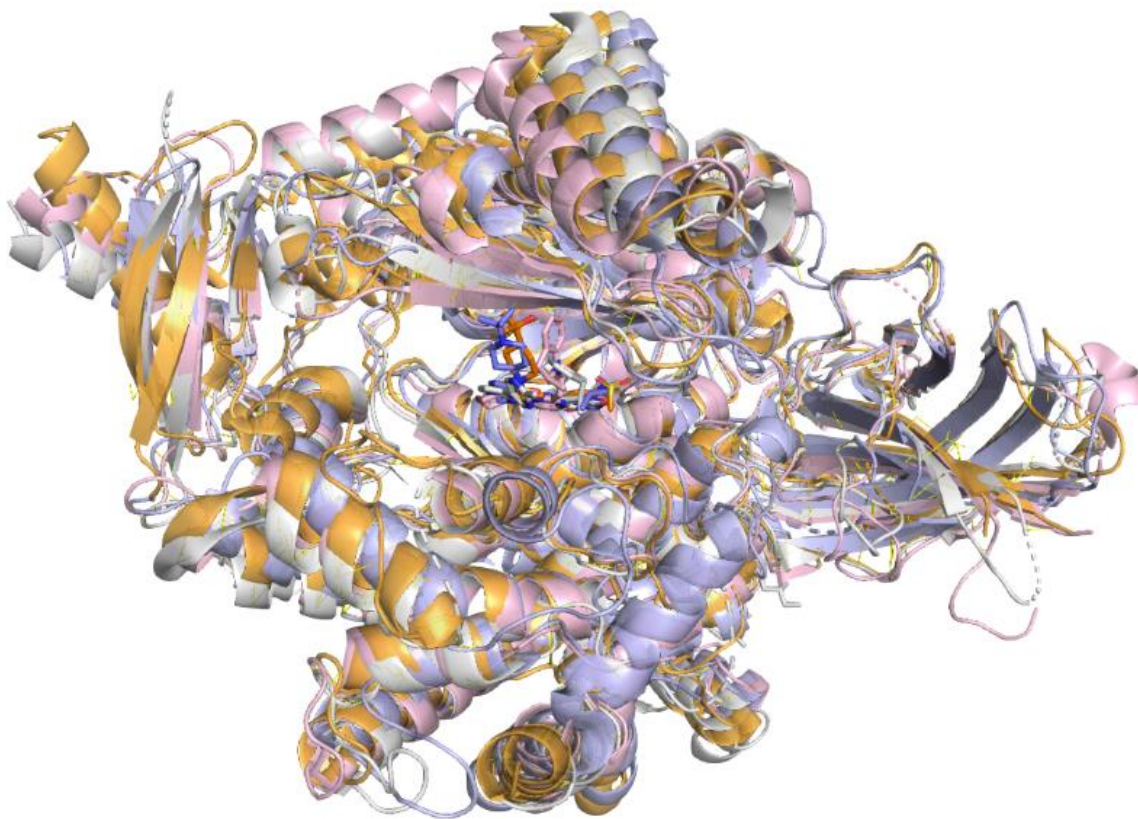


Figure 10 Alignment of the tertiary structures of PI3K α (grey), PI3K β (pink), PI3K γ (blue) and PI3K δ (orange) together with their respective ligands. Image generated in PyMOL.

Due to the presence of some gaps in X-ray structure determination, the SWISS-MODEL homology-modelling server was used to predict the complete tertiary structure of the 4 targets and to fulfil these existing gaps (represented by dashes in Figure 10), making them suitable receptors for virtual screening as considering all amino acid residues.

The following 4 figures provide particular details concerning the active centre of each isoform and its interaction pattern with their original ligands (Figures 11-14). In all cases presented, a common pattern is observed in the interaction of the ligands with a Valine residue. Another observed pattern is the interaction with a Lysine residue that is 49 amino acids away from the Valine residue already mentioned in the *alpha*, *gamma* and *delta* isoforms (Figures 11, 13 and 14). Additionally, particularizing, an interaction with an aspartate residue in PI3K β (Figure 12); a lysine residue in PI3K γ (Figure 13) and a serine residue in PI3K δ (Figure 14) can be seen.

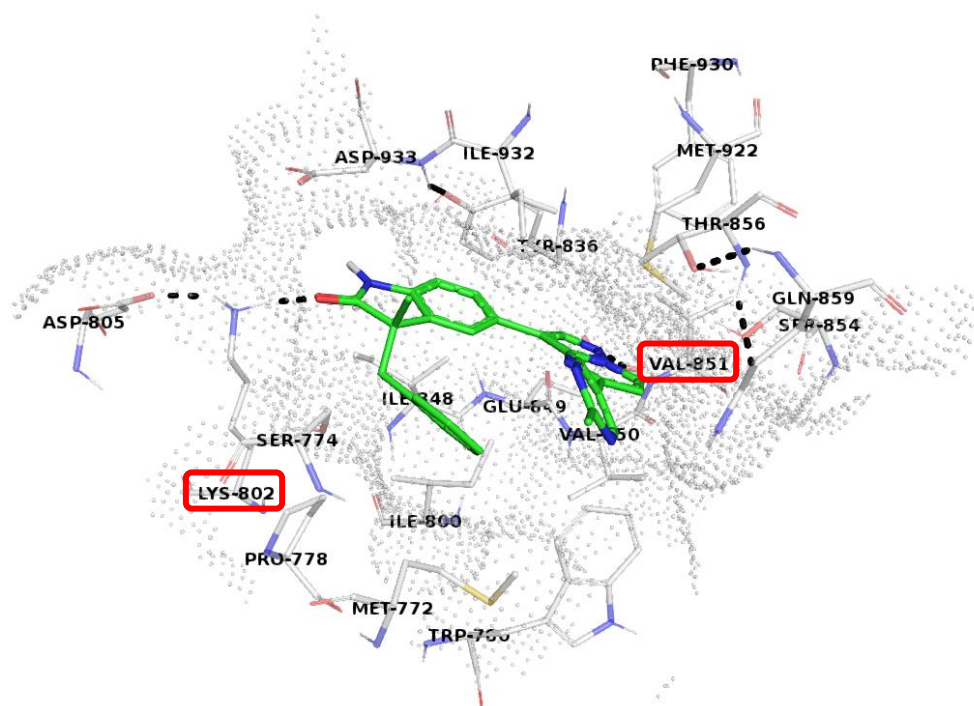


Figure 11 Interaction-binding mode of PI3K α active site with the respective original crystallographic ligand. Image generated in PyMOL.

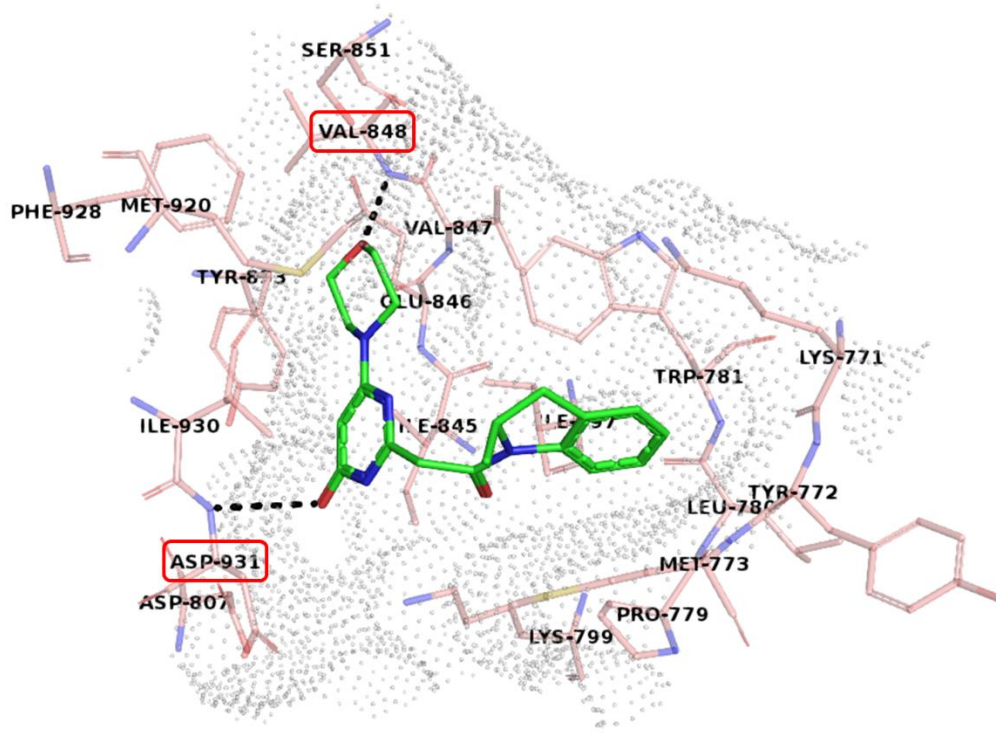


Figure 12 Interaction-binding mode of PI3K β active site with the respective original crystallographic ligand. Image generated in PyMOL.

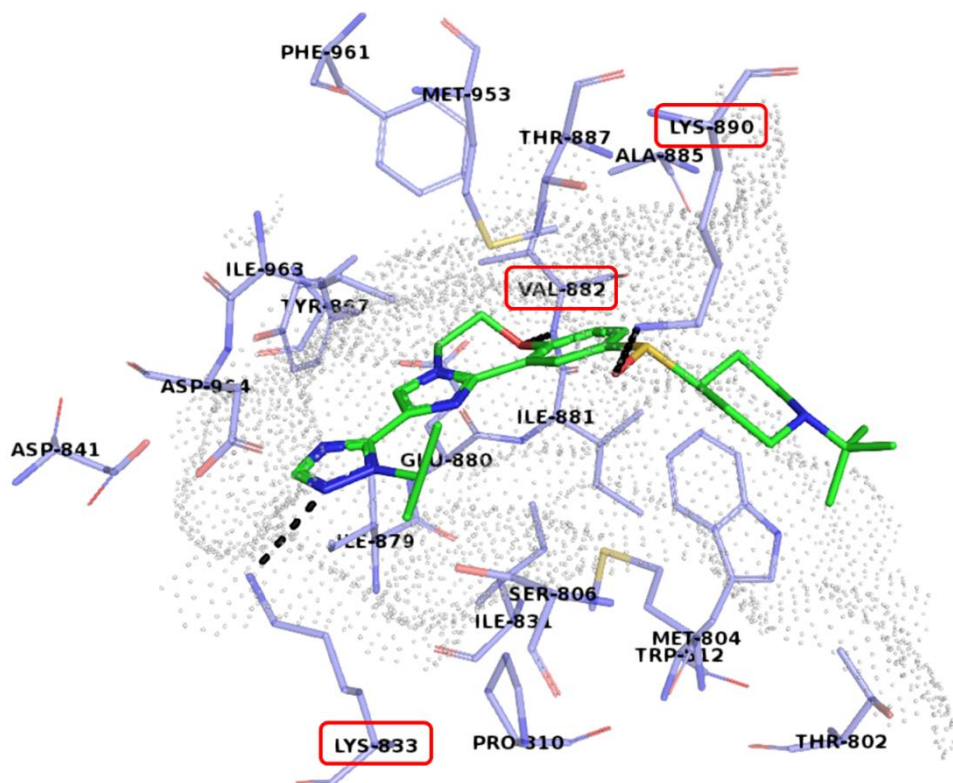


Figure 13 Interaction-binding mode of PI3K δ active site with the respective original crystallographic ligand. Image generated in PyMOL.

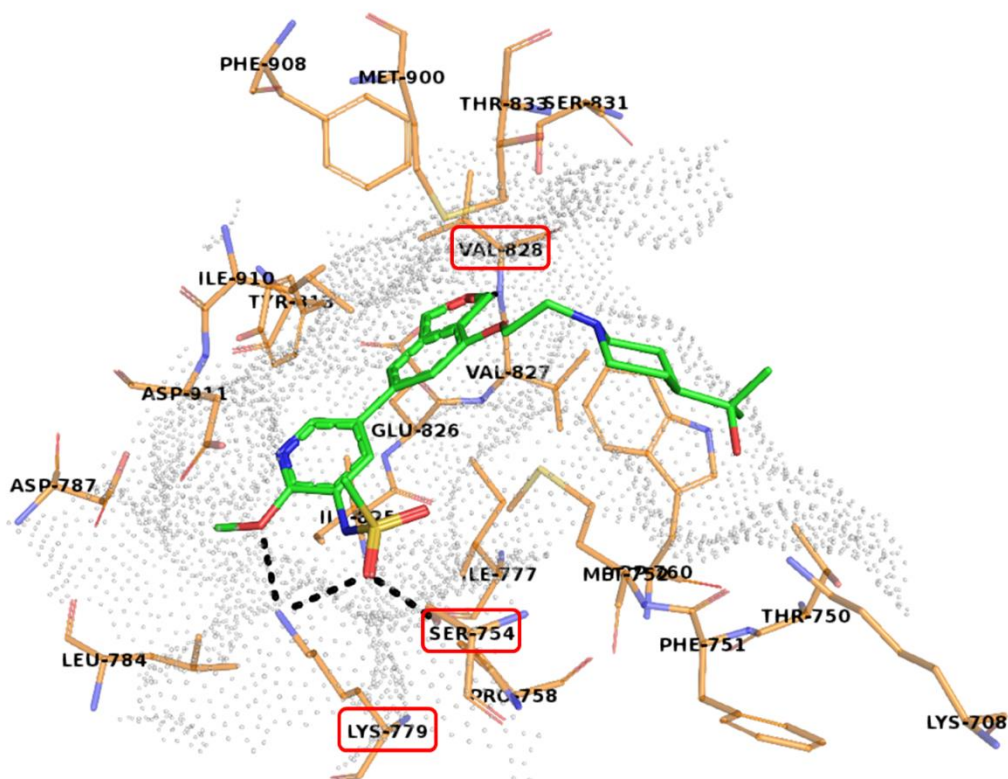


Figure 14 Interaction-binding mode of PI3K γ active site with the respective original crystallographic ligand. Image generated in PyMOL.

2.2. Ligands' design

A purine heterocycle base structure is reported in the literature as a selective inhibitor of PI3K α [26]. Figure 15 shows the scaffold and the binding interaction pattern of the constituent groups of this class of selective inhibitors with the active centre of PI3K α .

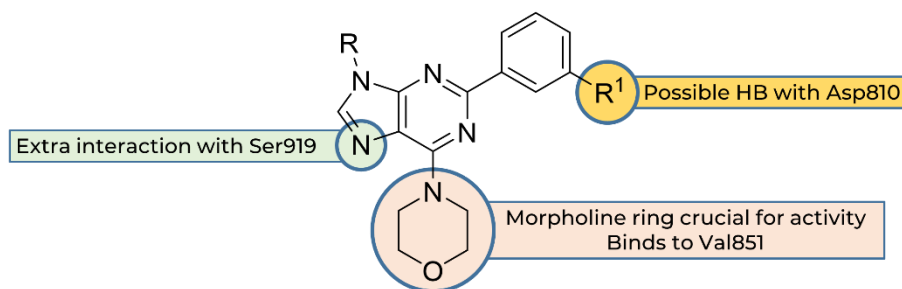


Figure 15 Reported scaffold and its interaction-binding for PI3K α . Image adapted from literature.

This is a base structure already familiar to the research group, from which some analogues with anticancer activity have already been synthesized. This structure was the basis for the design of new derivatives to explore novel interactions, while simultaneously increasing receptor binding affinity and water solubility, a common problem associated with this type of compounds.

All the derivatives maintain the same scaffold and vary essentially in 3 functional groups: amides (Classes 1, 2, 3, 5, 6 and 7); ureas (Classes 4 and 9) and carbamates (Class 8); as shown in Table 5.

Table 5 Global representation of the classes of ligands designed for Virtual Screening. R¹ and R² groups are shown on the compound numbering explanatory page.

Class 1	Class 2	Class 3
Class 4	Class 5	Class 6
Class 7	Class 8	Class 9

In addition to the classes mentioned in Table 5, the synthetic precursors of these classes were also designed and labelled as **(1-23)** and **Class 0**. (See the explanatory sheet of compound numbering).

All the ligands presented were designed, but due to a prolonged downtime period of the infrastructure containing the server with the program needed for the energy minimization of the ligands, only the complete minimization of compounds **(1-23)**, and **classes 0, 1, 2 and 3** was possible. The remaining classes needed to be restricted due to the limited period of this work. For this reason, only the results of the ligands with group R¹ ranging from **1-9** will be presented for the remaining classes (**Class 4-9**).

2.3. Virtual Screening

All the ligands presented in this chapter had their structure optimized to their minimum by quantum chemistry calculations and were virtually screened on the 4 receptors under study. The overall results are divided by class of compounds and are presented in Tables 2-12 in the Appendix. In the same tables, for each ligand, their respective physicochemical and structural properties are described, such as the total charge of the ligand and the number of hydrogen bond acceptor (HBA) and hydrogen bond donor (HBD) atoms at physiological pH. Other properties described are the partition coefficient (LogP), molecular weight (Mw) and refractivity (Rf). To facilitate the display, interpretation and discussion of all the results, a series of graphs will be presented in this section.

Firstly, the $\Delta G_{\text{binding}}$ results for the 4 proteins will be discussed and compared, by classes of ligands, aiming at the identification of selective compounds and evaluating structural similarities that may indicate an interaction pattern that justifies the selectivity obtained **(2.3.1.)**.

Afterwards, the correlations between the $\Delta G_{\text{binding}}$ results for the 4 proteins and the respective physicochemical properties of the ligands, both globally and more restrictedly, will be presented **(2.3.2)**, to once again find a possible correlation between the obtained $\Delta G_{\text{binding}}$ scores and one or more physicochemical properties.

Finally, the interactions between a set of ligands and the *alpha* and *gamma* isoforms of PI3K will be analysed in **2.3.3**. This analysis aims to identify established P-L interactions and compare them with those already reported, as well as explore new interaction sites.

2.3.1. Evaluation of ligand selectivity

For a ligand to be considered selective, the criterion defined was that the difference between its $\Delta G_{\text{binding}}$ in one isoform, and its values in the other targets, must be higher than 1 kcal/mol [$\Delta(\Delta G_{\text{binding}}) > 1 \text{ Kcal/mol}$]. This was done to surpass the average error involved in the binding estimation. A total of 68 compounds obeying this criterion were found, from which 5 presented a difference superior to 1.5 kcal/mol, consisting of more promising selective candidates.

In this subchapter, a series of line charts are presented. In general, each line represents the set of $\Delta G_{\text{binding}}$ scores of the ligands for each of the 4 targets under study. Therefore, the analysis of the differences between the results obtained by each ligand is facilitated.

Starting with the results for ligands **1-23** (Figure 16), there is an overall preference for PI3K α , followed by PI3K γ . None of the ligands shows selectivity for either isoform, however, ligand **11** has a higher binding energy for PI3K γ which is 0.9 kcal/mol away from the isoform with the second highest energy. It is also found that ligands **11, 13, 15-17** and **21** have a preferred affinity for PI3K γ . Except for ligand **16**, all these ligands have a common feature, being *meta* substituted with a nitrogen atom in the aromatic ring present in R¹.

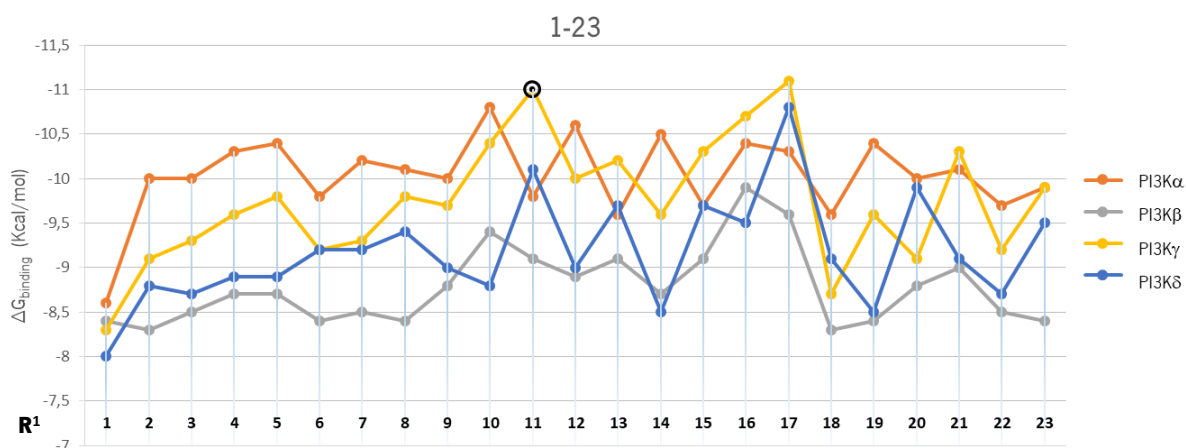


Figure 16 Graphical representation of the binding energies for the ligands **1-23** in the 4 isoforms of PI3K.

In analogy to ligands **1-23**, the results for the **class 0** ligands maintain an overall preferential affinity for PI3K α , followed by PI3K γ (Figure 17). In this case, it can be seen that the overall binding energies increased for all ligands. Additionally, there were found 3 ligands in this class that presented selectivity for PI3K α (ligands **6.0, 8.0** and **20.0**), highlighted in black in the graph of Figure 17. All these ligands have in common a substitution in *para* of the ring in R¹ by different groups. Note also that two

ligands have a relatively higher affinity (>0.5 kcal/mol) for PI3K γ (ligands **9.0** and **11.0**), both also structurally similar, with an amide function at the *meta* position of the ring in R¹.

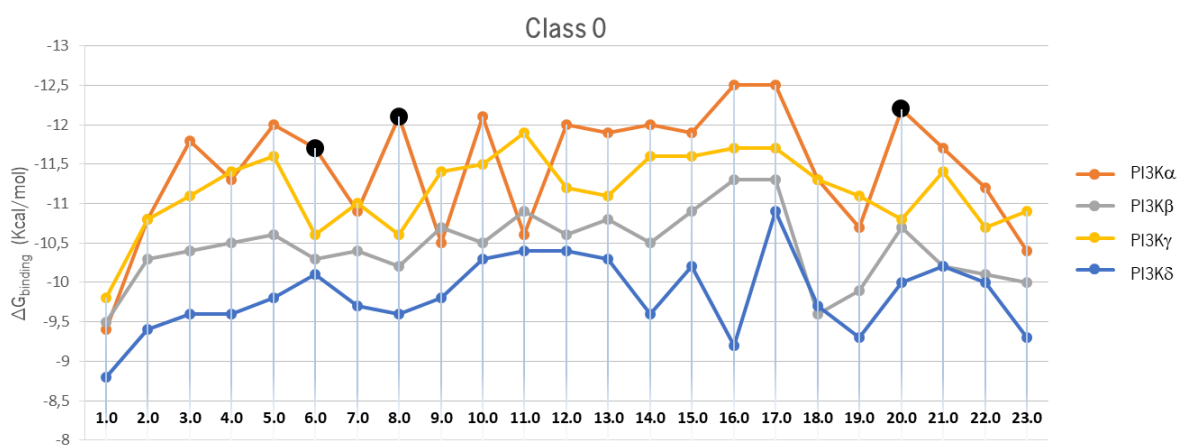


Figure 17 Graphical representation of the binding energies for the **Class 0** ligands in the 4 isoforms of PI3K.

All the ligands presented onwards, for each class, have 2 structural variations (R² and R¹). In the following graphs, the compounds are organized by keeping the R¹ group, shown in the first row of the x-axis, fixed, and varying the R² groups, shown below the corresponding R¹ in the x-axis, for the remaining classes of compounds.

Following the same pattern as the previously presented classes, **class 1** ligands exhibit preferential selectivity for the *alpha* and *gamma* isoforms of PI3K, as shown in Figure 18. In this class, highlighted with black dots, are 15 ligands, of which 8 show a higher affinity and selectivity for PI3K α (**4.1d**, **7.1d**, **11.1c**, **11.1e**, **12.1a**, **13.1e**, **14.1a** and **16.1c**) and 7 for PI3K γ (**1.1a**, **1.1b**, **1.1c**, **1.1d**, **3.1a**, **5.1a** and **22.1a**).

In the case of the PI3K γ selective ligands, there is a pattern in the R² group (**a**) that is consistent with the other ligands, which despite being non-selective, have a relatively high affinity for this isoform. Another consistency in the results for the *gamma* isoform of PI3K is the selectivity shown by ligands whose R¹ group is a hydrogen atom (**1**).

Regarding the results obtained for the **class 2** ligands (Figure 19), a significant overall increase in binding energies for all 4 isoforms stands out clearly. This is especially quite noticeable in PI3K δ . In this isoform, one ligand (**7.2b**), with a relatively high binding energy score, appeared for the first time, presenting a difference of 1 kcal/mol from the energy values for the other isoforms, making it practically selective.

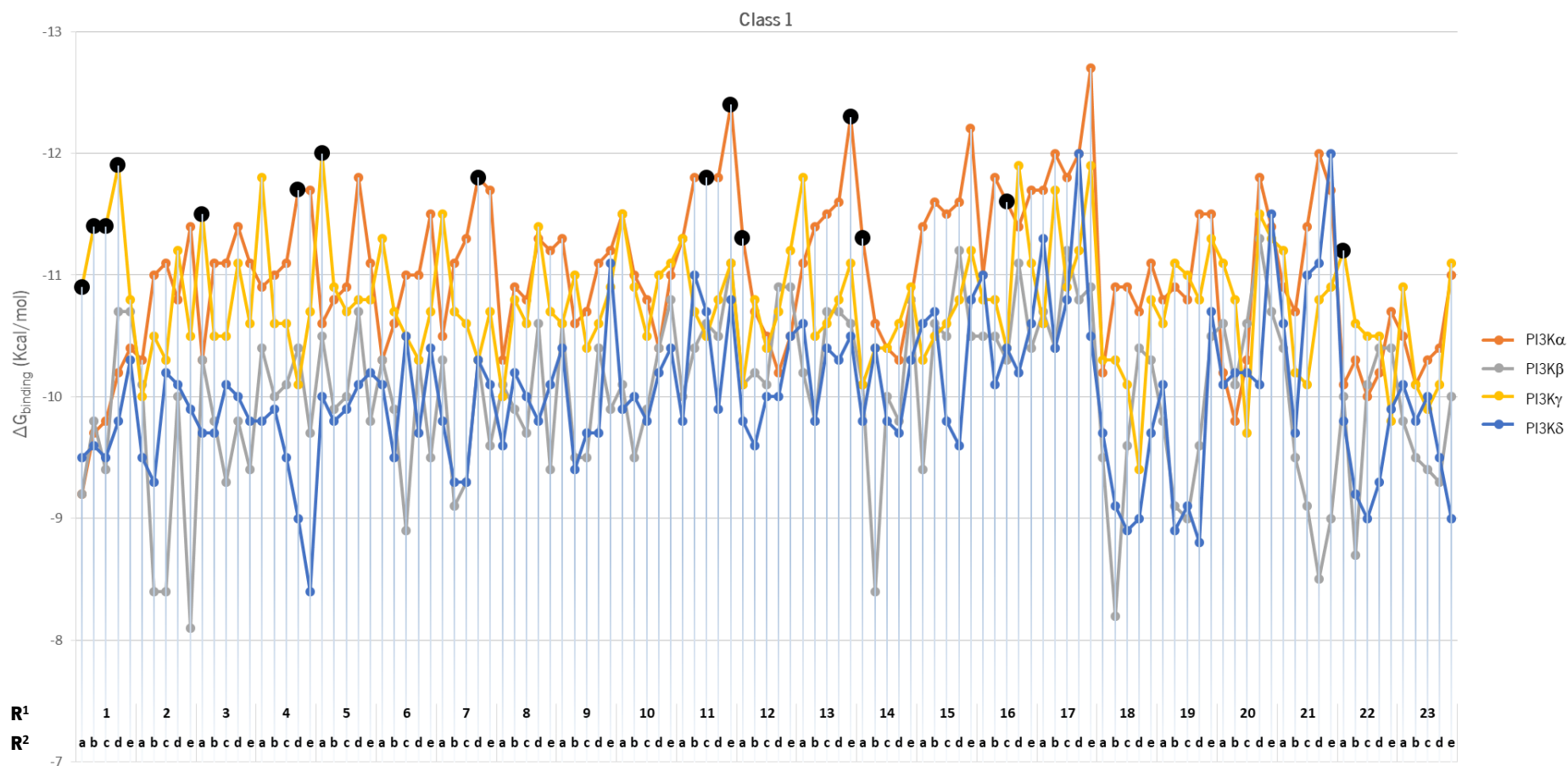


Figure 18 Graphical representation of the binding energies for the **Class 1** ligands in the 4 isoforms of PI3K.

Despite the overall increase in **class 2** ligands binding energies, only 3 were found selective for PI3K α (**3.2a**, **15.2e**, and **17.2e**). Still, in this class, the overall affinity results are in concordance with the previous classes, once the highest binding energies continue to be globally found for the *alpha* and *gamma* isoforms of PI3K.

Moving forward to **class 3**, after analysis of the graph in Figure 20 regarding the results obtained for the **class 3** ligands, 21 selective ligands were found and are highlighted in black in Figure 20. Of these, 20 are selective for PI3K α (**2.3d**, **3.3c**, **3.3d**, **4.3d**, **5.3d**, **6.3d**, **7.3d**, **11.3e**, **13.3a**, **13.3b**, **15.3a**, **15.3b**, **16.3b**, **16.3c**, **16.3d**, **17.3b**, **17.3e**, **18.3b**, **18.3d** and **19.3d**) and only 1 for PI3K γ (**21.3a**).

Regarding the 20 ligands selective for PI3K α , a pattern is noticeable in this class, as 9 of them have the common R² group (**d**). Additionally, like in **class 2**, an overall increase in the receptor affinity is evident for this class, for the ligands designed.

In a very general perspective, the highest binding energy scores are still evident for PI3K α , although there are also some prominent cases for the gamma isoform. A great example for a case where there is a partial selectivity for the PI3K γ isoform is the ligand **5.3a**, easily distinguished by its sharp yellow peak in Figure 20.

However, there is again a ligand with a relatively high affinity and partial selectivity for PI3K δ (**21.3b**). It will be interesting later on to try to understand why these two isolated cases for **classes 2** and **3** showed these results.

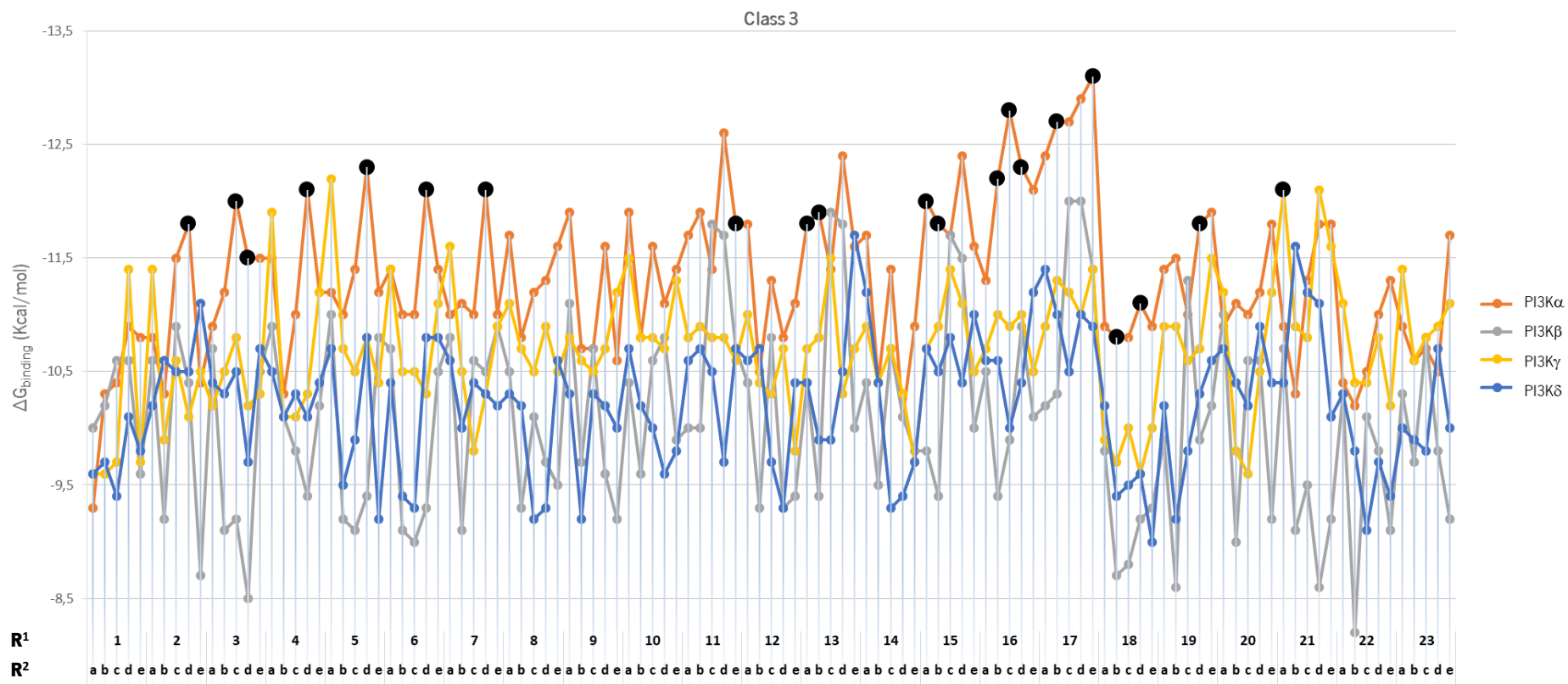


Figure 20 Graphical representation of the binding energies for the **Class 3** ligands in the 4 isoforms of PI3K.

Despite containing a more limited sample of ligands in comparison to the previous 3 classes, in **class 4**, 8 ligands selective for PI3K α were found and are highlighted in Figure 21 (**2.4a**, **4.4a**, **5.4c**, **7.4c**, **8.4e**, **9.4a**, **9.4b** and **9.4c**). It can be seen from the graph in Figure 21 that apart from when R¹ is **8**, there is one uniform increase in $\Delta G_{\text{binding}}$ when the R² group is a morpholine ring (**c**). In the same way, apart from when R¹ is **2**, there is one uniform increase when the R² is an amide (**e**).

Again, the overall affinity values are higher for PI3K α , however, there is a smaller difference between the binding energy associated with the remaining isoforms in comparison to the previously presented classes. In this graph, a parallel approximation of the affinity results for the *beta* and *delta* isoforms to the *gamma* is quite noticeable, although PI3K γ 's binding energy scores remained slightly higher.

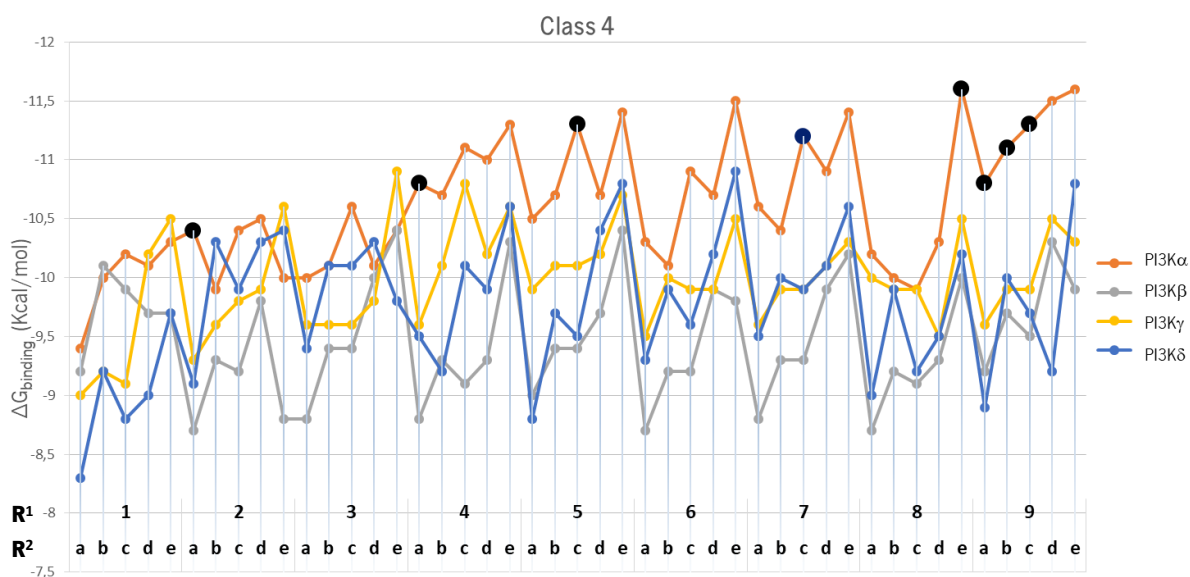


Figure 21 Graphical representation of the binding energies for the **Class 4** ligands in the 4 isoforms of PI3K.

Next, in Figure 22, the values of the binding energy score for **class 5** ligands are presented. Compared to previous classes, the overall values of binding energy are relatively lower. Despite this, a total of 6 ligands were found selective for PI3K α (**2.5b**, **2.5d**, **3.5b**, **5.5c**, **6.5b** and **7.5b**). These are highlighted in black dots in Figure 22. From these results and considering the peaks for PI3K α when *N*-methylpiperazine (**b**) is present in R², it is assumed that this group influences the affinity results for this isoform. On the other hand, contrary to the classes previously presented, a considerable increase of the binding energy for the *beta* isoform of PI3K is visible for a great amount of the **class 5** ligands, although remaining lower than for PI3K α .

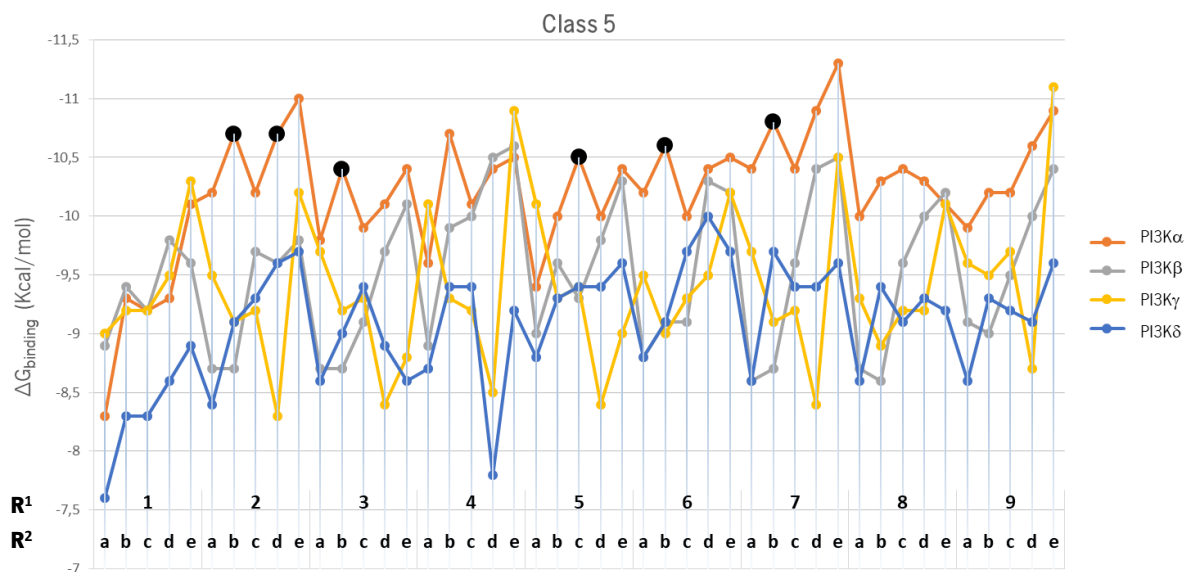


Figure 22 Graphical representation of the binding energies for the **Class 5** ligands in the 4 isoforms of PI3K.

Regarding the results obtained for the ligands of **class 6**, only one ligand was found selective for PI3K α (**7.6e**), represented in the graph of Figure 23 with a black dot. In this class, in accordance with the others, once again, there is a higher overall affinity of the ligands for the *alpha* isoform, although the scores are a little lower than those shown for the other classes.

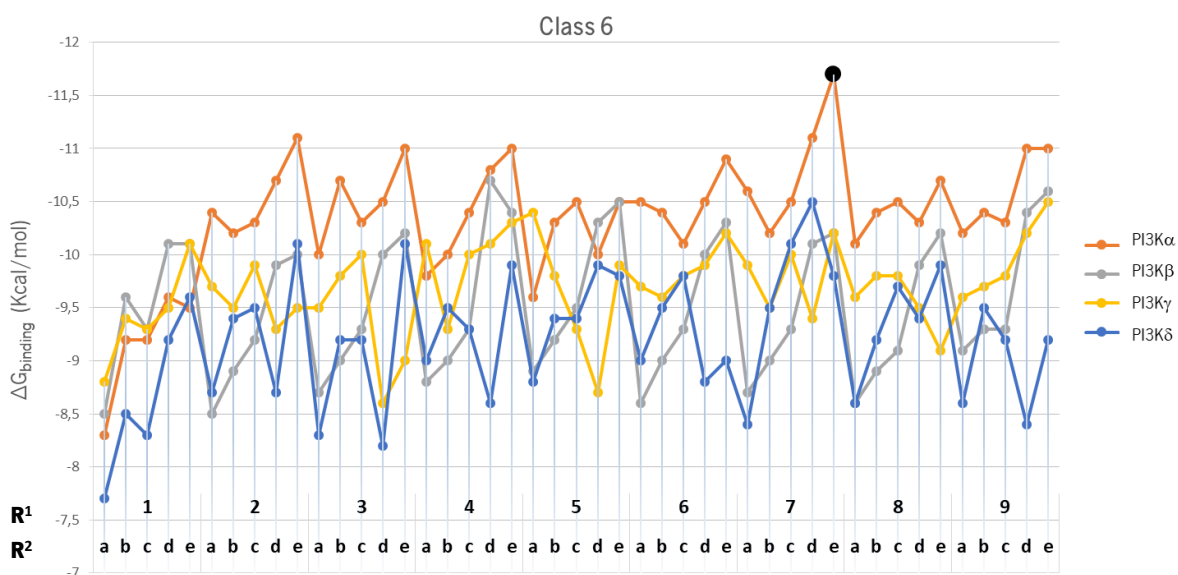


Figure 23 Graphical representation of the binding energies for the **Class 6** ligands in the 4 isoforms of PI3K.

For **class 7**, 3 selective ligands for PI3K α were found (**2.7e**, **5.7c** and **7.7e**) and are highlighted in black in Figure 24. The overall results continue to show a selective affinity for the *alpha* isoform of PI3K. However, distinguishable peaks are easily seen when an amide (**e**) is present in the R² group.

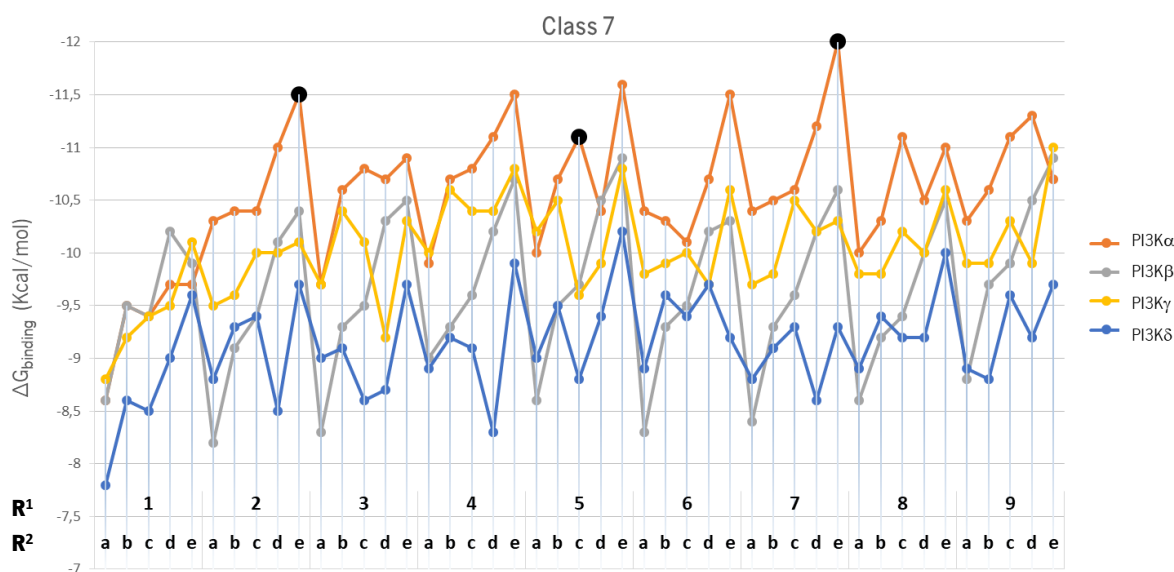


Figure 24 Graphical representation of the binding energies for the **Class 7** ligands in the 4 isoforms of PI3K.

Regarding **class 8**, the global results are similar to those presented for the 3 previous classes. In Figure 25, 2 ligands, highlighted with black dots, can be distinguished by their selectivity (**6.8a** and **7.8e**).

As in the two previous classes, the ligands that have in their structure the R¹ **7** and the R² **e**, show selectivity for PI3K α . The structural variations of these classes consist of a change in the number of carbons in the alkyl chain, and in the case of these 3 classes, this does not seem to be a determining factor in conferring selectivity between the different isoforms.

Also distinguished in Figure 25, a partial inhibitor for PI3k β can be easily identified (**1.8d**).

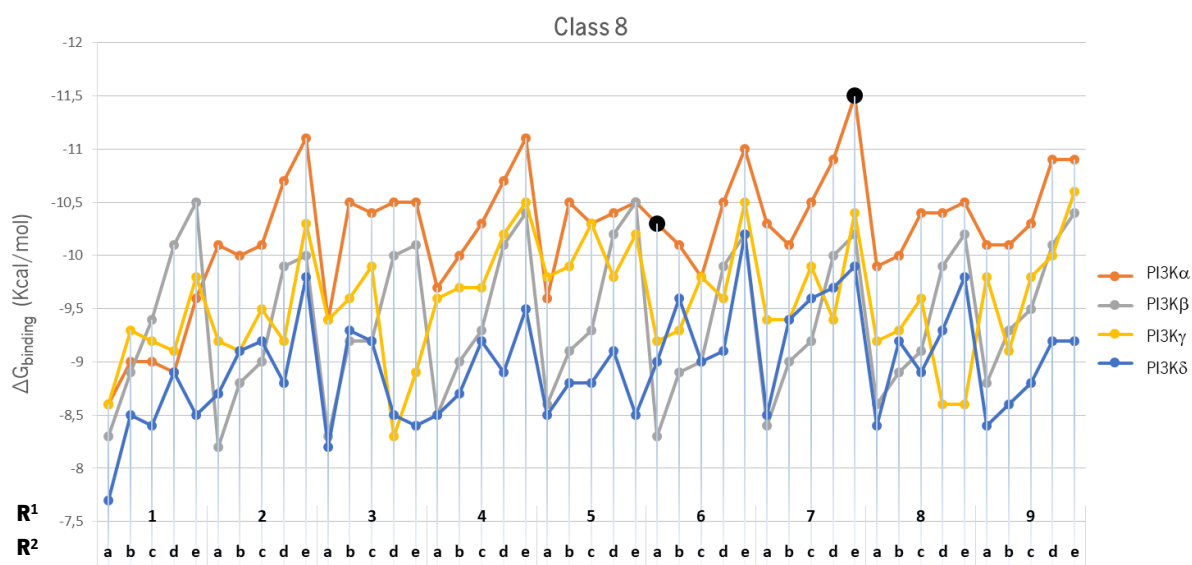


Figure 25 Graphical representation of the binding energies for the **Class 8** ligands in the 4 isoforms of PI3K.

Finally, Figure 26 shows the ligands' binding energies relative to **class 9** for the 4 isoforms. Of these, the ligands marked with black dots in Figure 26 (**2.9b**, **2.9c**, **2.9d**, **7.9d**, **8.9b** and **9.9c**) stand out for their selectivity for PI3K α . Overall, the results agree with those presented for all other classes, where a higher overall affinity of the ligands for the *alfa* isoform stands out.

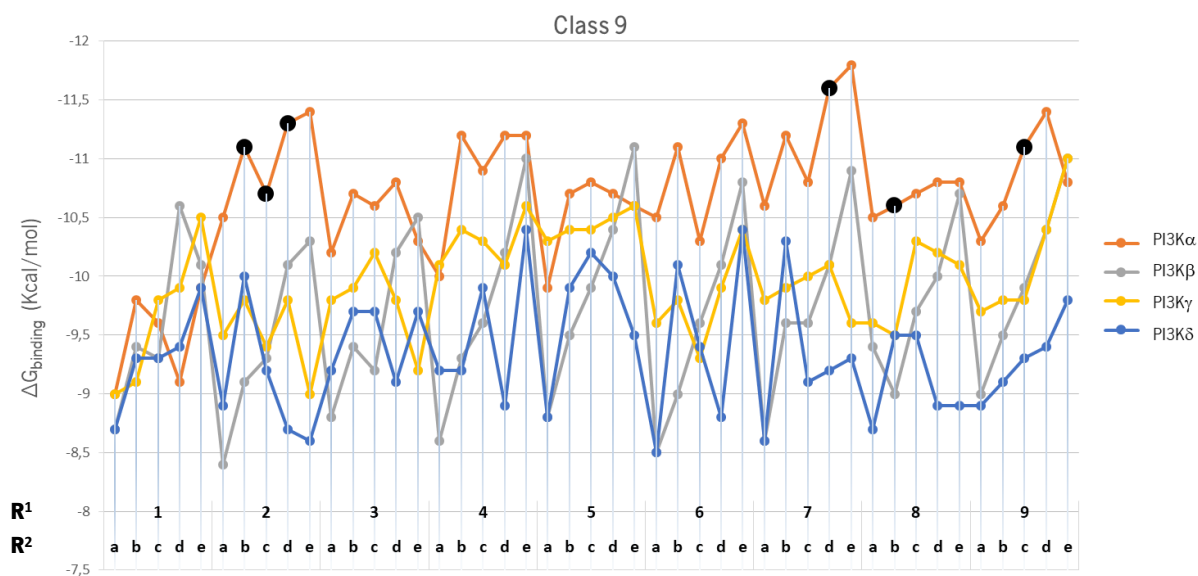


Figure 26 Graphical representation of the binding energies for the **Class 9** ligands in the 4 isoforms of PI3K.

When analysing all the results globally, from the 661 ligands virtually screened, a total of 68 selective ligands (approximately 10.3%) were identified in two classes, of which 60 for the *alpha* and 8 for the *gamma* isoform. This fact highlights the importance of computational studies on drug design, revealing that from a reasonable sample as the one showcased, only about 10% of the molecules are promising for the consecutive synthesis and studies of in vitro activity. Importantly, these results are in agreement with what is reported for these types of compounds, since the scaffold used in the design of all ligands tested here is stated as selective for PI3K α [26]. Additionally, there is also evidence for the activity of this scaffold, although slightly lower in the *gamma* isoform of PI3K [71].

From the 68 selective ligands mentioned, 5 stand out for presenting a $\Delta G_{\text{binding}}$ difference superior to 1.5 kcal/mol between the rest of the isoforms (**1.1b**, **1.1c**, **2.5b**, **7.3d** and **17.3e**). The minima optimized structures of these compounds are presented in Figure 27. Additionally, 4 ligands were found partially selective for the *beta* (**1.8d**), *delta* (**7.2b** and **21.3b**) and *gamma* (**5.3a**) isoforms.

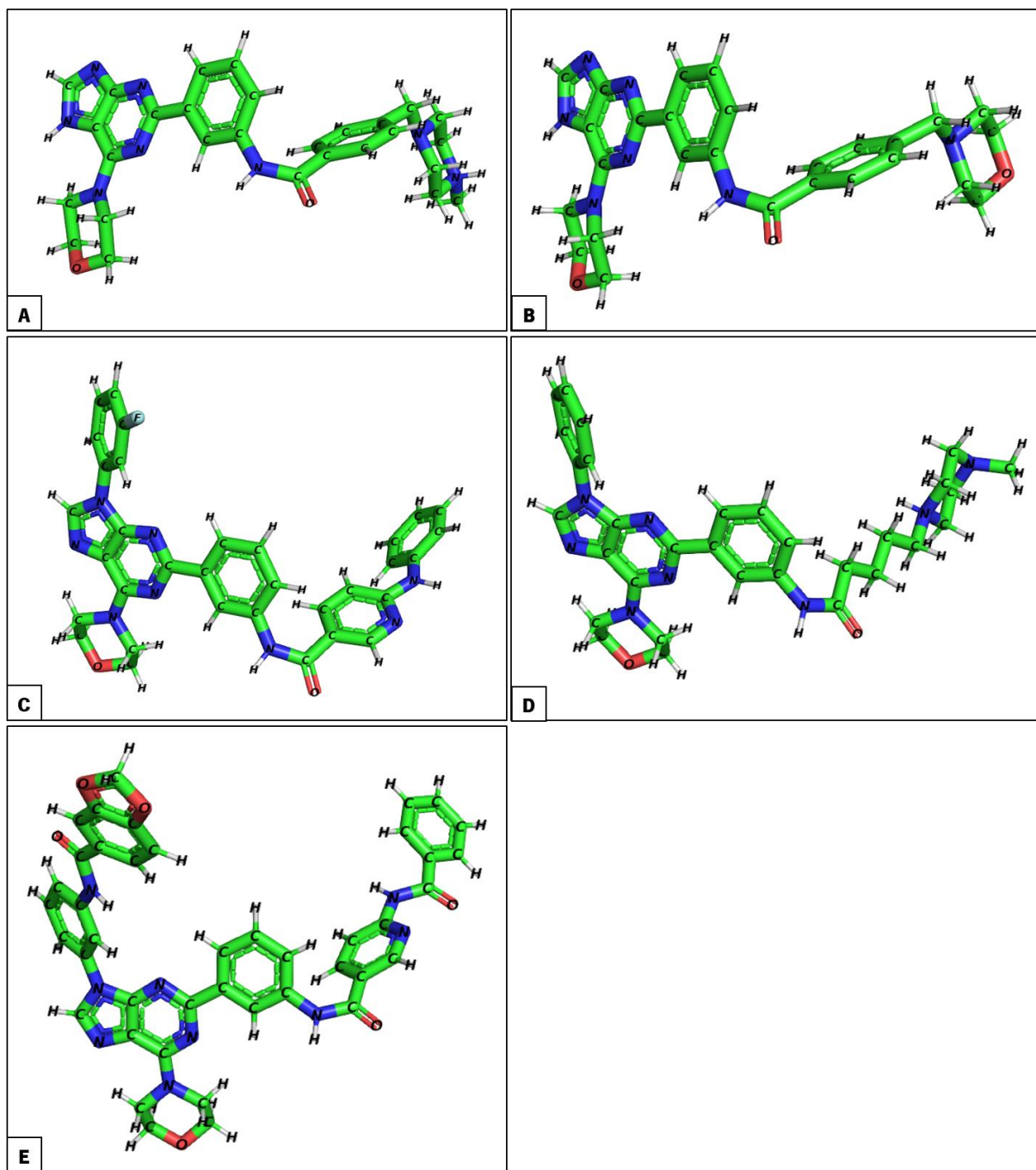


Figure 27 Local minima optimized structures of ligands **1.1b** (A), **1.1c** (B), **2.5b** (C), **7.3d** (D) and **17.3e** (E), obtained via DFT calculations. Images were prepared with PyMOL (Labelled atoms).

Table 6 shows all the selective ligands obtained for PI3K α (highlighted in orange) and PI3K γ (highlighted in yellow). These ligands were grouped according to their underlying structural groups. This makes it easier to identify possible structural patterns that may account for the selectivity of the ligands for their respective targets.

Table 6 Set of selective ligands obtained for PI3K α (highlighted in orange) and PI3K γ (highlighted in yellow), grouped according to structural clusters.

R ¹	Class 0	R ²									
		a	b	c	d	e					
1		1.1a	1.1b	1.1c	1.1d						
2		2.4a	2.5b 2.9b	2.9c	2.3d 2.5d 2.9d	2.7e					
3		3.1a	3.5b	3.3c	3.3d						
		3.2a									
4		4.4a			4.1d 4.3d						
5		5.1a [5.3a]*			5.4c 5.5c 5.7c		5.3d				
6		6.0			6.8a		6.5b	6.3d			
7		8.0		7.5b	7.4c		7.1d 7.3d 7.9d	7.6e 7.7e 7.8e			
8				8.9b				8.4e			
9			9.4a	9.4b	9.4c 9.9c						
11					11.1c				11.1e 11.3e		
12									12.1a		
13			13.3a	13.3b					13.1e		
14			14.1a								
15			15.3a	15.3b					15.2e		
16					16.3b				16.1c 16.3c	16.3d	
17					17.3b						17.2e 17.3e
18					18.3b						
19			20.0							18.3d	
20		19.3d									
21		21.3a									
22			22.1a								

*Partial selectivity for PI3K γ

Based on the results above, PI3K γ ligands selectivity can be correlated with structural patterns presented in some of the ligands displayed. For **class 1**, when R¹ is a hydrogen atom (**1**), 4 of the 5 ligands with variations in the R² group show selectivity. Another notable factor, for both **classes 1** and **3**, is the selectivity conferred when the R² group is a primary amine (**a**).

In the case of PI3K α , given the wider range of selective ligands, it is easier to find a more generic pattern. This is the case in the bold highlighted blocks from Table 6, where 4 clusters of ligands are shown that share the same R¹ and R² group with each other, varying only in class. The fact that they are grouped in these blocks by itself provides a pattern of selectivity, where the importance of the coexistence of these two groups in the ligand structure is emphasized.

On closer examination, the most representative classes when the R² group is replaced by **b** or **d**, are **classes 3, 5, and 9** respectively. In another perspective, it is also possible to verify that the most significant R¹ groups of the selective ligands are **2, 6, 7 and 16**. All this information will allow a rational design of more potent ligands for this PI3K isoform.

2.3.2. Correlation between the variation of $\Delta G_{\text{binding}}$ and ligand properties

After the identification of the selective ligands under study in **2.3.1.**, a possible correlation with one or more physicochemical characteristics of the ligands was investigated. For this purpose, 3 principal component analysis (PCA) plots were generated, aiming to reduce a set of variables (physicochemical properties) into a smaller set of uncorrelated components that represent most of the ligands' properties. By reducing the dimensionality, the interpretation of a few components rather than a large number of variables becomes possible [72].

The interpretation of the PCA graphs is mainly based on the analysis of the angles between the vectors that represent the various properties. Two properties will be more positively correlated (when one increases, the other also increases), the closer the angle between their respective vectors is to zero. On the other hand, the closer that an angle between vectors is to 180 degrees, the more negatively correlated the 2 properties are (when one increases the other decreases). Finally, two vectors whose angle is close to 90 degrees have a very weak or no correlation between the properties represented by them.

The data on the following graphs must take into account that $\Delta G_{\text{binding}}$ is given in negative values. Hence, the vectors respective to the $\Delta G_{\text{binding}}$ of the ligands for each isoform (represented in the graphs as PI3K α , PI3K β , PI3K γ and PI3K δ) are represented towards the negative chart (left side of the graph). When interpreting the graphs, the direction of the $\Delta G_{\text{binding}}$ vectors (PI3K) should be considered the opposite, i.e. if a $\Delta G_{\text{binding}}$ (PI3K) vector is at 180 degrees of another vector, it should be considered at 0 degrees, given the projection of this vector to the positive area of the plot.

Initially, the 661 ligands studied were analysed. All the physicochemical properties, as well as the binding energies for the 4 isoforms of PI3K, were set as variables, generating the graph in Figure 28. Here, over 65% of the data is described by the first two components.

In a first instance, from a global perspective, it can be seen that all the correlations presented for the 4 proteins under study are consistent since they present a close or almost null angle between them. The binding energies for the series of ligands, in all 4 environments, proved to be independent of charge and number of HBD, since a weak or no correlation between these properties and $\Delta G_{\text{binding}}$ (PI3K) are observed, due to the angle close to 90 degrees established.

On the other hand, there is an angle of approximately 180 degrees between one cluster of properties - refractivity (Rf), molecular weight (Mw), hydrogen bond acceptor atoms (HBA) and partition coefficient (LogP) - and the $\Delta G_{\text{binding}}$ of the 4 proteins. In this case, since $\Delta G_{\text{binding}}$ values are expressed negatively, the affinity of the ligands for the 4 isoforms is positively correlated with these properties.

In a more particular perspective, the affinity for the *beta* isoform stands out from the others by the optimal correlation (very close to 180 degrees) established with LogP. It is also notable, for this isoform, a higher correlation with the charge and HBD properties, and a lower correlation with the remaining properties in comparison with the other isoforms.

As for the other isoforms, although close, the $\Delta G_{\text{binding}}$ of the *delta* isoform establishes a higher correlation with the Rf, HBA and Mw properties, followed by the $\Delta G_{\text{binding}}$ of the *gamma* and *alpha* isoforms, respectively. The opposite happens in the correlation of these isoforms with LogP, since the biggest correlation happens with the $\Delta G_{\text{binding}}$ of PI3K α , followed by PI3K γ and PI3K δ , respectively.

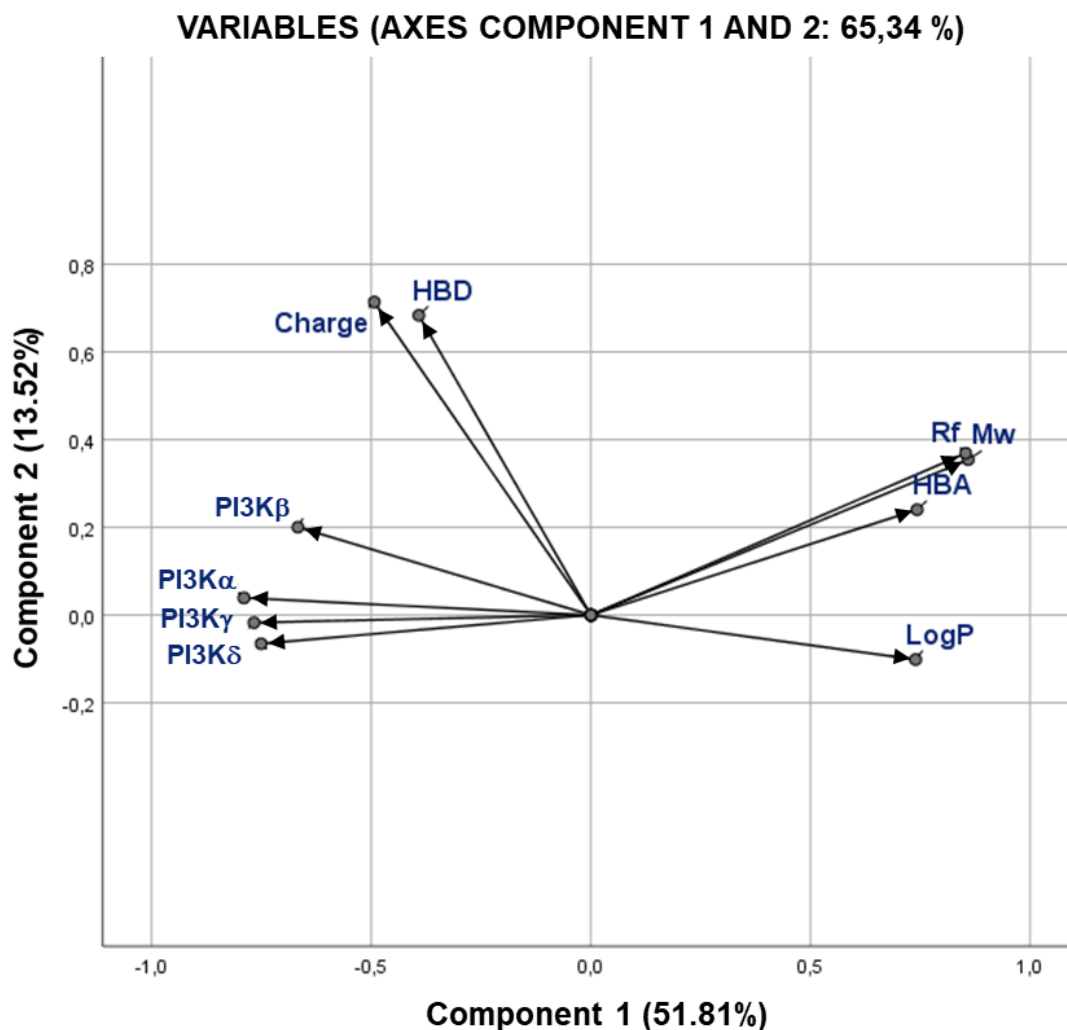


Figure 28 Principal component analysis (PCA) biplot of the first two components, objects factor scores and loadings, of data presented in Tables 2-12 from Appendix. Rotated component matrix and scores were calculated using IBM SPSS Statistics software. Black arrows represent the loadings of the ten variables.

Next, as an attempt to correlate the selectivity of the *alpha* and *gamma* isoforms to the physicochemical properties of the respective selective ligands, 2 additional PCA plots were performed (Figures 29 and 30).

Figure 29 depicts the PCA plot that correlates the $\Delta G_{\text{binding}}$ of the 60 selective ligands for PI3K α with their physicochemical properties. In this, more than 80% of the information is descended by components 1 and 2. The correlation between the properties and $\Delta G_{\text{binding}}$ of the ligands under analysis for the *alpha* isoform is similar to that shown in Figure 28 for all ligands. This means that there continues to be virtually no correlation between the $\Delta G_{\text{binding}}$ of PI3K α and the HBD and charge properties, although a small decrease in the angle between $\Delta G_{\text{binding}}$ and charge is noticeable. There is also an increase in the negative correlation of $\Delta G_{\text{binding}}$ with LogP, and a decrease with HBA, Mw, and Rf.

Additionally, a pattern in the dispersion of the ligands in the graph, represented by green diamonds, is noticeable in this graph. It can be seen that a considerable amount of the ligands in the positive chart of component 2 have R^2 groups that are protonated at physiological pH, such as the primary amine (**a**) and *N*-methylpiperazine (**b**). On the other hand, the ligands in the negative chart of this component are mostly ligands whose R^2 is not protonated at physiological pH, as is the case of the groups **c**, **d** and **e**.

In another perspective, it is also notable a dispersion of the ligands in the positive and negative charts of component 1. In the negative chart, the ligands with the less voluminous R^1 are clustered, as is the case of groups **2-9**. On the other hand, ligands with a larger R^1 group (**9-19**) are found in the positive chart.

Regarding the affinity of the ligands, it is expected that ligands with the highest R_f , M_w and number of HBA have a lower $\Delta G_{\text{binding}}$ score, which translates into a greater negative correlation between these variables. This is because the ligands shown on the right chart of component 1 in the graph, located where these variables' scores are higher, are the ones with the highest affinity for PI3K α . This is reinforced by the fact that the angle that $\Delta G_{\text{binding}}$ establishes with these properties is one of the widest presented.

In the overall analysis of the graph, it appears to have a similar profile to the two previously presented. Particularly, in this one, an angle of almost 90 degrees between the $\Delta G_{\text{binding}}$ and the ligand charge is visible. This is justified by the fact that there is a considerable range of charges, which do not follow a linear trend with the $\Delta G_{\text{binding}}$ score. This is because 6 of the 8 ligands show a charge different from 0 (**1.1a** (+1); **1.1b** (+1); **3.1a** (+1); **5.1a** (+1); **22.1a** (+2); **21.3a** (-1)). Thus, there is no consistency of values for the charge. If instead, the criteria for this variable were binary, where the presence of charge was 1 and the absence 0, there would certainly be a correlation, since 75% of the sample presented have a positive or negative charge at physiological pH.

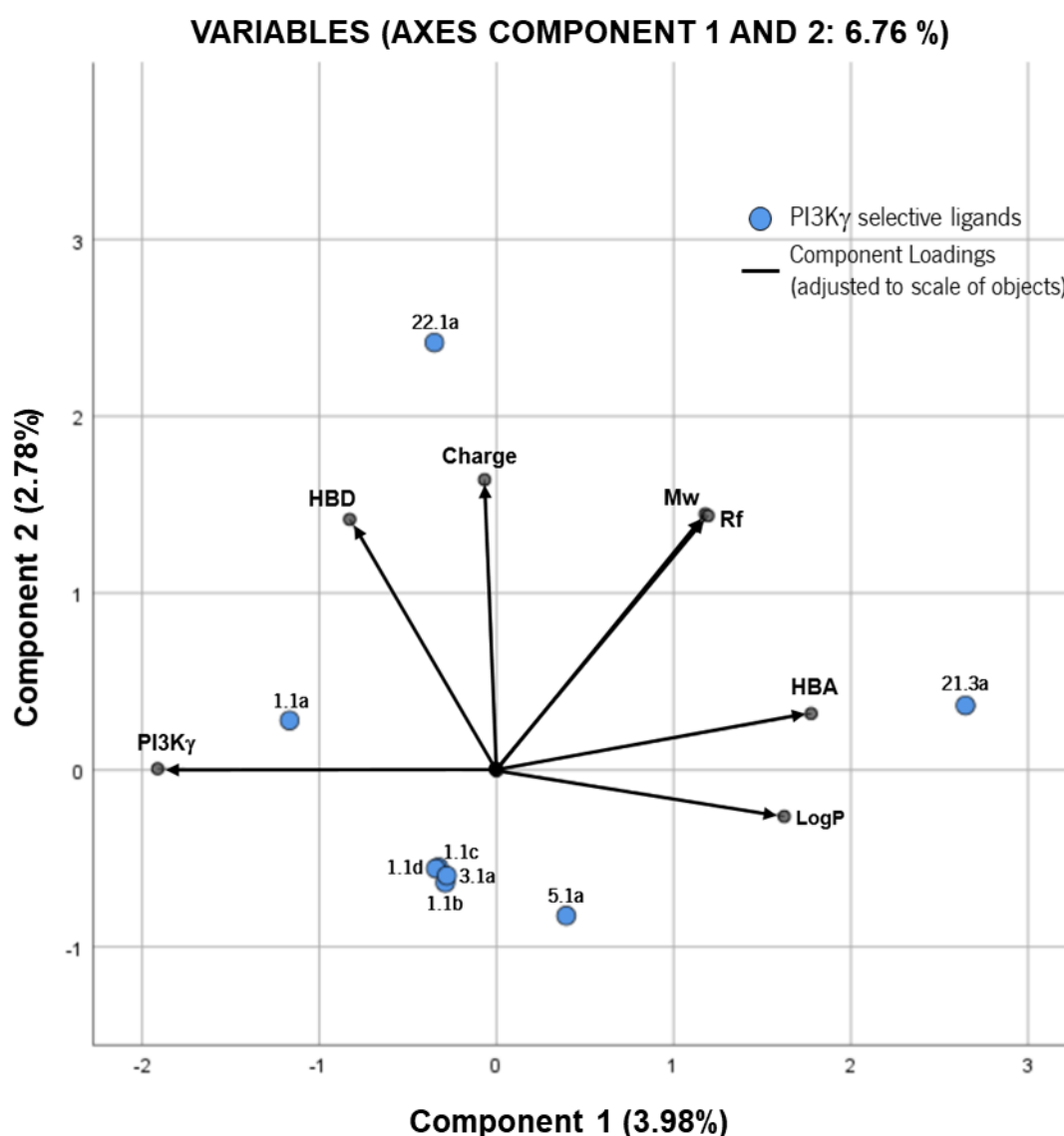


Figure 30 Principal component analysis (PCA) biplot of the first two components, objects factor scores and loadings, of filtered data presented in Tables 2-12 from Appendix. Rotated component matrix and scores were calculated using IBM SPSS Statistics software. Black arrows represent the loadings of the ten variables scaled to objects' values. Blue circles represent the selective ligands for PI3K γ .

Given that ligands **21.3a** and **5.1a** are the ones with the most negative $\Delta G_{\text{binding}}$ scores for PI3K γ , a pattern is noticeable since they are on the positive axis of component 1. There is an almost perfect negative correlation between the $\Delta G_{\text{binding}}$ and the number of HBA, given the approximate angle of 180 degrees established. Similarly, although with a smaller angle, a correlation with LogP is visible.

This information could be useful in the development of new selective inhibitors for the *gamma* isoform of PI3K, however, a larger sample of selective ligands is needed to confirm the patterns discussed.

2.3.3. Analysis of P-L interactions in PI3K α and PI3K γ

To analyse the interactions established between the ligands studied here with the 2 isoforms for which selectivity was obtained (PI3K α and PI3K γ), it was necessary to filter the results by selectivity and binding energy of the ligands. Thus, 5 ligands were chosen for analysis of interactions with PI3K α (**16.3b**, **16.3c**, **17.2e**, **17.3b** and **17.3e**), and 4 ligands were chosen for analysis of interactions with PI3K γ (**1.1b**, **1.1c**, **5.1a**, and **21.3a**). This analysis aims to identify established P-L interactions and compare them with those already reported, as well as explore new interaction sites.

Starting the analysis with the *alpha* isoform of PI3K, the overlap of the filtered ligands in the active centre of this receptor is shown in Figure 31. Since the ligands are found to be clustered in the

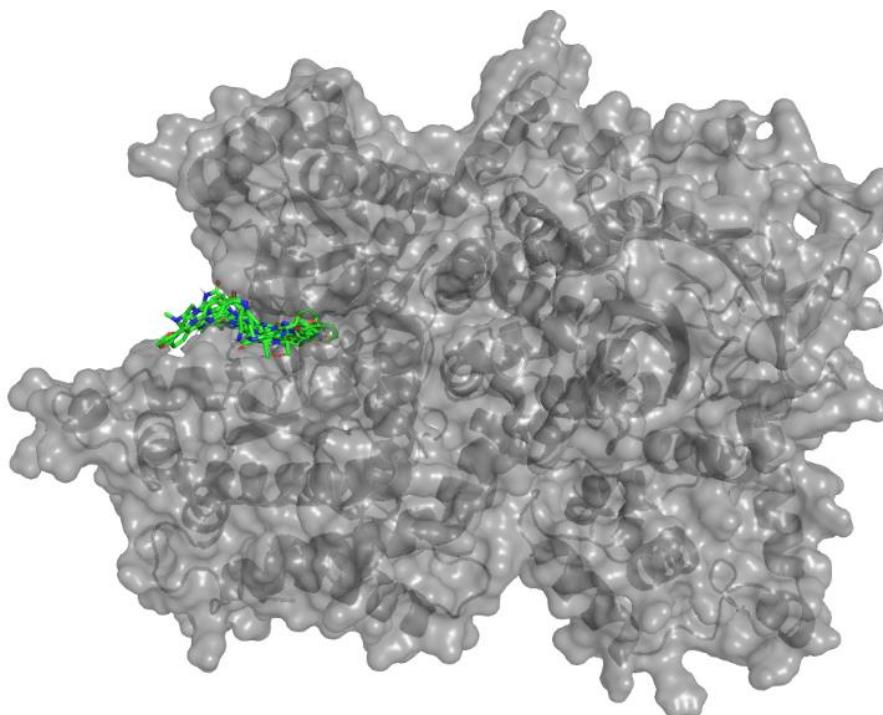


Figure 31 Overlay of the selected docked ligands for PI3K α (coloured by element (green-carbon, blue-nitrogen, red-oxygen and white-hydrogen) on the active centre of the respective receptor (both surface and cartoon in grey). Image generated in PyMOL.

same cavity on the target under study, it can be assumed that there is an optimal adaptation of their structure to the size of the pocket.

In a detailed perspective, the interaction of the ligands **16.3b** and **16.3c** with PI3K α can be seen in Figure 32 A and B, respectively. In here, there is a common interaction with the amino acid TYR-730 for both ligands (HBA), however, it occurs at different parts of the molecules as there is no overlap of the common structures. Additionally, in Figure 32 A, interactions with the residues ARG-664 (HBA) and SER-813 (HBD) are visible for ligand **16.3b**. In Figure 32 B, the non-common interactions between the ligand **16.3c** occur with the residues GLN-753 and SER-668, both as HBA. Although their structures are very similar, with only the *N*-methylpiperazine ring (**16.3b**) differing for the morpholine ring (**16.3c**), and given the higher affinity of the last one for the receptor [$\Delta G_{\text{binding}} = -12.8$ Kcal/mol] for ligand **16.3c** and ($\Delta G_{\text{binding}} = -12.2$ Kcal/mol) for ligand **16.3b**], there seems to be a probable steric block in the optimal interaction region for the ligand **16.3b**, given the larger volume of the associated R² group.

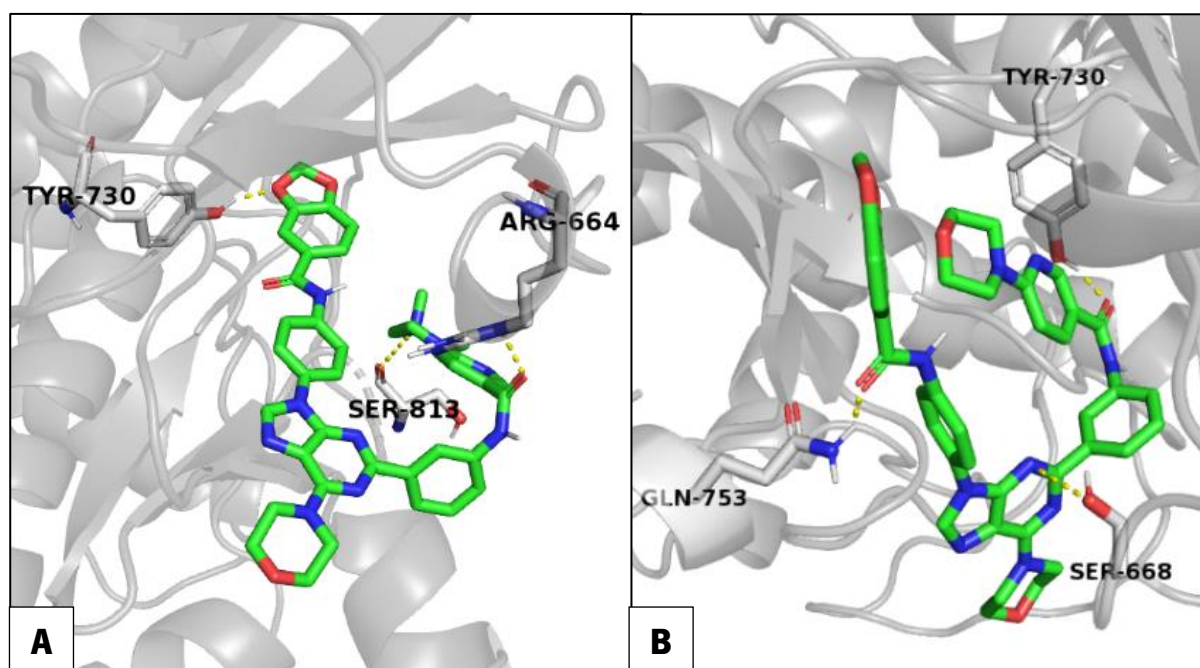


Figure 32 Interaction-binding mode of docked ligands **16.3b** (A) and **16.3c** (B) (coloured by element (green-carbon, blue-nitrogen, red-oxygen and white-hydrogen) on the active site of PI3K α (cartoon in grey). Image generated in PyMOL.

Next, the interaction of the ligands **17.2e**, **17.3b** and **17.3e** with PI3K α is displayed, respectively for the ligand **17.2e** in Figure 33 A, and the ligands **17.3b** and **17.3e** in Figure 33 B. Although very similar in structure, the class change seems to matter in the conformation adopted by the ligand when interacting with PI3K α . This is because, despite the common interaction (HBA in N7) of the

3 ligands with the SER-748 residue, ligand **17.2e** presents a conformation different from the two shown in Figure 33 B. These ligands (**17.3b** and **17.3e**) share the same class and vary only in the R² group, overlapping optimally.

Additionally, in Figure 33 A, the interactions of the ligand **17.2e** with the residue HIS-749, as HBD, and with the residue VAL-745, as HBA, are identified.

On the other hand, in Figure 33 B, an optimal overlap between ligands **17.3b** and **17.3e** can be observed. It should be noted that both R² substituent groups are quite voluminous, which supports the assumption made earlier for the non-overlap of the ligands in Figure 32. Here, in addition to the interaction already mentioned with the SER-748 residue, a HBD with the residue SER-668 and HBA with residues SER-667, LYS-696, TYR-730 AND ASP-827 are established with the target by both ligands.

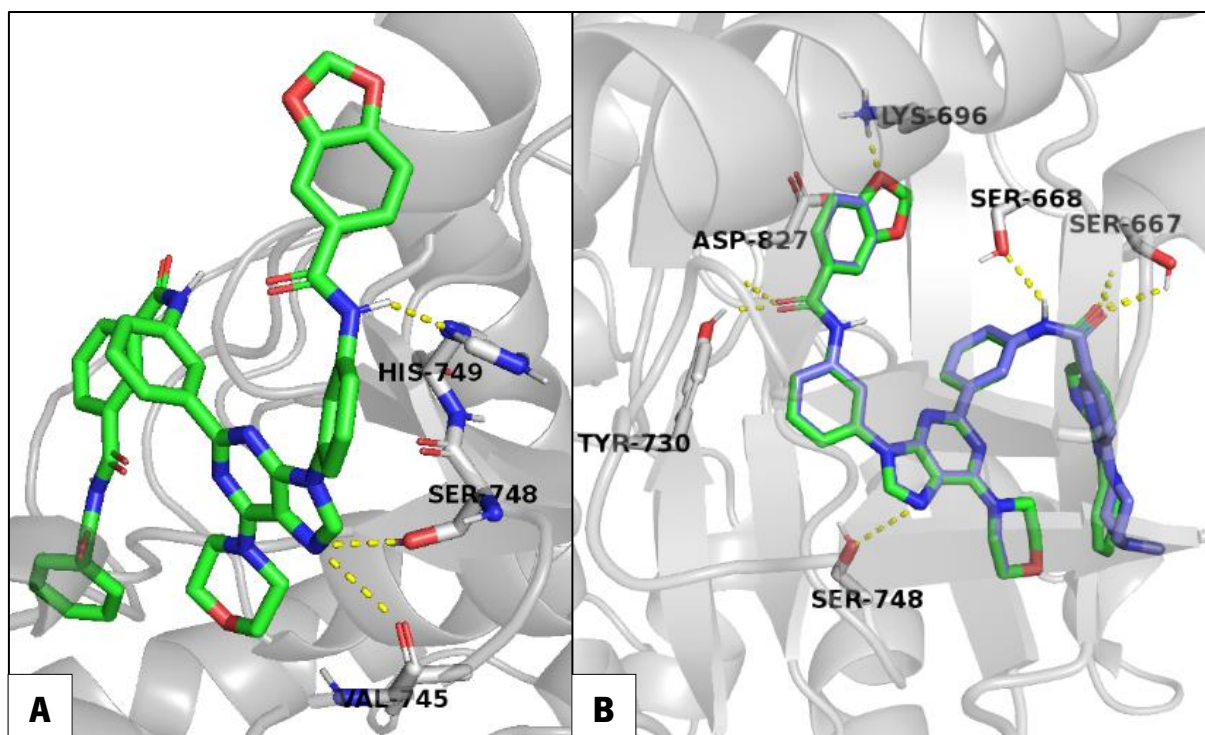


Figure 33 Interaction-binding mode of docked ligands **17.2e** (A) and overlapped ligands **17.3e** (B) (coloured by element (green-carbon, blue-nitrogen, red-oxygen and white-hydrogen) and **17.3b** (B) (coloured by element (purple-carbon, blue-nitrogen, red-oxygen and white-hydrogen) on the active site of PI3K α (cartoon in grey). Image generated in PyMOL.

Focusing now on the *gamma* isoform, the representation of the selected ligands clustered on the active site of the receptor (Figure 34) demonstrates, similarly to what happens in PI3K α , an optimal adaptation of the ligands' conformation to the cavity where the catalytic active centre of this isoform is located.

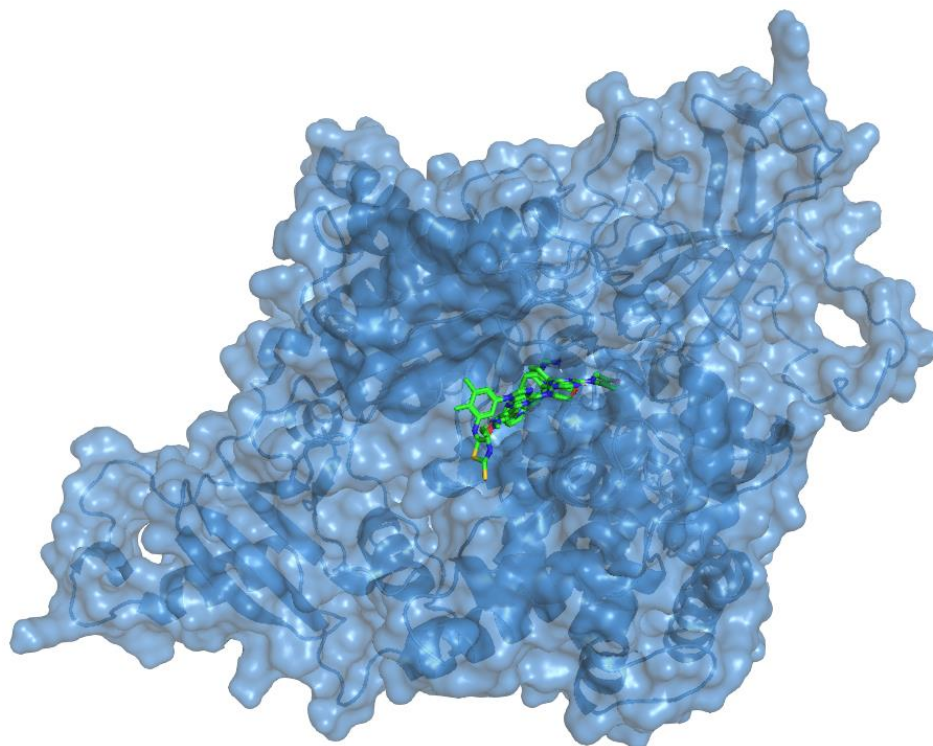


Figure 34 Overlay of the selected docked ligands for PI3K γ (coloured by element (green-carbon, blue-nitrogen, red-oxygen, yellow-sulphur and white-hydrogen) on the receptor's active centre (both surface and cartoon in blue). Image generated in PyMOL.

Looking now at the particular interactions of the 4 filtered ligands, it can be seen that there is an optimal overlap between ligands **1.1b** and **1.1c** (Figure 35 A), and ligands **5.1a** and **21.3a** (Figure 35 B) in the active centre of PI3K γ .

Overall, for PI3K γ , a consistent interaction is found between the class 1 ligands (**1.1b**, **1.1c** and **5.1a**) with the residues SER-664 and ASP-822. In the case of the ligands **1.1b** and **1.1c**, the interaction with the serine residue is established at N1 (HBA), whereas in ligand **5.1a**, the interaction is established by the protonated amino group (**a**) (HBD). On the other hand, the interaction with the aspartate residue occurs for ligands **1.1b** and **1.1c** simultaneously with the carbonyl group as HBA and the NH of the amide as HBD, for distinct groups of the same residue. As for the ligand **5.1a**, only one interaction occurs with the carbonyl group, which is HBA for ASP-822.

Given the structural similarities between the ligands of class 1, an overlap would be expected, which does not occur for ligand **5.1a**. This may be since this last ligand has a more voluminous R¹ group that can't fit properly the pocket of the protein, which causes it to slightly alter its conformation, which is common to larger ligands (**21.3a**) (Figure 35 B).

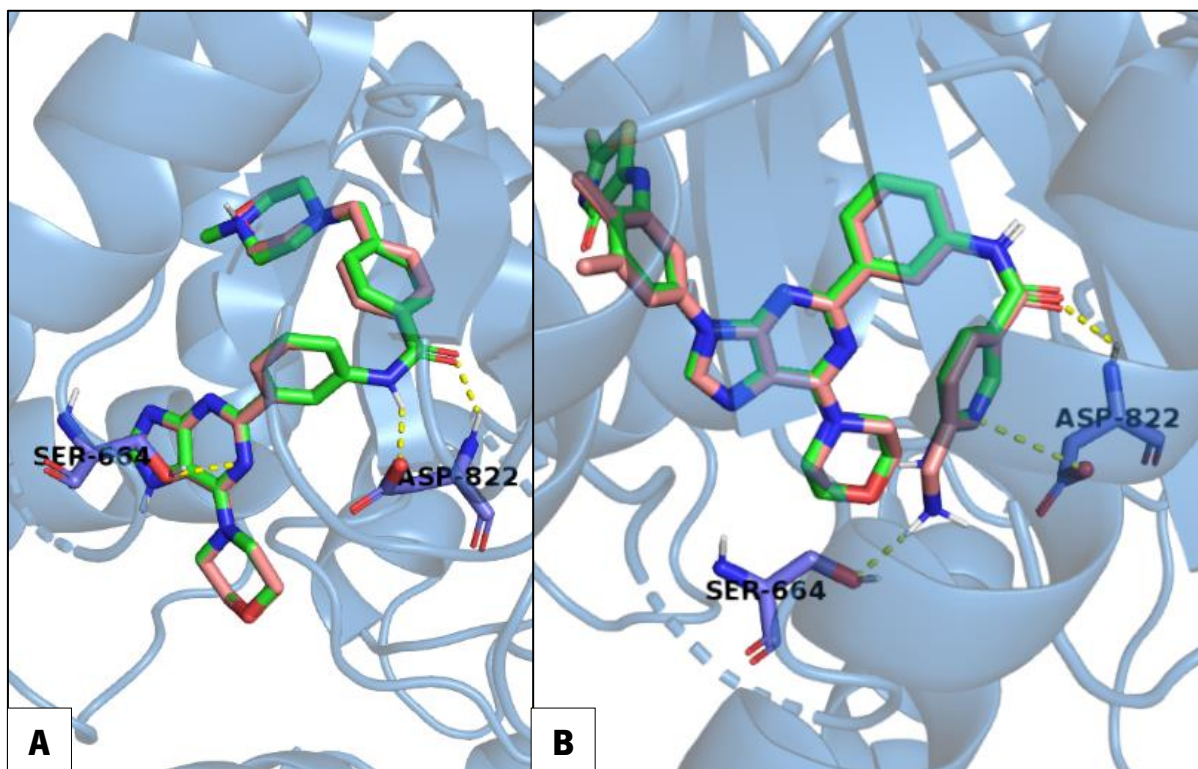


Figure 35 Interaction-binding mode of docked overlapped ligands **1.1b** and **1.1c** (A) and overlapped ligands **5.1a** and **21.3a** (B) on the active site of PI3K γ (cartoon in blue). Ligands **1.1b** and **21.3a** are coloured by element (green-carbon, blue-nitrogen, red-oxygen, yellow-sulphur and white-hydrogen), while ligands **1.1c** and **5.1a** elements' are (orange-carbon, blue-nitrogen, red-oxygen and white-hydrogen). Images generated in PyMOL.

Finally, since the $\Delta G_{\text{binding}}$ obtained for the ligand **21.3a** was the lowest among all the selective ligands for PI3K γ ($\Delta G_{\text{binding}} = -12.1$ Kcal/mol), a higher amount of polar interactions were expected than the ones visible in Figure 35 B.

Thus, in Figure 36 A the mode of interaction of this ligand with the residues of the active centre of PI3K γ is represented. In this figure, it is only possible to witness a polar interaction between the ligand and the aspartate residue, which is a common interaction to the rest of the ligands presented in Figure 35 (ASP-822).

Given the nature of the visualization program used (PyMOL), lesser common interactions such as π - π stacking interactions are not easily and directly identified. For this reason, AutoDock Tools (ADT) was used, where it was found that the π - π stacking interaction does indeed occur between the aromatic ring of the R¹ group and the TRP-670 residue (Figure 36 B).

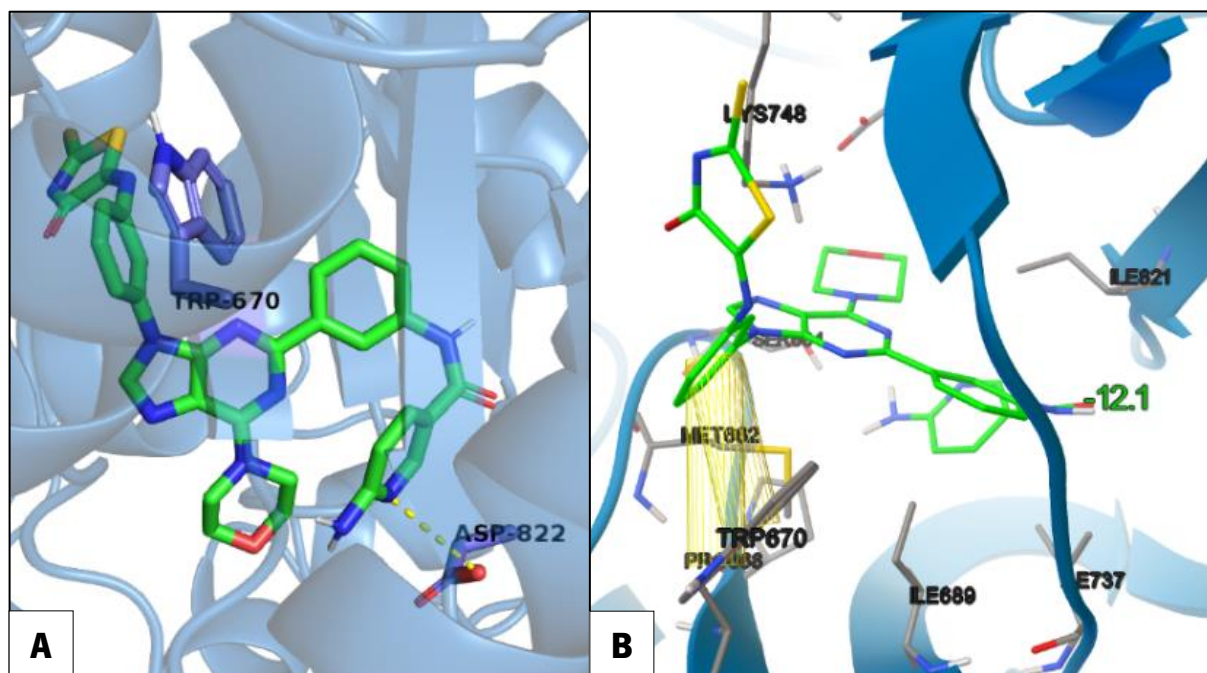


Figure 36 Interaction-binding mode of docked ligand **21.3a** in PyMOL (A) and in ADT (B) on the active site of PI3K γ (cartoon in blue). Ligand **21.3a** is coloured by element (green-carbon, blue-nitrogen, red-oxygen, yellow-sulphur and white-hydrogen). Image A generated in PyMOL and image B generated in ADT.

Summary

In review, this chapter presented the results from a Virtual Screening of 661 ligands, of which a total of 68 selective ligands were found (60 for PI3K α and 8 for PI3K γ). These results are in agreement with the information reported in the literature for ligands with this type of scaffold [26], [71].

Additionally, using statistical tools, some patterns were found between the affinity results and some physicochemical properties of the ligands, from both a global perspective, as well as a more specific, for the selective ligands. This study allowed the identification of properties on which $\Delta G_{\text{binding}}$ is most dependent in the 4 isoforms, such as the number of HBA, LogP, Mw and Rf. Additionally, a pattern was found regarding the volume of the R¹ group and protonation capacity of the R² group within the ligands selective for the *alpha* isoform in the PCA.

Finally, visualization tools were used to explore and detail the binding sites that the selective ligands establish with both PI3K α and PI3K γ . The most common polar interactions take place at the active centre of PI3K α with the amino acids TYR-730, SER-668, SER-748 and ASP-827. In the case of PI3K γ , in addition to the polar interactions of this isoform's selective ligands with the residues SER-664 and ASP-822, an additional π - π stacking interaction can be identified with TRP-670 (ligand **21.3a**).

Chapter 3

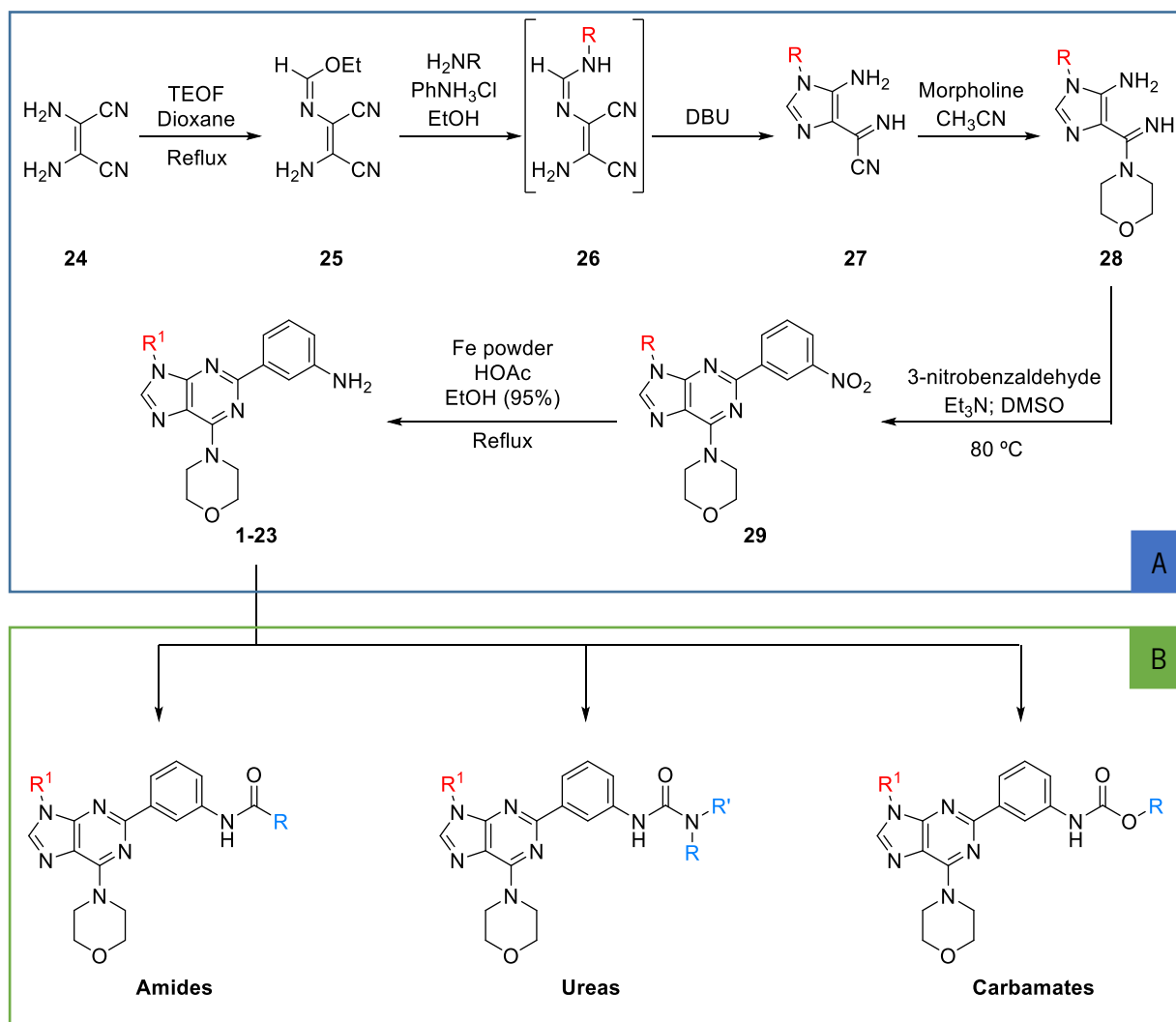
Chemical Synthesis
RESULTS AND DISCUSSION

Introduction

To synthesize some of the compounds submitted to the virtual screening reported in chapter **2**, an extensive synthetic route was carried out, which was divided fundamentally into two parts: Synthesis of starting reagents (**3.1**) and synthesis of final products (**3.2**).

The synthesis of starting reagents contemplates the preparation of new 2-(3-aminophenyl)-purine derivatives (**1-23**) through a multi-step synthetic approach (Scheme 2 A). Subsequently, a new series of different amides, ureas and carbamates were synthesized from 2-(3-aminophenyl)-purine derivatives in **3.2**, via different methodologies (Scheme 2 B).

All the compounds not yet reported were also characterized by physical and spectroscopic methods.



Scheme 2 Schematic representation of the synthetic approach used for the synthesis of 2-(3-aminophenyl)-purine derivatives (**1-23**) (**A**), and the general structure of the final synthesized products (**B**).

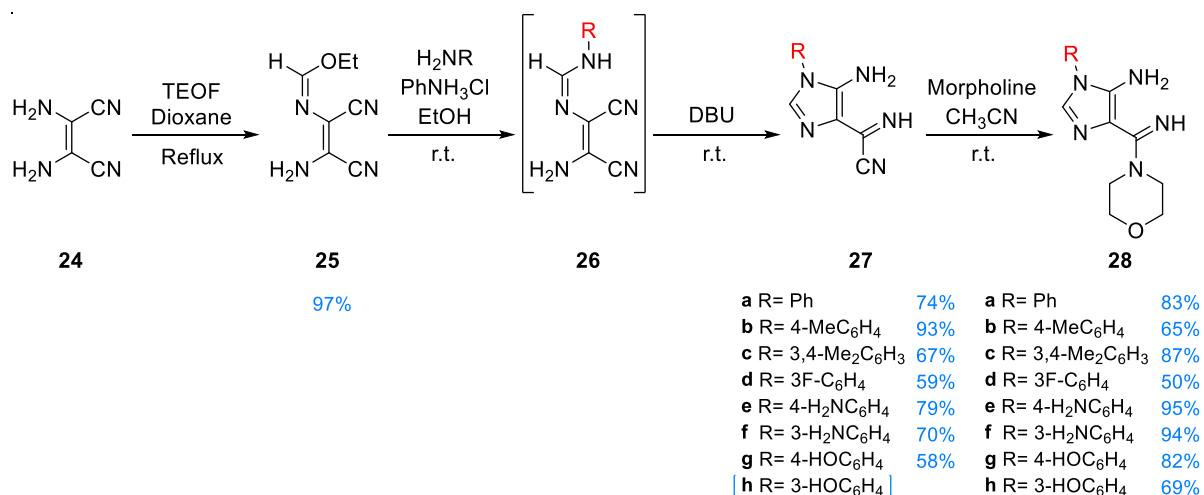
3.1. Synthesis of starting reagents

The synthesis of the starting reagents is divided into two distinct parts. Initially, the work is focused on the synthesis and the physical and spectroscopic characterization of a series of 5-amino-4-amidino-imidazoles **28**.

Then, a set of 2-(3-nitrophenyl)-purine derivatives **29** was synthesized from **28**, where, in the presence of an amine group in **R**¹, protection was necessary by using acylation agents. Finally, the 2-(3-aminophenyl)-purine derivatives (**1-23**) were synthesized by reduction of the nitro group of **29** and used as a starting point for the synthesis of the final products reported in this work. All the new purine derivatives **29** and (**1-23**) were also synthesized and characterized by physical and spectroscopic methods.

3.1.1. Synthesis of 5-amino-4-amidino-imidazoles (28)

The synthesis of the starting reagents (Scheme 3) begins with the synthesis of ethyl (*Z*)-*N*[(*Z*)-2-amino-1,2-dicyanovinyl]formimidate **25** from the commercial reagent **24** (diaminomaleonitrile) and triethyl orthoformate (TEOF) in dioxane under reflux conditions. This reaction has been previously optimized and reported with excellent yields [73].



Scheme 3 Global reaction scheme for the synthesis of 5-amino-4-amidino-imidazoles **28**. Representation of all reaction steps, synthesized compounds and the best-obtained yields highlighted in blue.

Subsequently, imidazoles **27** were generated by the reaction of **25** with aromatic amines (H₂NR) in ethanol under acid catalysis, using anilinium chloride (PhNH₃Cl) as a catalyst, applying previously reported conditions [74], [75]. The reactions were followed by thin-layer chromatography (TLC), and upon the disappearance of **25**, DBU was added. A solution resulted, from which products **27a-g** precipitated,

and were later filtered and washed with cold ethanol and diethyl ether, with good yields. Compound **27h** did not precipitate from the reaction mixture. Hence, the solvent was evaporated, originating a viscous black oil, to which acetonitrile and 4 equivalents of morpholine were added, at room temperature. The product **28h** was isolated after 26 hours of reaction, at room temperature and efficient magnetic stirring. The remaining products **28a-g**, were obtained by reaction of the respective precursors **27** with morpholine in acetonitrile, according to procedures already described in the literature, and were isolated with good to excellent yields [76].

All the new compounds were characterized by physical (melting point (m.p.)) and spectroscopic (IR, ^1H and ^{13}C NMR) methods (Section **3.1.2.**).

3.1.2. Characterization of 5-amino-4-amidino-imidazoles (**28**)

3.1.2.1. Physical and analytical characterization

The physical and analytical data presented in Table 7 is relative to the newly synthesized 5-amino-4-amidino-imidazoles (**28**) that have not yet been reported in the literature. The elemental analysis and mass spectrometry data could not be acquired until the deadline of this dissertation. For this reason, the values presented for these components are only theoretical.

Table 7 Physical and theoretical analytical data of the newly synthesized 5-amino-4-amidino-imidazoles (**28**).

Compound	m.p. (°C)	Molecular Formula*	Molecular Weight (g/mol)*	Elemental analysis (%) (Expected values)*		
				C	H	N
28c	175 - 176	C ₁₆ H ₂₁ N ₅ O	299.38	64.19	7.07	23.39
28d	142 - 144	C ₁₄ H ₁₆ FN ₅ O	289.31	58.12	5.57	24.21
28e	178 - 179	C ₁₄ H ₁₈ N ₆ O	286.34	58.73	6.34	29.35
28f	191 - 192	C ₁₄ H ₁₈ N ₆ O	286.34	58.73	6.34	29.35
28g	196 - 198	C ₁₄ H ₁₇ N ₅ O ₂	287.32	58.52	5.96	24.38
28h	190 - 192	C ₁₄ H ₁₇ N ₅ O ₂	287.32	58.52	5.96	24.38

* Data collected from ChemDraw software.

3.1.2.2. Infra-red spectroscopy (IR) characterization

In general, the identification of the structure of imidazoles (**28**) can be confirmed by the disappearance of the nitrile stretching band, which appears between 2260 and 2222 cm^{-1} , characteristic of the synthetic precursors **27** [74], [75], [77].

In addition, imidazoles (**28**) present between 3 and 6 bands of varying intensity between 3070 and 3441 cm^{-1} . These are typical of N-H and C-H bonds stretching bands (Table 8) [77].

Finally, 3 to 5 bands, overall with strong intensity, are visible between 1700 and 1500 cm^{-1} in Table 8. These bands correspond to the stretching vibrations of C=N and C=C bonds as well as N-H bending [77].

Table 8 IR spectroscopic data (Nujol/ cm^{-1}) for the newly synthesized 5-amino-4-amidino-imidazoles (**28**).

Compound	3500-2500 cm^{-1}	1700-1500 cm^{-1}
28c	3377, 3285 (w), 3119 (s)	1624, 1595 (s), 1586 (s), 1548, 1515 (s)
28d	3338 (w), 3257, 3140, 3092, 3070	1613 (s), 1595 (s), 1574 (s), 1533 (s)
28e	3441 (w), 3377 (w), 3322, 3288, 3196, 3113	1626 (s), 1609 (s), 1586 (s), 1550, 1521 (s)
28f	3403 (w), 3361 (w), 3285 (w), 3189, 3136 (w)	1665 (w), 1612, 1586 (s), 1545 (w), 1519 (s)
28g	3400, 3299 (w), 3263 (w), 3161, 3115	1601, 1576, 1547, 1518 (s)
28h	3404 (w), 3330 (w), 3252, 3117 (w)	1580 (s), 1546, 1514

Weak (w) and strong (s) intensity peaks are denoted after their respective value. The remaining peaks have medium intensity.

3.1.2.3. ^1H and ^{13}C NMR spectroscopy characterization

Table 9 shows the ^1H -NMR spectroscopic data of imidazoles **28**, which overall, for their base structure present a singlet corresponding to the H-C₂ proton, between 7.18 and 7.45 ppm. For the amine group, a broad singlet (s) is present between 4.7 and 6.7 ppm. To this singlet, in the case of compounds **28e** and **28f**, there is an additional integration of 2 protons corresponding to the amine groups in the substituent group R¹. Additionally, in the base structure, two triplets (t) are found with integration for 4 protons each, corresponding to the protons of the morpholine ring. As expected, given the higher electronegativity of the oxygen atom, there is a larger shift for the H-C₈ protons, between 3.66 and 3.67 ppm, while the H-C₇ protons, adjacent to the nitrogen atom, present a smaller chemical shift, between 3.30 and 3.34 ppm.

The ^{13}C -NMR spectroscopic data of imidazoles **28** is presented in Table 10. HMQC shows the direct correlation between the protons H-C₂ and C₂, whose chemical shifts vary between 129.81 and 130.49 ppm. In addition, H-C₇ and C₇, as well as H-C₈ and C₈, also correlate and present chemical shifts varying between 47.13 and 47.28 ppm and 66.06 and 66.12 ppm, respectively. The same happens for the protons of the R¹ group.

With HMBC it is possible to identify the chemical shifts of C₄, C₅ and C_i of the R¹ group, from the correlation from H-C₂, once these are 3-bond apart. Similarly, by this same method, it is also possible to identify C₆ from the coupling with H-C₇.

Table 9 ¹H-NMR spectroscopic data (400 MHz, DMSO-d₆) for the new compounds **28**.

Compound	Base structure	R ¹	R ¹ - H	Base Structure - H
28c			7.29 (d, 1H, <i>J</i> = 8.0 Hz, H _m) 7.25 (t, 1H, <i>J</i> = 2.0 Hz, H _{o'}) 7.17 (dd, 1H, <i>J</i> = 8.0, 2.0 Hz, H _o) 2.27 (s, 3H, Me _m) 2.26 (s, 3H, Me _p)	7.31 (s, 1H, H ₂) 4.7 – 6.7 (br.s, 2H, NH ₂) 3.67 (t, 4H, <i>J</i> = 4.8 Hz, H ₈) 3.33 (t, 4H, <i>J</i> = 4.8 Hz, H ₇)
28d			7.58 (dt, 1H, <i>J</i> = 8.4, 6.4 Hz, H _m) 7.44 (dt, 1H, <i>J</i> = 10.0, 2.4 Hz, H _{o'}) 7.36 (ddd, 1H, <i>J</i> = 8.4, 2.4, 0.8 Hz, H _o) 7.30 (tdd, 1H, <i>J</i> = 8.4, 2.4, 0.8 Hz, H _p)	7.45 (s, 1H, H ₂) 5.2 – 6.2 (br.s, 2H, NH ₂) 3.66 (t, 4H, <i>J</i> = 4.8 Hz, H ₈) 3.32 (t, 4H, <i>J</i> = 4.8 Hz, H ₇)
28e			7.04 (d, 2H, <i>J</i> = 8.4 Hz, H _o) 6.66 (d, 2H, <i>J</i> = 8.4 Hz, H _m) 4.7 – 6.0 (br.s, 2H, NH ₂) *	7.18 (s, 1H, H ₂) 3.66 (t, 4H, <i>J</i> = 4.4 Hz, H ₈) 3.30 (t, 4H, <i>J</i> = 4.4 Hz, H ₇) 4.7 – 6.0 (br.s, 2H, NH ₂) *
28f			7.15 (d, 1H, <i>J</i> = 8.0 Hz, H _m) 6.62 (ddd, 1H, <i>J</i> = 8.0, 2.0, 0.8 Hz, H _o) 6.59 (t, 1H, <i>J</i> = 2.0 Hz, H _{o'}) 6.53 (ddd, 1H, <i>J</i> = 8.0, 2.0, 0.8 Hz, H _p) 5.4 – 6.0 (br.s, 4H, NH ₂) *	7.28 (s, 1H, H ₂) 3.66 (t, 4H, <i>J</i> = 4.8 Hz, H ₈) 3.31 (t, 4H, <i>J</i> = 4.8 Hz, H ₇) 5.4 – 6.0 (br.s, 4H, NH ₂) *
28g			7.20 (d, 2H, <i>J</i> = 8.8 Hz, H _o) 6.86 (d, 2H, <i>J</i> = 8.8 Hz, H _m)	7.27 (s, 1H, H ₂) 3.66 (t, 4H, <i>J</i> = 4.8 Hz, H ₈) 3.34 (t, 4H, <i>J</i> = 4.8 Hz, H ₇)
28h			7.30 (t, 1H, <i>J</i> = 8.0 Hz, H _m) 6.77 – 6.85 (m, 3H, H _o + H _{o'} + H _p)	7.36 (s, 1H, H ₂) 3.66 (t, 4H, <i>J</i> = 4.4 Hz, H ₈) 3.34 (t, 4H, <i>J</i> = 4.4 Hz, H ₇)

* Overlay of the signals from the amine groups of R¹ and the base structure of imidazoles **28**.

Rational design and synthesis of novel selective PI3K inhibitors for cancer therapy

Table 10 ^{13}C -NMR spectroscopic data (100 MHz, DMSO-d_6) for the new compounds **28**.

Compound	Base structure	R^1	R^1	Base Structure					
				C_2	C_4	C_5	C_6	C_7	C_8
28c			137.90 ($\text{C}_{\text{m}'}$) 136.33 (C_{p}) 132.45 (C_{i}) 130.47 (C_{m}) 125.66 ($\text{C}_{\text{o}'}$) 122.02 (C_{o}) 19.33 (Me_{m}) 18.93 (Me_{p})	129.86	114.27	139.41	163.23	47.13	66.07
28d			163.58, 161.14 (d, $J = 244$ Hz, $\text{C}_{\text{m}'}$) 136.42, 136.32 (d, $J = 10$ Hz, C_{i}) 131.55, 131.46 (d, $J = 9$ Hz, C_{m}) 120.79, 120.76 (d, $J = 3$ Hz, C_{o}) 114.99, 114.78 (d, $J = 21$ Hz, C_{p}) 112.26, 112.01 (d, $J = 25$ Hz, $\text{C}_{\text{o}'}$)	130.06	114.74	139.29	163.07	47.17	66.09
28e			148.99 (C_{p}) 126.13 (C_{o}) 122.66 (C_{i}) 114.10 (C_{m})	130.31	113.76	139.51	163.55	47.25	66.12
28f			150.13 ($\text{C}_{\text{m}'}$) 135.45 (C_{i}) 130.14 (C_{m}) 113.49 (C_{o}) 111.47 (C_{p}) 109.48 ($\text{C}_{\text{o}'}$)	129.81	113.95	139.26	163.33	47.22	66.11
28g			158.88 (C_{p}) 126.54 (C_{o}) 124.79 (C_{i}) 116.32 (C_{m})	130.49	113.26	139.91	162.97	47.28	66.06
28h			159.16 ($\text{C}_{\text{m}'}$) 135.65 (C_{i}) 130.52 (C_{m}) 115.36 (C_{p}) 114.52 (C_{o}) 111.74 ($\text{C}_{\text{o}'}$)	130.13	113.60	139.63	162.79	47.28	66.06

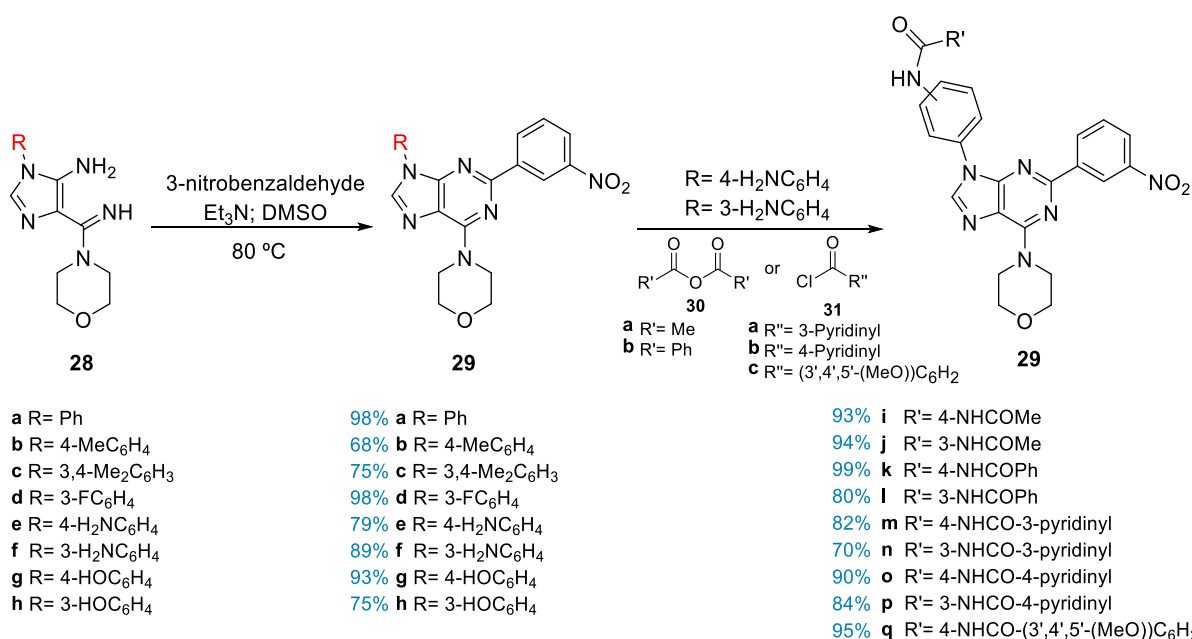
3.1.3. Synthesis of the purine derivatives (29) and (1-23)

Many synthetic methodologies have been reported to incorporate several functional groups in the purine core [78]. However, our research group has developed a mild, simple and inexpensive synthetic approach to purine derivatives having different substituents in N₉ [79]. Herein we report the synthesis of novel 2-(3-nitrophenyl)-purine derivatives (**29a-h**), from the reaction of 5-amino-4-amidino-imidazoles (**28**) with 3-nitrobenzaldehyde. Additionally, **29e** and **29f** reacted with different acylation agents to give compounds **29i-q**. Finally, **29a-d** and **29i-q** were converted to the corresponding amino derivatives (**1-23**) using an optimised iron powder/acetic acid methodology.

All the new compounds were characterized by physical (melting point (m.p.)) and spectroscopic (IR, ¹H and ¹³C NMR) methods (Section 3.1.4.).

3.1.3.1. Synthesis of 2-(3-nitrophenyl)-purine derivatives (29)

The derivatives **29a-h** were obtained using experimental conditions previously optimised in the research group [79]. As shown in Scheme 4, the imidazoles **28** reacted with 3-nitrobenzaldehyde using an excess of triethylamine (Et₃N) as base and the minimum amount of DMSO as solvent, at 80°C. The reactions were controlled by TLC, and upon the disappearance of the starting reagent **28**, after 16 hours to 3 days, the products were isolated in good to excellent yields.



Scheme 4 Global reaction scheme for the synthesis of 2-(3-nitrophenyl)-purine derivatives **29** from 5-amino-4-amidino-imidazoles **28**, followed by the acylation of **29e** and **29f** with different acylation agents (**30** and **31**). Representation of all reaction steps, synthesized compounds and the best obtained yields highlighted in blue.

Overall, the compounds **29a-h** were obtained from clean reactions, however, when the more insoluble products (**29b** and **29c**) precipitated from the reaction mixture, the magnetic stirring was no longer efficient and the reaction became slower and difficult to follow. In such cases, more solvent was added to the reaction mixture and the reaction was left to finish. This factor, as expected, led to increased reaction times. Also, in the rare cases, when the presence of starting reagent in small percentages was identified, by ¹H-NMR, the solid containing the mixture was recrystallized from ethanol.

3.1.3.2. Acylation of 9-(amino-aryl) purine derivatives

The second part of Scheme 4 depicts the acylation reactions with compounds **29e** and **29f** as starting reagents. These compounds have in the group R a primary amine in positions 4 and 3, respectively. So, the synthesis of the derivatives **29i-q** occurred by the reaction of **29e** and **29f** with anhydrides (**30**) and acyl chlorides (**31**), under different reaction conditions.

Firstly, acylation with acetic (**30a**) and benzoic (**30b**) anhydrides took place in a very straightforward way and led to the relatively fast generation of the desired products (**29i-l**) with very good to excellent yields. These reactions were carried out in DMSO with 1.5 to 1.7 molar equivalents of anhydride **30** and triethylamine (Et₃N), taking 2 to 4.5 hours to be completed.

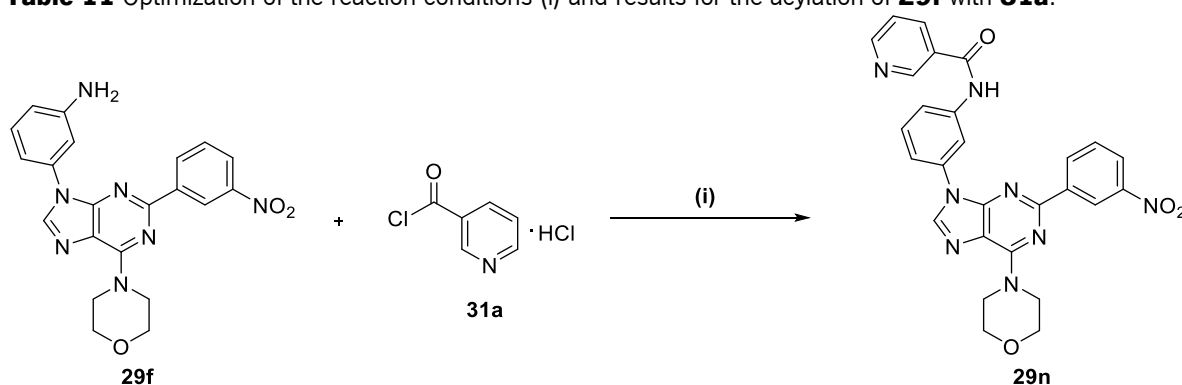
In contrast, acylation with acyl chlorides **31** was relatively difficult. Due to the strong reactivity of these compounds combined with the low solubility of the starting reagents **29e-f**, these reactions were rather challenging. Thus, it was necessary to establish the best reaction conditions for the synthesis of the derivatives **29m-q** (Tables 11-13).

Firstly, attempts were made to establish the most suitable conditions for the acylation of compound **29f** with the acyl chloride **31a**. Table 11 shows the optimisation attempts that were carried out, all under anhydrous conditions and at 80°C. First, the acylation of **29f** was tested with only 1.05 eq. of **31a** and 2.1 eq. of triethylamine in dry acetonitrile (Table 11 - Entry 1). After 2.5 hours a solid was isolated with a mixture of starting reagent **29f** (75%) and product **29n** (25%). With this test, acetonitrile proved not to be a suitable solvent because of the low solubility of the starting reagent. Therefore, solubility tests were performed with several non-nucleophilic solvents and **29f** was found to be more soluble in both dioxane and THF than the other solvents.

For this same reason, an assay was performed in dry dioxane, this time with an excess of base to facilitate the nucleophilic attack (Table 11 - Entry 2). After 2 hours, a solid with the same mixture as in the previous attempt was obtained. However, this time the desired product **29n** was in a greater percentage in the mixture (65%). In this attempt, despite a higher solubility of **29f**, it was found that the

acylation agent **31a** was poorly dissolved. For this reason, a mixture of solvents (dioxane and acetonitrile) was used in the following trial (Table 11 - Entry 3). This allowed both reagents **29f** and **31a** to be in solution at 80°C. After 2 hours, the solid suspension was filtered and identified as the pure product **29n**. However, TLC of the mother liquor showed that the reaction had not been yet completed. For this reason, the concentration of the reaction mixture was increased and the reaction time was prolonged (Table 11 - Entry 4). After 6.5 hours the reaction was finished. Based on the proportions of the components in the mixture obtained, and taking into account that the mother liquor also contained a mixture of starting reagent and product, it was decided to increase the number of equivalents of **31a** to 2 eq. (Table 11 - Entry 5). After 12 hours the pure product **29n** was isolated with a good yield.

Table 11 Optimization of the reaction conditions (i) and results for the acylation of **29f** with **31a**.



Entry	Reaction Conditions (i)	Results ^{a)}
1	29f (71.5 mg, 0.17 mmol), 31a (1.05 eq., 32.0 mg, 0.18 mmol) Et ₃ N (2.1 eq., 50.0 μL, 0.36 mmol) Dry acetonitrile (8 mL), 80°C, N ₂ , 2.5 h	29f (75%) + 29n (25%) (86.0 mg)
2	29f (0.57 g, 1.36 mmol), 31a (1.3 eq., 0.32 g, 1.77 mmol) Et ₃ N (6 eq., 1.14 mL, 8.18 mmol) Dry dioxane (10 mL), 80°C, N ₂ , 2 h	29f (35%) + 29n (65%) (0.53 g)
3	29f (64.0 mg, 0.15 mmol), 31a (1.2 eq., 32.5 mg, 0.18 mmol) Et ₃ N (2.5 eq., 53.0 μL, 0.38 mmol) Dry dioxane : Dry acetonitrile (1 mL : 1 mL), 80°C, N ₂ , 2 h	29n (43.4 mg, 0.08 mmol, 55%) ^{b)}
4	29f (1.00 g, 2.41 mmol), 31a (1.2 eq., 0.51 g, 2.89 mmol) Et ₃ N (2.5 eq., 0.84 mL, 6.01 mmol) Dry dioxane : Dry acetonitrile (2 mL : 2 mL), 80°C, N ₂ , 6.5 h	29f (4.5%) + 29n (95.5%) (0.60 g) ^{b)}
5	29f (67.0 mg, 0.16 mmol), 31a (2 eq., 57.0 mg, 0.32 mmol) Et ₃ N (6 eq., 0.13 mL, 0.96 mmol) Dry dioxane : Dry acetonitrile (1 mL : 1 mL), 80°C, N ₂ , 12 h	29n (58.3 mg, 0.11 mmol, 70%)

a) By ¹H-NMR spectroscopy.
b) The solution obtained after the filtration of the solid contained a mixture of **29f** and **29n**. (Evidenced by TLC).

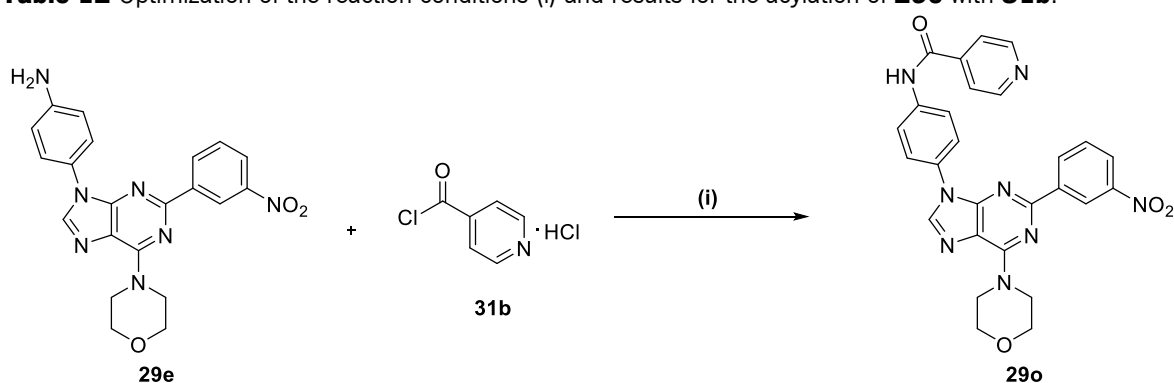
These last optimized reaction conditions were tested in the acylation of compound **29e** with the acylating agent **31b** (Table 12 - Entry 1). However, compound **29e** proved to be less soluble than **29f** in dioxane. For this reason, the proportion of the solvent mixture was changed so that, when heated, the

reagent was solubilised. Under these conditions, the pure product **29o** was obtained with a good yield (78%). On the other hand, it was found that the reaction time increased considerably.

Thus, the base was changed in order to check whether there was any change in the reaction time (Table 12 - Entry 2). So, the triethylamine was replaced by 4-(dimethylamino)-pyridine (DMAP), but the reaction time increased by 3.5 hours and the yield dropped to 53%.

Finally, the temperature of the reaction was increased to 100°C, still using DMAP as a base (Table 12 - Entry 3). This resulted in a faster reaction (5 h). In addition, there was a significant increase in the yield (90%).

Table 12 Optimization of the reaction conditions (i) and results for the acylation of **29e** with **31b**.



Entry	Reaction Conditions (i)	Results ^{a)}
1	29e (0.13 g, 0.30 mmol), 31b (2.15 eq., 0.12 g, 0.65 mmol) Et ₃ N (5 eq., 0.21 mL, 1.50 mmol) Dry dioxane : Dry acetonitrile (3 mL : 2 mL), 80°C, N ₂ , 24 h	29o (0.12 g, 0.24 mmol, 78%)
2	29e (0.11 g, 0.27 mmol), 31b (2 eq., 97.0 mg, 0.53 mmol) DMAP (4 eq., 0.13 g, 1.06 mmol) Dry dioxane : Dry acetonitrile (4 mL : 2 mL), 80°C, N ₂ , 27.5 h	29o (73.0 mg, 0.14 mmol, 53%) ^{b)}
3	29e (0.16 g, 0.39 mmol), 31b (2.5 eq., 0.17 g, 0.97 mmol) DMAP (5 eq., 0.23 mL, 1.94 mmol) Dry dioxane : Dry acetonitrile (4 mL : 2 mL), 100°C, N ₂ , 5 h	29o (0.18 g, 0.35 mmol, 90%)

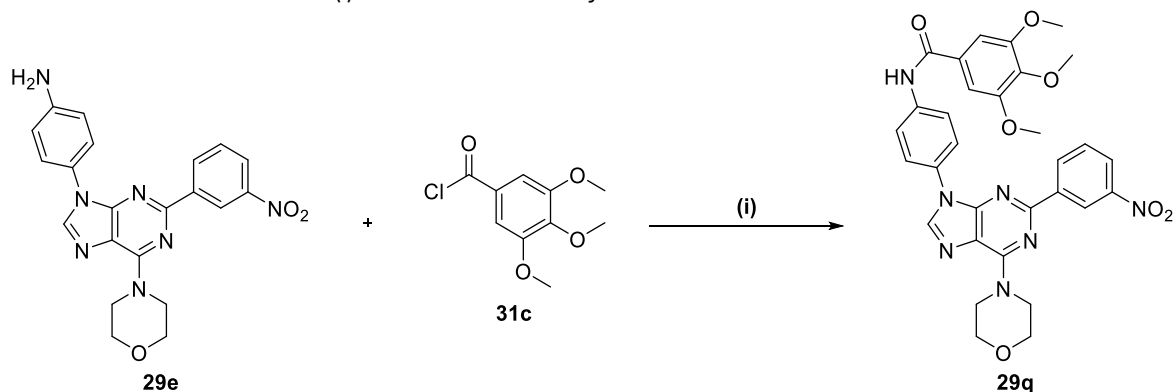
a) By ¹H-NMR spectroscopy.
b) The solution obtained after the filtration of the solid originated a viscous oil containing a mixture of DMAP and **29o**. (Evidenced by TLC).

After the reactions with acyl chlorides **31a** and **31b**, the acylation of compound **29e** with acyl chloride **31c** was tested. First, the reaction was tested under similar conditions as the previous reactions (Table 13- Entry 1). The reaction occurred rapidly, however, a mixture of 93% of the intended product **29q**, and 7% of starting reagent **29e** was obtained. Given the structural difference of the acylation agent, the reaction was tested only in one of the solvents. The acylation agent **31c** was shown to be quite soluble in dioxane and THF. For this reason, the reaction was tested in dry dioxane (Table 13 - Entry 2). As both reagents solubilised at room temperature it was decided to leave the reaction at this condition. After 5

hours, the TLC showed absence of starting reagent, however, the $^1\text{H-NMR}$ spectrum of the isolated solid showed traces of starting reagent **29e**.

Another attempt was made changing the base and solvent of the reaction (Table 13 – Entry 3). It was decided to use dry THF as solvent and a water-soluble base, as the final product precipitated very well in this solvent. The reaction mixture was then heated to speed up the reaction, however, even under heating, it proved to be slow. Nevertheless, the product **29q** was isolated pure with an excellent yield.

Table 13 Reaction conditions (i) and results for the acylation of **29e** with **31c**.



Entry	Reaction Conditions (i)	Results ^{a)}
1	29e (0.53 g, 1.27 mmol), 31c (1.25 eq., 0.36 g, 1.58 mmol) DMAP (3 eq., 0.34 g, 3.81 mmol) Dry dioxane : Dry acetonitrile (6 mL : 3 mL), 80°C, N ₂ , 2 h	29e (7%) + 29q (93%) (0.73 g)
2	29e (0.10 g, 0.24 mmol), 31c (1.1 eq., 61.0 mg, 0.26 mmol) DMAP (2 eq., 59.0 mg, 0.48 mmol) Dry dioxane (1.5 mL), r.t., N ₂ , 5 h	29e (traces) + 29q (0.17 g)
3	29e (0.37 g, 0.89 mmol), 31c (1.5 eq., 0.31 g, 1.34 mmol) K ₂ CO ₃ (3 eq., 0.37 g, 2.70 mmol) Dry THF (5 mL), 70°C, N ₂ , 28 h	29q (0.52 g, 0.85 mmol, 95%)

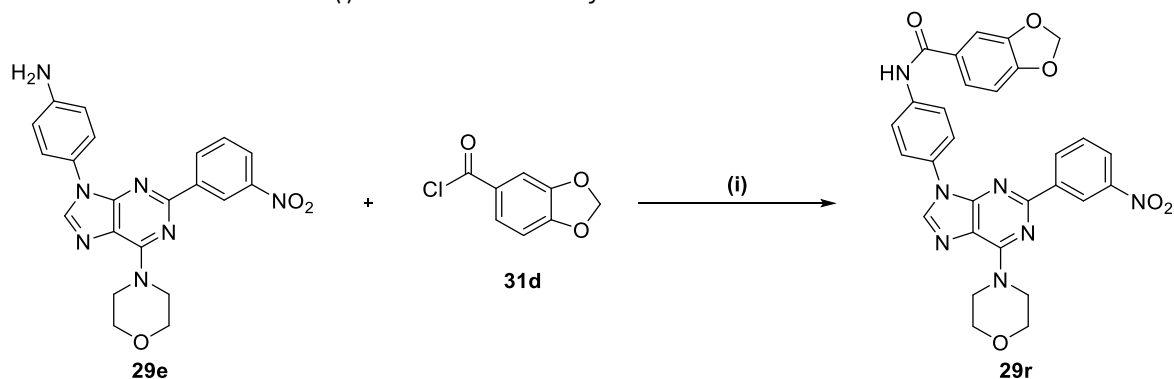
a) By $^1\text{H-NMR}$ spectroscopy.

Finally, Table 14 describes 5 attempts for the acylation of compound **29e** with the acylation agent **31d**. In all cases, the starting material **29e** was collected and no reaction occurred. Firstly, the conditions previously used in the acylation of **29e** with **31b** and **31c** were tested (Table 14 - Entries 1 and 2). After no reaction occurred, a new reaction attempt was left for 22 hours at 80°C in a mixture of dry dioxane and THF (Table 14 - Entry 3). Again, no reaction was observed. In all these 3 cases, **31d** seemed to never solubilise. For this reason, the same reaction was then carried out in DMSO, using K₂CO₃ as a base, but again without success (Table 14 - Entry 4).

As no trace of the desired product **29r** was found, information about the solubility and reactivity of the acylation agent **31d** was searched in the literature. Although little information was found, the reaction with this same reagent in benzene was reported [80]. Given the hazards associated with this solvent, an attempt was made with toluene as a solvent, due to its much lower toxicity (Table 14 - Entry

4) [81]. However, after 28.5 hours, no reaction occurred. Due to the restricted time, no further reaction conditions were tested and product **29r** was not synthesised.

Table 14 Reaction conditions (i) and results for the acylation of **29e** with **31d**.

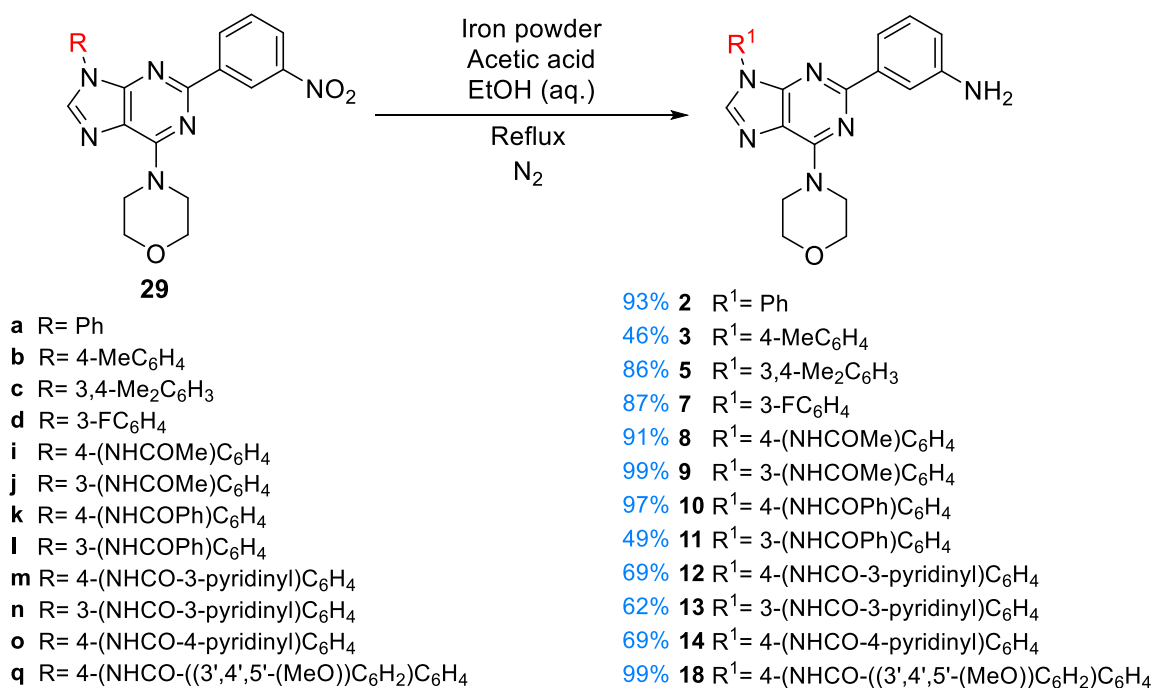


Entry	Reaction Conditions (i)	Results ^{a), b)}
1	29e (0.10 g, 0.25 mmol), 31d (1.25 eq., 57.2 mg, 0.31 mmol) DMAP (3 eq., 91.0 mg, 0.74 mmol) Dry dioxane : Dry acetonitrile (1 mL : 1 mL), 80°C, N ₂ , 2 h	No reaction
2	29e (0.12 g, 0.28 mmol), 31d (1.25 eq., 59.0 mg, 0.32 mmol) DMAP (3 eq., 0.10 g, 0.83 mmol) Dry dioxane (1 mL), 80°C, N ₂ , 6 h	No reaction
3	29e (0.35 g, 0.84 mmol), 31d (1.2 eq., 0.19 g, 1.01 mmol) K ₂ CO ₃ (1.3 eq., 0.15 g, 1.10 mmol) Dry dioxane : Dry THF (3 mL : 2 mL), 80°C, N ₂ , 22 h	No reaction
4	29e (25.4 mg, 0.06 mmol), 31d (1.25 eq., 14.04 mg, 0.08 mmol) K ₂ CO ₃ (2.5 eq., 21.0 mg, 0.15 mmol) DMSO (0.5 mL), 80°C, N ₂ , 20 h	No reaction
5	29e (0.13 g, 0.31 mmol), 31d (1.2 eq., 67.6 mg, 0.37 mmol) K ₂ CO ₃ (2 eq., 84.4 mg, 0.61 mmol) Toluene (4 mL), 80°C, N ₂ , 28.5 h	No reaction

a) By ¹H-NMR spectroscopy.
b) All assays resulted in the recovery of the starting material **29e**.

3.1.3.3. Reduction of 2-(3-nitrophenyl)-purine derivatives (29)

Very recently in the research group, a methodology based on the classic use of iron powder and acetic acid in an aqueous ethanol solution was reported [79]. However, this methodology required extractions in which large volumes of dichloromethane were used. Although this solvent can be recycled, an optimization of the protocol as well as of the reaction conditions was attempted to avoid this elaborate and time-consuming step. In scheme 5 the global conditions applied in the reduction of derivatives **29a-q** are represented, as well as the yields obtained by using this new methodology, whose optimization conditions are presented in Table 15.



Scheme 5 Global reaction scheme for the synthesis of 2-(3-aminophenyl)-purine derivatives **2-18** from the reduction of 2-(3-nitrophenyl)-purine derivatives **29**. Representation of the general conditions, synthesized compounds and the best obtained yields highlighted in blue.

In all the tests performed, the number of acetic acid equivalents was kept constant (20 eq.) while the number of iron powder equivalents and the proportion of ethanol:water were changed.

Firstly, the protocol reported in the research group for the reduction of compound **29i** was applied (Table 15 - Entry 1). After 4 hours of reaction, it was treated according to the described procedure, resulting in the isolation of the pure product **11** with a low yield (22%). In an attempt to accelerate the reaction, the number of iron equivalents was increased to 12 and at the same time, the proportion of ethanol in the aqueous solution was also increased to 80 % (Table 15 - Entry 2). In fact, the reaction was faster, however, in the isolation attempt, this time without resorting to extraction, it was found that there was inorganic material mixed with the product **11**. The organic material in this mixture was subsequently solubilised in THF and purified by flash chromatography.

The inorganic material isolated may have resulted from several factors, including the increased number of iron powder equivalents; excess of water in the aqueous ethanol solution; the waiting time after the addition of ammonia (NH₃ (aq)) to the reaction mixture and the inefficient saturation of the system with nitrogen. Because of these factors, in all subsequent reactions, an efficient saturation with nitrogen of the reaction system was performed, to avoid the formation of iron oxide, characterised by the

formation of an orange film on the walls of the reaction mixture flask. Also, this flask was kept closed for 12 to 18 hours after the addition of ammonia at the end of the following reactions.

In a third attempt, the use of 12 iron equivalents was maintained, but the percentage of ethanol in the aqueous solution was increased to 90% (Table 15 - Entry 3). According to TLC, all the starting reagent **29i** was converted to **11** after 3.5 hours. Thus, and applying the previously established conditions, the flask was left closed for 16 hours after the addition of ammonia. Two phases were observed in the flask after this time, a dark suspension at the bottom and a yellowish solution at the top. The content of the flask was then carefully filtered on diatomaceous earth and from the solution obtained, the organic solvent was evaporated and the solid was filtered off and identified as the pure product **11**. There was, however, one important detail in this reaction. During the diatomaceous earth filtration, the presence of some crystals in the retained layer was noted. This factor reveals that for a better yield a larger quantity of ethanol is necessary to guarantee that the largest possible amount of the product remains in solution.

Table 15 Reaction conditions and results for the reduction of **29i** and **29f**.

Entry	Reaction Conditions					Results ^{a)}
	Starting Material	Acetic acid (20 eq.)	Iron powder	Solvent	Time	
1	29i (0.10 g, 0.20 mmol)	(0.23 mL, 4.01 mmol)	8 eq. (90.0 mg, 1.60 mmol)	EtOH (70%) 30 mL	4 h	11 ^{b)} (0.02 g, 0.04 mmol, 22%)
2	29i (0.16 g, 0.31 mmol)	(0.35 mL, 6.17 mmol)	12 eq. (0.21 g, 3.70 mmol)	EtOH (80%) 66 mL	2.5 h	Inorganic Material ^{c)} (0.16 g)
3	29i (0.11 g, 0.22 mmol)	(0.25 mL, 4.37 mmol)	12 eq. (0.15 g, 2.63 mmol)	EtOH (90%) 45 mL	3.5 h	11 (0.05 g, 0.11 mmol, 49%)
4	29j (0.13 g, 0.29 mmol)	(0.33 mL, 5.72 mmol)	8 eq. (0.13 g, 2.29 mmol)	EtOH (95%) 70 mL	4.5 h	9 (0.12 g, 0.28 mmol, 97%)
5	29j (0.59 g, 1.27 mmol)	(1.46 mL, 25.48 mmol)	8 eq. (0.57 g, 10.20 mmol)	EtOH (95%) 200 mL	7.5 h	9 (0.55 g, 1.27 mmol, 99%)

a) By ¹H-NMR spectroscopy.
b) Application of the reported approach in the literature, with extraction.
c) Mixture of inorganic compounds and **11**. (Evidence by TLC).

In this same sense, the reaction conditions presented in Entries 4 and 5 of Table 15 were applied in all the following cases (8 iron powder equivalents and an aqueous solution of ethanol (95%)). These conditions made it possible to obtain derivative **9**, as well as the others presented in Scheme 5 with good to excellent yields. The decrease in the number of iron equivalents is justified by the fact that it is easier to retain the iron if it is in smaller quantities in the reaction mixture, and the difference in the speed of the reaction is not significant enough to justify its increase. On the other hand, the volume and proportion

of ethanol allow greater solubilisation of the starting reagent and product and lower solubilisation of inorganic material, given the lower amount of water present.

Although this new methodology proved to be very efficient and functional for the overall derivatives, in the reduction of **29b** to **3**, it was necessary to stop the filtration of the reaction mixture on diatomaceous earth, and this factor affected the overall yield of the reaction since the product precipitated abundantly on the porous plate. In addition, compounds **12 - 14** were found to be partially water-soluble, which explains their relatively lower yields. A way to counteract this was found through a higher addition of ammonia in the procedure.

In summary, a new and simpler approach to the reduction procedure already reported by the research group was found. Through this, it is possible to avoid an extraction using large volumes of dichloromethane. The purification method of these derivatives when inorganic material was isolated in a mixture with the desired product has also been described, consisting in a flash chromatography using THF as the solvent, given the overall solubility of the synthesized derivatives in this solvent.

3.1.4. Characterization of the purine derivatives (29) and (1-23)

The physical, analytical and spectroscopic characterisation of the newly synthesized 2-(3-nitrophenyl)-purine derivatives (**29**) and 2-(3-aminophenyl)-purine derivatives (**1-23**) is reported as a whole in this subchapter to simplify the discussion between the differences presented by these two classes of compounds, in particular for the spectroscopic characterisation.

The compounds **29a** and **29d** and the respective corresponding amines **2** and **7** were synthesised, however, the full characterisation of these derivatives is already reported in the literature [79].

3.1.4.1. Physical and analytical characterization

The physical and analytical data for all the newly synthesized purine derivatives are presented in Table 16. Again, it was not possible to acquire mass spectrometry and elemental analysis data for the samples until the dissertation deadline. For this reason, the values presented for these components in Table 16 are only theoretical.

Table 16 Physical and theoretical analytical data of the new synthesized purine derivatives.

Compound	m.p. (°C)	Molecular Formula*	Molecular Weight (g/mol)*	Elemental analysis (%) (Expected values)*		
				C	H	N
29b	219 – 220	C ₂₂ H ₂₀ N ₆ O ₃	416.44	63.45	4.84	20.18
29c	227 – 229	C ₂₃ H ₂₂ N ₆ O ₃	430.47	64.18	5.15	19.52
29e	218 – 220	C ₂₁ H ₁₉ N ₇ O ₃	417.43	60.42	4.59	23.49
29f	235 – 236	C ₂₁ H ₁₉ N ₇ O ₃	417.43	60.42	4.59	23.49
29g	272 – 275	C ₂₁ H ₁₈ N ₆ O ₄	418.41	60.28	4.34	20.09
29h	239 – 241	C ₂₁ H ₁₈ N ₆ O ₄	418.41	60.28	4.34	20.09
29i	253 – 256	C ₂₃ H ₂₁ N ₇ O ₄	459.47	60.12	4.61	21.34
29j	291 – 292	C ₂₃ H ₂₁ N ₇ O ₄	459.47	60.12	4.61	21.34
29k	266 – 269	C ₂₈ H ₂₃ N ₇ O ₄	521.54	64.48	4.45	18.80
29l	227 – 229	C ₂₈ H ₂₃ N ₇ O ₄	521.54	64.48	4.45	18.80
29m	> 280	C ₂₇ H ₂₂ N ₈ O ₄	522.53	62.06	4.24	21.45
29n	252 – 255	C ₂₇ H ₂₂ N ₈ O ₄	522.53	62.06	4.24	21.45
29o	283 – 286	C ₂₇ H ₂₂ N ₈ O ₄	522.53	62.06	4.24	21.45
29p	266 – 270	C ₂₇ H ₂₂ N ₈ O ₄	522.53	62.06	4.24	21.45
29q	256 – 260	C ₃₁ H ₂₉ N ₇ O ₇	611.62	60.88	4.78	16.03
3	218 – 220	C ₂₂ H ₂₂ N ₆ O	386.46	68.38	5.74	21.75
5	163 – 165	C ₂₃ H ₂₄ N ₆ O	400.49	68.98	6.04	20.99
8	270 – 272	C ₂₃ H ₂₃ N ₇ O ₂	430.19	64.32	5.40	22.83
9	160 – 162	C ₂₃ H ₂₃ N ₇ O ₂	430.19	64.32	5.40	22.83
10	258 – 261	C ₂₈ H ₂₅ N ₇ O ₂	491.56	68.42	5.13	19.95
11	260 – 262	C ₂₈ H ₂₅ N ₇ O ₂	491.56	68.42	5.13	19.95
12	264 – 271	C ₂₇ H ₂₄ N ₈ O ₂	492.54	65.84	4.91	22.75
13	> 280	C ₂₇ H ₂₄ N ₈ O ₂	492.54	65.84	4.91	22.75
14	245 – 248	C ₂₇ H ₂₄ N ₈ O ₂	492.54	65.84	4.91	22.75
18	201 – 204	C ₃₁ H ₃₁ N ₇ O ₅	581.63	64.02	5.37	16.86

* Data collected from ChemDraw software.

3.1.4.2. Infra-red spectroscopy (IR) characterization

In general, the identification of 2-(3-nitrophenyl)-purine derivatives (**29**) can be confirmed by the disappearance of several bands of variable intensity between 2500 and 3500 cm⁻¹, typical of N-H bond stretching bands of the precursors **28**. However, when the R group has an amine or amide functional group, additional bands appear in this region, compared to the other derivatives. This is the case for the derivatives **29e**, **29f** and **29i-q**. Overall, it is seen in Table 17 that the region between 1500 and 1700 cm⁻¹ presents a set of bands of variable intensity resulting from stretching vibrations of the C=C, C=N and N-O bonds. In the particular cases of compounds **29i-q**, stretching vibrations of medium or strong intensity, characteristic of the C=O bond are visible in this same region. In these cases are also visible bands of weak or medium intensity associated with N-H bending vibrations.

The new 2-(3-aminophenyl)-purine derivatives (**3-18**) differ structurally from their respective precursors **29** only in the nitro group, which was transformed into an amine. Thus, and as verified in Table 17, there are no significant changes in the bands present in the region between 1500 and 1700 cm^{-1} . However, there is an overall increase in the number of bands in the region between 2500 and 3500 cm^{-1} . These are typical bands of the stretching of N-H bonds.

Table 17 IR spectroscopic data ($\text{Nujol}/\text{cm}^{-1}$) for the new synthesized purine derivatives.

Compound	3500-2500 cm^{-1}	1700-1500 cm^{-1}
29b	3112	1590, 1573, 1563, 1519
29c	3102 (w)	1594, 1573, 1530, 1504 (w)
29e	3435, 3341, 3100	1593 (s), 1572 (s), 1523 (s)
29f	3373 (s), 3333, 3228 (s)	1609, 1588, 1561 (s), 1522
29g	3604 (w), 3105	1594 (s), 1572 (s), 1524 (s)
29h	3116	1593 (s), 1573 (s), 1523 (s)
29i	3645, 3330, 3100	1691, 1588 (s), 1569 (s), 1525 (s)
29j	3407	1695, 1606, 1589, 1573, 1537, 1519
29k	3427, 3286	1665, 1648, 1591 (s), 1569 (s), 1521 (s)
29l	3287, 3112 (w)	1652, 1602, 1590 (s), 1572 (s), 1534
29m	3296 (w), 3110	1682 (s), 1592 (s), 1571 (s), 1547, 1531 (s)
29n	3288, 3124	1646, 1592 (s), 1573, 1531, 1515
29o	3397 (w), 3289 (w), 3109 (w)	1692, 1682, 1593 (s), 1573 (s), 1537 (s)
29p	3293 (w), 3108 (w)	1656, 1592, 1574 (w), 1529
29q	3434, 3104	1675, 1594 (s), 1577, 1557, 1529 (s)
3	3449, 3432, 3356, 3243, 3120, 3100	1644, 1636, 1589 (s), 1576 (s), 1522 (s)
5	3433 (w), 3354 (w), 3239 (w), 3098 (w)	1636 (w), 1577 (s), 1515
8	3358 (w), 3308 (w)	1682 (w), 1665 (w), 1574, 1547, 1522
9	3245 (w), 3074 (w)	1670 (w), 1610 (w), 1574, 1510 (w)
10	3458 (w), 3324 (w), 3133 (w)	1651, 1584, 1531
11	3353 (w)	1660 (w), 8s1605, 1574
12	3345	1673, 1605, 1574, 1540, 1522
13	3424, 3354, 3287, 3106	1646 (s), 1603 (s), 1576 (s), 1535, 1511
14	3405, 3335	1661 (w), 1574, 1522
18	3434, 3343 (s), 3104	1658 (s), 1630, 1576 (s), 1525 (s)

Weak (w) and strong (s) intensity peaks are denoted after their respective value. The remaining peaks have medium intensity.

3.1.4.3. ^1H and ^{13}C -NMR spectroscopy characterization

Generally, the ^1H -NMR spectra of all purine derivatives (Table 18) show a singlet between 8.40 and 8.66 ppm, typical of H-C₈. In addition, a 4 proton integrated signal is visible for all these derivatives between 4.27 and 4.39 ppm, identifying the H-C₁₀ protons. This signal is most often presented as a broad singlet, however, there are rare exceptions where it is presented as a triplet. Also common to all compounds is the signal integrating also for 4 protons between 3.75 and 3.83 ppm, identifying H-C₁₁ protons.

In comparison with the synthetic precursors **28**, there is a relative increase in the chemical shifts of the corresponding protons of the purine derivatives (H-C₂ and H-C₈, H-C₇ and H-C₁₀, and H-C₈ and H-C₁₁, respectively). However, the most significant increase corresponds to the H-C₁₀ protons. Due to the electronic ring current effect, these protons, which in theory, should be at a lower chemical shift (δ) than the H-C₁₁ protons given the electronegativity of the nearest heteroatom, appear at a higher chemical shift.

Next, regarding derivatives **29e** and **29f**, they show a distinct signal among all the other 2-(3-nitrophenyl)-purine derivatives **29**. Because they have an amine in their structure, a singlet with a chemical shift between 5.43 and 5.50 ppm is visible in their ¹H-NMR spectra. These derivatives were used as starting reagents for the synthesis of **29i-q** derivatives. In these, in turn, the amine peak disappeared and a singlet, relative to the corresponding amide appeared between 10.18 and 10.80 ppm in the spectrum. The peaks relating to the remaining hydrogens of the R¹ group also underwent slight changes reported in Table 18, when compared to the precursors **29e** and **29f**.

Finally, in the ¹H-NMR spectrum of the 2-(3-aminophenyl)-purine derivatives (**1-23**), it is distinguished the appearance of a singlet between 4.5 and 5.4 ppm relative to the protons of the amine group, from A. Regarding the signals of the protons related to the R¹, these overall remain coherent with their respective precursors. However, a significant change in the standard chemical deviation of the protons of the aromatic ring A (Figure 37) is registered. It can be seen that in these derivatives, the chemical shifts for this aromatic ring A are lower compared to the respective synthetic precursors **29**. This change is more significant in H-C_p, which, when the R group is -NO₂, presents chemical shifts varying between 8.21 and 8.29 ppm. However, when the R group is -NH₂, H-C_p shows chemical shifts varying between 6.63 and 6.65 ppm. On the other hand, the protons H-C_o, H-C_{o'} and H-C_m show a range of deviations respectively of 8.64 - 8.67, 8.90 - 9.09 and 7.67- 7.76 ppm for the 2-(3-nitrophenyl)-purine derivatives (**29**). However, these same protons are shifted to lower chemical shifts of respectively 7.51 - 7.67 ppm for H-C_o, 7.53 - 7.72 for H-C_{o'}, and 7.08 - 7.09 for H-C_m, for the amino derivatives. This effect can be explained by the electronic resonance effect, withdrawing on the part of the nitro group in derivatives **29** and donor on the part of the amino group in the remaining derivatives (**1-23**).

Table 19 presents all the ¹³C spectroscopic data of the newly synthesised purine derivatives. Through HMQC it was possible to establish a direct correlation between H-C₈ and C₈, where the chemical shifts vary between 139.16 and 140.25 ppm. Additionally, direct correlations are established between H-C₁₀ and C₁₀, (45.08 - 45.38 ppm), and H-C₁₁ and C₁₁ (65.71 - 66.86 ppm). On the other hand, correlations are also identified between the chemical shifts of C_o, C_{o'}, C_m and C_p of group A with the

respective protons. However, as happened in the $^1\text{H-NMR}$ spectrum, depending on the R group (NO_2 or NH_2), these chemical shifts are also significantly different.

Figure 37 shows a model example (**29b** or **3**, depending on the R) of the general structure discussed here. With HMBC it was possible to identify several carbon atoms through the three bond correlation H – C. The H-C₈ identified carbons C₄ (150.94 - 152.04 ppm) and C₅ (118.45 - 119.36 ppm) of the purine nucleus, as well as the C_i of the R¹ groups. It was also possible to identify C₆ (153.08 - 153.74 ppm) in the purine nucleus by the coupling of H-C₁₀. Also, in the purine nucleus, C₂, as well as the carbons of the ring A, undergo a relatively small shift in the chemical shift values depending on whether the R group is NO_2 (154.84 - 155.60 ppm) or NH_2 (158.17 - 158.89 ppm). In both cases, this value can be confirmed by correlation with the H-C_o and H-C_{o'} from ring A, as highlighted in red in Figure 37.

Regarding group A, the identification of the chemical shifts of the quaternary carbon C_i can be done by the correlation of H-C_m, and H-C_o (C_i (139.60 - 139.85 ppm (R = NO_2) and 138.35 - 139.27 ppm (R = NH_2))). On the other hand, as for the C_{m'} shifts (147.94 - 148.33 ppm (R = NO_2) and 148.18 - 148.82 ppm (R = NH_2)), these were identified by their correlation with H-C_m and the H-C_p. The remaining chemical shifts regarding the carbons C_o, C_m, C_p and C_{o'}, as mentioned before, were identified by HMQC. C_o shows a chemical shift ranging between 133.14 and 134.32 ppm when R= NO_2 , however, when R= NH_2 , the shift ranges between 115.80 and 116.84 ppm. Next, C_m shows a chemical shift ranging between 129.32 and 130.24 ppm when R= NO_2 , again, however, when R= NH_2 , the shift ranges between 128.60 and 129.45 ppm. Then, C_p exhibits a chemical shift ranging between 123.51 and 124.65 ppm when R= NO_2 , however, when R= NH_2 , the shift ranges between 115.56 and 116.61 ppm. Finally, C_{o'} shows a chemical shift ranging between 121.42 and 122.21 ppm, when R= NO_2 , and when R= NH_2 , the shift ranges between 113.41 and 114.21 ppm.

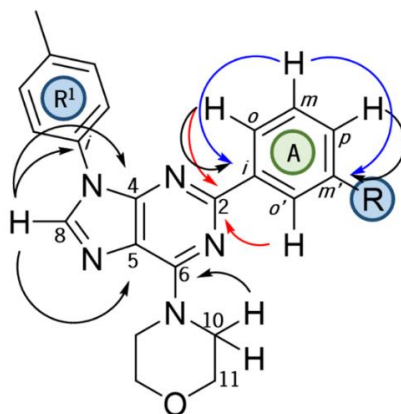


Figure 37 Generic model of the most significant correlations between the protons of the represented base structure and the identified carbons of the purine derivatives (R= NO_2 (**29b**) or R= NH_2 (**3**)).

Table 18 $^1\text{H-NMR}$ spectroscopic data (400 MHz, $\text{DMSO-}d_6$) for the new synthesized purine derivatives.

Comp.	Base structure	R ¹	R	R ¹ - H	Base Structure - H	Group A - H			
29b			NO ₂	7.76 (d, 2H, $J = 8.4$ Hz, H _o) 7.41 (d, 2H, $J = 8.4$ Hz, H _m) 2.41 (s, 3H, Me)	8.56 (s, 1H, H ₈) 4.30 (br.s, 4H, H ₁₀) 3.78 (t, 4H, $J = 4.8$ Hz, H ₁₁)	8.94 (t, 1H, $J = 1.6$ Hz, H _{o'}) 8.67 (d, 1H, $J = 8.0$ Hz, H _o) 8.24 (dd, 1H, $J = 8.0, 1.6$ Hz, H _p) 7.71 (t, 1H, $J = 8.0$ Hz, H _m)			
3				NH ₂	7.78 (d, 2H, $J = 8.4$ Hz, H _o) 7.41 (d, 2H, $J = 8.4$ Hz, H _m) 2.39 (s, 3H, Me)	8.50 (s, 1H, H ₈) 4.31 (br.s, 4H, H ₁₀) 3.77 (t, 4H, $J = 4.8$ Hz, H ₁₁)	7.59 (t, 1H, $J = 1.6$ Hz, H _{o'}) 7.52 (d, 1H, $J = 7.6$ Hz, H _o) 7.08 (t, 1H, $J = 7.6$ Hz, H _m) 6.63 (dd, 1H, $J = 7.6, 1.6$ Hz, H _p) 5.11 (s, 2H, NH ₂)		
29c			NO ₂	7.72 (s, 1H, H _o) 7.62 (dd, 1H, $J = 8.4, 2.0$ Hz, H _o) 7.37 (d, 1H, $J = 8.4$ Hz, H _m) 2.38 (s, 3H, Me _{m'}) 2.35 (s, 3H, Me _p)	8.48 (s, 1H, H ₈) 4.36 (t, 4H, $J = 4.8$ Hz, H ₁₀) 3.83 (t, 4H, $J = 4.8$ Hz, H ₁₁)	9.06 (t, 1H, $J = 2.0$ Hz, H _{o'}) 8.72 (dt, 1H, $J = 8.0, 2.0$ Hz, H _o) 8.24 (ddd, 1H, $J = 8.0, 2.0, 0.8$ Hz, H _p) 7.75 (t, 1H, $J = 8.0$ Hz, H _m)			
5				NH ₂	7.64 (m, 2H, H _o + H _{o'}) 7.36 (d, 1H, $J = 8.0$ Hz, H _m) 2.33 (s, 3H, Me _{m'}) 2.30 (s, 3H, Me _p)	8.50 (s, 1H, H ₈) 4.32 (br.s, 4H, H ₁₀) 3.78 (t, 4H, $J = 4.8$ Hz, H ₁₁)	7.59 (t, 1H, $J = 1.6$ Hz, H _{o'}) 7.52 (d, 1H, $J = 8.0$ Hz, H _o) 7.08 (t, 1H, $J = 8.0$ Hz, H _m) 6.63 (dd, 1H, $J = 8.0, 1.6$ Hz, H _p) 5.13 (s, 2H, NH ₂)		
29e			NO ₂	NH ₂	7.43 (d, 2H, $J = 8.4$ Hz, H _o) 6.76 (d, 2H, $J = 8.4$ Hz, H _m) 5.43 (s, 2H, NH ₂)	8.40 (s, 1H, H ₈) 4.30 (br.s, 4H, H ₁₀) 3.77 (t, 4H, $J = 4.8$ Hz, H ₁₁)	8.97 (t, 1H, $J = 2.0$ Hz, H _{o'}) 8.68 (dd, 1H, $J = 8.0, 2.0$ Hz, H _o) 8.25 (ddd, 1H, $J = 8.0, 2.0, 0.8$ Hz, H _p) 7.71 (t, 1H, $J = 8.0$ Hz, H _m)		
29f						NO ₂	7.24 (t, 1H, $J = 8.0$ Hz, H _m) 7.06 (t, $J = 1.2$ Hz, 1H, H _{o'}) 6.93 (dd, 1H, $J = 8.0, 1.2$ Hz, H _o) 6.67 (dd, 1H, $J = 8.0, 1.2$ Hz, H _p) 5.50 (s, 3H, NH ₂)	8.51 (s, 1H, H ₈) 4.33 (br.s, 4H, H ₁₀) 3.79 (t, 4H, $J = 4.8$ Hz, H ₁₁)	9.02 (t, 1H, $J = 2.4$ Hz, H _{o'}) 8.75 (dt, 1H, $J = 8.0, 1.2$ Hz, H _o) 8.28 (ddd, 1H, $J = 8.0, 2.4, 1.2$ Hz, H _p) 7.75 (t, 1H, $J = 8.0$ Hz, H _m)
29g								NO ₂	9.87 (s, 1H, OH) 7.63 (d, 2H, $J = 8.8$ Hz, H _o) 6.98 (d, 2H, $J = 8.8$ Hz, H _m)

Table 18 ¹H-NMR spectroscopic data (400 MHz, DMSO-*d*₆) for the new synthesized purine derivatives. (continuation)

Comp.	Base structure	R ¹	R	R ¹ - H	Base Structure - H	Group A - H
29h			NO ₂	10.03 (br.s, 1H, OH) 7.39 (t, 1H, <i>J</i> = 8.0 Hz, H _m) 7.35 (t, 1H, <i>J</i> = 2.0 Hz H _{o'}) 7.28 (dd, 1H, <i>J</i> = 8.0, 2.0 Hz, H _o) 6.88 (dd, 1H, <i>J</i> = 8.0, 2.0 Hz, H _p)	8.53 (s, 1H, H ₈) 4.27 (br.s, 4H, H ₁₀) 3.76 (t, 4H, <i>J</i> = 4.8 Hz, H ₁₁)	8.93 (dd, 1H, <i>J</i> = 2.0, 1.6 Hz, H _{o'}) 8.67 (dd, 1H, <i>J</i> = 8.0, 1.6 Hz, H _o) 8.22 (ddd, 1H, <i>J</i> = 8.0, 2.0, 0.8 Hz, H _p) 7.69 (t, 1H, <i>J</i> = 8.0 Hz, H _m)
29i			NO ₂	10.18 (s, 1H, NH) 7.79 (br.s, 4H, H _o + H _m) 2.10 (s, 3H, Me)	8.51 (s, 1H, H ₈) 4.27 (br.s, 4H, H ₁₀) 3.76 (t, 4H, <i>J</i> = 4.4 Hz, H ₁₁)	8.90 (t, 1H, <i>J</i> = 2.0 Hz, H _{o'}) 8.64 (dd, 1H, <i>J</i> = 8.0, 1.2 Hz, H _o) 8.21 (ddd, 1H, <i>J</i> = 8.0, 2.0, 1.2 Hz, H _p) 7.67 (t, 1H, <i>J</i> = 8.0 Hz, H _m)
8			NH ₂	10.21 (s, 1H, NH) 7.79 (m, 4H, H _o + H _m) 2.08 (s, 3H, Me)	8.47 (s, 1H, H ₈) 4.30 (br.s, 4H, H ₁₀) 3.76 (t, 4H, <i>J</i> = 4.4 Hz, H ₁₁)	7.58 (t, 1H, <i>J</i> = 2.0 Hz, H _{o'}) 7.51 (dt, 1H, <i>J</i> = 8.0, 0.8 Hz, H _o) 7.08 (t, 1H, <i>J</i> = 8.0 Hz, H _m) 6.63 (ddd, 1H, <i>J</i> = 8.0, 2.0, 0.8 Hz, H _p) 5.09 (s, 2H, NH ₂)
29j			NO ₂	10.24 (s, 1H, NH) 8.42 (s, 1H, H _{o'}) 7.55 (m, 3H, H _o + H _m + H _p) 2.10 (s, 3H, Me)	8.59 (s, 1H, H ₈) 4.32 (br.s, 4H, H ₁₀) 3.79 (t, 4H, <i>J</i> = 4.8 Hz, H ₁₁)	9.02 (t, 1H, <i>J</i> = 2.4 Hz, H _{o'}) 8.79 (dt, 1H, <i>J</i> = 8.0, 0.8 Hz, H _o) 8.26 (ddd, 1H, <i>J</i> = 8.0, 2.4, 0.8 Hz, H _p) 7.72 (t, 1H, <i>J</i> = 8.0 Hz, H _m)
9			NH ₂	10.24 (s, 1H, NH) 8.29 (s, 1H, H _{o'}) 7.63 (m, 1H, H _p) 7.53 (br.s, 1H, H _o) 7.52 (br.s, 1H, H _m) 2.10 (s, 3H, Me)	8.53 (s, 1H, H ₈) 4.32 (br.s, 4H, H ₁₀) 3.78 (t, 4H, <i>J</i> = 4.8 Hz, H ₁₁)	7.69 (t, 1H, <i>J</i> = 2.0 Hz, H _{o'}) 7.57 (dt, 1H, <i>J</i> = 8.0, 0.8 Hz, H _o) 7.08 (t, 1H, <i>J</i> = 8.0 Hz, H _m) 6.63 (ddd, 1H, <i>J</i> = 8.0, 2.0, 0.8 Hz, H _p) 5.09 (s, 2H, NH ₂)
29k			NO ₂	10.49 (s, 1H, NH) 7.97 – 8.02 (m, 4H, H _m + H _{o'}) 7.28 (d, 2H, <i>J</i> = 8.0 Hz, H _o) 7.52 – 7.63 (m, 3H, H _{p'} + H _m)	8.58 (s, 1H, H ₈) 4.32 (br.s, 4H, H ₁₀) 3.78 (t, 4H, <i>J</i> = 4.8 Hz, H ₁₁)	8.99 (t, 1H, <i>J</i> = 2.4 Hz, H _{o'}) 8.71 (dd, 1H, <i>J</i> = 8.0, 2.4 Hz, H _o) 8.25 (ddd, 1H, <i>J</i> = 8.0, 2.4, 0.8 Hz, H _p) 7.73 (t, 1H, <i>J</i> = 8.0 Hz, H _m)
10			NH ₂	10.50 (s, 1H, NH) 7.93 (m, 4H, H _m + H _{o'}) 7.85 (d, 2H, <i>J</i> = 9.2 Hz, H _o) 7.58 (m, 2H, H _p)* 7.52 (m, 3H, H _m)* ¹	8.46 (s, 1H, H ₈) 4.28 (br.s, 4H, H ₁₀) 3.75 (t, 4H, <i>J</i> = 4.8 Hz, H ₁₁)	7.58 (m, 2H, H _{o'})* 7.52 (m, 3H, H _o)* ¹ 7.09 (t, 1H, <i>J</i> = 8.0 Hz, H _m) 6.64 (ddd, 1H, <i>J</i> = 8.0, 2.4, 0.8 Hz, H _p)

*, *¹ - Overlay of signals on the spectrum.

Table 18 ¹H-NMR spectroscopic data (400 MHz, DMSO-*d*₆) for the new synthesized purine derivatives. (continuation)

Comp.	Base structure	R ¹	R	R ¹ - H	Base Structure - H	Group A - H
29i			NO₂	10.57 (s, 1H, NH) 8.65 (s, 1H, H _o) 8.00 (d, 2H, <i>J</i> = 8.0 Hz, H _{o''}) 7.84 (m, 1H, H _o) 7.63–7.53 (m, 5H, H _m + H _p + H _{p'} + H _{m''})	8.66 (s, 1H, H ₈) 4.39 (br.s, 4H, H ₁₀) 3.80 (t, 4H, <i>J</i> = 4.8 Hz, H ₁₁)	9.09 (t, 1H, <i>J</i> = 2.4 Hz, H _o) 8.87 (dt, 1H, <i>J</i> = 8.0, 0.8 Hz, H _o) 8.27 (ddd, 1H, <i>J</i> = 8.0, 2.4, 0.8 Hz, H _p) 7.75 (t, 1H, <i>J</i> = 8.0 Hz, H _m)
11			NH₂	10.55 (s, 1H, NH) 8.52 (t, 1H, <i>J</i> = 1.6 Hz, H _o) 7.99 (m, 2H, H _{o''}) 7.83 (dt, 1H, <i>J</i> = 8.0, 1.6 Hz, H _p) 7.64–7.53 (m, 5H, H _o + H _m + H _{p'} + H _{m''})*	8.57 (s, 1H, H ₈) 4.33 (br.s, 4H, H ₁₀) 3.79 (t, 4H, <i>J</i> = 4.8 Hz, H ₁₁)	7.72 (t, 1H, <i>J</i> = 1.6 Hz, H _o) 7.64–7.53 (m, 1H, H _o)* 7.08 (t, 1H, <i>J</i> = 8.0 Hz, H _m) 6.63 (ddd, 1H, <i>J</i> = 8.0, 2.4, 0.8 Hz, H _p) 5.07 (s, 2H, NH ₂)
29m			NO₂	10.55 (s, 1H, NH) 9.17 (d, 1H, <i>J</i> = 1.6 Hz, H _{o''}) 8.77 (m, 1H, H _p)* 8.34 (dt, 1H, <i>J</i> = 8.0, 1.6 Hz, H _o) 8.03 (d, 2H, <i>J</i> = 8.8 Hz, H _m) 7.93 (d, 2H, <i>J</i> = 8.8 Hz, H _o) 7.58 (m, 1H, H _{m'})	8.59 (s, 1H, H ₈) 4.37 (br.s, 4H, H ₁₀) 3.82 (t, 4H, <i>J</i> = 4.8 Hz, H ₁₁)	9.05 (t, 1H, <i>J</i> = 2.0 Hz, H _o) 8.77 (m, 1H, H _o)* 8.27 (ddd, 1H, <i>J</i> = 8.0, 2.0, 1.2 Hz, H _p) 7.76 (t, 1H, <i>J</i> = 8.0 Hz, H _m)
12			NH₂	10.67 (s, 1H, NH) 9.15 (d, 1H, <i>J</i> = 1.6 Hz, H _{o''}) 8.79 (dd, 1H, <i>J</i> = 4.8, 1.6 Hz, H _p) 8.33 (dt, 1H, <i>J</i> = 8.0, 1.6 Hz, H _o) 8.02 (d, 2H, <i>J</i> = 8.8 Hz, H _m) 7.94 (d, 2H, <i>J</i> = 8.8 Hz, H _o) 7.53 - 7.61 (m, 2H, H _m)*	8.57 (s, 1H, H ₈) 4.33 (br.s, 4H, H ₁₀) 3.79 (t, 4H, <i>J</i> = 4.8 Hz, H ₁₁)	7.53 - 7.61 (m, 2H, H _o + H _{o''})* 7.09 (t, 1H, <i>J</i> = 8.0 Hz, H _m) 6.63 (ddd, 1H, <i>J</i> = 8.0, 2.4, 0.8 Hz, H _p) 5.14 (s, 2H, NH ₂)
29n		NO₂	10.74 (s, 1H, NH) 9.14 (s, 1H, H _{o''}) 8.77 (d, 1H, <i>J</i> = 4.0 Hz, H _p) 8.68 (s, 1H, H _o) 8.32 (dt, 1H, <i>J</i> = 8.0, 2.0 Hz, H _{o''}) 8.02 (d, 2H, <i>J</i> = 8.8 Hz, H _m) 7.78 (m, 1H, H _p) 7.63 - 7.57 (m, 3H, H _m + H _o + H _{m''})	8.64 (s, 1H, H ₈) 4.32 (br.s, 4H, H ₁₀) 3.79 (t, 4H, <i>J</i> = 4.8 Hz, H ₁₁)	9.06 (t, 1H, <i>J</i> = 2.0 Hz, H _o) 8.84 (d, 1H, <i>J</i> = 8.0 Hz, H _o) 8.25 (ddd, 1H, <i>J</i> = 8.0, 2.0, 0.8 Hz, H _p) 7.72 (t, 1H, <i>J</i> = 8.0 Hz, H _m)	

* - Overlay of signals on the spectrum.

Table 18 ¹H-NMR spectroscopic data (400 MHz, DMSO-*d*₆) for the new synthesized purine derivatives. (continuation)

Comp.	Base structure	R ¹	R	R ¹ - H	Base Structure - H	Group A - H
13			NH ₂	10.75 (s, 1H, NH) 9.13 (d, 1H, <i>J</i> = 1.6 Hz, H _{o''}) 8.77 (dd, 1H, <i>J</i> = 4.8, 1.2 Hz, H _{p'}) 8.52 (t, 1H, <i>J</i> = 2.0 Hz, H _{o'}) 8.32 (dt, 1H, <i>J</i> = 8.0, 1.6 Hz, H _{o''}) 7.82 (dt, 1H, <i>J</i> = 8.0, 2.0 Hz, H _p) 7.67 - 7.57 (m, 3H, H _o + H _m + H _{m''})	8.57 (s, 1H, H ₈) 4.33 (br.s, 4H, H ₁₀) 3.79 (t, 4H, <i>J</i> = 4.8 Hz, H ₁₁)	7.72 (t, 1H, <i>J</i> = 2.0 Hz, H _{o'}) 7.67 - 7.57 (m, 1H, H _o) * ¹ 7.09 (t, 1H, <i>J</i> = 8.0 Hz, H _m) 6.65 (dd, 1H, <i>J</i> = 8.0, 2.0 Hz, H _p) 5.9 - 4.5 (br.s, 2H, NH ₂)
29o			NO ₂	10.74 (s, 1H, NH) 8.81 (d, 2H, <i>J</i> = 6.0 Hz, H _m) 8.03 (d, 2H, <i>J</i> = 9.2 Hz, H _m) 7.93 (d, 2H, <i>J</i> = 9.2 Hz, H _o) 7.90 (d, 2H, <i>J</i> = 6.0 Hz, H _{o'})	8.64 (s, 1H, H ₈) 4.35 (br.s, 4H, H ₁₀) 3.81 (t, 4H, <i>J</i> = 4.8 Hz, H ₁₁)	9.04 (t, 1H, <i>J</i> = 2.4 Hz, H _{o'}) 8.77 (dt, 1H, <i>J</i> = 8.0, 0.8 Hz, H _o) 8.29 (ddd, 1H, <i>J</i> = 8.0, 2.4, 0.8 Hz, H _p) 7.76 (t, 1H, <i>J</i> = 8.0 Hz, H _m)
14			NH ₂	10.75 (s, 1H, NH) 8.79 (d, 2H, <i>J</i> = 6.0 Hz, H _m) 7.98 (d, 2H, <i>J</i> = 11.6 Hz, H _m) 7.93 (d, 2H, <i>J</i> = 11.6 Hz, H _o) 7.88 (d, 2H, <i>J</i> = 6.0 Hz, H _{o'})	8.54 (s, 1H, H ₈) 4.31 (br.s, 4H, H ₁₀) 3.77 (t, 4H, <i>J</i> = 4.8 Hz, H ₁₁)	7.60 (t, 1H, <i>J</i> = 2.0 Hz, H _{o'}) 7.54 (dt, 1H, <i>J</i> = 8.0, 0.8 Hz, H _o) 7.09 (t, 1H, <i>J</i> = 8.0 Hz, H _m) 6.64 (ddd, 1H, <i>J</i> = 8.0, 2.0, 0.8 Hz, H _p) 5.12 (s, 2H, NH ₂)
29p			NO ₂	10.80 (s, 1H, NH) 8.77 - 8.81 (m, 2H, H _m) * 8.64 (d, 1H, <i>J</i> = 2.0 Hz, H _{o'}) 7.87 (d, 2H, <i>J</i> = 6.0 Hz, H _{o''}) 7.75 (dt, 1H, <i>J</i> = 7.2, 2.0 Hz, H _o) 7.56 - 7.62 (m, 2H, H _m + H _p)	8.59 (s, 1H, H ₈) 4.29 (br.s, 4H, H ₁₀) 3.76 (t, 4H, <i>J</i> = 4.8 Hz, H ₁₁)	9.01 (t, 1H, <i>J</i> = 2.0 Hz, H _{o'}) 8.77 - 8.81 (m, 1H, H _o) * 8.22 (ddd, 1H, <i>J</i> = 8.0, 2.0, 0.8 Hz, H _p) 7.69 (t, 1H, <i>J</i> = 8.0 Hz, H _m)
29q			NO ₂	10.35 (s, 1H, NH) 7.97 (d, 2H, <i>J</i> = 8.8 Hz, H _m) 7.88 (d, 2H, <i>J</i> = 8.8 Hz, H _o) 7.30 (s, 2H, H _{o'}) 3.87 (s, 6H, Me _m) 3.73 (s, 3H, Me _p)	8.58 (s, 1H, H ₈) 4.31 (br.s, 4H, H ₁₀) 3.78 (t, 4H, <i>J</i> = 4.8 Hz, H ₁₁)	8.98 (s, 1H, H _{o'}) 8.70 (d, 1H, <i>J</i> = 8.0 Hz, H _o) 8.24 (dd, 1H, <i>J</i> = 8.0, 1.6 Hz, H _p) 7.71 (t, 1H, <i>J</i> = 8.0 Hz, H _m)
18			NH ₂	10.35 (s, 1H, NH) 8.00 (d, 2H, <i>J</i> = 8.8 Hz, H _m) 7.93 (d, 2H, <i>J</i> = 8.8 Hz, H _o) 7.32 (s, 2H, H _{o'}) 3.89 (s, 6H, Me _m) 3.75 (s, 3H, Me _p)	8.57 (s, 1H, H ₈) 4.34 (t, 4H, <i>J</i> = 4.8 Hz, H ₁₀) 3.79 (t, 4H, <i>J</i> = 4.8 Hz, H ₁₁)	7.62 (t, 1H, <i>J</i> = 2.0 Hz, H _{o'}) 7.55 (dt, 1H, <i>J</i> = 8.0, 0.8 Hz, H _o) 7.09 (t, 1H, <i>J</i> = 8.0 Hz, H _m) 6.64 (ddd, 1H, <i>J</i> = 8.0, 2.0, 0.8 Hz, H _p) 5.14 (s, 2H, NH ₂)

* - Overlay of signals on the spectrum.

Rational design and synthesis of novel selective PI3K inhibitors for cancer therapy

Table 19 ^{13}C -NMR spectroscopic data (100 MHz, $\text{DMSO-}d_6$) for the new synthesized purine derivatives.

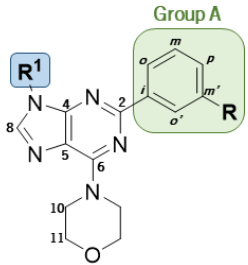
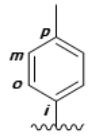
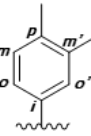
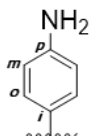
Comp.	Base structure	R^1	R	R^1	Base Structure	Group A					
						C_i	C_o	C_m	C_p	$\text{C}_{o'}$	$\text{C}_{m'}$
29b			NO_2	155.18 (C_2)	139.71	133.81	130.03	124.37	121.76	148.07	
137.41 (C_p)				153.19 (C_6)							
132.30 (C_i)		151.08 (C_4)	138.86	116.00	128.77	115.78	113.58	148.60			
129.94 (C_m)		139.96 (C_8)									
123.42 (C_o)		119.07 (C_5)									
20.62 (Me)		66.20 (C_{11})									
45.19 (C_{10})	158.33 (C_2)	137.23 (C_p)	NH_2	153.26 (C_6)	120.78 (C_o)	18.97 (Me_p)	18.68 ($\text{Me}_{m'}$)				
151.55 (C_4)	139.35 (C_8)										
139.70	133.14	129.32	123.51	121.42	147.96						
137.07 (C_m)	135.52 (C_p)	132.19 (C_i)	129.80 (C_m)	123.87 ($\text{C}_{o'}$)	120.19 (C_o)	18.68 ($\text{Me}_{m'}$)	18.18 (Me_p)				
154.84 (C_2)	139.82	133.72	129.90	124.18	121.70	147.98					
153.11 (C_6)							151.19 (C_4)				
148.75 (C_p)	140.21 (C_8)	118.85 (C_5)	66.21 (C_{11})	45.34 (C_{10})							
124.97 (C_o)	123.10 (C_i)	113.88 (C_m)									
113.88 (C_m)	66.21 (C_{11})	45.34 (C_{10})									
5		NO_2	154.84 (C_2)	139.82	133.72	129.90	124.18	121.70	147.98		
153.11 (C_6)			151.19 (C_4)								
151.08 (C_4)		139.96 (C_8)	138.79	115.80	128.60	115.56	113.44	148.52			
139.96 (C_8)		119.07 (C_5)									
119.07 (C_5)		66.26 (C_{11})									
66.26 (C_{11})		45.20 (C_{10})									
45.20 (C_{10})	158.17 (C_2)	137.61 (C_m)	NH_2	153.12 (C_6)	120.78 (C_o)	18.97 (Me_p)	18.68 ($\text{Me}_{m'}$)				
151.46 (C_4)	139.24 (C_8)										
139.79	133.14	129.32	123.51	121.42	147.96						
137.61 (C_m)	135.79 (C_p)	132.79 (C_i)	130.27 (C_m)	124.21 ($\text{C}_{o'}$)	120.78 (C_o)	19.52 ($\text{Me}_{m'}$)	18.97 (Me_p)				
154.84 (C_2)	139.82	133.72	129.90	124.18	121.70	147.98					
153.11 (C_6)							151.19 (C_4)				
148.75 (C_p)	140.21 (C_8)	118.85 (C_5)	66.21 (C_{11})	45.34 (C_{10})							
124.97 (C_o)	123.10 (C_i)	113.88 (C_m)									
113.88 (C_m)	66.21 (C_{11})	45.34 (C_{10})									
29e		NO_2	154.84 (C_2)	139.82	133.72	129.90	124.18	121.70	147.98		
153.11 (C_6)			151.19 (C_4)								
151.08 (C_4)		139.96 (C_8)	138.79	115.80	128.60	115.56	113.44	148.52			
139.96 (C_8)		119.07 (C_5)									
119.07 (C_5)		66.26 (C_{11})									
66.26 (C_{11})		45.20 (C_{10})									
45.20 (C_{10})	158.17 (C_2)	137.61 (C_m)	NH_2	153.12 (C_6)	120.78 (C_o)	18.97 (Me_p)	18.68 ($\text{Me}_{m'}$)				
151.46 (C_4)	139.24 (C_8)										
139.79	133.14	129.32	123.51	121.42	147.96						
137.61 (C_m)	135.79 (C_p)	132.79 (C_i)	130.27 (C_m)	124.21 ($\text{C}_{o'}$)	120.78 (C_o)	19.52 ($\text{Me}_{m'}$)	18.97 (Me_p)				

Table 19 ^{13}C -NMR spectroscopic data (100 MHz, $\text{DMSO-}d_6$) for the new synthesized purine derivatives. (continuation)

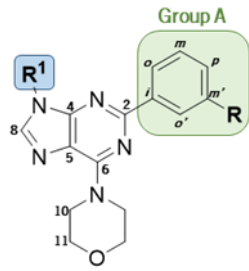
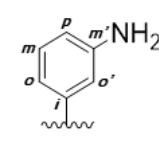
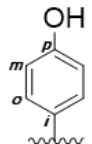
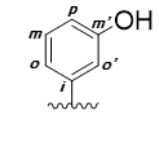
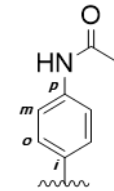
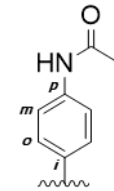
Comp.	Base structure	R^1	R	R^1	Base Structure	Group A					
						C_i	C_o	C_m	C_p	$\text{C}_{o'}$	$\text{C}_{m'}$
29f			NO_2	149.92 (C_m) 135.46 (C_i) 129.83 (C_m) 113.26 (C_p) 110.59 (C_o) 108.71 ($\text{C}_{o'}$)	155.12 (C_2) 153.19 (C_6) 151.10 (C_4) 140.02 (C_8) 119.12 (C_5) 66.19 (C_{11}) 45.20 (C_{10})	139.79	133.91	129.99	124.34	121.85	148.07
29g			NO_2	157.17 (C_p) 126.15 (C_i) 125.43 (C_o) 115.87 (C_m)	155.10 (C_2) 153.20 (C_6) 151.23 (C_4) 140.25 (C_8) 118.90 (C_5) 66.21 (C_{11}) 45.33 (C_{10})	139.79	133.82	130.04	124.34	121.79	148.08
29h			NO_2	158.32 (C_m) 135.88 (C_i) 130.41 (C_m) 114.83 (C_p) 113.82 (C_o) 110.56 ($\text{C}_{o'}$)	155.20 (C_2) 153.18 (C_6) 151.03 (C_4) 139.86 (C_8) 119.22 (C_5) 66.26 (C_{11}) 45.26 (C_{10})	139.74	133.87	129.99	124.39	121.85	148.07
29i			NO_2	168.62 ($\text{C}=\text{O}$) 138.80 (C_p) 129.58 (C_i) 123.81 (C_o) 119.53 (C_m) 24.06 (Me)	155.04 (C_2) 153.08 (C_6) 150.95 (C_4) 139.69 (C_8) 118.97 (C_5) 66.19 (C_{11}) 45.49 (C_{10})	139.61	133.73	129.88	124.24	121.71	147.94
8			NH_2	169.15 ($\text{C}=\text{O}$) 138.79 (C_p) 130.20 (C_i) 124.18 (C_o) 120.05 (C_m) 24.20 (Me)	158.50 (C_2) 153.38 (C_6) 151.70 (C_4) 139.45 (C_8) 118.63 (C_5) 66.52 (C_{11}) 45.47 (C_{10})	138.98	116.24	128.97	116.00	113.72	148.68

Table 19 ^{13}C -NMR spectroscopic data (100 MHz, $\text{DMSO}-d_6$) for the new synthesized purine derivatives. (continuation)

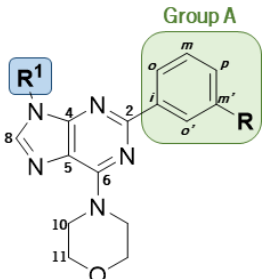
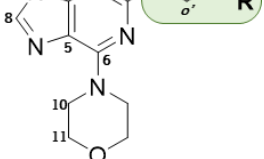
Comp.	Base structure	R^1	R	R^1	Base Structure	Group A					
						C_i	C_o	C_m	C_p	$\text{C}_{o'}$	$\text{C}_{m'}$
29j			NO_2	168.67 (C=O) 140.34 (C_m) 135.03 (C_i) 129.73 (C_m) 117.99 (C_p) 117.63 (C_o) 114.05 ($\text{C}_{o'}$) 24.05 (Me)	155.26 (C_2) 153.20 (C_6) 151.01 (C_4) 139.70 (C_8) 119.11 (C_5) 66.18 (C_{11}) 45.10 (C_{10})	139.67	134.00	129.94	124.36	121.93	148.08
9			NH_2	168.77 (C=O) 140.31 (C_m) 135.34 (C_i) 129.80 (C_m) 118.01 (C_p) 117.85 (C_o) 114.08 ($\text{C}_{o'}$) 24.13 (Me)	158.36 (C_2) 153.17 (C_6) 151.44 (C_4) 139.16 (C_8) 118.51 (C_5) 66.27 (C_{11}) 45.22 (C_{10})	138.69	116.00	128.62	115.61	113.76	148.47
29k			NO_2	166.07 (C=O) 138.84 (C_p) 134.82 (C_i) 132.02 (C_p) 130.35 (C_i) 128.70 (C_m) 127.89 (C_o) 124.05 (C_o) 121.25 (C_m)	155.42 (C_2) 153.38 (C_6) 151.27 (C_4) 140.00 (C_8) 119.18 (C_5) 66.40 (C_{11}) 45.44 (C_{10})	139.85	134.05	130.24	124.58	121.96	148.23
10			NH_2	166.84 (C=O) 138.82 (C_p) 135.00 (C_i) 132.59 (C_p) 131.14 (C_i) 129.23 (C_m) 128.21 (C_o) 124.47 (C_o) 122.03 (C_m)	158.89 (C_2) 153.74 (C_6) 152.04 (C_4) 139.76 (C_8) 118.89 (C_5) 66.86 (C_{11}) 45.81 (C_{10})	139.27	116.84	129.45	116.61	114.21	148.82

Table 19 ^{13}C -NMR spectroscopic data (100 MHz, $\text{DMSO}-d_6$) for the new synthesized purine derivatives. (continuation)

Comp.	Base structure	R^1	R	R^1	Base Structure	Group A					
						C_i	C_o	C_m	C_p	$\text{C}_{o'}$	$\text{C}_{m'}$
29i			NO_2	165.88 (C=O) 140.31 (C_m) 135.02 (C_i) 134.73 (C_i) 131.79 (C_p) 129.72 (C_m) 128.46 ($\text{C}_{m'}$) 127.75 ($\text{C}_{o'}$) 119.28 (C_p) 118.27 (C_o) 115.26 (C_o)	155.36 (C_2) 153.27 (C_6) 151.10 (C_4) 139.77 (C_8) 119.16 (C_5) 66.21 (C_{11}) 45.39 (C_{10})	139.72	134.10	129.99	124.43	122.00	148.16
11			NH_2	166.00 (C=O) 140.25 (C_m) 135.35 (C_i) 134.80 (C_i) 131.86 (C_p) 129.78 (C_m) 128.54 ($\text{C}_{m'}$) 127.77 ($\text{C}_{o'}$) 119.39 (C_p) 118.56 (C_o)* 115.40 (C_o)	158.40 (C_2) 153.23 (C_6) 151.53 (C_4) 139.18 (C_8) 118.56 (C_5)* 66.31 (C_{11}) 45.38 (C_{10})	138.72	116.09	128.67	115.68	113.83	148.50
29m				NO_2	163.96 (C=O) 151.88 (C_p) 148.42 ($\text{C}_{o'}$) 138.14 (C_p) 135.13 (C_o) 130.25 (C_i) 130.17 (C_i) 123.63 (C_o) 123.16 (C_m) 120.90 (C_m)	155.15 (C_2) 153.16 (C_6) 151.02 (C_4) 139.53 (C_8) 118.92 (C_5) 65.95 (C_{11}) 45.17 (C_{10})	139.66	133.54	129.69	123.97	121.60

* - Overlay of signals on the spectrum.

Rational design and synthesis of novel selective PI3K inhibitors for cancer therapy

Table 19 ^{13}C -NMR spectroscopic data (100 MHz, $\text{DMSO}-d_6$) for the new synthesized purine derivatives. (continuation)

Comp.	Base structure	R^1	R	R^1	Base Structure	Group A						
						C_i	C_o	C_m	C_p	$\text{C}_{o'}$	$\text{C}_{m'}$	
12			NH_2	164.24 (C=O) 152.27 (C_p) 148.71 ($\text{C}_{o'}$) 138.12 (C_p) 135.52 (C_o) 130.76 (C_i) 130.40 (C_i) 123.81 (C_o) 123.56 (C_m) 121.07 (C_m)		158.27 (C_2) 153.14 (C_6) 151.47 (C_4) 139.19 (C_8) 118.45 (C_5) 66.26 (C_{11}) 45.21 (C_{10})	138.72	115.84	128.62	115.58	113.41	148.55
29n			NO_2	164.43 (C=O) 152.35 (C_p) 148.77 ($\text{C}_{o''}$) 139.96 (C_m) 135.62 ($\text{C}_{o''}$) 135.14 (C_i) 130.44 (C_i) 129.85 (C_m) 123.63 ($\text{C}_{m''}$) 119.30 (C_p) 118.47 (C_o) 115.23 ($\text{C}_{o'}$)		155.39 (C_2) 153.28 (C_6) 151.09 (C_4) 139.69 (C_8) 119.21 (C_5) 66.25 (C_{11}) 45.48 (C_{10})	139.72	134.14	130.01	124.46	122.04	148.18
13			NH_2	164.56 (C=O) 152.38 (C_p) 148.77 ($\text{C}_{o''}$) 139.93 (C_m) 135.68 ($\text{C}_{o''}$) 135.43 (C_i) 130.55 (C_i) 129.94 (C_m) 123.71 ($\text{C}_{m''}$) 119.44 (C_p) 118.87 (C_o) 115.45 ($\text{C}_{o'}$)		158.41 (C_2) 153.27 (C_6) 151.54 (C_4) 139.20 (C_8) 118.60 (C_5) 66.35 (C_{11}) 45.31 (C_{10})	138.76	116.40	128.75	115.94	114.05	148.18

Table 19 ^{13}C -NMR spectroscopic data (100 MHz, $\text{DMSO}-d_6$) for the new synthesized purine derivatives. (continuation)

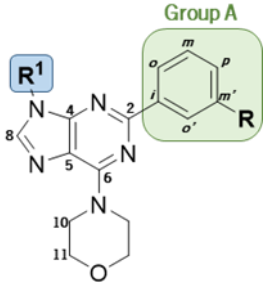
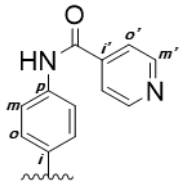
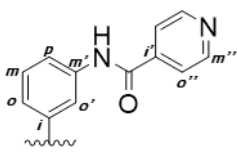
Comp.	Base structure	R^1	R	R^1	Base Structure	Group A					
						C_i	C_o	C_m	C_p	$\text{C}_{o'}$	$\text{C}_{m'}$
29o			NO_2	164.21 (C=O) 150.34 ($\text{C}_{m'}$) 141.73 (C_i) 138.13 (C_p) 130.61 (C_i) 124.00 (C_o) 121.63 ($\text{C}_{o'}$) 121.19 (C_m)	155.29 (C_2) 153.25 (C_6) 151.14 (C_4) 139.90 (C_8) 119.05 (C_5) 66.23 (C_{11}) 45.28 (C_{10})	139.71	133.91	130.11	124.45	121.84	148.12
14			NH_2	164.44 (C=O) 150.49 ($\text{C}_{m'}$) 141.92 (C_i) 137.96 (C_p) 131.15 (C_i) 123.98 (C_o) 121.79 ($\text{C}_{o'}$) 121.47 (C_m)	158.45 (C_2) 153.30 (C_6) 151.62 (C_4) 139.30 (C_8) 118.60 (C_5) 66.43 (C_{11}) 45.34 (C_{10})	138.89	116.12	128.86	115.87	113.64	148.65
29p			NO_2	164.65 (C=O) 150.52 ($\text{C}_{m'}$) 142.02 (C_i) 139.85 ($\text{C}_{m'}$) 135.34 (C_i) 130.13 (C_m) 121.93 ($\text{C}_{o'}$) 119.66 (C_p) 118.86 (C_o) 115.52 ($\text{C}_{o'}$)	155.60 (C_2) 153.44 (C_6) 151.24 (C_4) 139.78 (C_8) 119.36 (C_5) 66.44 (C_{11}) 45.43 (C_{10})	139.82	134.32	130.20	124.65	122.21	148.33

Table 19 ^{13}C -NMR spectroscopic data (100 MHz, $\text{DMSO}-d_6$) for the new synthesized purine derivatives. (continuation)

Comp.	Base structure	R^1	R	R^1	Base Structure	Group A						
						C_i	C_o	C_m	C_p	$\text{C}_{o'}$	$\text{C}_{m'}$	
29q			NO_2	165.05 (C=O) 152.61 (C_m) 140.40 (C_p) 138.48 (C_p) 130.15 (C_i) 129.66 (C_i) 123.71 (C_o) 121.21 (C_m) 105.30 ($\text{C}_{o'}$) 60.12 (Me_p) 56.09 (Me_m)		155.12 (C_2) 153.12 (C_6) 150.99 (C_4) 139.72 (C_8) 118.96 (C_5) 66.16 (C_{11}) 45.16 (C_{10})	139.60	133.77	129.95	124.31	121.71	147.97
18			NH_2	165.05 (C=O) 152.67 (C_m) 140.46 (C_p) 138.75 (C_p) 130.54 (C_i) 129.79 (C_i) 123.72 (C_o) 121.26 (C_m) 105.37 ($\text{C}_{o'}$) 60.14 (Me_p) 56.13 (Me_m)		158.24 (C_2) 153.14 (C_6) 151.46 (C_4) 139.16 (C_8) 118.46 (C_5) 66.26 (C_{11}) 45.26 (C_{10})	138.35	115.85	128.61	115.58	113.43	148.54

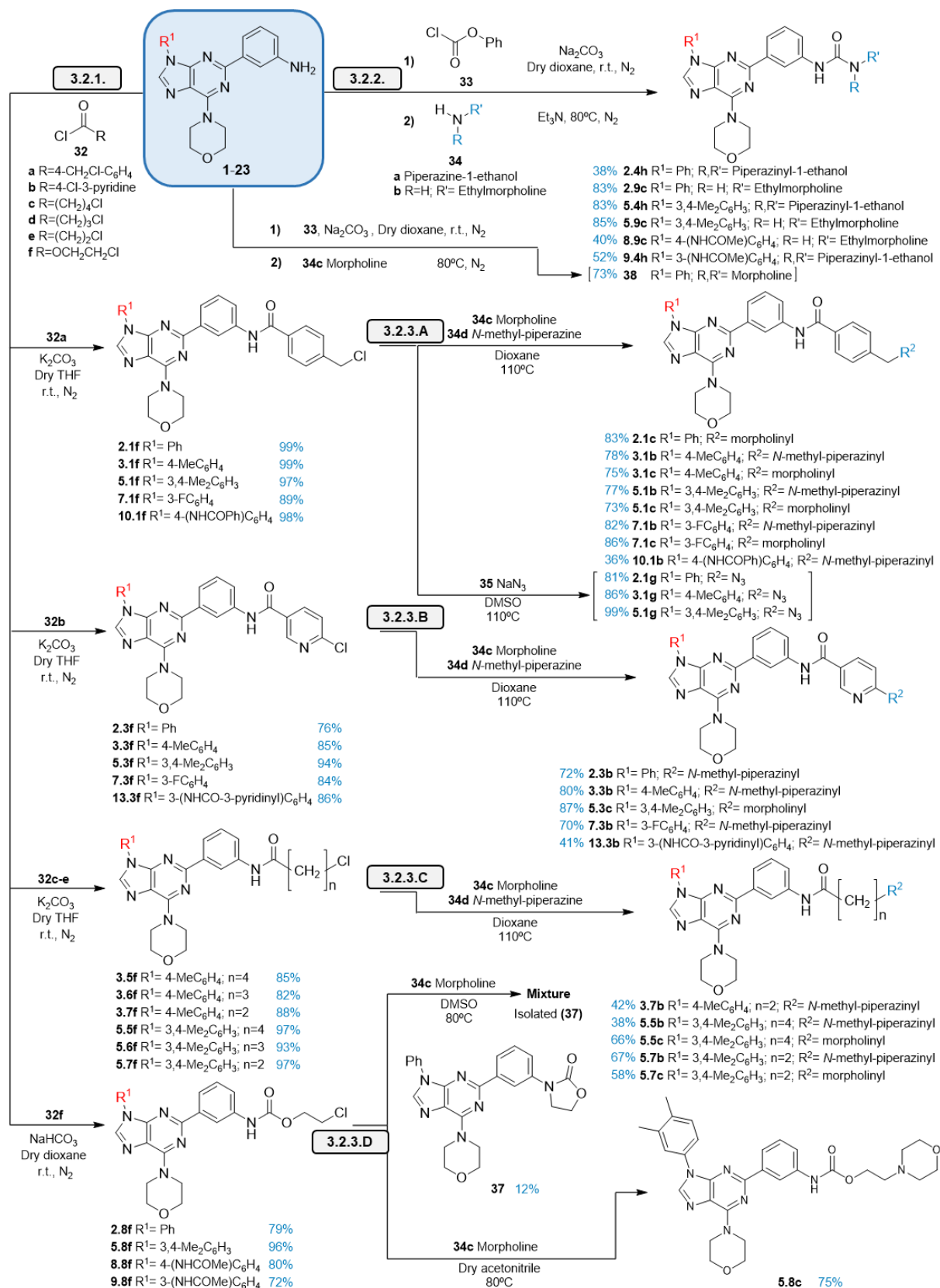
3.2. Synthesis of final products

The synthesis of final products is focused on the preparation of a series of derivatives containing in their structure either an amide, urea or carbamate functional group. In scheme 6, the synthesized compounds and their respective synthetic approach from 2-(3-aminophenyl)-purine derivatives are summarized.

The respective syntheses will be discussed throughout this subchapter, being divided into the acylation of 2-(3-aminophenyl)-purine derivatives (**3.2.1.**), one-pot synthesis of ureas from 2-(3-aminophenyl)-purine derivatives (**3.2.2.**), and the reaction of the acylated 2-(3-aminophenyl)-purine derivatives with nitrogen nucleophiles (**3.2.3.**). This last subchapter was divided according to the starting reagent used, that is, (**3.2.3.A**) – chloromethylphenyl derivatives, (**3.2.3.B**) – chloropyridine derivatives, (**3.2.3.C**) – chloroalkylamide derivatives and (**3.2.3.D**) – chloroalkylcarbamate derivatives. In addition, attempts towards the reduction of azides are presented in (**3.2.4.**)

Finally, all the pure final compounds obtained are physically, analytically and spectroscopically characterized in (**3.2.5.**).

Rational design and synthesis of novel selective PI3K inhibitors for cancer therapy

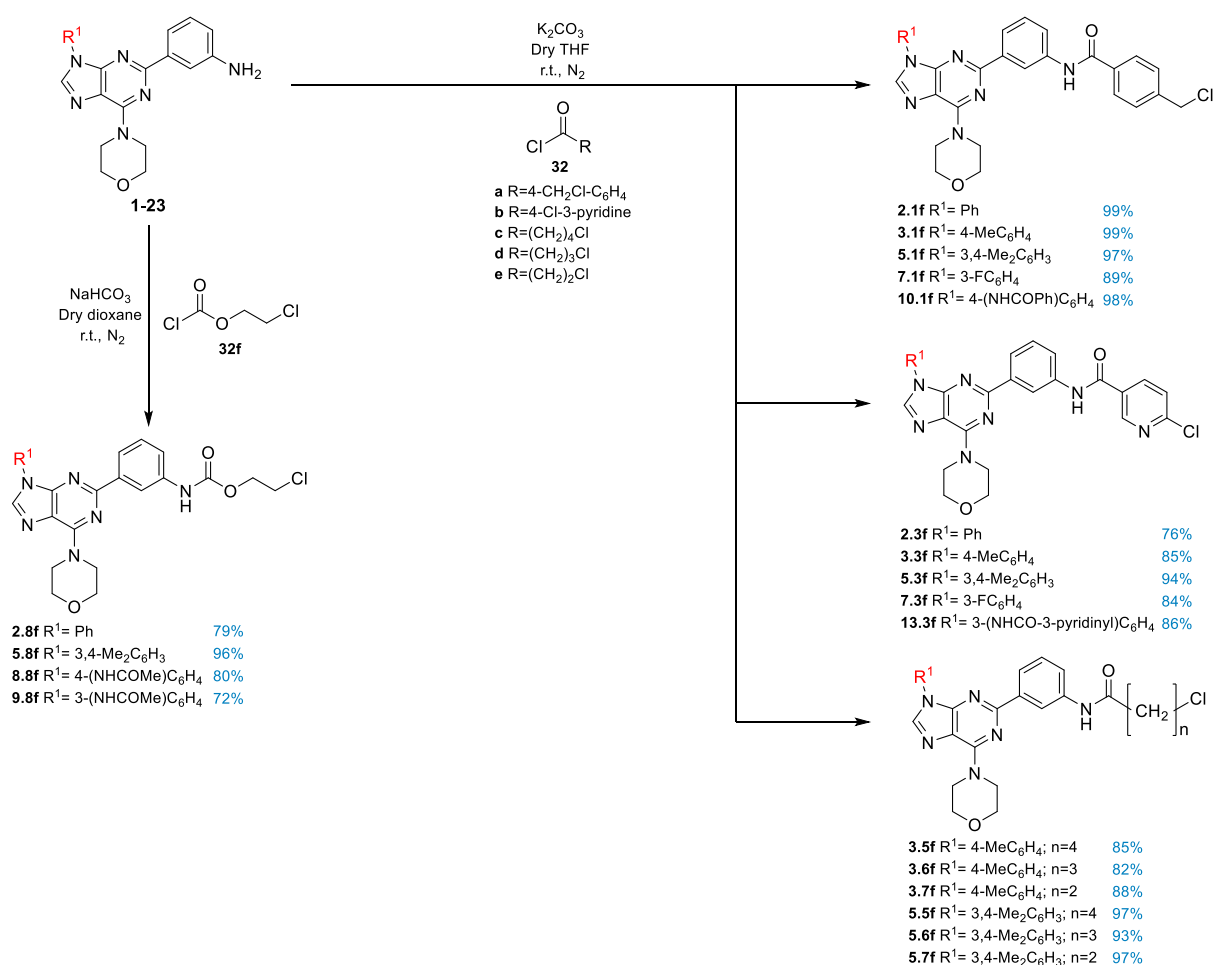


Scheme 6 Schematic representation of the synthetic approach used for the synthesis of the final products from 2-(3-aminophenyl)-purine derivatives.

Representation of all reaction steps, synthesized compounds and the best obtained yields highlighted in blue.

3.2.1. Acylation of 2-(3-aminophenyl)-purine derivatives

The derivatives shown in Scheme 7 were synthesized using a relatively simple approach by reacting the 2-(3-aminophenyl)-purine derivatives (**1-23**) with different acylation agents **32a-f** under a basic medium (NaHCO_3 or K_2CO_3) in dry dioxane or THF. The reactions were carried out in a closed vial, under anhydrous conditions and were controlled by TLC. The disappearance of the limiting reagent was verified after 1 to 3.5 hours of reaction. All the products were isolated with good to excellent yields.

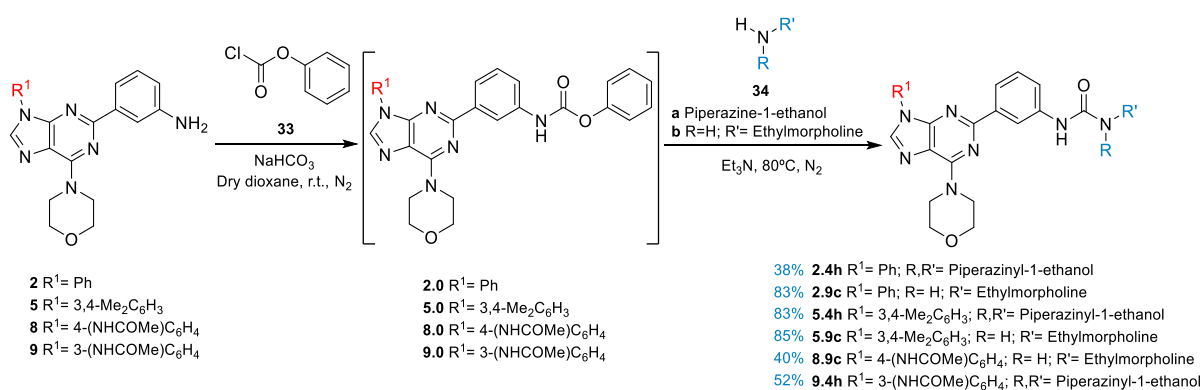


Scheme 7 Schematic representation of the acylation of 2-(3-aminophenyl)-purine derivatives and the best obtained yields highlighted in blue.

3.2.2. One-pot synthesis of ureas from 2-(3-aminophenyl)-purine derivatives

The synthesis of ureas started with the acylation of 2-(3-aminophenyl)-purine derivatives, however, due to some difficulties encountered in the isolation of the reaction intermediate, the reaction was carried out as a one-pot reaction, as described below.

The reaction approach presented in Scheme 8 was already reported for the synthesis of ureas [82], [83]. However, in our approach, the synthetic intermediates identified in the scheme are not isolated, in contrast to the reported reactions.



Scheme 8 Schematic representation of the one-pot synthesis of ureas from 2-(3-aminophenyl)-purine derivatives and the best obtained yields highlighted in blue.

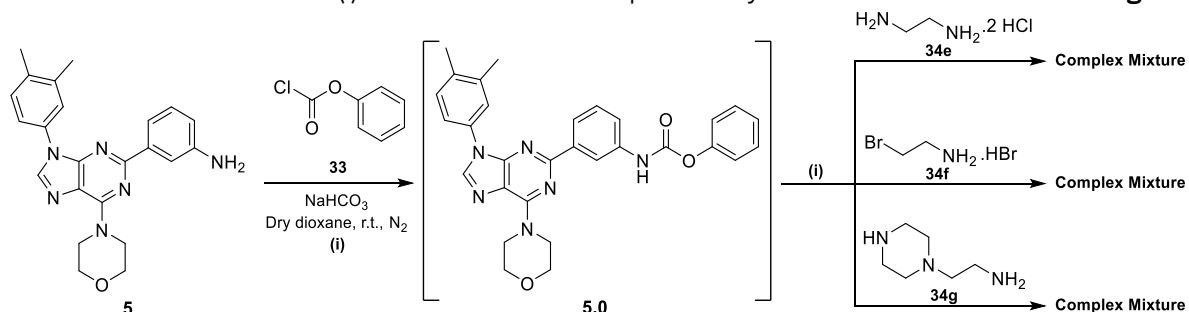
This methodology revealed an overall satisfactory performance for the products presented in Scheme 8. However, products **2.4h**, **8.9c** and **9.4h** were isolated in lower yields in comparison with the other derivatives, due to their increased solubility in water and the need for recrystallization from acetone.

Nevertheless, when the reaction with the amines **34e-g** was tested, complex mixtures were obtained in all of the assays (Table 20). The results obtained are most likely due to the nature of the amines used. In the case of diamines **34e** and **34g**, they have two nitrogen atoms to attack the intermediate carbamate **5.0** which can lead to competitive reaction products or may even promote the formation of polymers. In the case of the diamine **34g**, it is not symmetrical, having 2 different amines in its structure, one primary and one secondary. It would be expected that the secondary amine would attack the intermediate **5.0** first, given its higher nucleophilic nature. For this reason, two reactions were tested.

The first was performed at 80 °C (Entry 4) and the second at 45°C (Entry 5). No significant changes were observed in the ¹H-NMR spectrums of the solids isolated from each one of the reactions.

Then, we used the amine **34f**. The reaction was carried out at 80 °C (Entry 2) and at room temperature (Entry 3). A complex mixture of compounds was obtained in both cases. Considering that this amine can react with itself to generate polymers, the isolation of complex mixtures was not a surprise.

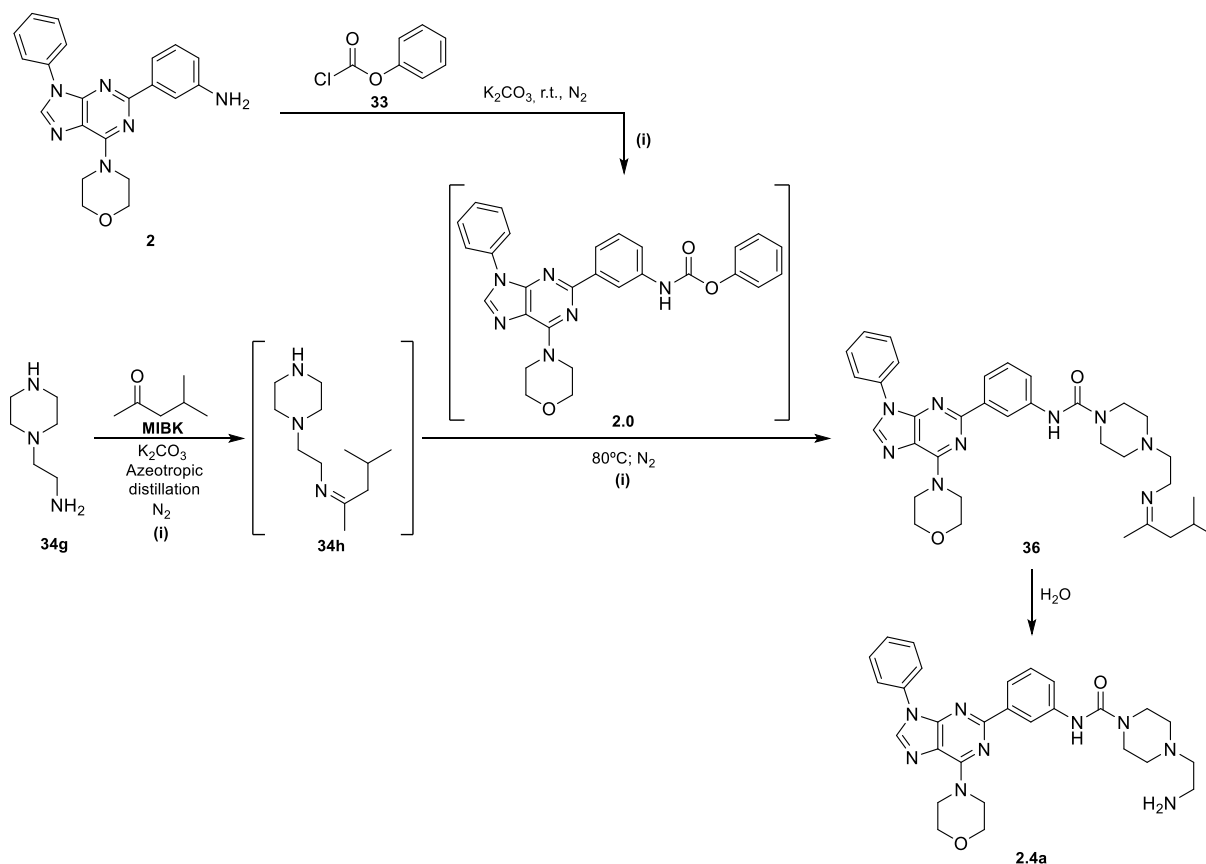
Table 20 Reaction conditions (i) and results for the attempts in the synthesis of ureas with amines **34e-g**.



Entry	Reaction Conditions (i)	Results ^{a)}
1	1. 5 (0.23 g, 0.56 mmol), 33 (1.15 eq., 78.1 μL , 0.62 mmol), NaHCO_3 (1.25 eq., 0.06 g, 0.71 mmol); Dry dioxane (3 mL), r.t., N_2 , 1 h 2. Et_3N (3 eq., 236 μL , 1.69 mmol); 34e (1.15 eq., 0.09 g, 0.65 mmol), N_2 , 80 °C, 2 h	Complex mixture (0.39 g)
2	1. 5 (0.18 g, 0.46 mmol), 33 (1.10 eq., 63.3 μL , 0.50 mmol), NaHCO_3 (1.25 eq., 0.05 g, 0.57 mmol); Dry dioxane (3 mL), r.t., N_2 , 1 h 2. Et_3N (3 eq., 191 μL , 1.37 mmol); 34f (1.15 eq., 0.09 g, 5.10 mmol), N_2 , 80 °C, 3 h	Complex mixture (0.24 g)
3	1. 5 (0.25 g, 0.62 mmol), 33 (1.25 eq., 100 μL , 0.78 mmol), NaHCO_3 (2.5 eq., 0.13 g, 1.56 mmol); Dry dioxane (3 mL), r.t., N_2 , 1.5 h 2. Et_3N (3 eq., 261 μL , 1.87 mmol); 34f (1.25 eq., 0.16 g, 0.78 mmol), N_2 , r.t., 2 days	Complex mixture (0.17 g)
4	1. 5 (0.05 g, 0.13 mmol), 33 (1.25 eq., 20.5 μL , 0.16 mmol), NaHCO_3 (2.5 eq., 0.03 g, 0.33 mmol); Dry dioxane (1.5 mL), r.t., N_2 , 1 h 2. Et_3N (3 eq., 54.5 μL , 0.39 mmol); 34g (1.2 eq., 21.0 μL , 0.16 mmol), N_2 , 80 °C, 2.5 h	Complex mixture (0.05 g)
5	1. 5 (0.05 g, 0.13 mmol), 33 (1.25 eq., 21.2 μL , 0.17 mmol), NaHCO_3 (2.5 eq., 0.03 g, 0.34 mmol); Dry dioxane (1 mL), r.t., N_2 , 1 h 2. Et_3N (3 eq., 56.2 μL , 0.40 mmol); 34g (1.2 eq., 21.3 μL , 0.16 mmol), N_2 , 45 °C, 14 h	Complex mixture (0.06 g)

a) By $^1\text{H-NMR}$ spectroscopy.

In order to try to eliminate the selectivity problem in the reaction with the diamine **34g**, a protocol described in the literature was adapted for the reaction (Scheme 9) [84]. In this approach and according to the literature, the amine **34g** initially reacts with the solvent methyl isobutylketone (**MIBK**) to generate a temporary protecting group for the primary amine. Then, the intermediate **34h** reacts with **2.0** to generate **36**. After the reaction of the secondary amine with **2.0**, the resulting imine intermediate **36** is smoothly hydrolysed, leading to the free primary amine.



Scheme 9 Schematic representation of the synthetic approach used for the synthesis of **2.4a** from a selective reaction with **34g** using MIBK.

To test this approach, two trials were carried out. In both assays, the protection of the primary amine with MIBK in the presence of K_2CO_3 was performed by azeotropic distillation of water at $88^\circ C$. When finished, the contents were added to a vial with the reaction intermediate **2.0**. In this step, different conditions were used, which are presented in Table 21. Firstly, the reaction was tested using dry dioxane as solvent (Entry 1). In the second attempt, the reaction to form the intermediate **2.0** was carried out in MIBK, in order to keep only one solvent in the reaction mixture and with an excess of **34h**. Both cases resulted in complex mixtures. This may be due to the instability of imine **34h** associated with a possible poor maintenance of the anhydrous conditions required for this reaction. No more reactions were attempted with the amine **34g**.

Table 21 Reaction conditions (i) and results for the attempts in the synthesis of **2.4a** with MIBK.

Entry	Reaction Conditions (i)	Results ^{a)}
1	1. 2 (0.17 g, 0.44 mmol), 33 (1.25 eq., 70.0 μ L, 0.55 mmol), K_2CO_3 (2.5 eq., 0.15 g, 1.11 mmol); Dry dioxane (3 mL), r.t., N_2 , 1 h 2. Et ₃ N (1.5 eq., 93.0 μ L, 0.67 mmol); 34h (2 eq, 0.89 mmol), N_2 , $80^\circ C$, 12 h	Complex mixture (0.13 g)
2	1. 2 (0.10 g, 0.28 mmol), 33 (1.25 eq., 44.0 μ L, 0.35 mmol), K_2CO_3 (2.5 eq., 0.10 g, 0.70 mmol); MIBK (5 mL), r.t., N_2 , 1 h 2. 34h (2.5 eq., 0.70 mmol), N_2 , $80^\circ C$, 2 h	Complex mixture (0.08 g)

a) By 1H -NMR spectroscopy.

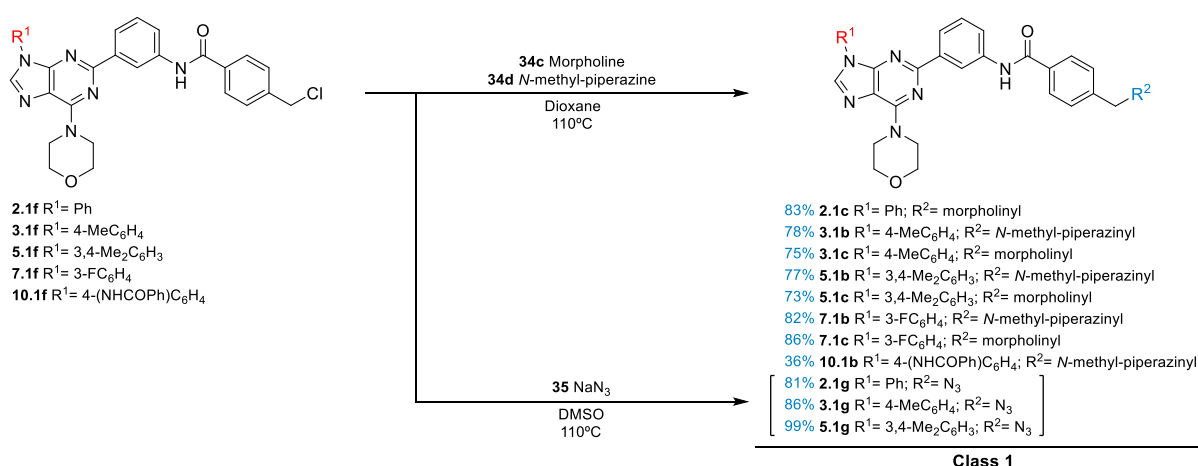
3.2.3. Reaction of the acylated 2-(3-aminophenyl)-purine derivatives with nitrogen nucleophiles

3.2.3.A – From chloromethylphenyl derivatives

To obtain the virtual screening final products of chapter 2, the acylated 2-(3-aminophenyl)-purine derivatives were reacted with morpholine, *N*-methyl-piperazine and sodium azide.

Through a bimolecular nucleophilic substitution, the acylated 2-(3-aminophenyl)-purine derivatives reacted with 5 equivalents of nucleophiles **34c** and **34d** in a closed vial at 110 °C. The reactions were again controlled by TLC. The compounds were isolated generally in good yields after 5-31 hours after the absence of starting material was confirmed (Scheme 10). However, compound **10.1b** proved to be quite soluble in water. For this reason, it had to be precipitated with diethyl ether, in contrast to the other derivatives, which were precipitated from water.

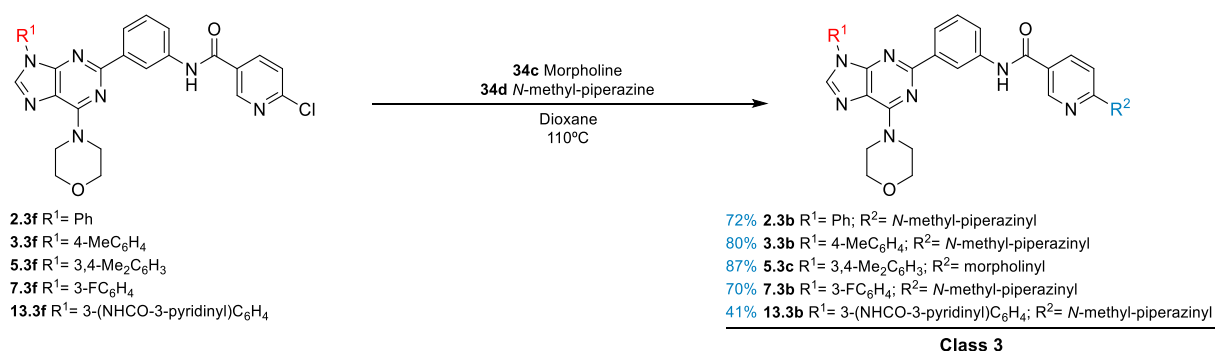
Aiming to synthesize derivatives **2.1g**, **3.1g** and **5.1g**, a few attempts were performed applying the reaction conditions used with the amines **34c** and **34d**. However, the reaction with sodium azide **35** in dioxane, at 110°C, proved to be too slow. Thus, the reaction solvent was replaced by DMSO and the respective precursors reacted with 5-6 equivalents of sodium azide **35**, at 110 °C, in a closed vial. After 1-14 hours, TLC showed the absence of starting material. The products were isolated with excellent yields and the presence of the azide functional group in the structure of the synthesized derivatives was confirmed by IR spectroscopy.



Scheme 10 Schematic representation of the reactions between the class 1 acylated 2-(3-aminophenyl)-purine derivatives with nitrogen nucleophiles, and their reaction conditions. Representation of the synthesized compounds and the best obtained yields are highlighted in blue.

3.2.3.B – From chloropyridine derivatives

Through an aromatic nucleophilic substitution, the class 3 compounds shown in Scheme 11, were obtained from the reaction of the respective synthetic precursors with 5 equivalents of the nucleophile (morpholine **34c** or *N*-methyl-piperazine **34d**). The reactions were carried out in a closed vial, at 110°C, in dioxane and controlled by TLC. After 12-24 hours of reaction, TLC showed absence of starting material and products **2.3b**, **3.3b**, **5.3c** and **7.3b** were isolated, after precipitation with water, in good yields. In the case of **13.3b**, due to its high solubility in water, it was isolated from diethyl ether. The lower relative yield of this product is probably due to its higher solubility in the solvents used.

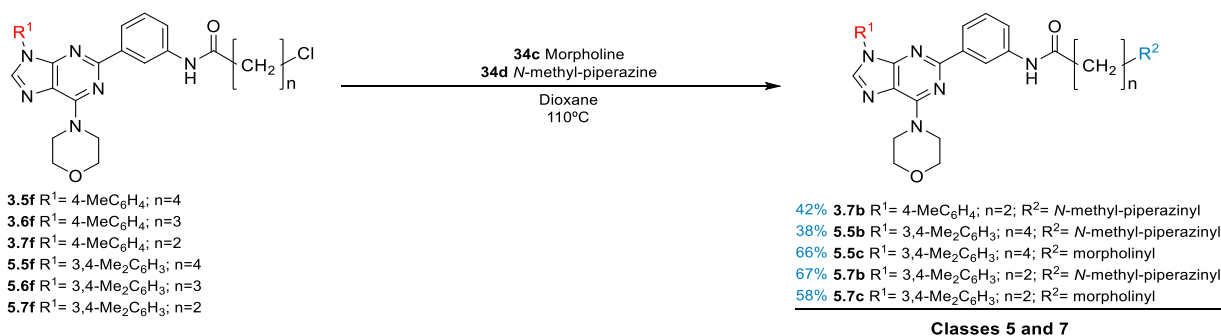


Scheme 11 Schematic representation of the synthesis of the class 3 compounds and the best obtained yields are highlighted in blue.

3.2.3.C – From chloroalkylamide derivatives

The same reaction conditions were applied in the synthesis of the derivatives of classes 5 and 7, from their synthetic precursors (Scheme 12). The precursors were reacted with the nucleophiles **34c** and **34d** in dioxane, in a closed vial, at 110°C. After 3.5 to 6 hours of reaction, TLC showed the absence of starting material. All compounds were subsequently precipitated with water and proved to be relatively soluble in this solvent, leading to pure products with moderate yields. In the case of compound **3.7b**, it was too much soluble in water and was isolated from diethyl ether.

When the same reaction conditions were applied to the synthesis of compounds from class 6, the isolated solids proved to be mixtures of compounds (Table 22).



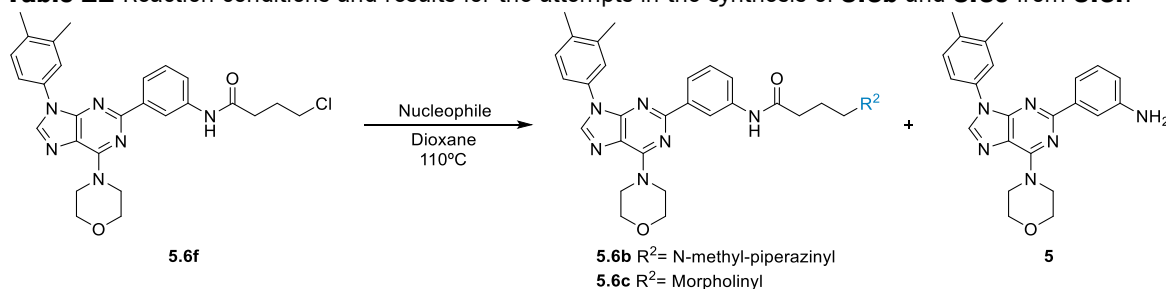
Scheme 12 Schematic representation of the reaction between the classes 5-7 acylated 2-(3-aminophenyl)-purine derivatives with the nitrogen nucleophiles.

Representation of the synthesized compounds and the best obtained yields are highlighted in blue.

Table 22 shows the results of the attempts for the synthesis of derivatives **5.6b** and **5.6c**. In both cases, the cleavage of the amide unit occurred. Through the control of the reactions by TLC, it was possible to see that the cleavage of the reagent **5.6f**, to generate **5**, and the formation of the products **5.6b/5.6c** took place simultaneously. The TLC showed the presence of the cleaved product (**5**) after 30 minutes of reaction. In addition, through ¹H-NMR spectroscopy, it was noticed that compound **5.6f** degrades with time when in solution (DMSO-*d*₆).

Due to time constraints relative to the deadline of the dissertation, it was not possible to perform additional tests. In the future, variations in the reaction conditions can be made in factors such as solvent, temperature and reaction time to obtain the desired products.

Table 22 Reaction conditions and results for the attempts in the synthesis of **5.6b** and **5.6c** from **5.6f**.



Entry	Reaction Conditions	Results ^{a)}
1	5.6f (0.10 g, 0.20 mmol), <i>N</i> -methyl-piperazine 34b (5 eq., 113 μL, 1.02 mmol) Dioxane (0.5 mL), 110°C, 5 h	5.6b (68%) + 5 (32%) (65.9 mg)
2	5.6f (82.3 mg, 0.16 mmol), morpholine 34c (5 eq., 71.0 μL, 0.82 mmol) Dioxane (0.5 mL), 110°C, 9 h	5.6c (55%) + 5 (45%) (56.2 mg)

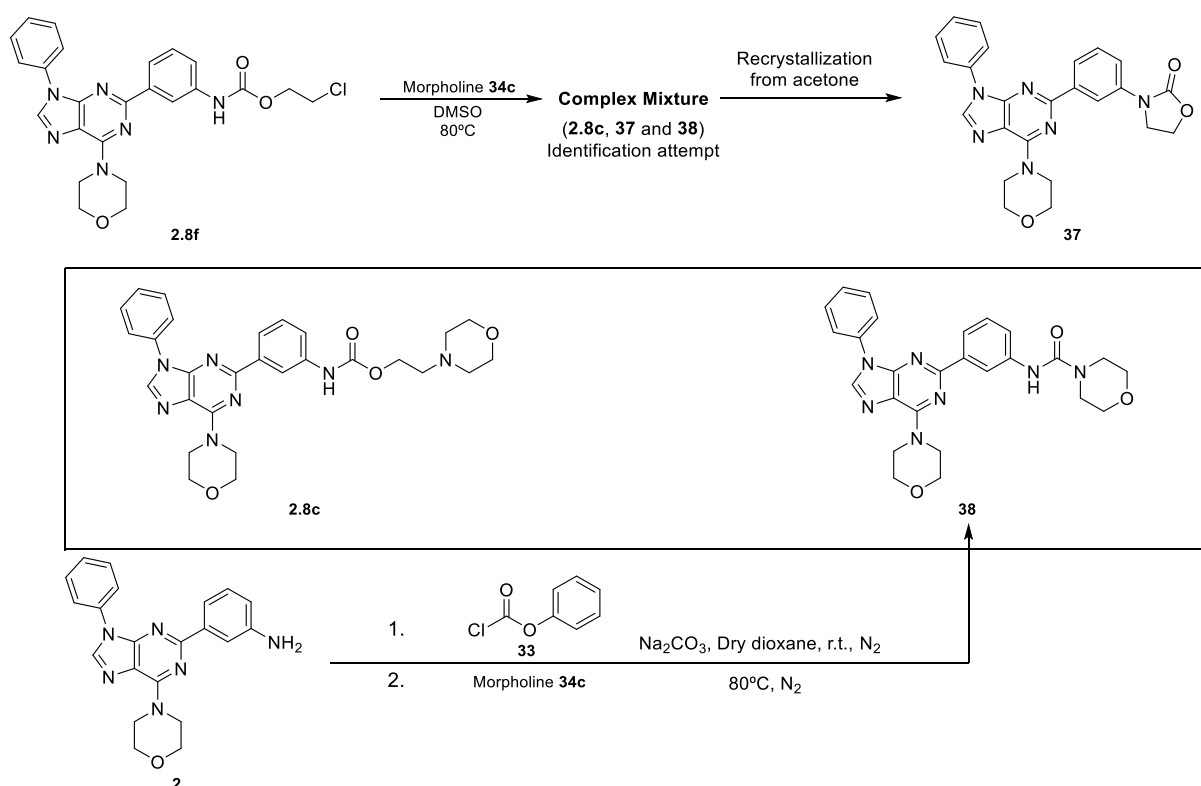
a) By ¹H-NMR spectroscopy.

3.2.3.D – From chloroalkylcarbamate derivatives

At last, to obtain the virtually screened products of class 8, for example, compound **2.8c** (Scheme 13), some synthetic approaches were tested, which are described hereafter.

First, the nucleophilic substitution of the chlorine atom of **2.8f** was tried with 5 equivalents of morpholine **34c** in DMSO, at 80°C. The reaction was carried out in a closed vial and controlled by TLC. After 16 hours, there were no traces of starting material. The resulting solid was isolated with water and the ¹H-NMR spectrum showed a complex mixture. An attempt to identify the compounds in the mixture was carried out. From the ¹H-NMR data, we tentatively identified 3 compounds, as shown in Scheme 13.

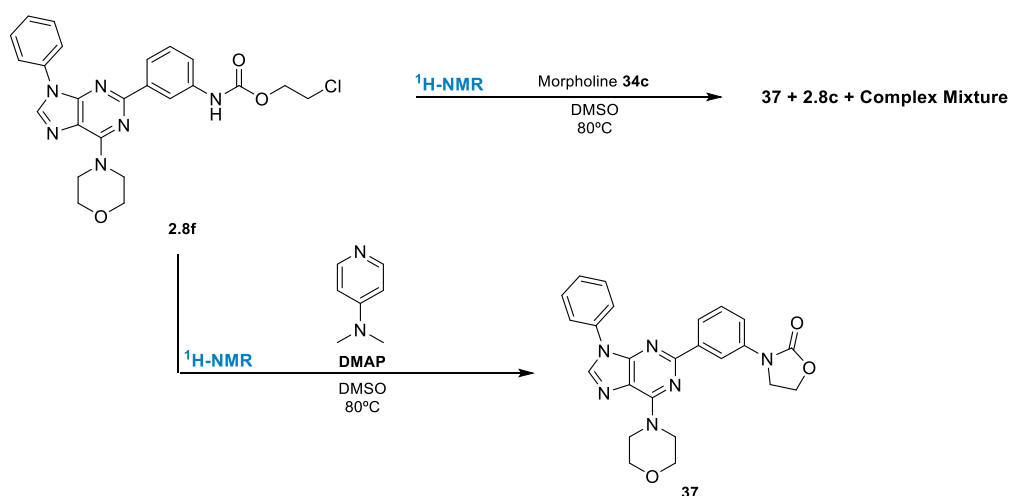
In order to isolate the major component, the solid obtained was recrystallized from acetone. The compound **37** was isolated pure in an overall 12% yield. Then, to confirm the presence of compound **38** in the complex mixture, this compound was synthesized by the reaction of **2** with **33**, followed by reaction with morpholine **34c**, in accordance with the methodology described in section 3.2.2. The signals in the ¹H-NMR spectrum of product **38** showed to be different from the signals selected in the spectrum of the initial mixture. Thus, it was proven that the structure of the third product in the mixture was not compound **38** and it could not be identified.



Scheme 13 Schematic representation of the reaction of **2.8f** with **34c** and the proposed structures for the major compounds present in the complex mixture.

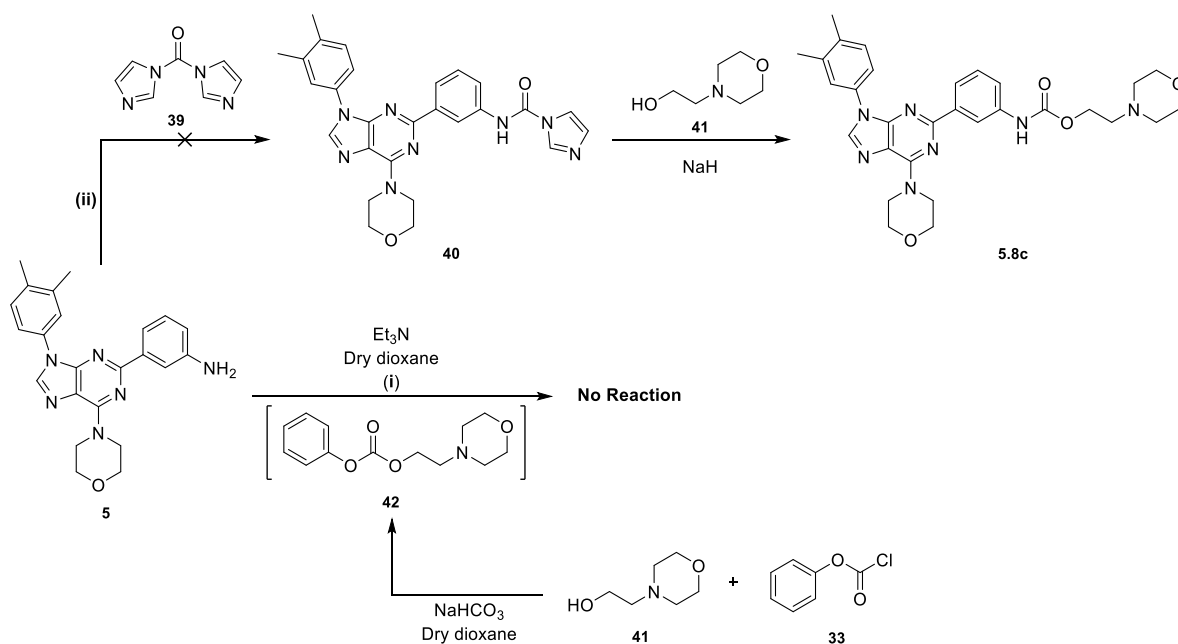
To understand the kinetic of the reaction, compound **2.8f** and 5 equivalents of morpholine **34c**, in 0.5 mL of DMSO- d_6 , were mixed in an NMR tube. The reaction was maintained at 80°C, over 4 days, and was punctually controlled (Scheme 14). The $^1\text{H-NMR}$ spectrum obtained confirmed the formation of the 3 products observed in the complex mixture isolated previously.

An additional NMR test was performed to understand the formation of compound **37**. For this purpose, instead of morpholine **34c**, a non-nucleophilic base was used. DMAP was chosen since the chemical shifts presented by this base's protons did not overlap with the chemical shifts found in the aliphatic zone of the original mixture. Compound **2.8f** and 5 equivalents of DMAP were reacted in 0.5 mL of DMSO- d_6 in an NMR tube, at 80°C. The reaction was carefully monitored by $^1\text{H-NMR}$ over 4 days. The disappearance of the NH-corresponding signal of the carbamate function in **2.8f**, together with a small shift associated with the aliphatic signals was noticeable, confirming the formation of compound **37**. This test proved that, in the presence of a base, compound **2.8f** undergoes an intramolecular reaction and forms an oxazolidinone ring through nucleophilic substitution of the chlorine by the N-H of the carbamate function (Scheme 14).



Scheme 14 Schematic representation of the reaction of **2.8f** with **34c**, and with DMAP, made in an NMR tube, in order to understand respectively the kinetics of the reaction and the formation of compound **37**.

After these results, synthetic alternatives for the synthesis of the desired derivatives were considered. In scheme 15, two synthetic alternatives are represented. Both alternatives use amine **5** and 2-morpholinoethanol **41** as starting reagents.



Scheme 15 Schematic representation of the two synthetic alternatives considered for the synthesis of the derivative **5.8c**, from the 2-(3-aminophenyl)-purine derivative **5**.

First, we reacted 2-morpholinoethanol **41** with phenyl chloroformate **33** to generate the carbonate **42**. After confirmation of the formation of **42** by TLC, compound **5** was solubilized in dry dioxane and added along with 3 equivalents of triethylamine. The purpose of this attempt was to verify if the attack of the nucleophile on the carbonyl of the carbonate **42** would happen, to generate **5.8c**, as reported in [85]. Two reactions were carried out using different temperatures. In both attempts, either at room temperature (Table 23- Entry 1) or at 80°C (Table 23- Entry 2), no reaction occurred and the starting material was recovered in the reaction isolation process.

Table 23 Reaction conditions and results for the attempts in the synthesis of **5.8c** from an adapted method used in the one-pot synthesis of the ureas.

Entry	Reaction Conditions (i)	Results ^{a)}
1	1. 45 (1.1 eq., 56.0 μL, 0.46 mmol), 33 (1.15 eq., 60.4 μL, 0.48 mmol), NaHCO ₃ (2.3 eq., 0.08 g, 0.96 mmol); Dry dioxane (1 mL), r.t., N ₂ , 1 h 2. 5 (0.17 g, 0.42 mmol), Et ₃ N (3 eq., 175 μL, 1.25 mmol), Dry dioxane (1 mL), N ₂ , r.t., 24 h	No reaction (0.13 g) of 5
2	1. 45 (1.1 eq., 56.0 μL, 0.46 mmol), 33 (1.15 eq., 60.4 μL, 0.48 mmol), NaHCO ₃ (2.3 eq., 0.08 g, 0.96 mmol); Dry dioxane (0.5 mL), r.t., N ₂ , 1 h 2. 5 (0.17 g, 0.42 mmol), Et ₃ N (3 eq., 175 μL, 1.25 mmol), Dry dioxane (1.5 mL), N ₂ , 80°C, 24 h	No reaction (0.13 g) of 5

a) By ¹H-NMR spectroscopy.

Given the unsuccessful outcomes of the strategy used, the second synthetic alternative presented in Scheme 15 (ii) was tried, based on conditions reported in the literature [86], [87]. This approach

consists on the reaction of compound **5** with carbonyldiimidazole (CDI) (**39**) to synthesize compound **40**. This intermediate can later react with 2-morpholinoethanol **41** in the presence of a hydride (NaH). The respective alkoxide is supposed to attack the carbonyl of the synthetic intermediate **40**, thus giving the desired product **5.8c**. For this purpose, **5** (0.13 mmol) was reacted with a total of 3.7 equivalents of CDI (**39**) in THF, at 0°C, according to the reported reaction conditions [87]. After 10 days, only a minimal amount of product was visible by TLC. Therefore, the reaction mixture was composed essentially of the starting material. The reaction was expected to occur more rapidly and for this reason, the proposed alternative route was abandoned.

Considering that changing the solvent may change the reactivity of the starting reagent, new attempts were carried out. Thus, the reaction of the compounds **2.8f** or **5.8f** with morpholine **34c** were tested again under the reaction conditions described in Table 24. All these reactions were carefully monitored by TLC.

Table 24 Reaction conditions and results for the attempts in the synthesis of **2.8c** or **5.8c** through the reaction of their respective synthetic precursors (**2.8f** and **5.8f**, respectively) with morpholine **34c**.

Entry	Reaction Conditions (i)	Results ^{a)}
1	2.8f (76.8 mg, 0.16 mmol), 34c (5 eq., 69.9 μ L, 0.80 mmol) Dry dioxane (1 mL), 110°C, 24 h	2 (50%) + 2.8c (50%) (25.1 mg)
2	2.8f (64.5 mg, 0.14 mmol), 34c (5 eq., 58.7 μ L, 0.67 mmol) Dry dioxane (0.5 mL), 70°C, 5 days	2.8f (22%) + 2 (9%) + 2.8c (69%) (53.0 mg)
3	5.8f (52.3 mg, 0.10 mmol), 34c (10 eq., 89.7 μ L, 1.03 mmol) Dry THF (1 mL), 80°C, 38 h	F ₁ - 22.0 mg - 5.8f (traces) + 5.8c F ₂ - 20.0 mg - 5.8f (28%) + 5 (19%) + 5.8c (53%)
4	5.8f (50.2 mg, 0.10 mmol), 34c (10 eq., 86.1 μ L, 0.99 mmol) Dry acetonitrile (0.25 mL), 80°C, 22 h	5 (8%) + 5.8c (92%) (51.5 mg)

a) By ¹H-NMR spectroscopy.

In the first trial, the solvent was changed to dry dioxane and the reaction temperature was raised to 110°C (Table 24 - Entry 1). Under these conditions, in a closed vial, the reaction of compound **2.8f** with 5 equivalents of **34c** gave, after 24 hours, a mixture of the desired product **2.8c** (50%) and compound **2** (50%), resulting either from the cleavage of the starting material **2.8f** or the product **2.8c**. To test the effect of the reaction temperature on the formation of compound **2**, in a second trial, the temperature was decreased to 70°C (Table 24 - Entry 2). After 5 days, the starting material was still present. However, there was a significant decrease in the percentage of compound **2** in the mixture (9%).

Considering the results obtained in these last 2 trials, the temperature of 80°C was maintained for the following trials. In both, 10 equivalents of **34c** were reacted with **5.8f** in different solvents, as a way to speed up the reaction. In the first attempt, the solvent used was dry THF (Table 24 - Entry 3). In the later attempt (Table 24 - Entry 4), dry acetonitrile was used as the solvent. Both reactions were carried out in a closed vial, under efficient magnetic stirring, at 80°C, as stated. It was confirmed that at this temperature, only a relatively low percentage of compound **5** was present in the mixture. When the reaction was made in dry THF, after 38 hours, it was completed. Water was added to the reaction mixture and a solid precipitated. It was filtered off and washed with ethanol. The ¹H-NMR spectrum showed **5.8c** and traces of starting reagent. A second fraction was obtained after concentration of the mother liquor. The ¹H-NMR spectrum of this sample showed the mixture described in Table 24.

This information was taken into account for the last trial, in dry acetonitrile. After 22 hours of reaction, the solid from the reaction mixture was precipitated with water. By ¹H-NMR, this solid proved to be a mixture of the desired product **8.8c** (92%) and compound **5** (8%). The sample was then recrystallized from ethanol, giving the desired pure product **8.8c**, with an overall good yield of 75%. In the future, these same conditions will be applied to different derivatives to validate this synthetic approach.

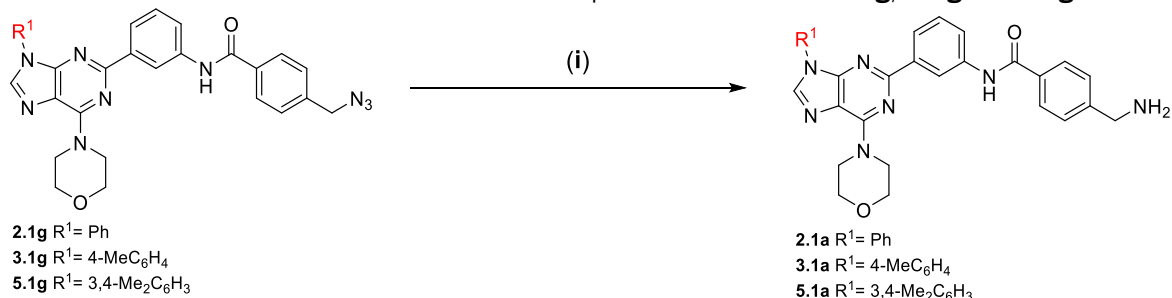
3.2.4. Attempts towards the reduction of azides

Several reported approaches are known for the synthesis of amines. In this work, we selected the reduction of azides for the synthesis of the derivatives with R²=NH₂ (Table 25). For this purpose, different methodologies found in the literature were applied in 5 trials, using the derivatives **2.1g**, **3.1g** and **5.1g**.

We started with a catalytic hydrogenation of **5.1g** using Pd/C [88]. In the first experiment, compound **5.1g** was solubilized in dry THF under anhydrous conditions. To this solution, Pd/C (10%) was added and the reaction atmosphere was saturated with hydrogen (Table 25 - Entry 1). The reaction was carefully controlled by TLC, and after 6 days the TLC still showed the presence of starting material. However, after an aliquot of the mixture was analysed by ¹H-NMR, it was noticed that the signal of the CH₂ adjacent to the azide, was not present. The reaction was then stopped and a solid was isolated, which showed to be a complex mixture, in which no starting material was identified. To verify that the complex mixture was caused by the excessive reaction time, a second experiment (Table 25 - Entry 2) was carried out under the same conditions, but this time controlled by ¹H-NMR. After 22 hours, the ¹H-NMR spectrum showed the disappearance of the signal of the CH₂ adjacent to the azide. This means that there was no more starting reagent in the reaction mixture. However, a complex mixture was again

obtained upon isolation of the solid. Different purification methods were tested, namely dry flash and recrystallization, without success.

Table 25 Reaction conditions and results of the attempts of the reduction of **2.1g**, **3.1g** and **5.1g**.



Entry	Reaction Conditions (i)	Results ^{a)}
1	5.1g (135 mg, 0.26 mmol), Pd/C 10% (13.5 mg) Dry THF (32 mL), H ₂ , r.t., 6 days	Complex mixture (88.3 mg)
2	5.1g (82.1 mg, 0.16 mmol), Pd/C 10% (8.21 mg) Dry THF (10 mL), H ₂ , r.t., 22 h	Complex mixture (68.5 mg)
3	5.1g (165 mg, 0.31 mmol), Zn (1.5 eq., 30.5 mg, 0.47 mmol), NH ₄ Cl (2.5 eq., 42.0 mg, 0.78 mmol) EtOH:H ₂ O (6 mL : 2 mL), 80°C., 3 h	No reaction (124 mg)
4	3.1g (57.0 mg, 0.10 mmol), NaI (4 eq., 62.7 mg, 0.42 mmol), Amberlite (0.2 g) DCM : MeOH (10 mL : 1.5 mL), r.t., 3 days	No reaction ^{b)}
5	1. 2.1g (68.5 mg, 0.13 mmol), PPh ₃ (2 eq., 67.6 mg, 0.26 mmol) Dry THF (5 mL), 80°C., 24 h 2. H ₂ O (1 mL), 80°C, 16 h.	Mixture ^{c)}

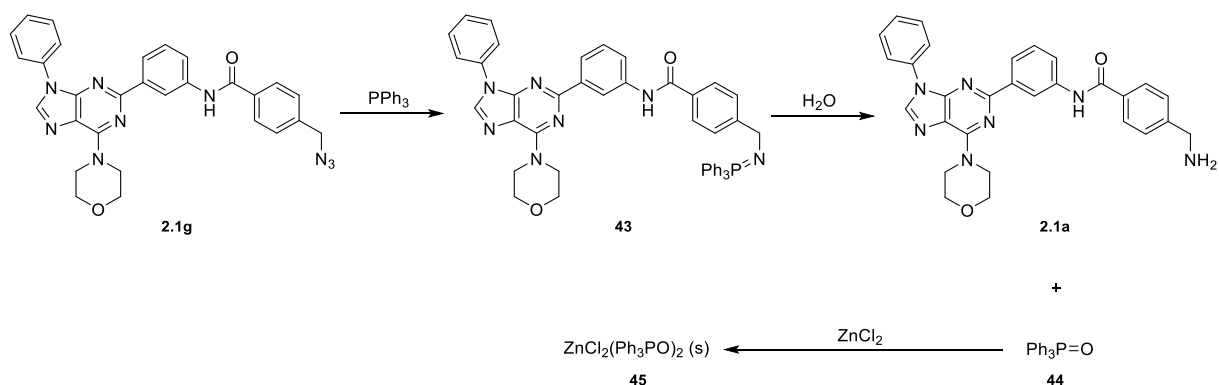
a) By ¹H-NMR spectroscopy.
b) Attempts in the isolation of the reaction gave rise to an oil.
c) The attempt made to isolate the desired product did not work as expected, leading to the isolation of **44**.

Based on these results, a new reported approach was tried to reduce the azide in compound **5.1g**. This compound was reacted with 1.5 eq. of zinc (Zn) and 2.5 eq. of ammonium chloride (NH₄Cl) in an aqueous solution of ethanol under reflux (Table 25 - Entry 3). The reported conditions [89] describe the reaction as fast and clean, lasting from 10 minutes to 2 hours. However, after 3 hours of reaction, only reagent **5.1g** was identified by TLC. It was collected after addition of water to the reaction mixture.

Next, the compound **3.1g** was reacted with sodium iodide (NaI) and amberlite (IR-120 H⁺) in a mixture of dichloromethane (DCM) and methanol (MeOH) (Table 25 - Entry 4), according to reported conditions [90]. The reaction was carried out at room temperature for 3 days. Since the TLC did not show the formation of any product, an aliquot of the reaction mixture was analysed by ¹H-NMR, to confirm this observation.

Finally, the Staudinger reaction [91] was implemented to try the reduction of compound **2.1g** (Table 25 - Entry 5). This compound was solubilised in dry THF and 2 eq. of triphenylphosphine (PPh₃) were added to the solution. The reaction was carried out in a closed vial, at 80°C. After 24 hours, TLC

showed the absence of starting reagent **2.1g**. Distilled water was then added to the reaction mixture. The TLC showed the formation of two new products, after 16 hours. One of the products of this reaction is triphenylphosphine oxide **44** as shown in Scheme 16. This by-product can be difficult to separate from the reaction product **2.1a**. For this reason, a procedure reported in the literature was attempted [92]. In All the solvent of the reaction mixture was evaporated. Then, we solubilized the obtained crude in THF and 3 equivalents of zinc chloride (ZnCl_2) were added to the solution according to the reported conditions. After 24 hours, a white solid had precipitated from the solution. The solid was filtered and discarded, and the solution was evaporated. The resulting solid was a mixture, by $^1\text{H-NMR}$, in which traces of the desired product were identified. However, the major component was **44**, revealing that the separation attempt was not successful.



Scheme 16 Schematic representation of the Staudinger reaction applied to compound **2.1g**, and subsequent attempt for the separation of the by-product **44** by a reported method using zinc chloride.

3.2.5. Characterization of final compounds

All the newly synthesized products described in **3.2.** have their physical, analytical and spectroscopic characterisation reported in this subchapter. The compounds **2.1f**, **7.1f** and **7.1b** were synthesised, however, the full characterisation of these derivatives is already reported in [93].

In order to facilitate the characterization of the compounds, a generic structure was constructed (Figure 38) based on their structural similarities. In this structure, the purine core and group **A** are common to all compounds. The structural variations occur only in groups **R¹** and **B**, whose respective structure fragments are presented in Tables 28 and 29.

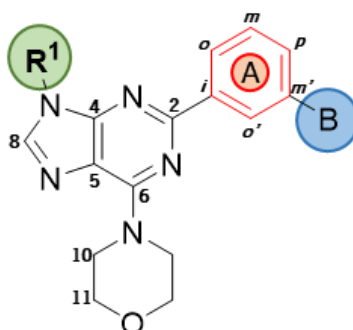


Figure 38 Generic structure of the compounds, where the purine core and group **A** are maintained in all of the compounds, while variations occur in the **R¹** and **B** groups.

3.2.5.1. Physical and analytical characterization

The physical and analytical data for all the newly synthesized compounds are presented in Table 26. It was not possible to acquire mass spectrometry and elemental analysis data for the samples until the dissertation deadline. For this reason, the values presented for these components in Table 26 are only theoretical.

Table 26 Physical and theoretical analytical data of the compounds synthesized in subchapter 3.2.

Compound	m.p. (°C)	Molecular Formula*	Molecular Weight (g/mol)*	Elemental analysis (%) (Expected values)*		
				C	H	N
2.1c	247 – 249	C ₃₃ H ₃₃ N ₇ O ₃	575.67	68.85	5.78	17.03
2.1g	184 – 186	C ₂₉ H ₂₅ N ₉ O ₂	531.58	65.53	4.74	23.71
2.3b	277 – 279	C ₃₂ H ₃₃ N ₉ O ₂	575.68	66.77	5.78	21.90
2.3f	> 280	C ₂₇ H ₂₂ ClN ₇ O ₂	511.97	63.34	4.33	19.15
2.4h	223 – 225	C ₂₈ H ₃₂ N ₈ O ₃	528.62	63.62	6.10	21.20
2.8f	175 – 177	C ₂₄ H ₂₃ ClN ₆ O ₃	478.94	60.19	4.84	17.55
2.9c	268 – 270	C ₂₈ H ₃₂ N ₈ O ₃	528.62	63.62	6.10	21.20
37	> 280	C ₂₄ H ₂₂ N ₆ O ₃	442.48	65.15	5.01	18.99
38	199 – 201	C ₂₆ H ₂₇ N ₇ O ₃	485.55	64.32	5.61	20.19
3.1b	251 – 253	C ₃₅ H ₃₈ N ₈ O ₂	602.74	69.75	6.35	18.59
3.1c	> 280	C ₃₄ H ₃₅ N ₇ O ₃	589.70	69.25	5.98	16.63
3.1f	254 – 256	C ₃₀ H ₂₇ ClN ₆ O ₂	539.04	66.85	5.05	15.59
3.1g	235 – 237	C ₃₀ H ₂₇ N ₉ O ₂	545.61	66.04	4.99	23.11
3.3b	> 280	C ₃₃ H ₃₅ N ₉ O ₂	589.70	67.21	5.98	21.38
3.3f	269 – 271	C ₂₈ H ₂₄ ClN ₇ O ₂	526.00	63.94	4.60	18.64
3.5f	200 – 202	C ₂₇ H ₂₉ ClN ₆ O ₂	505.02	64.21	5.79	16.64
3.6f	179 – 181	C ₂₆ H ₂₇ ClN ₆ O ₂	490.99	63.60	5.54	17.12
3.7b	206 – 208	C ₃₀ H ₃₆ N ₈ O ₂	540.67	66.64	6.71	20.73
3.7f	208 – 210	C ₂₅ H ₂₅ ClN ₆ O ₂	476.97	62.96	5.28	17.62
5.1b	216 – 217	C ₃₆ H ₄₀ N ₈ O ₂	616.77	70.11	6.54	18.17
5.1c	219 – 220	C ₃₅ H ₃₇ N ₇ O ₃	603.73	69.63	6.18	16.24
5.1f	228 – 230	C ₃₁ H ₂₉ ClN ₆ O ₂	553.06	67.32	5.29	15.20
5.1g	181 – 183	C ₃₁ H ₂₉ N ₉ O ₂	559.63	66.53	5.22	22.53
5.3c	168 – 170	C ₃₃ H ₃₄ N ₈ O ₃	590.69	67.10	5.80	18.97
5.3f	262 – 264	C ₂₉ H ₂₆ ClN ₇ O ₂	540.02	64.50	4.85	18.16
5.4h	150 – 152	C ₃₀ H ₃₆ N ₈ O ₃	556.67	64.73	6.52	20.13
5.5b	195 – 197	C ₃₃ H ₄₂ N ₈ O ₂	582.75	68.02	7.26	19.23
5.5c	154 – 156	C ₃₂ H ₃₉ N ₇ O ₃	569.71	67.46	6.90	17.21
5.5f	198 – 200	C ₂₈ H ₃₁ ClN ₆ O ₂	519.05	64.79	6.02	16.19
5.6f	201 – 203	C ₂₇ H ₂₉ ClN ₆ O ₂	505.02	64.21	5.79	16.64
5.7b	195 – 197	C ₃₁ H ₃₈ N ₈ O ₂	554.70	67.12	6.91	20.20
5.7c	189 – 191	C ₃₀ H ₃₅ N ₇ O ₃	541.66	66.52	6.51	18.10
5.7f	226 – 228	C ₂₆ H ₂₇ ClN ₆ O ₂	490.99	63.60	5.54	17.12
5.8c	180 – 181	C ₃₀ H ₃₅ N ₇ O ₄	557.66	64.62	6.33	17.58
5.8f	209 – 211	C ₂₆ H ₂₇ ClN ₆ O ₃	506.99	61.60	5.35	16.58
5.9c	228 – 229	C ₃₀ H ₃₆ N ₈ O ₃	556.67	64.73	6.52	20.13
7.1c	208 – 210	C ₃₃ H ₃₂ FN ₇ O ₃	593.66	66.77	5.43	16.52
7.3b	260 – 262	C ₃₂ H ₃₂ FN ₉ O ₂	593.67	64.74	5.43	21.23
7.3f	262 – 263	C ₂₇ H ₂₁ ClFN ₇ O ₂	529.96	61.19	3.99	18.50
8.8f	240 – 242	C ₂₆ H ₂₆ ClN ₇ O ₄	535.99	58.26	4.89	18.29
8.9c	218 – 220	C ₃₀ H ₃₅ N ₉ O ₄	585.67	61.52	6.02	21.52
9.4h	231 – 233	C ₃₀ H ₃₅ N ₉ O ₄	585.67	61.52	6.02	21.52
9.8f	269 – 271	C ₂₆ H ₂₆ ClN ₇ O ₄	535.99	58.26	4.89	18.29
10.1b	273 – 275	C ₄₁ H ₄₁ N ₉ O ₃	707.84	69.57	5.84	17.81
10.1f	236 – 238	C ₃₆ H ₃₀ ClN ₇ O ₃	644.13	67.13	4.69	15.22
13.3b	187 – 189	C ₃₈ H ₃₇ N ₁₁ O ₃	695.79	65.60	5.36	22.14
13.3f	199 – 201	C ₃₃ H ₂₆ ClN ₉ O ₃	632.08	62.71	4.15	19.94

* Data collected from ChemDraw software.

3.2.5.2. Infra-red spectroscopy (IR) characterization

Overall, the identification of the structures of the final compounds can be confirmed by the appearance of one to three bands between 1600 and 1735 cm^{-1} . These bands of medium or strong intensity are characteristic of the stretching vibrations of the new C=O bond, common to all compounds presented in Table 27 [77]. In this same region, there are also a few bands of weak or medium intensity associated with N-H bending vibrations [77]. However, when the R¹ group has an amide functional group (**8.8f**, **8.9c**, **9.4h**, **9.8f**, **10.1b**, **10.1f**, **13.3b** and **13.3f**), additional bands appear in this region, in comparison to the other derivatives.

Regarding the region between 1500 and 1600 cm^{-1} , a set of bands of variable intensity can be seen, representing the stretching vibrations of the C=C and C=N bonds. The region between 3000 to 3500 cm^{-1} shows one or a few bands of variable intensity, which are typical of the stretching of N-H bonds [77].

Furthermore, the presence of the azide functional group in the structure of the compounds **2.1g**, **3.1g** and **5.1g** was confirmed by the presence of a band of medium or strong intensity between 2093 and 2101 cm^{-1} , characteristic of the stretching of the N=N=N bond [77].

Rational design and synthesis of novel selective PI3K inhibitors for cancer therapy

Table 27 IR spectroscopic data (Nujol/cm⁻¹) for the compounds synthesized in subchapter 3.2.

Compound	3500 – 3000 cm ⁻¹	3000 – 2000 cm ⁻¹	2000 – 1500 cm ⁻¹
2.1c	3316	-	1648, 1607, 1576 (s), 1542 (s), 1513
2.1g	3315, 3142 (w)	2093	1637 (s), 1605, 1580 (s), 1542 (s), 1510
2.3b	3293, 3058	-	1643, 1605, 1577, 1532, 1513
2.3f	3292	-	1643 (s), 1601, 1578 (s), 1538
2.4h	3397 (w), 3309 (w)	-	1625 (s), 1580, 1524
2.8f	3431, 3296 (s)	-	1728 (s), 1610 (s), 1601, 1575 (s), 1558 (s), 1514
2.9c	3311 (s)	-	1633 (s), 1596 (s), 1580 (s), 1532 (s), 1521 (s)
37	3087	-	1735 (s), 1595 (s), 1580 (s), 1519
38	3358, 3132	-	1635 (s), 1600, 1579 (s), 1531, 1515
3.1b	3332	-	1645, 1606, 1577, 1538, 1524
3.1c	3337	-	1644, 1606 (w), 1573, 1540, 1523
3.1f	3329, 3139	-	1646 (s), 1605, 1577 (s), 1534
3.1g	3326, 3139 (w)	2099	1644, 1605, 1579 (s), 1537
3.3b	3323, 3289	-	1642 (s), 1600 (s), 1582 (s), 1530 (s)
3.3f	3311 (s), 3127, 3052	-	1650 (s), 1604 (s), 1575 (s), 1561 (s), 1538 (s), 1525 (s)
3.5f	3290, 3137	-	1660 (s), 1600, 1582 (s), 1567, 1540, 1524
3.6f	3278, 3138 (w)	-	1654 (s), 1606, 1579 (s), 1547 (s), 1524
3.7b	3280 (s)	-	1666 (s), 1609 (s), 1578 (s), 1523 (s)
3.7f	3281 (w), 3137 (w)	-	1673 (w), 1655, 1606, 1579, 1547, 1525
5.1b	3281	-	1646, 1608, 1575 (s), 1534
5.1c	3280	-	1646 (s), 1607, 1573 (s), 1516 (s)
5.1f	3282	-	1645 (s), 1609, 1575 (s), 1533 (s), 1508
5.1g	3313 (w)	2101 (s)	1658, 1609, 1575 (s), 1515
5.3c	3346	-	1651, 1602 (s), 1575 (s), 1503
5.3f	3303 (s), 3120, 3054	-	1687, 1650 (s), 1606 (s), 1574 (s), 1539 (s), 1516 (s)
5.4h	3356	-	1637, 1597, 1573 (s), 1548, 1519
5.5b	3219	-	1640, 1598, 1573, 1544, 1517
5.5c	3224 (s)	-	1641 (s), 1598 (s), 1573 (s), 1517 (s)
5.5f	3245 (s), 3121, 3060	-	1650 (s), 1599, 1574 (s), 1540, 1519
5.6f	3310 (s), 3111, 3020	-	1654 (s), 1598 (s), 1567 (s), 1525 (s)
5.7b	3218	-	1640, 1598, 1573 (s), 1516 (s)
5.7c	3246, 3129	-	1641, 1599, 1578 (s), 1538, 1520

Weak (w) and strong (s) intensity peaks are denoted after their respective value. The remaining peaks have medium intensity.

Table 27 IR spectroscopic data (Nujol/cm⁻¹) for the compounds synthesized in subchapter 3.2. (continuation)

Compound	3500 – 3000 cm ⁻¹	3000 – 2000 cm ⁻¹	2000 – 1500 cm ⁻¹
5.7f	3260 (s), 3127, 3059 (w)	-	1661 (s), 1607, 1600 (s), 1577 (s), 1547 (s), 1520 (s)
5.8c	3251 (w), 3079 (w)	-	1731, 1576 (s), 1517
5.8f	3295, 3101 (w)	-	1729 (s), 1614, 1571 (s), 1517
5.9c	3318, 3129 (w)	-	1636 (s), 1600, 1575 (s), 1519
7.1c	3306, 3131 (w)	-	1650 (s), 1607, 1575 (s), 1532
7.3b	3306	-	1644 (s), 1604 (s), 1577 (s), 1534, 1507 (s)
7.3f	3274, 3122	-	1646 (s), 1604, 1567 (s), 1542 (s), 1518
8.8f	3402, 3259 (w), 3105 (w)	-	1729, 1712 (w), 1674, 1581 (s), 1524
8.9c	3296	-	1658, 1634, 1600, 1569 (s), 1548, 1522 (s)
9.4h	3355 (w), 3263 (w), 3207 (w), 3118, 3080 (w)	-	1691, 1627, 1603 (s), 1560 (s)
9.8f	3307 (w), 3311 (w), 3133	-	1741, 1727, 1685, 1661, 1618, 1603 (s), 1578 (s), 1557 (s)
10.1b	3333	-	1675 (s), 1640 (s), 1584 (s), 1534 (s), 1508 (s)
10.1f	3417 (s)	-	1782, 1716 (w), 1650 (s), 1606, 1578 (s), 1527 (s)
13.3b	3279	-	1653, 1603, 1575, 1550
13.3f	3295, 3104	-	1645 (s), 1607, 1575 (s), 1543 (s), 1511

Weak (w) and strong (s) intensity peaks are denoted after their respective value. The remaining peaks have medium intensity.

3.2.5.3. $^1\text{H-NMR}$ spectroscopy characterization

The compounds synthesized in subchapter 3.2. were synthesised from the 2-(3-aminophenyl)-purine derivatives (**1-23**). To facilitate the discussion of the overall variations in the $^1\text{H-NMR}$ chemical shifts of the different compounds, the structural model in Figure 39 was constructed.

Generally, in comparison with the synthetic precursors, the $^1\text{H-NMR}$ data of the compounds in Table 28 is consistent for the chemical shifts of the protons of the R^1 group and the protons of the purine nucleus. The final compounds are distinguished from the precursors (**1-23**), upon the disappearance of the singlet, between 4.5 and 5.4 ppm, correspondent to the amine group protons. In addition, there is an overall increase in the chemical shifts of the protons of ring A, with emphasis on the *para* (*p*), *ortho'* (*o'*) and *ortho* (*o*) protons. This increase can be justified by the change of the electronic resonance effect conferred by the functional group in B. The new functional groups (amides, carbamates and ureas) are withdrawing, which enhances the chemical shifts of these protons. However, these chemical shifts are still lower than the chemical shifts of the 2-(3-nitrophenyl)-purine derivatives **29**.

No significant differences are visible in the chemical shifts of the ring A protons, upon change of the functional group between amides ($\text{X}=\text{C}$), ureas ($\text{X}=\text{N}$) and carbamates ($\text{X}=\text{O}$). The more pronounced variation corresponds to the change in the chemical shift of the N-H proton, adjacent to ring A (Figure 39). When $\text{X}=\text{C}$, the chemical shift of this proton varies between 9.97 and 10.62 ppm. However, when $\text{X}=\text{N}$, the chemical shift oscillates between 8.62 and 8.75 ppm. Lastly, in carbamates ($\text{X}=\text{O}$), the chemical shift of this proton ranges between 9.77 and 9.92 ppm.

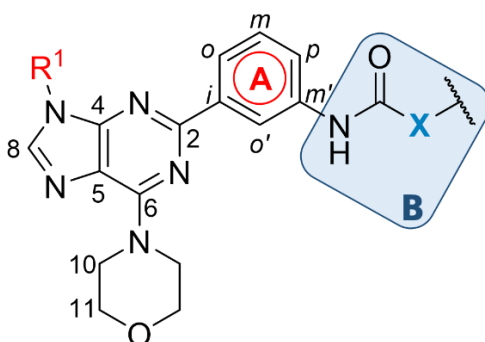
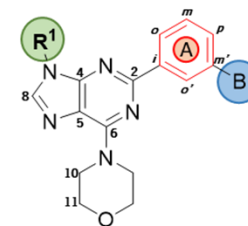
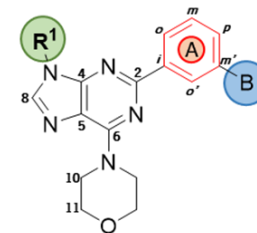


Figure 39 Representative structural model of the majority of the final products reported. Variations in X identify the functional groups of the final amides ($\text{X}=\text{C}$), ureas ($\text{X}=\text{N}$) and carbamates ($\text{X}=\text{O}$) synthesized.

**Table 28** ¹H-NMR spectroscopic data (400 MHz, DMSO-*d*₆) for the compounds synthesized in subchapter 3.2.

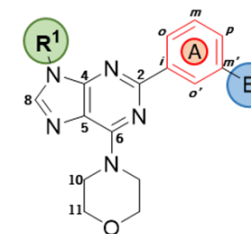
Comp.	R ¹	Group B	R ¹	Purine	Group A	Group B
2.1c			7.9 – 8.0 (m, 2H, H _o) * ¹ 7.64 (t, 2H, <i>J</i> = 8.0 Hz, H _m) 7.4 – 7.5 (m, 1H, H _p) * ²	8.63 (s, 1H, H _a) 4.37 (br s, 4H, H ₁₀) 3.80 (t, 4H, <i>J</i> = 4.8 Hz, H ₁₁)	8.66 (s, 1H, H _o) 8.11 (dt, 1H, <i>J</i> = 8.0, 1.6 Hz, H _o) 7.9 – 8.0 (m, 1H, H _p) * ¹ 7.4 – 7.5 (m, 1H, H _m) * ²	10.35 (s, 1H, NH) 7.9 – 8.0 (m, 2H, H _o) * ¹ 7.4 – 7.5 (m, 2H, H _m) * ² 3.58 (t, 4H, <i>J</i> = 4.8 Hz, H ₃) 3.53 (s, 2H, H ₁) 2.36 (t, 4H, <i>J</i> = 4.8 Hz, H ₂)
2.1g			7.9 – 8.0 (m, 2H, H _o) * ¹ 7.65 (t, 2H, <i>J</i> = 8.0 Hz, H _m) 7.49 (t, 1H, <i>J</i> = 8.0 Hz, H _p)	8.63 (s, 1H, H _a) 4.37 (br s, 4H, H ₁₀) 3.80 (t, 4H, <i>J</i> = 4.8 Hz, H ₁₁)	8.67 (t, 1H, <i>J</i> = 2.0 Hz, H _o) 8.11 (dt, 1H, <i>J</i> = 8.0, 1.2 Hz, H _o) 7.9 – 8.0 (m, 1H, H _p) * ¹ 7.45 (t, 1H, <i>J</i> = 8.0 Hz, H _m)	10.42 (s, 1H, NH) 7.9 – 8.0 (m, 2H, H _o) * ¹ 7.53 (d, 2H, <i>J</i> = 8.0 Hz, H _m) 4.56 (s, 2H, CH ₂)
2.3f			7.96 (m, 2H, H _o) * ¹ 7.63 (t, 2H, <i>J</i> = 7.6 Hz, H _m) 7.47 (m, 1H, H _p) * ²	8.60 (s, 1H, H _a) 4.35 (br s, 4H, H ₁₀) 3.80 (t, 4H, <i>J</i> = 4.8 Hz, H ₁₁)	8.64 (s, 1H, H _o) 8.13 (d, 1H, <i>J</i> = 8.0 Hz, H _o) 7.96 (m, 1H, H _p) * ¹ 7.47 (m, 1H, H _m) * ²	10.61 (s, 1H, NH) 8.97 (s, 1H, H _o) 8.36 (d, 1H, <i>J</i> = 8.4 Hz, H _o) 7.69 (d, 1H, <i>J</i> = 8.4 Hz, H _m)
2.3c			7.97 (m, 2H, H _o) * ¹ 7.64 (t, 2H, <i>J</i> = 6.8 Hz, H _m) 7.48 (t, 1H, <i>J</i> = 6.8 Hz, H _p)	8.61 (s, 1H, H _a) * ² 4.36 (br s, 4H, H ₁₀) 3.80 (s, 4H, H ₁₁)	8.61 (s, 1H, H _o) * ² 8.08 (m, 1H, H _o) * ³ 7.97 (m, 1H, H _p) * ¹ 7.42 (t, 1H, <i>J</i> = 7.6 Hz, H _m)	10.13 (s, 1H, NH) 8.76 (s, 1H, H _o) 8.08 (m, 1H, H _o) * ³ 6.90 (d, 1H, <i>J</i> = 8.4 Hz, H _m) 3.62 (s, 4H, H ₁) 2.38 (s, 4H, H ₂) 2.20 (s, 3H, H ₃)
2.4h			7.95 (m, 2H, H _o) * ¹ 7.63 (m, 2H, H _m) * ² 7.49 (tt, 1H, <i>J</i> = 8.0, 1.2 Hz, H _p)	8.60 (s, 1H, H _a) 4.35 (br s, 4H, H ₁₀) 3.79 (t, 4H, <i>J</i> = 4.8 Hz, H ₁₁)	8.32 (t, 1H, <i>J</i> = 2.0 Hz, H _o) 7.95 (m, 1H, H _o) * ¹ 7.63 (m, 1H, H _p) * ² 7.31 (t, 1H, <i>J</i> = 8.0 Hz, H _m)	8.63 (s, 1H, NH) 4.43 (t, 1H, <i>J</i> = 5.6 Hz, OH) 3.52 (q, 2H, <i>J</i> = 5.6 Hz, H ₄) 3.45 (t, 4H, <i>J</i> = 4.8 Hz, H ₁) 2.42 (m, 6H, H ₂ + H ₃)
2.8f			7.99 (m, 2H, H _o) * ¹ 7.66 (m, 2H, H _m) * ² 7.49 (m, 1H, H _p)	8.63 (s, 1H, H _a) 4.36 (m, 4H, H ₁₀) * ³ 3.80 (t, 4H, <i>J</i> = 4.8 Hz, H ₁₁)	8.46 (s, 1H, H _o) 7.99 (m, 1H, H _o) * ¹ 7.66 (m, 1H, H _p) * ² 7.37 (t, 1H, <i>J</i> = 8.0 Hz, H _m)	9.92 (s, 1H, NH) 4.36 (m, 2H, H ₁) 3.87 (m, 2H, H ₂)
2.9c			7.95 (dt, 2H, <i>J</i> = 7.6, 1.2 Hz, H _o) 7.64 (t, 2H, <i>J</i> = 7.6 Hz, H _m) 7.49 (tt, 1H, <i>J</i> = 7.6, 1.2 Hz, H _p)	8.60 (s, 1H, H _a) 4.35 (br s, 4H, H ₁₀) 3.79 (t, 4H, <i>J</i> = 4.8 Hz, H ₁₁)	8.17 (t, 1H, <i>J</i> = 1.6 Hz, H _o) 7.89 (dt, 1H, <i>J</i> = 8.0, 1.6 Hz, H _o) 7.70 (ddd, 1H, <i>J</i> = 8.0, 2.4, 0.8 Hz, H _p) 7.30 (t, 1H, <i>J</i> = 8.0 Hz, H _m)	8.75 (s, 1H, NH _A) 6.06 (t, 1H, <i>J</i> = 5.6 Hz, NH _B) 3.58 (t, 4H, <i>J</i> = 4.8 Hz, H ₄) 3.22 (q, 2H, <i>J</i> = 5.6 Hz, H ₁) 2.38 (m, 6H, H ₂ + H ₃)

*¹, *², *³ – Overlay of signals on the spectrum.

**Table 28** ¹H-NMR spectroscopic data (400 MHz, DMSO-*d*₆) for the compounds synthesized in subchapter 3.2. (continuation)

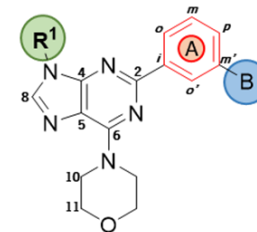
Comp.	R ¹	Group B	R ¹	Purine	Group A	Group B
37			7.99 (d, 2H, <i>J</i> = 8.0 Hz, H _o) 7.63 (m, 2H, H _m) * ¹ 7.48 (m, 1H, H _p) * ²	8.58 (s, 1H, H ₈) 4.36 (s, 4H, H ₁₀) 3.81 (t, 4H, <i>J</i> = 4.8 Hz, H ₁₁)	8.60 (s, 1H, H _o) 8.11 (d, 1H, <i>J</i> = 8.0 Hz, H _o) 7.63 (m, 1H, H _p) * ¹ 7.48 (m, 1H, H _m) * ²	4.47 (t, 2H, <i>J</i> = 7.6 Hz, H ₂) 4.13 (t, 2H, <i>J</i> = 7.6 Hz, H ₁)
38			7.96 (m, 2H, H _o) * ¹ 7.64 (m, 2H, H _m) * ² 7.49 (m, 1H, H _p)	8.61 (s, 1H, H ₈) 4.35 (br s, 4H, H ₁₀) 3.79 (t, 4H, <i>J</i> = 4.8 Hz, H ₁₁)	8.32 (t, 1H, <i>J</i> = 2.0 Hz, H _o) 7.96 (m, 1H, H _o) * ¹ 7.64 (m, 1H, H _p) * ² 7.32 (t, 1H, <i>J</i> = 8.0 Hz, H _m)	8.67 (s, 1H, NH) 3.61 (t, 4H, <i>J</i> = 4.8 Hz, H ₂) 3.44 (t, 4H, <i>J</i> = 4.8 Hz, H ₁)
3.1f			7.81 (d, 2H, <i>J</i> = 8.4 Hz, H _o) 7.42 (d, 2H, <i>J</i> = 8.4 Hz, H _m) 2.40 (s, 3H, Me)	8.56 (s, 1H, H ₈) 4.36 (br s, 4H, H ₁₀) 3.80 (t, 4H, <i>J</i> = 4.8 Hz, H ₁₁)	8.64 (t, 1H, <i>J</i> = 1.6 Hz, H _o) 8.10 (d, 1H, <i>J</i> = 8.0 Hz, H _o) 7.94 (d, 1H, <i>J</i> = 8.0 Hz, H _p) 7.44 (t, 1H, <i>J</i> = 8.0 Hz, H _m)	10.42 (s, 1H, NH) 7.98 (d, 2H, <i>J</i> = 8.0 Hz, H _o) 7.59 (d, 2H, <i>J</i> = 8.0 Hz, H _m) 4.84 (s, 2H, CH ₂)
3.1b			7.82 (d, 2H, <i>J</i> = 8.0 Hz, H _o) 7.43 (m, 2H, H _m) * ¹ 2.42 (br s, 3H, Me) * ²	8.47 (s, 1H, H ₈) 4.37 (t, 4H, <i>J</i> = 4.8 Hz, H ₁₀) 3.82 (t, 4H, <i>J</i> = 4.8 Hz, H ₁₁)	8.64 (s, 1H, H _o) 8.10 (d, 1H, <i>J</i> = 8.0 Hz, H _o) 7.92 (br s, 1H, H _p) 7.43 (m, 1H, H _m) * ¹	10.11 (s, 1H, NH) 7.93 (d, 2H, <i>J</i> = 8.0 Hz, H _o) 7.43 (m, 2H, H _m) * ¹ 3.54 (s, 2H, H ₁) 2.42 (br s, 4H, H ₂) * ² 2.34 (t, 4H, <i>J</i> = 4.8 Hz, H ₃) 2.17 (s, 3H, H ₄)
3.1c			7.82 (d, 2H, <i>J</i> = 8.4 Hz, H _o) 7.43 (m, 2H, H _m) * ¹ 2.40 (s, 3H, Me)	8.56 (s, 1H, H ₈) 4.36 (br s, 4H, H ₁₀) 3.80 (s, 4H, H ₁₁)	8.63 (s, 1H, H _o) 8.10 (d, 1H, <i>J</i> = 8.0 Hz, H _o) 7.94 (m, 1H, H _p) * ² 7.43 (m, 1H, H _m) * ¹	10.34 (s, 1H, NH) 7.94 (m, 2H, H _o) * ² 7.43 (m, 2H, H _m) * ¹ 3.57 (m, 6H, H ₁ + H ₃) 2.37 (s, 4H, H ₂)
3.1g			7.81 (d, 2H, <i>J</i> = 8.4 Hz, H _o) 7.43 (d, 2H, <i>J</i> = 8.4 Hz, H _m) 2.40 (s, 3H, Me)	8.56 (s, 1H, H ₈) 4.35 (br s, 4H, H ₁₀) 3.80 (t, 4H, <i>J</i> = 4.8 Hz, H ₁₁)	8.64 (t, 1H, <i>J</i> = 2.0 Hz, H _o) 8.10 (dt, 1H, <i>J</i> = 8.0, 1.2 Hz, H _o) 7.96 (ddd, 1H, <i>J</i> = 8.0, 2.0, 1.2 Hz, H _p) 7.44 (t, 1H, <i>J</i> = 8.0 Hz, H _m)	10.41 (s, 1H, NH) 7.99 (d, 2H, <i>J</i> = 8.0 Hz, H _o) 7.53 (d, 2H, <i>J</i> = 8.0 Hz, H _m) 4.56 (s, 2H, CH ₂)
3.3f			7.80 (d, 2H, <i>J</i> = 8.4 Hz, H _o) 7.43 (d, 2H, <i>J</i> = 8.4 Hz, H _m) 2.40 (s, 3H, Me)	8.55 (s, 1H, H ₈) 4.35 (br s, 4H, H ₁₀) 3.79 (t, 4H, <i>J</i> = 4.8 Hz, H ₁₁)	8.61 (t, 1H, <i>J</i> = 1.6 Hz, H _o) 8.13 (d, 1H, <i>J</i> = 8.0 Hz, H _o) 7.95 (dd, 1H, <i>J</i> = 8.0, 1.6 Hz, H _p) 7.45 (t, 1H, <i>J</i> = 8.0 Hz, H _m)	10.61 (s, 1H, NH) 8.96 (d, 1H, <i>J</i> = 2.4 Hz, H _o) 8.36 (dd, 1H, <i>J</i> = 8.4, 2.4 Hz, H _o) 7.70 (d, 1H, <i>J</i> = 8.4 Hz, H _m)

*¹, *² – Overlay of signals on the spectrum.

**Table 28** ¹H-NMR spectroscopic data (400 MHz, DMSO-*d*₆) for the compounds synthesized in subchapter 3.2. (continuation)

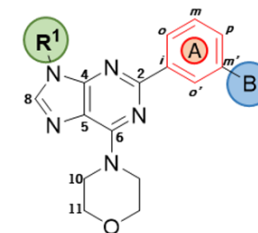
Comp.	R ¹	Group B	R ¹	Purine	Group A	Group B
3.3b			7.82 (d, 2H, <i>J</i> = 8.4 Hz, H _o) 7.43 (d, 2H, <i>J</i> = 8.4 Hz, H _m) 2.40 (s, 3H, Me)	8.56 (s, 1H, H ₈) 4.36 (br s, 4H, H ₁₀) 3.80 (t, 4H, <i>J</i> = 4.8 Hz, H ₁₁)	8.58 (s, 1H, H _o) 8.08 (m, 1H, H _o) * 7.96 (d, 1H, <i>J</i> = 8.0, H _p) 7.41 (t, 1H, <i>J</i> = 8.0 Hz, H _m)	10.13 (s, 1H, NH) 8.75 (d, 1H, <i>J</i> = 2.0 Hz, H _o) 8.08 (m, 1H, H _o) * 6.90 (d, 1H, <i>J</i> = 9.2 Hz, H _m) 3.62 (t, 4H, <i>J</i> = 4.8 Hz, H ₁) 2.38 (t, 4H, <i>J</i> = 4.8 Hz, H ₂) 2.21 (s, 3H, H ₃)
3.5f			7.80 (d, 2H, <i>J</i> = 8.0 Hz, H _o) 7.43 (d, 2H, <i>J</i> = 8.0 Hz, H _m) 2.41 (s, 3H, Me)	8.55 (s, 1H, H ₈) 4.34 (br s, 4H, H ₁₀) 3.79 (t, 4H, <i>J</i> = 4.8 Hz, H ₁₁)	8.40 (s, 1H, H _o) 8.02 (d, 1H, <i>J</i> = 8.0 Hz, H _o) 7.87 (d, 1H, <i>J</i> = 8.0 Hz, H _p) 7.36 (t, 1H, <i>J</i> = 8.0 Hz, H _m)	10.01 (s, 1H, NH) 3.67 (t, 2H, <i>J</i> = 6.4 Hz, H ₄) 2.37 (t, 2H, <i>J</i> = 6.8 Hz, H ₁) 1.75 (m, 4H, H ₂ + H ₃)
3.6f			7.80 (d, 2H, <i>J</i> = 8.4 Hz, H _o) 7.42 (d, 2H, <i>J</i> = 8.4 Hz, H _m) 2.40 (s, 3H, Me)	8.54 (s, 1H, H ₈) 4.34 (br s, 4H, H ₁₀) 3.79 (t, 4H, <i>J</i> = 4.8 Hz, H ₁₁)	8.41 (s, 1H, H _o) 8.02 (d, 1H, <i>J</i> = 8.0 Hz, H _o) 7.88 (d, 1H, <i>J</i> = 8.0 Hz, H _p) 7.36 (t, 1H, <i>J</i> = 8.0 Hz, H _m)	10.10 (s, 1H, NH) 3.71 (t, 2H, <i>J</i> = 6.4 Hz, H ₃) 2.51 (m, 2H, H ₁) 2.02 (m, 2H, H ₂)
3.7f			7.80 (d, 2H, <i>J</i> = 8.4 Hz, H _o) 7.42 (d, 2H, <i>J</i> = 8.4 Hz, H _m) 2.40 (s, 3H, Me)	8.54 (s, 1H, H ₈) 4.34 (br s, 4H, H ₁₀) 3.80 (t, 4H, <i>J</i> = 4.8 Hz, H ₁₁)	8.41 (s, 1H, H _o) 8.04 (d, 1H, <i>J</i> = 8.0 Hz, H _o) 7.89 (d, 1H, <i>J</i> = 8.0 Hz, H _p) 7.38 (t, 1H, <i>J</i> = 8.0 Hz, H _m)	10.18 (s, 1H, NH) 3.90 (t, 2H, <i>J</i> = 6.0 Hz, H ₂) 2.85 (t, 2H, <i>J</i> = 6.0 Hz, H ₁)
3.7b			7.80 (d, 2H, <i>J</i> = 8.4 Hz, H _o) 7.43 (d, 2H, <i>J</i> = 8.4 Hz, H _m) 2.41 (s, 3H, Me)	8.55 (s, 1H, H ₈) 4.34 (br s, 4H, H ₁₀) 3.79 (t, 4H, <i>J</i> = 4.8 Hz, H ₁₁)	8.37 (s, 1H, H _o) 8.01 (d, 1H, <i>J</i> = 8.0 Hz, H _o) 7.84 (d, 1H, <i>J</i> = 8.0 Hz, H _p) 7.37 (t, 1H, <i>J</i> = 8.0 Hz, H _m)	10.20 (s, 1H, NH) 2.61 (t, 2H, <i>J</i> = 6.4 Hz, H ₂) 2.47 (br s, 2H, H ₁) 2.31 (br s, 8H, H ₃ + H ₄) 2.12 (s, 3H, H ₅)
5.1f			7.73 (d, 1H, <i>J</i> = 2.0 Hz, H _o) 7.64 (dd, 1H, <i>J</i> = 8.0, 2.0 Hz, H _o) 7.36 (d, 1H, <i>J</i> = 8.0 Hz, H _m) 2.35 (s, 3H, Me _m) 2.30 (s, 3H, Me _p)	8.54 (s, 1H, H ₈) 4.35 (br s, 4H, H ₁₀) 3.79 (t, 4H, <i>J</i> = 4.8 Hz, H ₁₁)	8.71 (t, 1H, <i>J</i> = 2.0 Hz, H _o) 8.09 (dt, 1H, <i>J</i> = 8.0, 0.8 Hz, H _o) 7.90 (ddd, 1H, <i>J</i> = 8.0, 2.0, 0.8 Hz, H _p) 7.44 (t, 1H, <i>J</i> = 8.0 Hz, H _m)	10.41 (s, 1H, NH) 7.96 (d, 2H, <i>J</i> = 8.0 Hz, H _o) 7.58 (d, 2H, <i>J</i> = 8.0 Hz, H _m) 4.84 (s, 2H, CH ₂)

* – Overlay of signals on the spectrum.

**Table 28** ¹H-NMR spectroscopic data (400 MHz, DMSO-*d*₆) for the compounds synthesized in subchapter 3.2. (continuation)

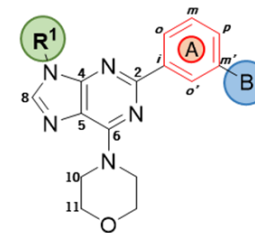
Comp.	R ¹	Group B	R ¹	Purine	Group A	Group B
5.1b			7.74 (d, 1H, <i>J</i> = 2.0 Hz, H _o) 7.65 (dd, 1H, <i>J</i> = 8.0, 2.0 Hz, H _o) 7.4 – 7.5 (m, 1H, H _m) *1 2.36 (s, 3H, Me _m) 2.31 (s, 3H, Me _p)	8.56 (s, 1H, H ₈) 4.36 (br s, 4H, H ₁₀) 3.80 (t, 4H, <i>J</i> = 4.8 Hz, H ₁₁)	8.70 (t, 1H, <i>J</i> = 1.6 Hz, H _o) 8.09 (dt, 1H, <i>J</i> = 8.0, 1.6 Hz, H _o) 7.90 (m, 1H, H _p) 7.4 – 7.5 (m, 1H, H _m) *1	10.33 (s, 1H, NH) 7.91 (d, 2H, <i>J</i> = 8.0 Hz, H _o) 7.4 – 7.5 (m, 2H, H _m) *1 3.52 (s, 2H, H ₁) 2.3 – 2.5 (m, 8H, H ₂ + H ₃) 2.14 (s, 3H, H ₄)
5.1c			7.74 (s, 1H, H _o) 7.65 (d, 1H, <i>J</i> = 8.0 Hz, H _o) 7.4 – 7.5 (m, 1H, H _m) *1 2.36 (br s, 3H, Me _m) *2 2.31 (s, 3H, Me _p)	8.56 (s, 1H, H ₈) 4.36 (br s, 4H, H ₁₀) 3.80 (br s, 4H, H ₁₁)	8.70 (s, 1H, H _o) 8.09 (d, 1H, <i>J</i> = 8.0 Hz, H _o) 7.89 (m, 1H, H _p) 7.4 – 7.5 (m, 1H, H _m) *1	10.34 (s, 1H, NH) 7.92 (d, 2H, <i>J</i> = 8.0 Hz, H _o) 7.4 – 7.5 (m, 1H, H _m) *1 3.5 – 3.6 (m, 6H, H ₁ + H ₃) 2.36 (br s, 4H, H ₂) *2
5.1g			7.75 (s, 1H, H _o) 7.65 (d, 1H, <i>J</i> = 8.0 Hz, H _o) 7.37 (d, 1H, <i>J</i> = 8.0 Hz, H _m) 2.36 (s, 3H, Me _m) 2.31 (s, 3H, Me _p)	8.56 (s, 1H, H ₈) 4.36 (br s, 4H, H ₁₀) 3.80 (s, 4H, H ₁₁)	8.71 (s, 1H, H _o) 8.10 (d, 1H, <i>J</i> = 8.0 Hz, H _o) 7.92 (d, 1H, <i>J</i> = 8.0 Hz, H _p) 7.44 (t, 1H, <i>J</i> = 8.0 Hz, H _m)	10.41 (s, 1H, NH) 8.00 (d, 2H, <i>J</i> = 8.0 Hz, H _o) 7.53 (d, 2H, <i>J</i> = 8.0 Hz, H _m) 4.56 (s, 2H, CH ₂)
5.3f			7.73 (d, 1H, <i>J</i> = 2.0 Hz, H _o) 7.64 (dd, 1H, <i>J</i> = 8.0, 2.0 Hz, H _o) 7.36 (d, 1H, <i>J</i> = 8.0 Hz, H _m) 2.35 (s, 3H, Me _m) 2.30 (s, 3H, Me _p)	8.54 (s, 1H, H ₈) 4.35 (br s, 4H, H ₁₀) 3.79 (t, 4H, <i>J</i> = 4.8 Hz, H ₁₁)	8.68 (s, 1H, H _o) 8.11 (d, 1H, <i>J</i> = 8.0 Hz, H _o) 7.90 (d, 1H, <i>J</i> = 8.0 Hz, H _p) 7.45 (t, 1H, <i>J</i> = 8.0 Hz, H _m)	10.62 (s, 1H, NH) 8.96 (d, 1H, <i>J</i> = 2.4 Hz, H _o) 8.36 (dd, 1H, <i>J</i> = 8.0, 2.4 Hz, H _o) 7.70 (d, 1H, <i>J</i> = 8.0 Hz, H _m)
5.3c			7.74 (d, 1H, <i>J</i> = 2.0 Hz, H _o) 7.64 (dd, 1H, <i>J</i> = 8.0, 2.0 Hz, H _o) 7.42 (d, 1H, <i>J</i> = 8.0 Hz, H _m) 2.35 (s, 3H, Me _m) 2.30 (s, 3H, Me _p)	8.54 (s, 1H, H ₈) 4.35 (br s, 4H, H ₁₀) 3.79 (t, 4H, <i>J</i> = 4.8 Hz, H ₁₁)	8.68 (t, 1H, <i>J</i> = 2.0 Hz, H _o) 8.07 (d, 1H, <i>J</i> = 8.0 Hz, H _o) 7.90 (d, 1H, <i>J</i> = 8.0 Hz, H _p) 7.37 (t, 1H, <i>J</i> = 8.0 Hz, H _m)	10.17 (s, 1H, NH) 8.78 (d, 1H, <i>J</i> = 2.4 Hz, H _o) 8.12 (dd, 1H, <i>J</i> = 8.8, 2.4 Hz, H _o) 6.90 (d, 1H, <i>J</i> = 8.8 Hz, H _m) 3.70 (t, 4H, <i>J</i> = 4.8 Hz, H ₂) 3.59 (t, 4H, <i>J</i> = 4.8 Hz, H ₁)
5.4h			7.72 (d, 1H, <i>J</i> = 2.0 Hz, H _o) 7.60 (dd, 1H, <i>J</i> = 8.0, 2.0 Hz, H _o) 7.34 (d, 1H, <i>J</i> = 8.0 Hz, H _m) 2.33 (s, 3H, Me _m) 2.29 (s, 3H, Me _p)	8.50 (s, 1H, H ₈) 4.32 (br s, 4H, H ₁₀) 3.77 (t, 4H, <i>J</i> = 4.8 Hz, H ₁₁)	8.37 (t, 1H, <i>J</i> = 2.0 Hz, H _o) 7.92 (dt, 1H, <i>J</i> = 8.0, 0.8 Hz, H _o) 7.55 (ddd, 1H, <i>J</i> = 8.0, 2.0, 0.8 Hz, H _p) 7.30 (t, 1H, <i>J</i> = 8.0 Hz, H _m)	8.62 (s, 1H, NH) 4.50 (t, 1H, <i>J</i> = 5.6 Hz, OH) 3.51 (q, 2H, <i>J</i> = 5.6 Hz, H ₄) 3.41 (t, 4H, <i>J</i> = 4.8 Hz, H ₁) 2.41 (m, 6H, H ₂ + H ₃)

*1, *2 – Overlay of signals on the spectrum.

**Table 28** $^1\text{H-NMR}$ spectroscopic data (400 MHz, $\text{DMSO-}d_6$) for the compounds synthesized in subchapter 3.2. (continuation)

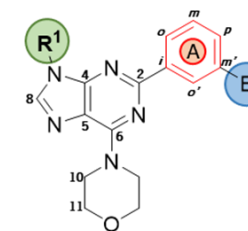
Comp.	R ¹	Group B	R ¹	Purine	Group A	Group B
5.5f			7.73 (d, 1H, $J = 2.0$ Hz, H_o) 7.63 (dd, 1H, $J = 8.0, 2.0$ Hz, H_o) 7.36 (m, 1H, H_m) * ¹ 2.36 (m, 3H, Me_m) * ² 2.31 (s, 3H, Me_p)	8.54 (s, 1H, H_a) 4.34 (br s, 4H, H_{10}) 3.79 (t, 4H, $J = 4.8$ Hz, H_{11})	8.49 (t, 1H, $J = 1.6$ Hz, H_o) 8.01 (dt, 1H, $J = 8.0, 1.6$ Hz, H_o) 7.79 (dd, 1H, $J = 8.0, 0.8$ Hz, H_p) 7.36 (m, 1H, H_m) * ¹	10.01 (s, 1H, NH) 3.67 (t, 2H, $J = 6.4$ Hz, H_4) 2.36 (m, 2H, H_1) * ² 1.75 (m, 4H, $H_2 + H_3$)
5.5b			7.71 (d, 1H, $J = 2.0$ Hz, H_o) 7.62 (dd, 1H, $J = 8.0, 2.0$ Hz, H_o) 7.34 (m, 1H, H_m) * ¹ 2.33 (s, 3H, Me_m) 2.28 (s, 3H, Me_p)	8.50 (s, 1H, H_a) * ² 4.33 (br s, 4H, H_{10}) 3.78 (t, 4H, $J = 4.8$ Hz, H_{11})	8.50 (s, 1H, H_o) * ² 8.00 (d, 1H, $J = 8.0$ Hz, H_o) 7.78 (d, 1H, $J = 8.0$ Hz, H_p) 7.34 (m, 1H, H_m) * ¹	9.98 (s, 1H, NH) 2.2 – 2.3 (m, 12H, $H_1 + H_4 + H_5 + H_6$) 2.09 (s, 3H, H_7) 1.59 (m, 2H, H_2) 1.43 (m, 2H, H_3)
5.5c			7.72 (d, 1H, $J = 2.0$ Hz, H_o) 7.63 (dd, 1H, $J = 8.0, 2.0$ Hz, H_o) 7.36 (m, 1H, H_m) * 2.34 (s, 3H, Me_m) 2.30 (s, 3H, Me_p)	8.52 (s, 1H, H_a) 4.34 (br s, 4H, H_{10}) 3.79 (t, 4H, $J = 4.8$ Hz, H_{11})	8.49 (s, 1H, H_o) 8.01 (d, 1H, $J = 8.0$ Hz, H_o) 7.79 (d, 1H, $J = 8.0$ Hz, H_p) 7.36 (t, 1H, H_m) *	9.97 (s, 1H, NH) 3.54 (t, 4H, $J = 4.8$ Hz, H_6) 2.2 – 2.3 (m, 8H, $H_1 + H_4 + H_5$) 1.61 (m, 2H, H_2) 1.45 (m, 2H, H_3)
5.6f			7.72 (d, 1H, $J = 1.6$ Hz, H_o) 7.63 (dd, 1H, $J = 8.0, 1.6$ Hz, H_o) 7.36 (m, 1H, H_m) * 2.35 (s, 3H, Me_m) 2.30 (s, 3H, Me_p)	8.54 (s, 1H, H_a) 4.34 (br s, 4H, H_{10}) 3.78 (t, 4H, $J = 4.8$ Hz, H_{11})	8.49 (s, 1H, H_o) 8.01 (d, 1H, $J = 8.0$ Hz, H_o) 7.79 (d, 1H, $J = 8.0$ Hz, H_p) 7.36 (m, 1H, H_m) *	10.07 (s, 1H, NH) 3.70 (t, 2H, $J = 6.4$ Hz, H_3) 2.48 (m, 2H, H_1) 2.04 (m, 2H, H_2)
5.7f			7.72 (d, 1H, $J = 2.0$ Hz, H_o) 7.63 (dd, 1H, $J = 8.0, 2.0$ Hz, H_o) 7.38 (m, 1H, H_m) * 2.35 (s, 3H, Me_m) 2.31 (s, 3H, Me_p)	8.55 (s, 1H, H_a) 4.35 (br s, 4H, H_{10}) 3.79 (t, 4H, $J = 4.8$ Hz, H_{11})	8.50 (s, 1H, H_o) 8.04 (d, 1H, $J = 8.0$ Hz, H_o) 7.81 (d, 1H, $J = 8.0$ Hz, H_p) 7.38 (m, 1H, H_m) *	10.18 (s, 1H, NH) 3.89 (t, 2H, $J = 6.0$ Hz, H_2) 2.84 (t, 2H, $J = 6.0$ Hz, H_1)
5.7b			7.72 (s, 1H, H_o) 7.64 (d, 1H, $J = 8.0$ Hz, H_o) 7.37 (m, 1H, H_m) * 2.35 (s, 3H, Me_m) 2.31 (s, 3H, Me_p)	8.54 (s, 1H, H_a) 4.34 (br s, 4H, H_{10}) 3.79 (s, 4H, H_{11})	8.45 (s, 1H, H_o) 8.01 (d, 1H, $J = 8.0$ Hz, H_o) 7.78 (d, 1H, $J = 8.0$ Hz, H_p) 7.37 (m, 1H, H_m) *	10.20 (s, 1H, NH) 2.62 (t, 2H, $J = 6.8$ Hz, H_2) 2.3 – 2.5 (br s, 10H, $H_1 + H_3 + H_4$) 2.11 (s, 3H, H_5)

*, *1, *2 – Overlay of signals on the spectrum.

**Table 28** ¹H-NMR spectroscopic data (400 MHz, DMSO-*d*₆) for the compounds synthesized in subchapter 3.2. (continuation)

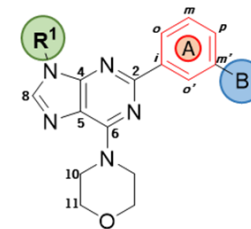
Comp.	R ¹	Group B	R ¹	Purine	Group A	Group B
5.7c			7.71 (s, 1H, H _o) 7.63 (d, 1H, <i>J</i> = 8.0 Hz, H _o) 7.36 (m, 1H, H _m) * 2.35 (s, 3H, Me _m) 2.30 (s, 3H, Me _p)	8.53 (s, 1H, H ₈) 4.34 (br s, 4H, H ₁₀) 3.79 (s, 4H, H ₁₁)	8.45 (s, 1H, H _o) 8.01 (d, 1H, <i>J</i> = 8.0 Hz, H _o) 7.80 (d, 1H, <i>J</i> = 8.0 Hz, H _p) 7.36 (m, 1H, H _m) *	10.18 (s, 1H, NH) 3.57 (s, 4H, H ₄) 2.63 (s, 2H, H ₂) 2.49 (s, 2H, H ₁) 2.41 (s, 4H, H ₃)
5.8f			7.74 (d, 1H, <i>J</i> = 2.0 Hz, H _o) 7.65 (dd, 1H, <i>J</i> = 8.0, 2.4 Hz, H _o) 7.36 (m, 1H, H _m) * ¹ 2.35 (s, 3H, Me _m) 2.30 (s, 3H, Me _p)	8.55 (s, 1H, H ₈) 4.36 (m, 4H, H ₁₀) * ² 3.79 (t, 4H, <i>J</i> = 4.8 Hz, H ₁₁)	8.51 (s, 1H, H _o) 7.99 (dt, 1H, <i>J</i> = 8.0, 1.2 Hz, H _o) 7.62 (d, 1H, <i>J</i> = 8.0 Hz, H _p) 7.36 (m, 1H, H _m) * ¹	9.91 (s, 1H, NH) 4.36 (m, 2H, H ₁) * ² 3.88 (m, 2H, H ₂)
5.8c			7.73 (s, 1H, H _o) 7.64 (br s, 1H, H _o) 7.36 (br s, 1H, H _m) * 2.35 (s, 3H, Me _m) 2.30 (s, 3H, Me _p)	8.54 (s, 1H, H ₈) 4.33 (br s, 4H, H ₁₀) 3.78 (br s, 4H, H ₁₁)	8.48 (s, 1H, H _o) 7.96 (br s, 1H, H _o) 7.61 (br s, 1H, H _p) 7.36 (br s, 1H, H _m) *	9.77 (s, 1H, NH) 4.19 (br s, 4H, H ₁) 3.55 (s, 2H, H ₄) 2.57 (m, 6H, H ₂ + H ₃)
5.9c			7.73 (d, 1H, <i>J</i> = 1.6 Hz, H _o) 7.63 (m, 1H, H _o) * 7.37 (d, 1H, <i>J</i> = 8.0 Hz, H _m) 2.36 (s, 3H, Me _m) 2.31 (s, 3H, Me _p)	8.54 (s, 1H, H ₈) 4.34 (br s, 4H, H ₁₀) 3.79 (t, 4H, <i>J</i> = 4.4 Hz, H ₁₁)	8.24 (s, 1H, H _o) 7.87 (d, 1H, <i>J</i> = 8.0 Hz, H _o) 7.63 (m, 1H, H _p) * 7.29 (t, 1H, <i>J</i> = 8.0 Hz, H _m)	8.74 (s, 1H, NH _A) 6.05 (t, 1H, <i>J</i> = 5.2 Hz, NH _B) 3.59 (t, 4H, <i>J</i> = 4.4 Hz, H ₄) 3.22 (q, 2H, <i>J</i> = 5.2 Hz, H ₁) 2.39 (br s, 6H, H ₂ + H ₃)
7.1c			7.92 – 7.98 (m, 2H, H _o + H _o) * ¹ 7.65 – 7.71 (m, 1H, H _m) 7.33 (td, 1H, <i>J</i> = 8.0, 1.6 Hz, H _p)	8.69 (s, 1H, H ₈) * ² 4.36 (br s, 4H, H ₁₀) 3.80 (t, 4H, <i>J</i> = 4.8 Hz, H ₁₁)	8.69 (s, 1H, H _o) * ² 8.10 (d, 1H, <i>J</i> = 8.0 Hz, H _o) 7.92 – 7.98 (m, 1H, H _p) * ¹ 7.45 (t, 1H, <i>J</i> = 8.0 Hz, H _m)	10.35 (s, 1H, NH) 7.92 – 7.98 (m, 2H, H _o) * ¹ 7.46 (d, 2H, <i>J</i> = 8.0 Hz, H _m) 3.58 (t, 4H, <i>J</i> = 4.4 Hz, H ₃) 3.54 (s, 2H, H ₁) 2.36 (t, 4H, <i>J</i> = 4.4 Hz, H ₂)
7.3f			7.92 – 7.97 (m, 2H, H _o + H _o) * ¹ 7.65 – 7.72 (m, 1H, H _m) * ² 7.33 (tdd, 1H, <i>J</i> = 8.4, 2.4, 0.8 Hz, H _p)	8.68 (s, 1H, H ₈) 4.35 (br s, 4H, H ₁₀) 3.80 (t, 4H, <i>J</i> = 4.8 Hz, H ₁₁)	8.67 (t, 1H, <i>J</i> = 1.6 Hz, H _o) 8.13 (dt, 1H, <i>J</i> = 8.0, 1.6 Hz, H _o) 7.92 – 7.97 (m, 1H, H _p) * ¹ 7.47 (t, 1H, <i>J</i> = 8.0 Hz, H _m)	10.61 (s, 1H, NH) 8.96 (dd, 1H, <i>J</i> = 2.4, 0.8 Hz, H _o) 8.37 (dd, 1H, <i>J</i> = 8.4, 2.4 Hz, H _o) 7.65 – 7.72 (m, 1H, H _m) * ²

*, *1, *2 – Overlay of signals on the spectrum.

**Table 28** ¹H-NMR spectroscopic data (400 MHz, DMSO-*d*₆) for the compounds synthesized in subchapter 3.2. (continuation)

Comp.	R ¹	Group B	R ¹	Purine	Group A	Group B
7.3b			7.93 – 7.98 (m, 2H, H _o + H _{o'}) * ¹ 7.68 (dt, 1H, J = 8.4, 6.4 Hz, H _m) 7.33 (tdd, 1H, J = 8.4, 2.4, 0.8 Hz, H _p)	8.68 (s, 1H, H _a) 4.35 (br s, 4H, H ₁₀) 3.80 (s, 4H, H ₁₁)	8.64 (t, 1H, J = 1.6 Hz, H _o) 8.06 – 8.10 (m, 1H, H _o) * ² 7.93 – 7.98 (m, 1H, H _p) * ¹ 7.43 (t, 1H, J = 8.0 Hz, H _m)	10.13 (s, 1H, NH) 8.76 (d, 1H, J = 2.4 Hz, H _o) 8.06 – 8.10 (m, 1H, H _o) * ² 6.90 (d, 1H, J = 8.8 Hz, H _m) 3.62 (t, 4H, J = 4.8 Hz, H ₁) 2.38 (t, 4H, J = 4.8 Hz, H ₂) 2.21 (s, 3H, H ₃)
8.8f			10.18 (s, 1H, NH) 7.87 (d, 2H, J = 9.2 Hz, H _o) 7.81 (d, 2H, J = 9.2 Hz, H _m) 2.10 (s, 3H, Me)	8.55 (s, 1H, H _a) 4.34 (br s, 4H, H ₁₀) 3.79 (t, 4H, J = 4.8 Hz, H ₁₁)	8.43 (s, 1H, H _o) 7.99 (dt, 1H, J = 8.0, 1.2 Hz, H _o) 7.69 (d, 1H, J = 8.0 Hz, H _p) 7.37 (t, 1H, J = 8.0 Hz, H _m)	9.92 (s, 1H, NH) 4.36 (t, 2H, J = 5.2 Hz, H ₁) 3.88 (t, 2H, J = 5.2 Hz, H ₂)
8.9c			10.18 (s, 1H, NH) 7.79 – 7.90 (m, 4H, H _o + H _m) * 2.09 (s, 3H, Me)	8.53 (s, 1H, H _a) 4.34 (br s, 4H, H ₁₀) 3.79 (t, 4H, J = 4.8 Hz, H ₁₁)	8.13 (s, 1H, H _o) 7.79 – 7.90 (m, 2H, H _o + H _p) * 7.30 (t, 1H, J = 8.0 Hz, H _m)	8.75 (s, 1H, NH _A) 6.06 (t, 1H, J = 5.6 Hz, NH _B) 3.58 (t, 4H, J = 4.8 Hz, H ₄) 3.21 (q, 2H, J = 5.6 Hz, H ₁) 2.38 (m, 6H, H ₂ + H ₃)
9.4h			10.23 (s, 1H, NH) 8.27 (s, 1H, H _o) 7.66 – 7.70 (m, 1H, H _p) * 7.51 – 7.56 (m, 2H, H _o + H _m) 2.10 (s, 3H, Me)	8.56 (s, 1H, H _a) 4.35 (br s, 4H, H ₁₀) 3.80 (t, 4H, J = 4.8 Hz, H ₁₁)	8.32 (t, 1H, J = 1.6 Hz, H _o) 8.00 (dt, 1H, J = 8.0, 1.6 Hz, H _o) 7.66 – 7.70 (m, 1H, H _p) * 7.31 (t, 1H, J = 8.0 Hz, H _m)	8.58 (s, 1H, NH) 4.42 (t, 1H, J = 5.2 Hz, OH) 3.52 (q, 2H, J = 5.2 Hz, H ₄) 3.44 (t, 4H, J = 4.8 Hz, H ₁) 2.41 (m, 6H, H ₂ + H ₃)
9.8f			10.25 (s, 1H, NH) 8.39 (s, 1H, H _o) 7.61 (dt, 1H, J = 8.4, 1.6 Hz, H _p) 7.51 – 7.57 (m, 2H, H _o + H _m) 2.12 (s, 3H, Me)	8.58 (s, 1H, H _a) 4.36 (br s, 4H, H ₁₀) * 3.80 (t, 4H, J = 4.8 Hz, H ₁₁)	8.53 (s, 1H, H _o) 8.04 (d, 1H, J = 8.0 Hz, H _o) 7.71 (d, 1H, J = 8.0 Hz, H _p) 7.37 (t, 1H, J = 8.0 Hz, H _m)	9.83 (s, 1H, NH) 4.36 (br s, 2H, H ₁) * 3.88 (t, 2H, J = 5.2 Hz, H ₂)
10.1f			10.49 (s, 1H, NH) 7.92 – 8.05 (m, 6H, H _o + H _m + H _{o'}) * ¹ 7.53 – 7.63 (m, 3H, H _p + H _m) * ²	8.59 (s, 1H, H _a) 4.36 (br s, 4H, H ₁₀) 3.80 (t, 4H, J = 4.8 Hz, H ₁₁)	8.65 (t, 1H, J = 1.6 Hz, H _o) 8.13 (d, 1H, J = 8.0 Hz, H _o) 7.92 – 8.05 (m, 1H, H _p) * ¹ 7.45 (t, 1H, J = 8.0 Hz, H _m)	10.43 (s, 1H, NH) 7.92 – 8.05 (m, 2H, H _o) * ¹ 7.53 – 7.63 (m, 2H, H _m) * ² 4.83 (s, 2H, CH ₂)

*, *¹, *² – Overlay of signals on the spectrum.

**Table 28** ¹H-NMR spectroscopic data (400 MHz, DMSO-*d*₆) for the compounds synthesized in subchapter 3.2. (continuation)

Comp.	R ¹	Group B	R ¹	Purine	Group A	Group B
10.1b			10.48 (s, 1H, NH) 7.91 – 8.05 (m, 6H, H _o + H _m + H _{o'}) * ¹ 7.62 (tt, 1H, J = 8.4, 1.6 Hz, H _p) 7.55 (t, 2H, J = 8.4 Hz, H _m)	8.60 (s, 1H, H ₈) 4.37 (br s, 4H, H ₁₀) 3.80 (t, 4H, J = 4.8 Hz, H ₁₁)	8.65 (t, 1H, J = 2.0 Hz, H _o) 8.12 (dt, 1H, J = 8.0, 1.2 Hz, H _o) 7.91 – 8.05 (m, 1H, H _p) * ¹ 7.44 (t, 1H, J = 8.0 Hz, H _m)	10.35 (s, 1H, NH) 7.91 – 8.05 (m, 2H, H _o) * ¹ 7.43 (d, 2H, J = 8.4 Hz, H _m) 3.51 (s, 2H, H ₁) 2.32 (br s, 8H, H ₂ + H ₃) 2.13 (s, 3H, H ₄)
13.3f			10.72 (s, 1H, NH) 9.12 (d, 1H, J = 1.6 Hz, H _{o''}) 8.72 (br s, 1H, H _p) * ¹ 8.59 (br s, 1H, H _o) 8.2 – 8.3 (m, 1H, H _{o''}) * ² 7.84 (d, 1H, J = 7.6 Hz, H _o) 7.6 – 7.7 (m, 2H, H _p + H _m) 7.4 – 7.5 (m, 1H, H _{m''}) * ³	8.62 (s, 1H, H ₈) 4.37 (br s, 4H, H ₁₀) 3.81 (s, 4H, H ₁₁)	8.72 (br s, 1H, H _o) * ¹ 8.2 – 8.3 (m, 1H, H _o) * ² 7.92 (d, 1H, J = 7.6 Hz, H _p) 7.4 – 7.5 (m, 1H, H _m) * ³	10.56 (s, 1H, NH) 8.90 (d, 1H, J = 2.0 Hz, H _o) 8.2 – 8.3 (m, 1H, H _o) * ² 7.4 – 7.5 (m, 1H, H _m) * ³
13.3b			10.82 (s, 1H, NH) 9.13 (dd, 1H, J = 2.4, 0.8 Hz, H _{o''}) 8.72 (m, 1H, H _p) * ¹ 8.55 (t, 1H, J = 1.6 Hz, H _o) 8.30 (dt, 1H, J = 8.0, 2.4 Hz, H _{o''}) 7.88 (dt, 1H, J = 7.6, 1.6 Hz, H _o) 7.6 – 7.7 (m, 2H, H _p + H _m) 7.49 (dd, 1H, J = 8.0, 4.8 Hz, H _{m''})	8.63 (s, 1H, H ₈) 4.37 (br s, 4H, H ₁₀) 3.81 (t, 4H, J = 4.8 Hz, H ₁₁)	8.68 (t, 1H, J = 2.0 Hz, H _o) 8.18 (d, 1H, J = 8.0 Hz, H _o) 7.96 (ddd, 1H, J = 8.0, 2.0, 0.8 Hz, H _p) 7.41 (t, 1H, J = 8.0 Hz, H _m)	10.13 (s, 1H, NH) 8.72 (m, 1H, H _o) * ¹ 8.03 (dd, 1H, J = 9.2, 2.4 Hz, H _o) 6.83 (d, 1H, J = 9.2 Hz, H _m) 3.61 (t, 4H, J = 4.8 Hz, H ₁) 2.39 (t, 4H, J = 4.8 Hz, H ₂) 2.21 (s, 3H, H ₃)

*¹, *², *³ – Overlay of signals on the spectrum.

3.2.5.4. $^{13}\text{C-NMR}$ spectroscopy characterization

The $^{13}\text{C-NMR}$ spectroscopic data of the compounds synthesized in subchapter 3.2. are presented in Table 29. Through HMQC, it was possible to establish a direct correlation between H-C₈ and C₈, H-C₁₀ and C₁₀, and H-C₁₁ and H-C₁₁ in the purine nucleus, as well as between C_o, C_{o'}, C_m and C_p in group A, with their respective protons.

With HMBC it was possible to identify several carbon atoms through the two or three bond H – C correlation, as seen in Figure 40. The H-C₈ identified carbons C₄ and C₅ of the purine nucleus, while C₆ was identified by the coupling with H-C₁₀. Also, C₂ was identified by the correlation with H-C_o and H-C_{o'} from ring A (red arrows). Regarding ring A, both C_i and C_{m'} are correlated to H-C_m (blue arrows). Finally, N-H, allowed the identification of the carbonyl (C=O), through the 2-bond correlation, and C_p and C_{o'}, through the 3-bond correlations (green arrows).

Overall, the $^{13}\text{C-NMR}$ chemical shifts of both the group R¹ and purine nucleus remained coherent with the ones presented for the corresponding carbons in the synthetic precursors (**1-23**), except for C₂. Despite presenting similar chemical shifts, a small decrease was observed in the chemical shifts of C₂ and C_{m'}, when compared to those presented in the precursors (**1-23**). On the other hand, there was a slight increase in the chemical shifts of C_o, C_{o'} and C_p of ring A, when compared to the precursors (**1-23**). The remaining carbons, C_i and C_m, remain consistent with the precursors.

No significant variations between the chemical shifts of the final products were recorded. However, depending on the functional group, the chemical shifts of the carbonyl (C=O) change. In amides (X=C), the chemical shifts vary between 162.96 and 170.33 ppm, in ureas (X=N) between 155.05 and 155.29 ppm, and in carbamates (X=O), the variation of the chemical shifts ranges between 153.16 and 154.62 ppm.

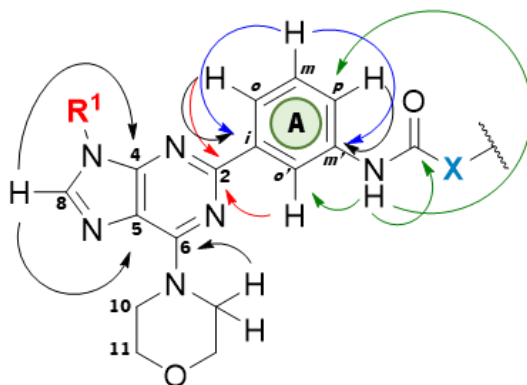
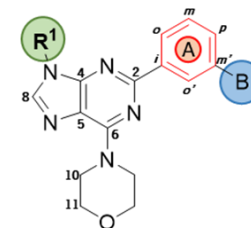
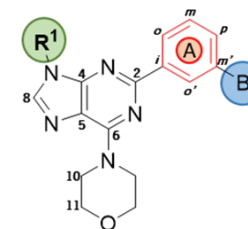


Figure 40 Representative model of the most significant correlations observed in HMBC spectra. Variations in X identify the functional groups of the final amides (X=C), ureas (X=N) and carbamates (X=O).

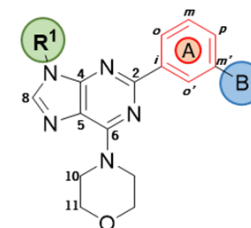
**Table 29** ^{13}C -NMR spectroscopic data (100 MHz, $\text{DMSO}-d_6$) for the compounds synthesized in subchapter 3.2.

Comp.	R ¹	Group B	R ¹	Purine	Group A	Group B
2.1c			135.04 (C _i) 129.57 (C _m) 127.60 (C _p) 123.34 (C _o)	157.42 (C ₂) 153.21 (C ₆) 151.37 (C ₄) 139.46 (C ₈) 118.75 (C ₅) 66.25 (C ₁₁) 45.33 (C ₁₀)	139.25 (C _m) 138.58 (C _i) 128.46 (C _m) 123.17 (C _o) 122.00 (C _p) 119.93 (C _o)	165.55 (C=O) 141.69 (C _p) 133.77 (C _i) 128.74 (C _m) 127.70 (C _o) 66.17 (C ₃) 61.96 (C ₁) 53.16 (C ₂)
				157.40 (C ₂) 153.21 (C ₆) 151.37 (C ₄) 139.49 (C ₈) 118.75 (C ₅) 66.25 (C ₁₁) 45.28 (C ₁₀)	139.12 (C _m) 138.61 (C _i) 128.49 (C _m) 123.27 (C _o) 122.01 (C _p) 119.93 (C _o)	165.32 (C=O) 139.17 (C _p) 134.72 (C _i) 128.26 (C _m) 128.17 (C _o) 53.09 (CH ₂)
2.1g			135.04 (C _i) 129.58 (C _m) 127.62 (C _p) 123.36 (C _o)	157.26 (C ₂) 153.19 (C ₆) 151.34 (C ₄) 139.46 (C ₈) 118.78 (C ₅) 66.24 (C ₁₁) 45.29 (C ₁₀)	138.70 (C _i + C _m) 128.59 (C _m) 123.64 (C _o) 121.96 (C _p) 119.88 (C _o)	163.02 (C=O) 152.72 (C _p) 149.37 (C _o) 139.09 (C _o) 130.02 (C _i) 124.07 (C _m)
2.3f			135.02 (C _i) 129.56 (C _m) 127.60 (C _p) 123.36 (C _o)	157.47 (C ₂) 153.21 (C ₆) 151.37 (C ₄) 139.44 (C ₈) 118.70 (C ₅) 66.27 (C ₁₁) 45.18 (C ₁₀)	139.36 (C _m) 138.56 (C _i) 128.43 (C _m) 122.94 (C _o) 121.95 (C _p) 119.84 (C _o)	164.16 (C=O) 159.89 (C _p) 148.48 (C _o) 137.00 (C _o) 118.75 (C _i) 105.53 (C _m) 54.29 (C ₂) 45.75 (C ₃) 44.21 (C ₁)
2.3c			135.05 (C _i) 129.58 (C _m) 127.61 (C _p) 123.35 (C _o)			

**Table 29** ^{13}C -NMR spectroscopic data (100 MHz, $\text{DMSO}-d_6$) for the compounds synthesized in subchapter 3.2. (continuation)

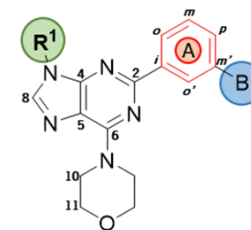
Comp.	R ¹	Group B	R ¹	Purine	Group A	Group B
2.4h			135.06 (C _i) 129.58 (C _m) 127.60 (C _p) 123.36 (C _o)	157.75 (C ₂) 153.20 (C ₆) 151.38 (C ₄) 139.39 (C ₈) 118.67 (C ₅) 66.26 (C ₁₁) 45.22 (C ₁₀)	140.55 (C _m) 138.34 (C _i) 128.13 (C _m) 121.55 (C _o) 121.52 (C _p) 119.18 (C _{o'})	155.10 (C=O) 60.22 (C ₃) 58.49 (C ₄) 53.10 (C ₂) 43.79 (C ₁)
2.8f			135.06 (C _i) 129.55 (C _m) 127.55 (C _p) 123.22 (C _o)	157.32 (C ₂) 153.16 (C ₆) * 151.33 (C ₄) 139.41 (C ₈) 118.75 (C ₅) 66.25 (C ₁₁) 45.27 (C ₁₀)	139.03 (C _m) 138.67 (C _i) 128.67 (C _m) 122.02 (C _o) 119.60 (C _p) 118.09 (C _{o'})	153.16 (C=O) * 64.32 (C ₁) 43.05 (C ₂)
2.9c			135.04 (C _i) 129.54 (C _m) 127.59 (C _p) 123.37 (C _o)	157.61 (C ₂) 153.17 (C ₆) 151.36 (C ₄) 139.40 (C ₈) 118.67 (C ₅) 66.22 (C ₁₁) 45.25 (C ₁₀)	140.60 (C _m) 138.54 (C _i) 128.54 (C _m) 120.64 (C _o) 119.14 (C _p) 116.96 (C _{o'})	155.16 (C=O) 66.16 (C ₄) 57.86 (C ₂) 53.22 (C ₃) 35.95 (C ₁)
37			134.81 (C _i) 129.10 (C _m) 127.15 (C _p) 122.79 (C _o)	157.03 (C ₂) 153.14 (C ₆) 151.13 (C ₄) 138.94 (C ₈) 118.67 (C ₅) 65.90 (C ₁₁) 45.11 (C ₁₀)	138.66 (C _m) 138.48 (C _i) 128.37 (C _m) 122.61 (C _o) 119.27 (C _p) 117.42 (C _{o'})	154.62 (C=O) 61.13 (C ₂) 44.56 (C ₁)
38			135.04 (C _i) 129.56 (C _m) 127.60 (C _p) 123.37 (C _o)	157.69 (C ₂) 153.19 (C ₆) 151.38 (C ₄) 139.41 (C ₈) 118.66 (C ₅) 66.24 (C ₁₁) 45.25 (C ₁₀)	140.38 (C _m) 138.35 (C _i) 128.16 (C _m) 121.63 (C _o) 121.54 (C _p) 119.17 (C _{o'})	155.28 (C=O) 65.99 (C ₂) 44.18 (C ₁)

* – Overlay of signals on the spectrum.

**Table 29** ^{13}C -NMR spectroscopic data (100 MHz, $\text{DMSO}-d_6$) for the compounds synthesized in subchapter 3.2. (continuation)

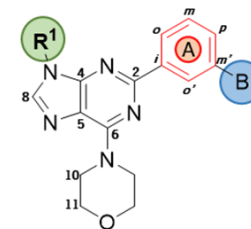
Comp.	R ¹	Group B	R ¹	Purine	Group A	Group B
3.1f			137.13 (C _p) 132.53 (C _i) 129.94 (C _m) 123.27 (C _o) * 20.60 (Me)	157.32 (C ₂) 153.18 (C ₆) 151.35 (C ₄) 139.48 (C ₈) 118.70 (C ₅) 66.25 (C ₁₁) 45.18 (C ₁₀)	139.12 (C _m) 138.64 (C _i) 128.88 (C _m) 123.27 (C _o) * 122.01 (C _p) 119.92 (C _o)	165.26 (C=O) 140.99 (C _p) 134.88 (C _i) 128.74 (C _m) 128.11 (C _o) 45.43 (CH ₂)
3.1b			136.74 (C _p) 132.32 (C _i) 129.50 (C _m) 122.92 (C _o) 20.11 (Me)	157.32 (C ₂) 153.10 (C ₆) 151.24 (C ₄) 138.90 (C ₈) 118.54 (C ₅) 65.88 (C ₁₁) 45.10 (C ₁₀)	138.86 (C _m) 138.53 (C _i) 127.84 (C _m) 122.86 (C _o) 121.78 (C _p) 119.90 (C _o)	165.20 (C=O) 141.80 (C _p) 133.48 (C _i) 128.13 (C _m) 127.17 (C _o) 61.23 (C ₁) 54.34 (C ₃) 52.16 (C ₂) 45.17 (C ₄)
3.1c			137.18 (C _p) 132.55 (C _i) 129.97 (C _m) 123.31 (C _o) 20.63 (Me)	157.37 (C ₂) 153.20 (C ₆) 151.39 (C ₄) 139.23 (C ₈) 118.71 (C ₅) 66.27 (C ₁₁) 45.27 (C ₁₀)	139.52 (C _m) 138.63 (C _i) 128.46 (C _m) 123.22 (C _o) 122.03 (C _p) 119.94 (C _o)	165.59 (C=O) 141.70 (C _p) 133.78 (C _i) 128.77 (C _m) 127.72 (C _o) 66.18 (C ₃) 61.97 (C ₁) 53.17 (C ₂)
3.1g			137.20 (C _p) 132.56 (C _i) 129.99 (C _m) 123.33 (C _o) * ¹ 20.64 (Me)	157.37 (C ₂) 153.22 (C ₆) 151.41 (C ₄) 139.53 (C ₈) 118.74 (C ₅) 66.29 (C ₁₁) 45.31 (C ₁₀)	139.16 (C _m) * ² 138.68 (C _i) 128.51 (C _m) 123.33 (C _o) * ¹ 122.06 (C _p) 119.96 (C _o)	165.38 (C=O) 139.16 (C _p) * ² 134.75 (C _i) 128.30 (C _m) 128.21 (C _o) 53.13 (CH ₂)

*, *1, *2 – Overlay of signals on the spectrum.

**Table 29** ^{13}C -NMR spectroscopic data (100 MHz, $\text{DMSO}-d_6$) for the compounds synthesized in subchapter 3.2. (continuation)

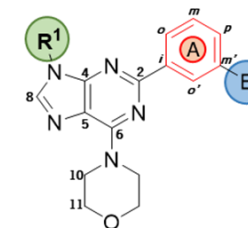
Comp.	R ¹	Group B	R ¹	Purine	Group A	Group B
3.3f			137.16 (C _p) 132.52 (C _i) 129.94 (C _m) 123.31 (C _o) 20.62 (Me)	157.20 (C ₂) 153.18 (C ₆) 151.35 (C ₄) 139.52 (C ₈) 118.73 (C ₅) 66.25 (C ₁₁) 45.26 (C ₁₀)	138.74 (C _m) 138.69 (C _i) 128.59 (C _m) 123.67 (C _o) 121.96 (C _p) 119.86 (C _o)	163.04 (C=O) 152.72 (C _p) 149.37 (C _o) 139.11 (C _o) 130.03 (C _i) 124.09 (C _m)
3.3b			137.13 (C _p) 132.54 (C _i) 129.95 (C _m) 123.27 (C _o) 20.61 (Me)	157.39 (C ₂) 153.19 (C ₆) 151.37 (C ₄) 139.46 (C ₈) 118.70 (C ₅) * 66.26 (C ₁₁) 45.28 (C ₁₀)	139.33 (C _m) 138.58 (C _i) 128.40 (C _m) 122.95 (C _o) 121.94 (C _p) 119.81 (C _o)	164.15 (C=O) 159.88 (C _p) 148.47 (C _o) 136.99 (C _o) 118.70 (C _i) * 105.52 (C _m) 54.29 (C ₂) 45.75 (C ₃) 44.20 (C ₁)
3.5f			137.14 (C _p) 132.53 (C _i) 129.93 (C _m) 123.32 (C _o) 20.61 (Me)	157.32 (C ₂) 153.17 (C ₆) 151.35 (C ₄) 139.48 (C ₈) 118.67 (C ₅) 66.23 (C ₁₁) 45.10 (C ₁₀) *	139.29 (C _m) 138.61 (C _i) 128.53 (C _m) 122.54 (C _o) 120.59 (C _p) 118.48 (C _o)	170.94 (C=O) 45.10 (C ₄) * 35.47 (C ₁) 31.60 (C ₂) 22.47 (C ₃)
3.6f			137.10 (C _p) 132.52 (C _i) 129.91 (C _m) 123.28 (C _o) 20.60 (Me)	157.29 (C ₂) 153.15 (C ₆) 151.34 (C ₄) 139.44 (C ₈) 118.67 (C ₅) 66.23 (C ₁₁) 45.23 (C ₁₀)	139.24 (C _m) 138.61 (C _i) 128.52 (C _m) 122.55 (C _o) 120.57 (C _p) 118.48 (C _o)	170.22 (C=O) 45.04 (C ₃) 33.42 (C ₁) 27.93 (C ₂)

* – Overlay of signals on the spectrum.

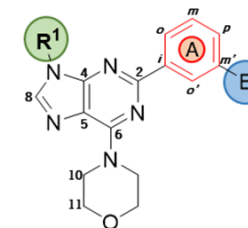
**Table 29** ^{13}C -NMR spectroscopic data (100 MHz, $\text{DMSO-}d_6$) for the compounds synthesized in subchapter 3.2. (continuation)

Comp.	R ¹	Group B	R ¹	Purine	Group A	Group B
3.7f			137.14 (C _p) 132.52 (C _i) 129.93 (C _m) 123.31 (C _o) 20.61 (Me)	157.24 (C ₂) 153.16 (C ₆) 151.34 (C ₄) 139.48 (C ₈) 118.69 (C ₅) 66.23 (C ₁₁) 45.20 (C ₁₀)	139.02 (C _m) 138.69 (C _i) 128.63 (C _m) 122.81 (C _o) 120.57 (C _p) 118.45 (C _o)	168.00 (C=O) 40.83 (C ₂) 39.27 (C ₁)
			137.14 (C _p) 132.52 (C _i) 129.94 (C _m) 123.31 (C _o) 20.62 (Me)	157.32 (C ₂) 153.18 (C ₆) 151.35 (C ₄) 139.51 (C ₈) 118.69 (C ₅) 66.23 (C ₁₁) 45.22 (C ₁₀)	139.26 (C _m) 138.67 (C _i) 128.59 (C _m) 122.59 (C _o) 120.57 (C _p) 118.38 (C _o)	170.25 (C=O) 54.74 (C ₄) 53.69 (C ₂) 52.33 (C ₃) 45.68 (C ₅) 34.09 (C ₁)
5.1f			137.80 (C _m) 135.99 (C _p) 132.79 (C _i) 130.39 (C _m) 124.28 (C _o) 120.73 (C _o) 19.55 (Me _m) 19.05 (Me _p)	157.37 (C ₂) 153.27 (C ₆) 151.46 (C ₄) 139.54 (C ₈) 118.77 (C ₅) 66.33 (C ₁₁) 45.50 (C ₁₀) *	139.18 (C _m) 138.73 (C _i) 128.58 (C _m) 123.36 (C _o) 122.07 (C _p) 120.04 (C _o)	165.34 (C=O) 141.10 (C _p) 134.91 (C _i) 128.86 (C _m) 128.16 (C _o) 45.50 (CH ₂) *
			137.73 (C _m) 135.92 (C _p) 132.76 (C _i) 130.33 (C _m) 124.23 (C _o) 120.68 (C _o) 19.51 (Me _m) 19.01 (Me _p)	157.36 (C ₂) 153.22 (C ₆) 151.42 (C ₄) 139.50 (C ₈) 118.73 (C ₅) 66.28 (C ₁₁) 45.24 (C ₁₀)	139.27 (C _m) 138.66 (C _i) 128.48 (C _m) 123.17 (C _o) 121.99 (C _p) 119.97 (C _o)	165.58 (C=O) 142.23 (C _p) 133.70 (C _i) 128.67 (C _m) 127.68 (C _o) 61.62 (C ₁) 54.70 (C ₃) 52.58 (C ₂) 45.74 (C ₄)

* – Overlay of signals on the spectrum.

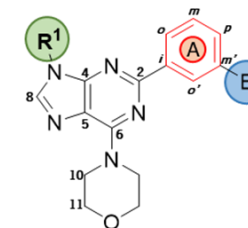
**Table 29** ^{13}C -NMR spectroscopic data (100 MHz, $\text{DMSO-}d_6$) for the compounds synthesized in subchapter 3.2. (continuation)

Comp.	R ¹	Group B	R ¹	Purine	Group A	Group B
5.1c			137.74 (C _m)	157.36 (C ₂)	139.26 (C _m) 138.66 (C _i) 128.50 (C _m) 123.19 (C _o) 122.00 (C _p) 119.98 (C _{o'})	165.56 (C=O)
			135.94 (C _p)	153.23 (C ₆)		141.73 (C _p)
			132.76 (C _i)	151.43 (C ₄)		133.78 (C _i)
			130.34 (C _m)	139.51 (C ₈)		128.80 (C _m)
			124.25 (C _{o'})	118.73 (C ₅)		127.71 (C _o)
			120.69 (C _o)	66.29 (C ₁₁)		66.20 (C ₃)
			19.52 (Me _m) 19.02 (Me _p)	45.30 (C ₁₀)		61.99 (C _i) 53.19 (C ₂)
5.1g		137.69 (C _m)	157.30 (C ₂)	139.13 (C _m) 138.66 (C _i) 128.47 (C _m) 123.24 (C _o) 121.96 (C _p) 119.95 (C _{o'})	165.27 (C=O)	
		135.89 (C _p)	153.20 (C ₆)		139.16 (C _p)	
		132.74 (C _i)	151.39 (C ₄)		134.71 (C _i)	
		130.30 (C _m)	139.48 (C ₈)		128.26 (C _m)	
		124.21 (C _{o'})	118.71 (C ₅)		128.15 (C _o)	
		120.65 (C _o)	66.25 (C ₁₁)		53.09 (CH ₂)	
		19.48 (Me _m) 18.98 (Me _p)	45.26 (C ₁₀)			
5.3f		137.67 (C _m)	157.17 (C ₂)	138.88 (C _m) 138.72 (C _i) 128.56 (C _m) 123.53 (C _o) 121.95 (C _p) 119.93 (C _{o'})	162.98 (C=O)	
		135.86 (C _p)	153.18 (C ₆)		152.66 (C _p)	
		132.72 (C _i)	151.36 (C ₄)		149.35 (C _{o'})	
		130.28 (C _m)	139.47 (C ₈)		139.07 (C _o)	
		124.21 (C _{o'})	118.72 (C ₅)		130.10 (C _i)	
		120.65 (C _o)	66.24 (C ₁₁)		124.07 (C _m)	
		19.46 (Me _m) 18.96 (Me _p)	45.26 (C ₁₀)			
5.3c		137.73 (C _m)	157.38 (C ₂)	139.33 (C _m) 138.63 (C _i) 128.45 (C _m) 122.99 (C _o) 121.93 (C _p) 119.90 (C _{o'})	164.12 (C=O)	
		135.90 (C _p)	153.22 (C ₆)		160.08 (C _p)	
		132.77 (C _i)	151.41 (C ₄)		148.42 (C _{o'})	
		130.33 (C _m)	139.45 (C ₈)		137.06 (C _o)	
		124.21 (C _{o'})	118.73 (C ₅)		119.22 (C _i)	
		120.64 (C _o)	66.36 (C ₁₁)		105.60 (C _m)	
		19.50 (Me _m) 19.00 (Me _p)	45.32 (C ₁₀)		66.29 (C ₂) 44.71 (C _i)	

**Table 29** ^{13}C -NMR spectroscopic data (100 MHz, $\text{DMSO}-d_6$) for the compounds synthesized in subchapter 3.2. (continuation)

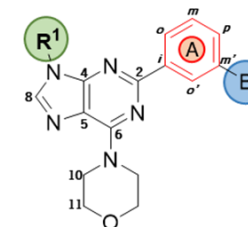
Comp.	R ¹	Group B	R ¹	Purine	Group A	Group B
5.4h			137.86 (C _m) 136.01 (C _p) 132.88 (C _i) 130.45 (C _m) 124.31 (C _o) 120.69 (C _o) 19.60 (Me _m) 19.12 (Me _p)	157.76 (C ₂) 153.32 (C ₆) 151.52 (C ₄) 139.46 (C ₈) 118.74 (C ₆) 66.40 (C ₁₁) 45.38 (C ₁₀)	140.62 (C _m) 138.51 (C _i) 128.29 (C _m) 121.65 (C _o + C _p) 119.47 (C _o)	155.29 (C=O) 60.28 (C ₃) 58.58 (C ₄) 53.20 (C ₂) 43.89 (C ₁)
5.5f			137.69 (C _m) 135.86 (C _p) 132.76 (C _i) 130.28 (C _m) 124.23 (C _o) 120.66 (C _o) 19.46 (Me _m) 18.97 (Me _p)	157.29 (C ₂) 153.17 (C ₆) 151.37 (C ₄) 139.46 (C ₈) 118.67 (C ₆) 66.23 (C ₁₁) 45.27 (C ₁₀)	139.30 (C _m) 138.63 (C _i) 128.54 (C _m) 122.52 (C _o) 120.56 (C _p) 118.54 (C _o)	170.92 (C=O) 45.10 (C ₄) 35.43 (C ₁) 31.57 (C ₂) 22.45 (C ₃)
5.5b			137.68 (C _m) 135.79 (C _p) 132.78 (C _i) 130.28 (C _m) 124.15 (C _o) 120.57 (C _o) * 19.50 (Me _m) 19.00 (Me _p)	157.36 (C ₂) 153.18 (C ₆) 151.37 (C ₄) 139.35 (C ₈) 118.73 (C ₆) 66.28 (C ₁₁) 45.14 (C ₁₀)	139.40 (C _m) 138.67 (C _i) 128.50 (C _m) 122.50 (C _o) 120.57 (C _p) * 118.62 (C _o)	171.33 (C=O) 57.58 (C ₄) 54.76 (C ₆) 52.70 (C ₆) 45.74 (C ₇) 36.30 (C ₁) 25.97 (C ₃) 23.12 (C ₂)
5.5c			137.69 (C _m) 135.83 (C _p) 132.75 (C _i) 130.28 (C _m) 124.20 (C _o) 120.63 (C _o) 19.48 (Me _m) 18.99 (Me _p)	157.33 (C ₂) 153.17 (C ₆) 151.38 (C ₄) 139.39 (C ₈) 118.70 (C ₆) 66.25 (C ₁₁) 45.25 (C ₁₀)	139.41 (C _m) 138.65 (C _i) 128.51 (C _m) 122.48 (C _o) 120.55 (C _p) 118.56 (C _o)	171.28 (C=O) 66.19 (C ₆) 57.98 (C ₄) 53.35 (C ₅) 36.25 (C ₁) 25.55 (C ₃) 23.02 (C ₂)

* – Overlay of signals on the spectrum.

**Table 29** ^{13}C -NMR spectroscopic data (100 MHz, $\text{DMSO-}d_6$) for the compounds synthesized in subchapter 3.2. (continuation)

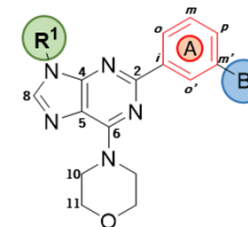
Comp.	R ¹	Group B	R ¹	Purine	Group A	Group B
5.6f			137.68 (C_m) 135.85 (C_p) 132.72 (C_i) 130.27 (C_m) 124.22 ($\text{C}_{o'}$) 120.65 (C_o) 19.46 (Me_m) 18.97 (Me_p)	157.27 (C_2) 153.16 (C_6) 151.36 (C_4) 139.45 (C_8) 118.67 (C_5) 66.22 (C_{11}) 45.20 (C_{10})	139.24 (C_m) 138.63 (C_i) 128.54 (C_m) 122.53 ($\text{C}_{o'}$) 120.53 (C_p) 118.52 ($\text{C}_{o'}$)	170.19 ($\text{C}=\text{O}$) 45.03 (C_3) 33.37 (C_1) 27.90 (C_2)
5.7f			137.72 (C_m) 135.91 (C_p) 132.73 (C_i) 130.31 (C_m) 124.27 ($\text{C}_{o'}$) 120.70 (C_o) 19.49 (Me_m) 19.00 (Me_p)	157.23 (C_2) 153.19 (C_6) 151.39 (C_4) 139.50 (C_8) 118.71 (C_5) 66.25 (C_{11}) 45.26 (C_{10})	139.04 (C_m) 138.72 (C_i) 128.66 (C_m) 122.80 ($\text{C}_{o'}$) 120.56 (C_p) 118.54 ($\text{C}_{o'}$)	168.01 ($\text{C}=\text{O}$) 40.85 (C_2) 39.27 (C_1)
5.7b			137.70 (C_m) 135.89 (C_p) 132.73 (C_i) 130.30 (C_m) 124.25 ($\text{C}_{o'}$) 120.70 (C_o) 19.49 (Me_m) 19.00 (Me_p)	157.30 (C_2) 153.30 (C_6) 151.38 (C_4) 139.50 (C_8) 118.70 (C_5) 66.24 (C_{11}) 45.23 (C_{10})	139.28 (C_m) 138.70 (C_i) 128.61 (C_m) 122.57 ($\text{C}_{o'}$) 120.54 (C_p) 118.45 ($\text{C}_{o'}$)	170.25 ($\text{C}=\text{O}$) 54.75 (C_4) 53.72 (C_2) 52.35 (C_3) 45.69 (C_5) 34.10 (C_1)
5.7c			137.69 (C_m) 135.89 (C_p) 132.72 (C_i) 130.28 (C_m) 124.24 ($\text{C}_{o'}$) 120.70 (C_o) 19.48 (Me_m) 18.99 (Me_p)	157.26 (C_2) 153.18 (C_6) 151.38 (C_4) 139.48 (C_8) 118.70 (C_5) 66.22 (C_{11}) * 45.11 (C_{10})	139.27 (C_m) 138.68 (C_i) 128.61 (C_m) 122.56 ($\text{C}_{o'}$) 120.54 (C_p) 118.46 ($\text{C}_{o'}$)	170.16 ($\text{C}=\text{O}$) 66.22 (C_4) * 54.15 (C_2) 53.01 (C_3) 33.83 (C_1)

* – Overlay of signals on the spectrum.

**Table 29** ^{13}C -NMR spectroscopic data (100 MHz, $\text{DMSO}-d_6$) for the compounds synthesized in subchapter 3.2. (continuation)

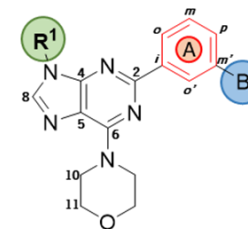
Comp.	R ¹	Group B	R ¹	Purine	Group A	Group B
5.8f			137.65 (C _m) 135.77 (C _p) 132.77 (C _i) 130.26 (C _m) 124.05 (C _o) 120.49 (C _o) 19.48 (Me _m) 18.98 (Me _p)	157.22 (C ₂) 153.16 (C ₆) * 151.34 (C ₄) 139.36 (C ₈) 118.71 (C ₆) 66.25 (C ₁₁) 45.31 (C ₁₀)	139.02 (C _m) 138.74 (C _i) 128.62 (C _m) 122.01 (C _o) 119.64 (C _p) 118.07 (C _o)	153.16 (C=O) * 64.30 (C _i) 43.31 (C ₂)
5.8c			137.77 (C _m) 135.91 (C _p) 132.82 (C _i) 130.37 (C _m) 124.17 (C _o) 120.61 (C _o) 19.56 (Me _m) 19.06 (Me _p)	157.37 (C ₂) 153.22 (C ₆) 151.42 (C ₄) 139.46 (C ₈) 118.76 (C ₆) 66.32 (C ₁₁) 45.36 (C ₁₀)	139.32 (C _m) 138.77 (C _i) 128.70 (C _m) 121.91 (C _o) 119.67 (C _p) 118.03 (C _o)	153.65 (C=O) 66.20 (C ₄) 61.19 (C _i) 57.04 (C ₂) 53.49 (C ₃)
5.9c			137.68 (C _m) 135.85 (C _p) 132.75 (C _i) 130.27 (C _m) 124.25 (C _o) 120.68 (C _o) 19.48 (Me _m) 18.98 (Me _p)	157.52 (C ₂) 153.17 (C ₆) 151.39 (C ₄) 139.42 (C ₈) 118.62 (C ₆) 66.22 (C ₁₁) 45.38 (C ₁₀)	140.60 (C _m) 138.59 (C _i) 128.52 (C _m) 120.61 (C _o) 119.07 (C _p) 117.01 (C _o)	155.16 (C=O) 66.16 (C ₄) 57.86 (C ₂) 53.23 (C ₃) 35.96 (C _i)
7.1c			163.47, 161.04 (d, $J = 243.0$ Hz, C _m) 136.56, 136.46 (d, $J = 10.0$ Hz, C _i) 131.36, 131.27 (d, $J = 9.0$ Hz, C _m) 118.98, 118.96 (d, $J = 2.0$ Hz, C _o) 114.35, 114.14 (d, $J = 21.0$ Hz, C _p) 110.46, 110.21 (d, $J = 25.0$ Hz, C _o)	157.56 (C ₂) 153.19 (C ₆) 151.31 (C ₄) 139.24 (C ₈) 118.76 (C ₆) 66.24 (C ₁₁) 45.35 (C ₁₀)	139.29 (C _m) 138.47 (C _i) 128.52 (C _m) 123.14 (C _o) 122.07 (C _p) 119.96 (C _o)	165.57 (C=O) 141.70 (C _p) 133.78 (C _i) 128.76 (C _m) 127.70 (C _o) 66.18 (C ₃) 61.96 (C _i) 53.16 (C ₂)

* – Overlay of signals on the spectrum.

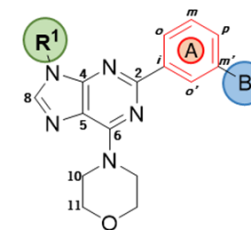
**Table 29** ^{13}C -NMR spectroscopic data (100 MHz, $\text{DMSO}-d_6$) for the compounds synthesized in subchapter 3.2. (continuation)

Comp.	R ¹	Group B	R ¹	Purine	Group A	Group B
7.3f			163.45, 161.03 (d, $J = 242.0$ Hz, $\text{C}_{m'}$) 136.53, 136.43 (d, $J = 10.0$ Hz, C_i) 131.35, 131.26 (d, $J = 9.0$ Hz, C_m) 119.01, 118.98 (d, $J = 3.0$ Hz, C_o) 114.36, 114.15 (d, $J = 21.0$ Hz, C_p) 110.49, 110.24 (d, $J = 25.0$ Hz, $\text{C}_{o'}$)	157.39 (C_2) 153.17 (C_6) 151.28 (C_4) 139.28 (C_8) 118.78 (C_5) 66.22 (C_{11}) 45.23 (C_{10})	138.74 ($\text{C}_{m'}$) 138.57 (C_i) 128.65 (C_m) 123.60 (C_o) 122.01 (C_p) 119.88 ($\text{C}_{o'}$)	163.03 ($\text{C}=\text{O}$) 152.72 (C_p) 149.36 ($\text{C}_{o'}$) 139.10 (C_o) 130.02 (C_i) 124.10 (C_m)
7.3b			163.46, 161.03 (d, $J = 243.0$ Hz, $\text{C}_{m'}$) 136.56, 136.46 (d, $J = 10.0$ Hz, C_i) 131.35, 131.25 (d, $J = 10.0$ Hz, C_m) 118.96, 118.93 (d, $J = 3.0$ Hz, C_o) 114.32, 114.12 (d, $J = 20.0$ Hz, C_p) 110.44, 110.18 (d, $J = 26.0$ Hz, $\text{C}_{o'}$)	157.58 (C_2) 153.18 (C_6) 151.29 (C_4) 139.21 (C_8) 118.69 (C_5) 66.24 (C_{11}) 45.37 (C_{10})	139.39 ($\text{C}_{m'}$) 138.42 (C_i) 128.46 (C_m) 122.88 (C_o) 121.97 (C_p) 119.85 ($\text{C}_{o'}$)	164.14 ($\text{C}=\text{O}$) 159.88 (C_p) 148.47 ($\text{C}_{o'}$) 136.98 (C_o) 118.75 (C_i) 105.53 (C_m) 54.29 (C_2) 45.75 (C_3) 44.20 (C_1)
8.8f			168.53 ($\text{C}=\text{O}$) 138.71 (C_p) 129.84 (C_i) 123.73 (C_o) 119.58 (C_m) * 24.03 (Me)	157.26 (C_2) 153.13 (C_6) 151.33 (C_4) 139.33 (C_8) 118.62 (C_5) 66.25 (C_{11}) 45.27 (C_{10})	139.00 ($\text{C}_{m'}$) 138.66 (C_i) 128.65 (C_m) 122.07 (C_o) 119.58 (C_p) * 118.11 ($\text{C}_{o'}$)	153.16 ($\text{C}=\text{O}$) 64.32 (C_1) 43.05 (C_2)
8.9c			168.56 ($\text{C}=\text{O}$) 138.72 (C_p) 129.80 (C_i) 124.00 (C_o) 119.61 (C_m) 24.03 (Me)	157.57 (C_2) 153.16 (C_6) 151.40 (C_4) 139.44 (C_8) 118.55 (C_5) 66.23 (C_{11}) 45.49 (C_{10})	140.59 ($\text{C}_{m'}$) 138.57 (C_i) 128.57 (C_m) 120.70 (C_o) 119.13 (C_p) 116.91 ($\text{C}_{o'}$)	155.17 ($\text{C}=\text{O}$) 66.18 (C_4) 57.87 (C_2) 53.23 (C_3) 35.97 (C_1)

* – Overlay of signals on the spectrum.

**Table 29** ^{13}C -NMR spectroscopic data (100 MHz, $\text{DMSO}-d_6$) for the compounds synthesized in subchapter 3.2. (continuation)

Comp.	R ¹	Group B	R ¹	Purine	Group A	Group B
9.4h			168.69 (C=O) 140.28 (C _m) 135.24 (C _i) 129.81 (C _m) 118.07 (C _p) 117.79 (C _o) 114.11 (C _{o'}) 24.08 (Me)	157.76 (C ₂) 153.20 (C ₆) 151.36 (C ₄) 139.29 (C ₈) 118.62 (C ₅) 66.24 (C ₁₁) 45.29 (C ₁₀)	140.47 (C _m) 138.28 (C _i) 128.14 (C _m) 121.66 (C _o) 121.48 (C _p) 119.28 (C _{o'})	155.05 (C=O) 60.20 (C ₃) 58.48 (C ₄) 53.09 (C ₂) 43.77 (C ₁)
			168.84 (C=O) 140.25 (C _m) 135.30 (C _i) 129.73 (C _m) 117.96 (C _p) 117.58 (C _o) 113.92 (C _{o'}) 24.08 (Me)	157.32 (C ₂) 153.09 (C ₆) 151.30 (C ₄) 139.23 (C ₈) 118.70 (C ₅) 66.23 (C ₁₁) 45.28 (C ₁₀)	138.95 (C _m) 138.62 (C _i) 128.67 (C _m) 122.10 (C _o) 119.45 (C _p) 118.37 (C _{o'})	153.16 (C=O) 64.33 (C ₁) 43.03 (C ₂)
10.1f			165.81 (C=O) 138.71 (C _p) 134.94 (C _i) 131.79 (C _p) 130.47 (C _i) 128.81 (C _m) 128.16 (C _o) 123.78 (C _{o'}) 122.09 (C _m)	157.43 (C ₂) 153.25 (C ₆) 151.46 (C ₄) 139.48 (C ₈) 118.72 (C ₅) 66.32 (C ₁₁) 45.21 (C ₁₀)	139.16 (C _m) 138.59 (C _i) 128.57 (C _m) 123.44 (C _o) 121.12 (C _p) 119.99 (C _{o'})	165.38 (C=O) 141.05 (C _p) 134.75 (C _i) 128.49 (C _m) 127.77 (C _o) 45.48 (CH ₂)
			165.76 (C=O) 138.65 (C _p) 134.73 (C _i) 131.76 (C _p) 130.44 (C _i) 128.66 (C _m) 127.70 (C _o) 123.77 (C _{o'}) 122.04 (C _m)	157.43 (C ₂) 153.23 (C ₆) 151.44 (C ₄) 139.47 (C ₈) 118.69 (C ₅) 66.29 (C ₁₁) 45.18 (C ₁₀)	139.27 (C _m) 138.57 (C _i) 128.50 (C _m) 123.28 (C _o) 121.07 (C _p) 119.95 (C _{o'})	165.66 (C=O) 142.21 (C _p) 133.73 (C _i) 128.46 (C _m) 127.73 (C _o) 61.62 (C ₁) 54.70 (C ₃) 52.57 (C ₂) 45.74 (C ₄)

**Table 29** ^{13}C -NMR spectroscopic data (100 MHz, $\text{DMSO}-d_6$) for the compounds synthesized in subchapter 3.2. (continuation)

Comp.	R ¹	Group B	R ¹	Purine	Group A	Group B			
13.3f			164.36 (C=O)	157.34 (C ₂)	138.65 (C _{m'} + C _i)	162.96 (C=O)			
			152.18 (C _p)				153.26 (C ₆)	128.61 (C _m)	152.69 (C _p)
			148.68 (C _{o''})				151.36 (C ₄)	123.91 (C _o)	149.29 (C _{o'})
			139.91 (C _m)				139.36 (C ₈)	122.10 (C _p)	138.95 (C _o)
			135.46 (C _{o'})				118.78 (C ₅)	120.20 (C _{o'})	129.91 (C _i)
			135.25 (C _i)				66.26 (C ₁₁)		124.04 (C _m)
			130.33 (C _i)				45.18 (C ₁₀)		
			129.83 (C _m)						
			123.42 (C _{m''})						
			119.35 (C _o)						
118.65 (C _p)									
115.42 (C _{o'})									
13.3b			164.42 (C=O)	157.53 (C ₂)	139.33 (C _{m'}) *2	164.11 (C=O)			
			152.14 (C _p)				153.25 (C ₆)	159.83 (C _p)	
			148.73 (C _{o''})				151.38 (C ₄)	148.43 (C _o)	
			140.06 (C _m)				139.33 (C ₈) *2	136.87 (C _o)	
			135.50 (C _{o'})				118.72 (C ₅)	118.63 (C _i) *1	
			135.24 (C _i)				66.26 (C ₁₁)	105.42 (C _m)	
			130.42 (C _i)				45.26 (C ₁₀)	54.30 (C ₂)	
			129.81 (C _m)					45.77 (C ₃)	
			123.42 (C _{m''})					44.19 (C ₁)	
			119.42 (C _o)						
118.63 (C _p) *1									
115.47 (C _{o'})									

*1, *2 – Overlay of signals on the spectrum.

Summary

In review, this chapter reports in **3.1.**, the synthesis of 2-(3-aminophenyl)-purine derivatives (**1-23**), using previously reported conditions. All the new synthesised compounds, including synthetic precursors (**24-29**) [74]–[76], [79], were characterised by physical and spectroscopic methods. The optimization of the conditions for the acylation of 9-(amino-aryl) purine derivatives **29e-f**, with different acylation agents, was attempted. Finally, the already reported procedure for the reduction of 2-(3-nitrophenyl)-purine derivatives **29** was also optimized [79].

The synthesized 2-(3-aminophenyl)-purine derivatives (**1-23**) were used as starting reagents for the synthesis of the final products in **3.2**. Here, the synthetic route started with the acylation of the 2-(3-aminophenyl)-purine derivatives to generate synthetic intermediates, namely amides and carbamates. Then, the one-pot synthesis of ureas from 2-(3-aminophenyl)-purine derivatives was performed, by adapting conditions reported in the literature [82], [83]. This approach proved to be efficient when realized with amines **34a-c**. However, some tests were performed with amines **34e-g**, which resulted in complex mixtures.

Subsequently, the acylated 2-(3-aminophenyl)-purine derivatives were reacted with nitrogen nucleophiles. Generally, the desired products were obtained efficiently. However, the reaction of chloroalkylamido derivatives with nucleophiles showed that, for class 6 derivatives, degradation of the reagent occurs under the conditions used. Hence, additional optimization is necessary for synthesizing these derivatives. Additionally, to synthesize the carbamates regarding class 8, different synthetic approaches reported in the literature were tested, given the unexpected outcome of the approach initially used. It was then possible to synthesize, after several attempts, the final product **5.8c**. At last, to synthesize the derivatives with ($R^2=NH_2$), the reduction of azides **2.1g**, **3.1g** and **5.1g** was tried. Four different reported methodologies were tested, however, none resulted as expected. So, future attempts or the adaptation of a new approach for the synthesis of these derivatives is necessary.

Finally, all the compounds obtained were physically and spectroscopically characterized.

Chapter 4

**Conclusions and Future
Perspectives**

One of the most common events in human cancer is the activation of the PI3K/AKT/mTOR signalling pathway. The effort to develop isoform-specific PI3K inhibitors, together with novel therapeutic strategies, aims for a more favourable safety inhibitory profile by reducing the toxicity and side-effects of current inhibitors [27], [44]. In the literature, compounds with a similar structure to the ones synthesized and tested by our research group are reported as selective PI3K inhibitors [26]. Considering the similarity of the structures published and the ones synthesized by us, we considered the hypothesis that our compounds could also be active in this type of receptors.

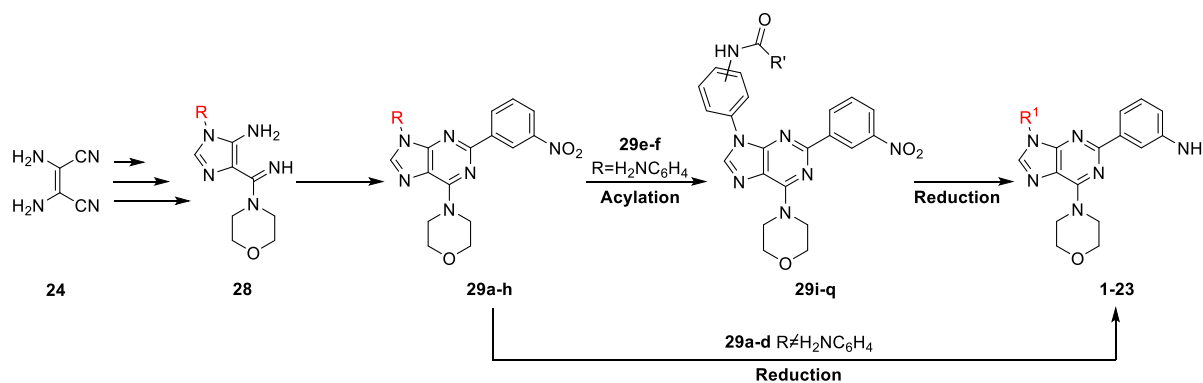
Aiming to identify selective inhibitors for the class I isoforms of PI3K, eleven classes of compounds incorporating the same base structure were designed, giving a total of 1081 ligands. The affinity of 661 of these ligands was evaluated, through molecular docking assays, for the 4 isoforms of the target under study. The Virtual Screening performed yielded a total of 68 selective ligands, 60 for PI3K α and 8 for PI3K γ . In order to finish the study, in the future, we aim to complete the Virtual Screening on the remaining 420 ligands on the four targets.

Additionally, a correlation between the variation of $\Delta G_{\text{binding}}$ for the four isoforms, and the physicochemical properties of the ligands was established. This study allowed the identification of properties on which $\Delta G_{\text{binding}}$ is most dependent in the 4 isoforms, such as the number of HBA, LogP, Mw and Rf. Furthermore, within the ligands selective for the *alpha* isoform, a pattern was discovered regarding the volume of the R¹ group and the protonation capacity of the R² group in the PCA graph. It was found that ligands with a larger R¹ group had an overall higher affinity for PI3K α , while ligands with less voluminous R¹ groups presented a lower affinity for this isoform. The same happened with ligands that have R² groups that are or aren't protonated at physiological pH. While ligands with protonated R² groups showed a lower affinity for PI3K α , ligands with non-protonated R² groups presented higher affinities for this isoform.

Moreover, visualization tools were employed to explore and detail the binding sites that the selective ligands established with PI3K α and PI3K γ . It was observed that in the active centre of PI3K α , the amino acids TYR-730, SER-668, SER-748, and ASP-827 form the most common polar interactions. In the case of PI3K γ , an extra π - π stacking contact was identified with TRP-670, in addition to the polar interactions of this isoform's selective ligands with the residues SER-664 and ASP-822. Regarding the ligands' structure, for both isoforms, it was concluded that different R¹ groups could orient the whole molecule to an optimal interaction position. This makes that there is no interaction pattern between the common groups of the molecules' base structure, with the amino acids of the active centre of the studied

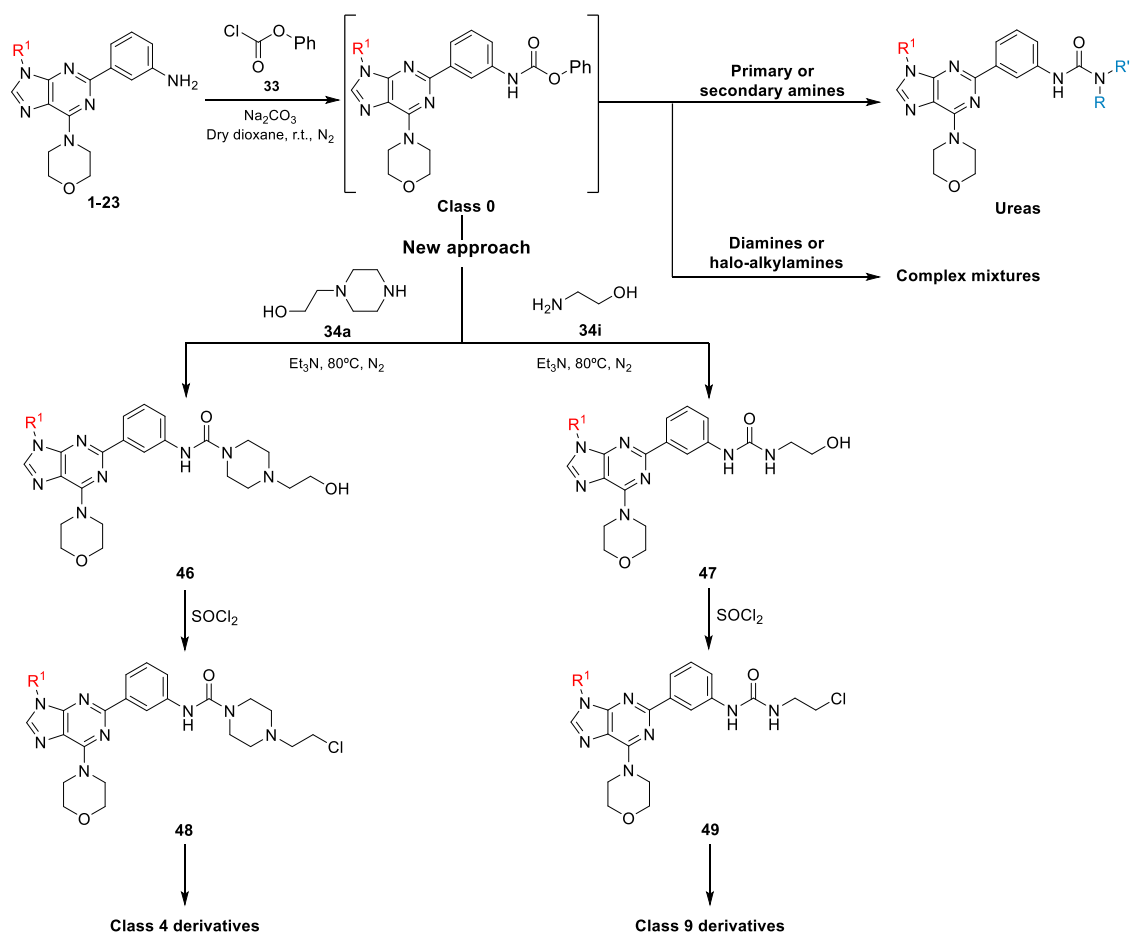
isoforms. However, the presence of the carbonyl group in the structures proved to be important, since its polar interactions with residues of the active centres were seen in the majority of the analysed ligands. In the future, in order to identify common interactions, it is necessary to generate more selective ligands with the same R^1 , while varying group R^2 for each class, or vice-versa, since the overlap of the ligands should be better, allowing a deeper analysis of the interactions established by them.

A set of the designed ligands were selected to be synthesized, using a synthetic route that started from commercial reagents. The total synthetic route was divided into two parts. The first part (Scheme 17) is focused on the synthesis of 2-(3-aminophenyl)-purine derivatives, **1-23**, using reported reaction conditions. The acylation of 9-(amino-aryl) purine derivatives **29e-f** was performed with different acylation agents, and the already reported procedure for the reduction of 2-(3-nitrophenyl)-purine derivatives **29** was optimized [79].



Scheme 17 Synthetic route used for the synthesis of 2-(3-aminophenyl)-purine derivatives (**1-23**) from commercial reagents.

The second part is focused on the synthesis of the final products. The 2-(3-aminophenyl)-purine derivatives, **1-23**, were reacted with several acylation reagents to generate the synthetic intermediates, amides and carbamates (Scheme 18). The reactions occurred smoothly at room temperature and the products were isolated in excellent yields.

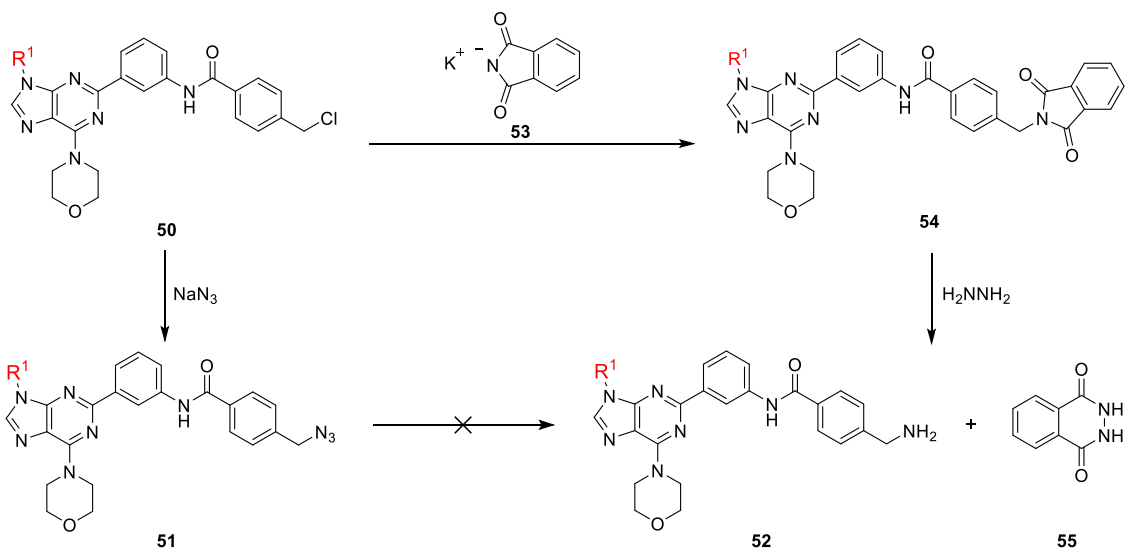


Scheme 19 Schematic representation of the one-pot synthesis of ureas with an alternative synthetic approach for the synthesis of classes 4 and 9 derivatives.

The acylated 2-(3-aminophenyl)-purine derivatives were reacted with nitrogen nucleophiles. The arylamide derivatives generated the products of nucleophilic substitution of the chlorine atom by the nitrogen nucleophiles. The products were isolated in good to excellent yields. However, the reaction of chloroalkylamide derivatives with nitrogen nucleophiles led to degradation of the starting reagent under the conditions used. Hence, additional optimizations are required for synthesizing derivatives of class 6.

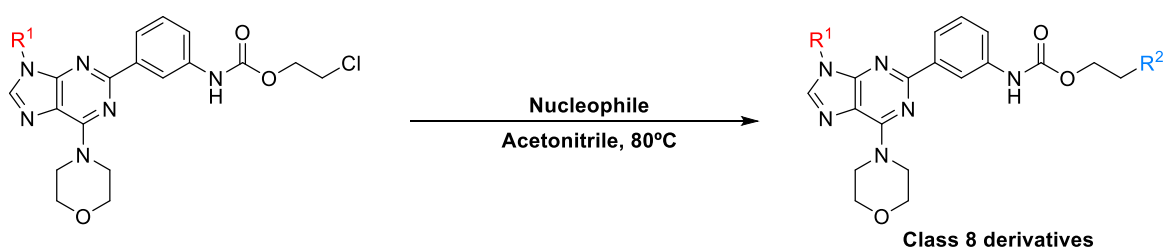
Furthermore, to synthesize the derivatives **52**, the reduction of azides **2.1g**, **3.1g** and **5.1g** was attempted. Four different reported methodologies were tested, however, without success (Scheme 20). In the future, additional attempts could be made to reduce the azides. However, some different approaches can be explored and used for the synthesis of derivatives **53**, such as the Gabriel synthesis presented in Scheme 20. It involves the reaction of **50** with potassium phthalimide **51**, followed by reaction with hydrazine to generate the free amine **53** [94].

Rational design and synthesis of novel selective PI3K inhibitors for cancer therapy



Scheme 20 Schematic representation of the Gabriel synthesis as an alternative synthetic approach to the reduction of azides, for the synthesis of derivatives **52**.

Additionally, the synthesis of the carbamates regarding derivatives of class 8, was tried with several approaches reported in the literature. These resulted in complex mixtures and the cleavage of the carbamate function. After several attempts, where solvent, temperature, amount of nucleophile, and reaction time were changed, one compound was obtained in the reaction of **5.8f** with **34c** in acetonitrile, at 80°C. The compound was obtained pure after recrystallization of the isolated solid from ethanol. Other derivatives of class 8 may be synthesized following the same reaction conditions (Scheme 21), in the future.



Scheme 21 Schematic representation of the optimised conditions for the synthesis of class 8 derivatives.

All the newly synthesized compounds were physically and spectroscopically characterized. In the future, the synthesized compounds will be tested *in vitro*, in cancer cell lines, in order to find potential inhibitors of PI3K and also, assess a possible correlation between the $\Delta G_{\text{binding}}$ scores of the different molecules and the IC_{50} of their *in vitro* biological activity.

Chapter 5

METHODS

Introduction

The methods chapter is essentially divided into two distinct subchapters. Firstly, in **5.1.**, all the methodologies used for the virtual screening will be presented, as well as the set of tools, software and databases used and consulted for collecting information on the ligands and the different biological targets, in addition to the tools for analysing the results from the virtual screening. Finally, in **5.2.**, the procedures employed for the synthesis of all the compounds that were reported in chapter **3** are described.

5.1. Virtual Screening

In order to perform the virtual screening, it was essential to collect data about the ligands and biological targets used. Thus, it was necessary to use databases and different computational chemistry tools to perform the virtual screening. The whole process and tools used for the preparation of the biological targets and ligands, as well as for the virtual screening itself, are described in the following subchapters.

5.1.1. Targets Preparation

Two targets were selected for each one of the four PI3K isoforms from Protein Data Bank (PDB) (november 2020) [95]. The chosen proteins were selected respectively according to their resolution, publication date and publisher, expression organism and structure of the original ligand (Table 1 - Appendix). Thus, the final PDB codes of the chosen proteins are 6PYS for PI3K α [96], 4BFR for PI3K β [97], 6AUD for PI3K γ [98] and 6TNR for PI3K δ [99].

From the canonical amino acid sequence, obtained in FASTA format from the same database for each protein, it was proved the necessity of completing small gaps in each one, to obtain the complete tertiary structure of the 4 targets. Overall, the active site of the proteins was intact in all of the 4 isoforms, with only a few gaps in areas relatively far from the binding site, which corresponds to more mobile regions, such as loop, turns or bends, as seen in orange in Figure 41A and green in Figure 41B, which should not interfere with the affinity result. In any case, the complete structures were those used as targets for the virtual screening.

For this purpose, SWISS-MODEL [100]–[104], a protein structure homology-modelling server, was used as a tool to obtain the complete structures. From all the generated structures, in all four cases, the model chosen was the one with the highest GMQE (Global Model Quality Estimate). Notably, these structures were constructed upon their respective PDB code, maintaining a great alignment and conformational similarity to the experimental protein.

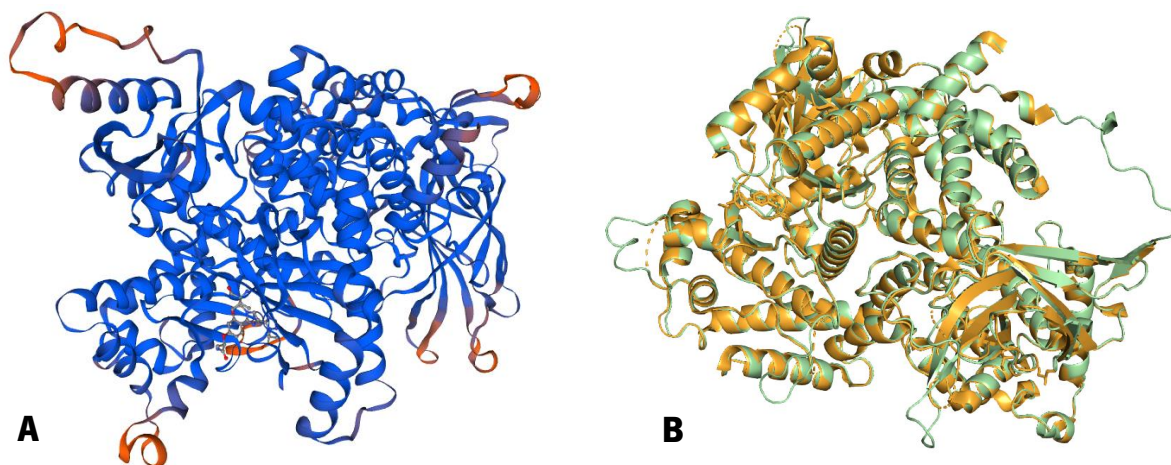


Figure 41 Example representation of the structure of PI3K α completed by SWISS-MODEL (A) and the overlap of the tertiary structures of the original (orange cartoon) and completed (green cartoon) PI3K α (B)

After obtaining the complete protein structures, PyMOL [105] was used to prepare each protein for the subsequent step of the methodology. Firstly, all hydrogens were added to all the amino acids of the respective macromolecules (Figure 42). Finally, the .pdb files were converted to .pdbqt in AutoDock Tools [106], resulting in a suitable format for the virtual screening. In this step, only the polar hydrogens are maintained.

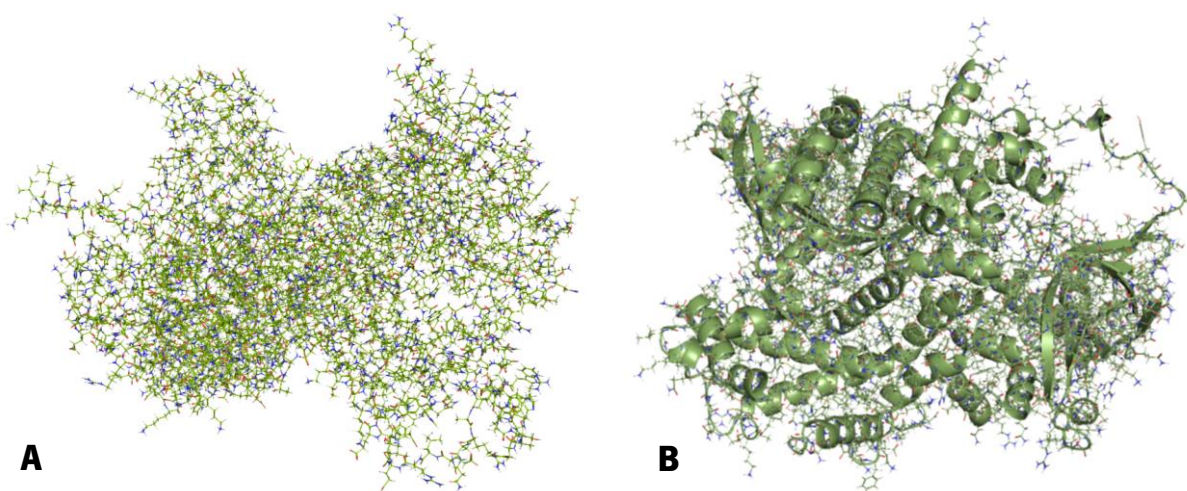


Figure 42 Representative model (PI3K α) of the final step of the receptor preparation with all hydrogen atoms represented in the amino acid structure without (A) and with the cartoon of the tertiary structure of the macromolecule (B).

5.1.2. Ligand Preparation

Due to the novelty of the molecules under study, their physicochemical properties were predicted and collected from Marvin Sketch 20.21. The properties LogP, MW and Rf were obtained directly from the programme. Importantly, to predict with some accuracy the charge, the number of HBA and number of HBD of the ligands under study, the pH of the medium had to be considered, since these values vary depending on the pH, as seen in Figures 43 and 44, respectively for charge and number of HBA/HBD. Therefore, the values of these properties were collected at physiological pH (7.4). In the case of the charge, the structure with the highest percentage was chosen. As for the number of HBA and HBD, the result was rounded to units.

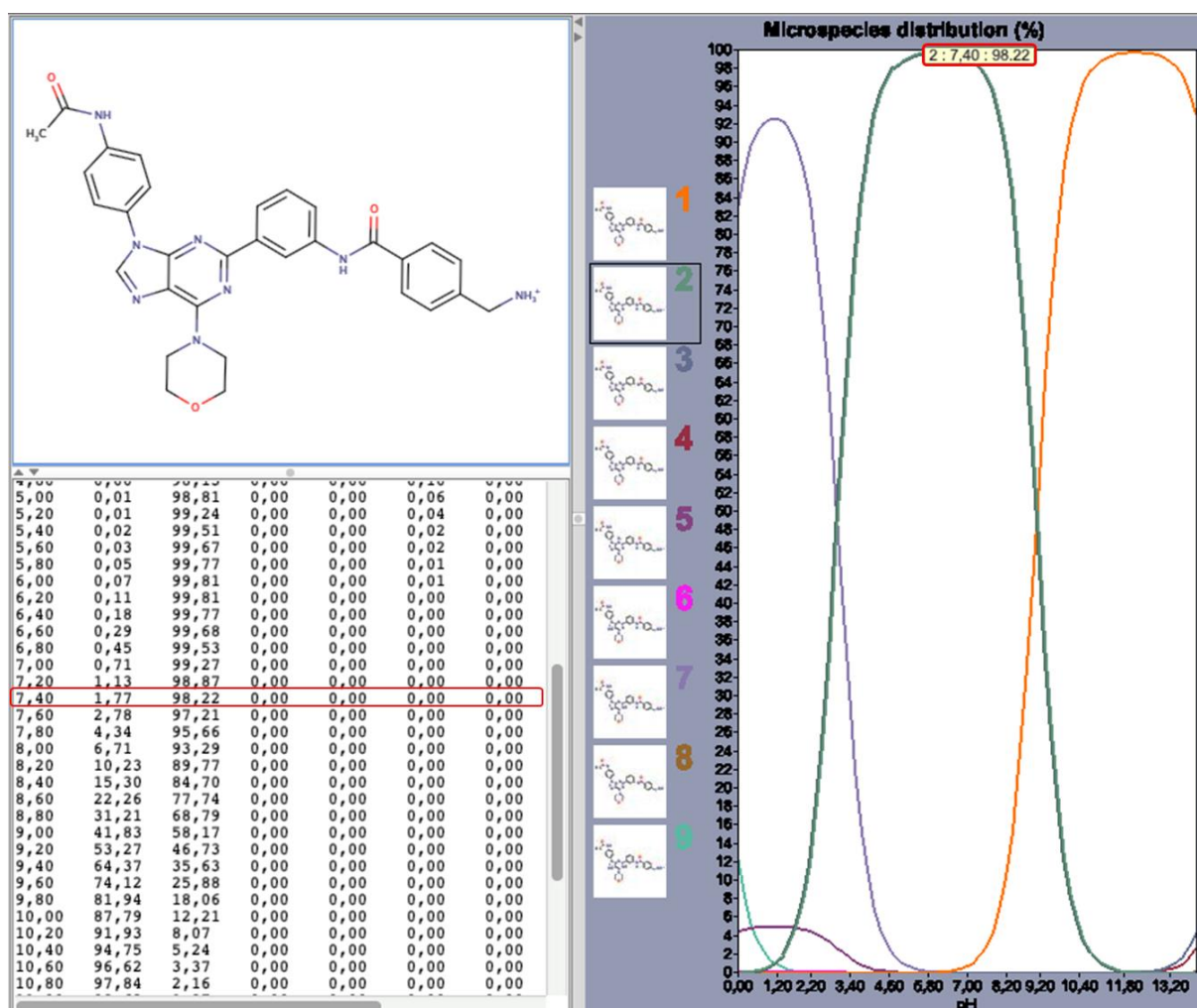


Figure 43 Illustrative model of the charge variations in the structure of the ligand **9.1a** at different pH values. Highlighted in red are the percentage values and the number of the structure conferred with the respective charge of the ligand at physiological pH.

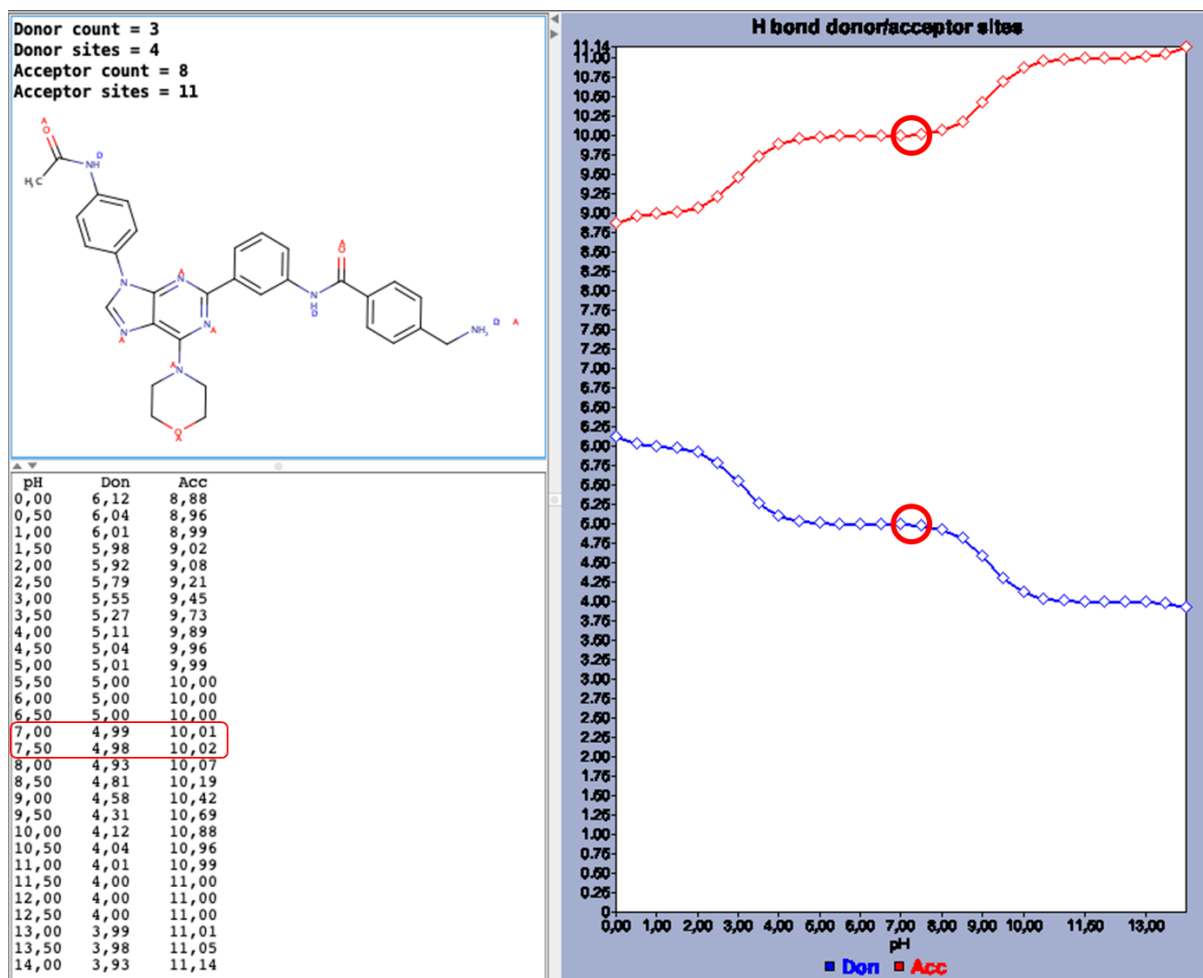


Figure 44 Illustrative model of the number of HBA (red) and HBD (blue) variations in the ligand **9.1a** at different pH values. Highlighted in red are the values registered for HBA and HBD at pH 7.0 and 7.5. For all the ligands reported in this work, these 2 values were always in concordance, so the reported numbers of HBA and HBD were rounded to units from both.

Quantum chemical calculations, at the DFT level, were then used to prepare all the ligands for docking aiming to obtain their optimized structure. Calculations were done with the hybrid density functional B3LYP together with the 6-31+G(d,p) basis set. This chosen method is proven to be adequate to study organic molecules such as the ones presented in this work, with similar size and atom types [107]. It also allows a proper description of the lower energy conformations and electronic distribution, combined with a decrease in computational cost (calculation speed). This is because the energy difference between experimental and DFT calculations is stated as approximated to the difference reported by more robust methods, like ab initio, of higher computational cost [107]–[109].

All molecules were computed with the Gaussian 09 suite of programs [110] in a vacuum and without vibrational corrections, except for 2 ligands (**21.1a** and **21.1b**), that, at physiological pH, are

found in their zwitterionic form. These ligands had to be solvated in water to stabilize the charges, otherwise, some errors would occur during the optimization.

After obtaining the most stable/probable conformation, OpenBabel [111] was used to transform Gaussian outputs into the PDBQT format, suitable to be used in AutoDock Vina [112]. The PDBQT format gathers information concerning atom position and charges.

5.1.3. Virtual Screening

To run the molecular docking experiments, the number of points and spacing of the grid box centre was determined. The centre was settled considering the special location of the original ligand found in each isoform. To assure that all the important residues at the active site were considered, the number of points was decided under the consideration that the final volume of the box could encompass both the ligand size and the amino acids from the active site. For this reason, for all the targets under study, the number of points in a dimension used for the grid box was 28 for all the 3 dimensions, with a spacing of 1.0 Å, usual in AutoDock Vina [112].

To sum up the information regarding the grid box, Table 30 describes the grid box options in all 4 proteins used. Figure 1 - 4 from Appendix shows the Vina grid box settled for all the targets studied in the virtual screening. These options were maintained fixed for all the series of compounds under study.

Table 30 Grid Box centre axial coordinates (x,y,z) for the 4 targets under study.

	PI3Kα	PI3Kβ	PI3Kγ	PI3Kδ
x center	-18.53	-26.22	17.04	-8.60
y center	11.64	21.24	-5.37	-30.25
z center	25.60	27.38	18.23	23.87

At last, the affinity ($\Delta G_{\text{binding}}$) of the 661 ligands was estimated by virtual screening against the 4 isoforms of PI3K, using AutoDock Vina [112]. An exhaustiveness of 20 and a number of modes =20 were used for each docking run.

All the energy values presented throughout the work refer to the conformation that presents the lowest $\Delta G_{\text{binding}}$ score within all the 20 obtained.

5.2. PCA analysis

Principal component analysis (PCA) from SPSS software [113] was used firstly to correlate the data listed for all the 661 reported ligands against the binding energy predicted for the 4 targets under study, by using docking experiments (Tables 2-12 - Appendix). Next, it was used to correlate the 60 PI3K α selective ligands' properties and the binding energy predicted for this target. The same process was then repeated for the 8 ligands found selective for PI3K γ .

This methodology allows the reduction of the dimensionality of data while increasing interpretability. It does so by creating new uncorrelated variables that successively maximize variance. This translates into finding new variables, principal components, which are linear functions of those in the original dataset, that successively maximize variance and that are uncorrelated with each other [114]. It is common practice to use some predefined percentage of total variance explained to decide how many principal components should be retained (70% of total variability is a common, if subjective, cut-off point), although the requirements of graphical representation often lead to the use of just the first two. Even in such situations, the percentage of total variance accounted for is a fundamental tool to assess the quality of these low-dimensional graphical representations of the dataset [114]. In conclusion, by using PCA, it is possible to, in a single graph, follow the relationship between the binding energy and all the properties of all the ligands, instead of using several linear correlation graphs (scatter plots) between only two variables that will not reveal some pattern as in PCA.

The PCA plot shows the original variables as vectors (arrows). These vectors can be interpreted in three ways, according to their orientation, length in space and angles between vectors [115]. First, regarding the orientation of the vector, concerning the principal component space, the more parallel to a principal component axis is a vector, the more it contributes only to that principal component. Second, the longer the vector, the more variability of this variable is represented by the two displayed principal components (short vectors are thus better represented in another dimension). At last, in PCA, patterns can be easily identified among variables according to the angle established between their respective vectors. So, when two vectors are close, forming a small angle, the two variables they represent are positively correlated. But, if they meet each other at 90°, they are not likely to be correlated. Finally, when they diverge and form a large angle (close to 180°), they are negatively correlated [115].

5.3. Chemical Synthesis – General techniques

Melting points (m.p., °C) were determined in a Gallenkamp apparatus and are uncorrected. ¹H and ¹³C NMR spectra, including HMQC and HMBC were recorded on a Bruker Avance III at 400 and 100.6 MHz, respectively. Chemical shifts (δ) are given in parts per million (ppm), downfield from tetramethylsilane (TMS), and coupling constants (J) in hertz (Hz).

Reactions were monitored by thin layer chromatography (TLC), using pre-coated TLC sheets Alugram Xtra SIL G/UV254, with revelation under UV light (254 nm). Infrared spectra were recorded with a FT-IR Bomem MB 104 using Nujol mulls and NaCl cells.

5.3.1. Starting reagents

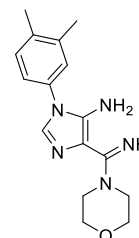
In this section are described only the experimental procedures of new compounds. Hence, compounds previously synthesized were obtained following the experimental protocols reported. Compound **25** is reported in [73], while compounds **27** are reported in [74] and [75]. Finally, compounds **28a**, **28b**, **29a**, **29d**, **2** and **3** reported in [76] and [79].

5.3.1.1. General procedure for the synthesis of 5-amino-4-amidino-imidazoles (**28**)

Morpholine (4-5 eq.) was added to a suspension of 5-amino-4-cyanoformimidoylimidazole (**27**) in acetonitrile. The mixture was stirred at room temperature until all the starting material was consumed (evidence by TLC). The suspension was cooled using an ice bath and the solid was filtered and washed with cold acetonitrile and diethyl ether to give compounds **28a-h**.

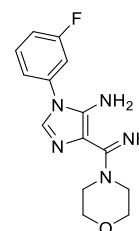
4-[Imino(morpholin-4-yl)methyl]-1-(3,4-dimethylphenyl)-1H-imidazol-5-amine (**28c**)

Compound **28c** (4.84 g, 16.17 mmol, 87%), was obtained as a grey solid from the reaction of [5-amino-1-(3,4-dimethylphenyl)-1H-imidazol-4-yl](imino)acetonitrile **27c** (4.43 g, 18.49 mmol) with morpholine (6.45 mL, 73.97 mmol, 4 eq.) in acetonitrile (30 mL) after 21 hours.



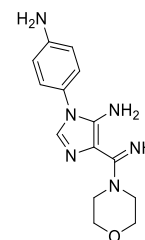
4-[Imino(morpholin-4-yl)methyl]-1-(3-fluorophenyl)-1H-imidazol-5-amine (**28d**)

Compound **28d** (1.40 g, 4.83 mmol, 50%), was obtained as an off white solid from the reaction of [5-amino-1-(3-fluorophenyl)-1H-imidazol-4-yl](imino)acetonitrile **27d** (2.24 g, 9.80 mmol) with morpholine (4.30 mL, 48.98 mmol, 5 eq.) in acetonitrile (31 mL) after 27 hours.

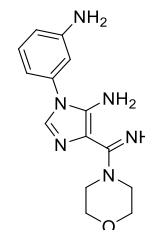


4-[Imino(morpholin-4-yl)methyl]-1-(4-aminophenyl)-1H-imidazol-5-amine (28e)

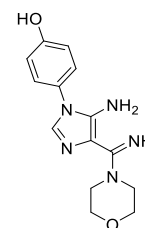
Compound **28e** (3.64 g, 12.72 mmol, 95%), was obtained as an off white solid from the reaction of [5-amino-1-(4-aminophenyl)-1H-imidazol-4-yl](imino)acetonitrile **27e** (3.04 g, 13.43 mmol) with morpholine (5.86 mL, 67.14 mmol, 5 eq.) in acetonitrile (23 mL) after 16 hours.

**4-[Imino(morpholin-4-yl)methyl]-1-(3-aminophenyl)-1H-imidazol-5-amine (28f)**

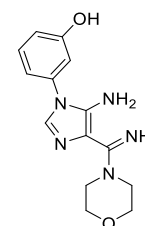
Compound **28f** (6.08 g, 21.22 mmol, 94%), was obtained as a grey solid from the reaction of [5-amino-1-(3-aminophenyl)-1H-imidazol-4-yl](imino)acetonitrile **27f** (5.09 g, 22.48 mmol) with morpholine (9.79 mL, 0.11 mol, 5 eq.) in acetonitrile (52 mL) after 19 hours.

**4-[Imino(morpholin-4-yl)methyl]-1-(4-phenol)-1H-imidazol-5-amine (28g)**

Compound **28g** (4.68 g, 16.28 mmol, 82%), was obtained as an off white solid from the reaction of [5-amino-1-(4-phenol)-1H-imidazol-4-yl](imino)acetonitrile **27g** (4.55 g, 20.02 mmol) with morpholine (6.98 mL, 88.01 mmol, 4 eq.) in acetonitrile (40 mL) after 20 hours.

**4-[Imino(morpholin-4-yl)methyl]-1-(3-phenol)-1H-imidazol-5-amine (28h)**

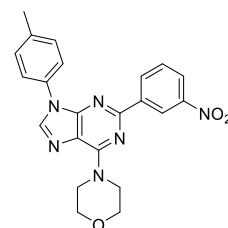
Compound **28h** (3.36 g, 11.69 mmol, 69%), was obtained as a grey solid from the reaction of [5-amino-1-(4-phenol)-1H-imidazol-4-yl](imino)acetonitrile **27h** (3.87 g (oil), 17.01 mmol) with morpholine (5.93 mL, 68.04 mmol, 4 eq.) in acetonitrile (40 mL) after 26 hours.

**5.3.1.2. General procedure for the synthesis of 2-(3-nitrophenyl)purine derivatives (29a-h)**

3-nitrobenzaldehyde (1.1 eq.) and triethylamine (Et₃N) (10 eq.) were added to a suspension of 5-amino-4-amidino-imidazoles (**28**) in DMSO. The reaction was carried out at 80 °C, under efficient magnetic stirring and was carefully monitored by TLC. When the starting reagent was absent, the reaction was cooled to room temperature and Et₃N was decanted. Then, acetonitrile and distilled water were added to the suspension. The resulting solid was filtered and washed with distilled water followed by cold acetonitrile and diethyl ether, and identified as compounds **29a-h**.

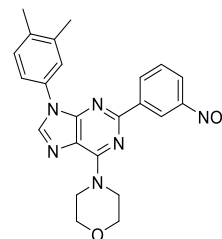
4-(2-(3-nitrophenyl)-9-(p-tolyl)-9H-purin-6-yl)morpholine (29b)

Compound **29b** (1.56 g, 3.75 mmol, 68%) was obtained as a yellow solid from the reaction of compound **28b** (1.58 g, 5.54 mmol) with 3-nitrobenzaldehyde (0.92 g, 6.09 mmol) and Et₃N (7.72 mL, 55.38 mmol) in DMSO (3 mL) after 18 hours.



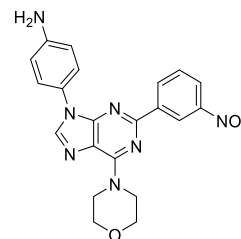
4-(2-(3-nitrophenyl)-9-(3,4-dimethylphenyl)-9H-purin-6-yl)morpholine (29c)

Compound **29c** (1.92 g, 4.46 mmol, 75%) was obtained as a light yellow solid from the reaction of compound **28c** (1.77 g, 5.92 mmol) with 3-nitrobenzaldehyde (0.98 g, 6.52 mmol) and Et₃N (8.26 mL, 59.20 mmol) in DMSO (3 mL) after 21.5 hours.



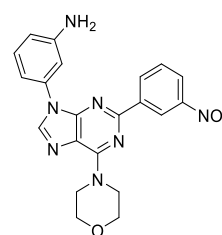
4-(2-(3-nitrophenyl)-9-(4-aniline)-9H-purin-6-yl)morpholine (29e)

Compound **29e** (1.72 g, 4.13 mmol, 79%) was obtained as a yellow solid from the reaction of compound **28e** (1.50 g, 5.25 mmol) with 3-nitrobenzaldehyde (0.88 g, 5.77 mmol) and Et₃N (7.31 mL, 52.46 mmol) in DMSO (3.5 mL) after 16 hours.



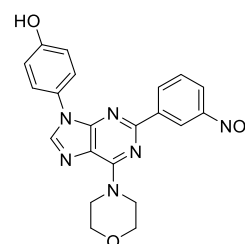
4-(2-(3-nitrophenyl)-9-(3-aniline)-9H-purin-6-yl)morpholine (29f)

Compound **29f** (1.95 g, 4.68 mmol, 89%) was obtained as an off white solid from the reaction of compound **28f** (1.50 g, 5.25 mmol) with 3-nitrobenzaldehyde (0.88 g, 5.77 mmol) and Et₃N (7.31 mL, 52.46 mmol) in DMSO (3.5 mL) after 16 hours.



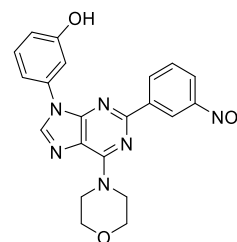
4-(2-(3-nitrophenyl)-9-(4-phenol)-9H-purin-6-yl)morpholine (29g)

Compound **29g** (2.40 g, 5.75 mmol, 93%) was obtained as a yellow solid from the reaction of compound **28g** (1.78 g, 6.19 mmol) with 3-nitrobenzaldehyde (1.03 g, 6.81 mmol) and Et₃N (8.63 mL, 61.90 mmol) in of DMSO (3 mL) after 28.5 hours.



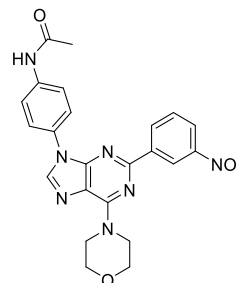
4-(2-(3-nitrophenyl)-9-(3-phenol)-9H-purin-6-yl)morpholine (29h)

Compound **29h** (1.58 g, 3.78 mmol, 75%) was obtained as a yellow solid from the reaction of compound **28h** (1.45 g, 5.04 mmol) with 3-nitrobenzaldehyde (0.84 g, 5.54 mmol) and Et₃N (7.03 mL, 50.40 mmol) in 1.7 mL of DMSO after 3 days.

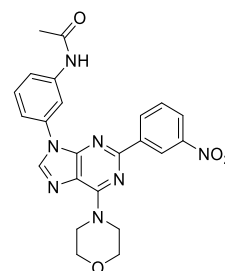


5.3.1.3. Acylation of 4-(2-(3-nitrophenyl)-9-(aniline)-9H-purin-6-yl)morpholine derivatives (29e-f)***N*-(4-(6-morpholino-2-(3-nitrophenyl)-9H-purin-9-yl)phenyl)acetamide (29i)**

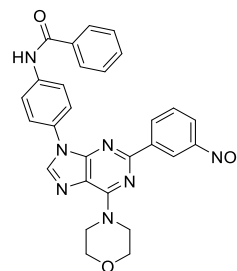
To a suspension of **29e** (0.77 g, 1.85 mmol), in DMSO (1 mL) and Et₃N (3 eq., 0.78 mL, 5.56 mmol), acetic anhydride **30a** (1.5 eq., 0.29 mL, 3.09 mmol) was added. The reaction was carried out in a closed vial, at 80°C, under efficient magnetic stirring and was carefully monitored by TLC. After 4 hours and 30 minutes the absence of the starting reagent **29e** was confirmed. The reaction was cooled down to room temperature. Then, acetonitrile and distilled water were added to the solution until a brown solid precipitated. The resulting suspension was cooled down in an ice bath, and the solid was filtered off and washed successively with water, cold acetonitrile and diethyl ether. The resulting light brown solid was identified as **29i** (0.79 g, 1.73 mmol, 93%).

***N*-(3-(6-morpholino-2-(3-nitrophenyl)-9H-purin-9-yl)phenyl)acetamide (29j)**

To a suspension of **29f** (0.77 g, 1.85 mmol), in DMSO (1 mL) and Et₃N (3 eq., 0.78 mL, 5.56 mmol), acetic anhydride **30a** (1.5 eq., 0.29 mL, 3.09 mmol) was added. The reaction was carried out in a closed vial, at 80°C, under efficient magnetic stirring and was carefully monitored by TLC. After 4 hours and 30 minutes the absence of the starting reagent **29f** was confirmed. The reaction was cooled down to room temperature. Then, acetonitrile and distilled water were added to the solution until an off white solid precipitated. The resulting suspension was cooled down in an ice bath, and the solid was filtered off and washed successively with water, cold acetonitrile and diethyl ether. The resulting off white solid was identified as **29j** (0.80 g, 1.74 mmol, 94%).

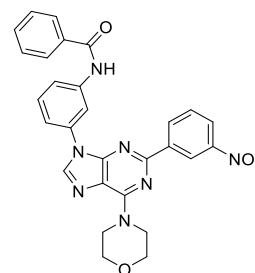
***N*-(4-(6-morpholino-2-(3-nitrophenyl)-9H-purin-9-yl)phenyl)benzamide (29k)**

A mixture of **29e** (0.74 g, 1.77 mmol) and benzoic anhydride **30b** (1.7 eq., 0.70 g, 3.07 mmol) was suspended in DMSO (1.5 mL) and Et₃N (1.7 eq., 0.43 mL, 3.07 mmol) was added. The reaction was carried out in a closed vial, at 80°C, under efficient magnetic stirring and was carefully monitored by TLC. After 3 hours and 30 minutes the absence of the starting reagent **29e** was confirmed. The reaction was cooled down to room temperature. Then, acetonitrile and distilled water were added to the solution until a grey solid precipitated. The resulting suspension was cooled down in an ice bath, and the solid was filtered off and washed successively with water, cold acetonitrile and diethyl ether. The resulting off white solid was identified as **29k** (0.92 g, 1.76 mmol, 99%).

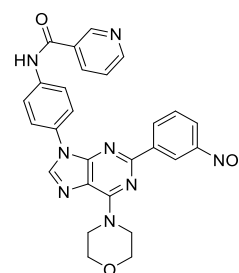


***N*-(3-(6-morpholino-2-(3-nitrophenyl)-9*H*-purin-9-yl)phenyl)benzamide (29l)**

A mixture of **29f** (0.55 g, 1.31 mmol) and benzoic anhydride **30b** (1.6 eq., 0.47 g, 2.11 mmol) was suspended in DMSO (1 mL) and Et₃N (1.6 eq., 0.29 mL, 2.11 mmol) was added. The reaction was carried out in a closed vial, at 80°C, under efficient magnetic stirring and was carefully monitored by TLC. After 2 hours and 25 minutes the absence of the starting reagent **29f** was confirmed. The reaction was allowed to cool down to room temperature. Then, acetonitrile and distilled water were added to the solution until an off white solid precipitated. The resulting suspension was cooled down in an ice bath, and the solid was filtered off and washed successively with water, cold acetonitrile and diethyl ether. The resulting off white solid was identified as **29l** (0.55 g, 1.06 mmol, 80%).

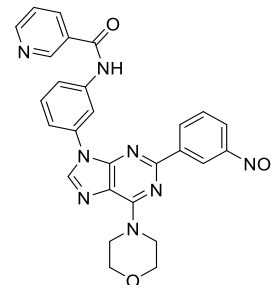
***N*-(4-(6-morpholino-2-(3-nitrophenyl)-9*H*-purin-9-yl)phenyl)nicotinamide (29m)**

Under anhydrous conditions, pyridine-3-carbonyl chloride hydrochloride **31a** (1.5 eq., 92.0 mg, 0.51 mmol) and DMAP (3 eq., 0.13 g, 1.03 mmol) were solubilized in dried acetonitrile (2 mL), in a closed vial. To the resulting pink solution, compound **29e** (0.14 g, 0.34 mmol), solubilized in dry dioxane (2 mL), was added dropwise. The reaction was carried out in a closed vial, at 80 °C, under efficient magnetic stirring and was carefully monitored by TLC. After 2 hours and 35 minutes, the absence of starting reagent **29e** was confirmed. The reaction was allowed to cool down to room temperature. Then, acetonitrile and distilled water were added to the solution, until a yellow solid precipitated. The resulting suspension was cooled down in an ice bath, and the solid was filtered off and washed successively with water, acetonitrile and diethyl ether. The resulting yellow solid was identified as **29m** (0.15 mg, 0.28 mmol, 82%).

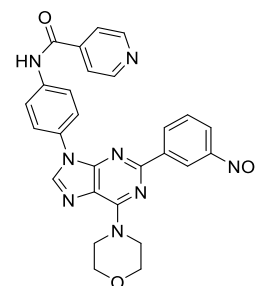


***N*-(3-(6-morpholino-2-(3-nitrophenyl)-9*H*-purin-9-yl)phenyl)nicotinamide (29n)**

Under anhydrous conditions, pyridine-3-carbonyl chloride hydrochloride **31a** (1.2 eq., 52.0 mg, 0.29 mmol) was solubilized in dried acetonitrile (1 mL) and distilled Et₃N (2.5 eq., 0.05 mL, 0.38 mmol), in a closed vial. To the resulting pink solution, compound **29f** (64.0 mg, 0.15 mmol), solubilized in dry dioxane (1 mL), was added dropwise. The reaction was carried out in a closed vial, at 80°C, under efficient magnetic stirring and was carefully monitored by TLC. After 2 hours the absence of starting reagent **29f** was confirmed. The reaction was allowed to cool down to room temperature. Then, acetonitrile and distilled water were added to the solution until a brown solid precipitated. The solid was filtered off and washed successively with water, acetonitrile and diethyl ether. The resulting brown solid was identified as **29n** (43.4 mg, 0.08 mmol, 55%).

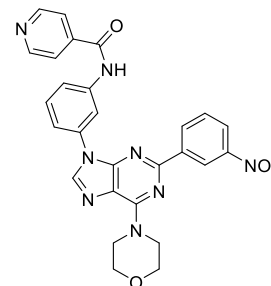
***N*-(4-(6-morpholino-2-(3-nitrophenyl)-9*H*-purin-9-yl)phenyl)isonicotinamide (29o)**

Under anhydrous conditions, isonicotinoyl-carbonyl chloride hydrochloride **31b** (2.5 eq., 0.17 g, 0.97 mmol) and DMAP (5 eq., 0.23 g, 1.94 mmol) were solubilized in dried acetonitrile (2 mL), in a closed vial. To the resulting pink solution, compound **29e** (0.16 g, 0.39 mmol), solubilized in dry dioxane (4 mL) was added dropwise. The reaction was carried out in a closed vial, at 100 °C, under efficient magnetic stirring and was carefully monitored by TLC. After 5 hours, the absence of starting reagent **29e** was confirmed. The reaction was allowed to cool down to room temperature. Then, acetonitrile and distilled water were added to the solution until a yellow solid precipitated. The resulting suspension was cooled down in an ice bath, and the solid was filtered off and washed successively with water, acetonitrile and diethyl ether. The resulting light yellow solid was identified as **29o** (0.18 g, 0.35 mmol, 90%).

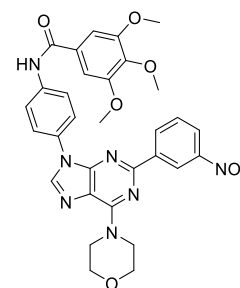


***N*-(3-(6-morpholino-2-(3-nitrophenyl)-9*H*-purin-9-yl)phenyl)isonicotinamide (29p)**

Under anhydrous conditions, isonicotinoyl-carbonyl chloride hydrochloride **31b** (2.15 eq., 0.12 g, 0.67 mmol) was solubilized in dried acetonitrile (2 mL) and distilled Et₃N (5 eq., 0.21 mL, 1.50 mmol), in a closed vial. To the resulting pink solution, compound **29f** (0.13 g, 0.30 mmol), solubilized in dried dioxane (2 mL), was added dropwise. The reaction was carried out in a closed vial, at 80°C, under efficient magnetic stirring and was carefully monitored by TLC. After 24 hours the absence of starting reagent **29f** was confirmed. The reaction was allowed to cool down to room temperature. Then, acetonitrile and distilled water were added to the solution until an off white solid precipitated. The solid was filtered off and washed successively with water, acetonitrile and diethyl ether. The resulting off white solid was identified as **29p** (0.13 g, 0.25 mmol, 84%).

***N*-(4-(3,4,5-trimethoxybenzoyl)-6-morpholino-2-(3-nitrophenyl)-9*H*-purin-9-yl)phenylbenzamide (29q)**

Under anhydrous conditions, 3,4,5-trimethoxybenzoyl chloride **31c** (1.5 eq., 0.31 g, 1.34 mmol) and K₂CO₃ (3 mol eq., 0.37 g, 2.70 mmol) were suspended in dried THF (3 mL), in a closed vial. To the resulting suspension, compound **29e** (0.37 g, 0.89 mmol), solubilized in dry THF (5 mL), was added dropwise. The reaction was carried out in a closed vial, at 70°C, under efficient magnetic stirring and was carefully monitored by TLC. After 28 hours, the absence of the starting reagent **29e** was confirmed. The reaction was allowed to cool down to room temperature. Then, the reaction solvent was evaporated and acetonitrile and distilled water were added to the suspension until a yellow solid precipitated. The resulting suspension was cooled down in an ice bath, and the solid was filtered off and washed successively with water, cold acetonitrile and diethyl ether. The resulting yellow solid was identified as **29q** (0.52 g, 0.85 mmol, 95%).

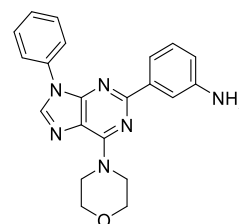


5.3.1.4. General procedure for the reduction of 2-(3-nitrophenyl)-purine derivatives (29)

2-nitrophenyl-purine derivatives **29** were combined, in a round bottom flask, with iron powder (8-12 eq.) and acetic acid (20 eq.) in a 90-95% ethanol solution. The reaction mixture, under nitrogen atmosphere, was submitted to reflux and the reaction was monitored by TLC (ethyl acetate). When the TLC showed absence of starting material, the suspension was cooled to approximately 20°C. A 25% aqueous ammonia solution was added to the suspension until pH=10-11. The suspension was kept at room temperature for 12-18 hours. The residue in suspension was filtered through a diatomaceous earth column (2-3 cm). The solution was concentrated using a rotary evaporator, until total removal of ethanol. The resulting suspension was cooled using an ice bath, and the solid was filtered, washed successively with water and diethyl ether and identified as compounds **1-23**. Analytical pure samples were obtained either by flash chromatography using THF as solvent, or by recrystallization of the solids from dichloromethane.

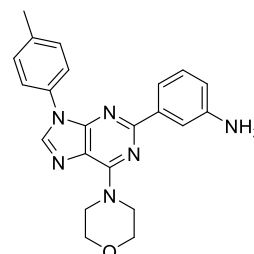
3-(6-morpholino-9-phenyl-9H-purin-2-yl)aniline (2)

Compound **2** (1.55 g, 4.17 mmol, 93%) was obtained as an off white solid from the reaction of compound **29a** (1.81 g, 4.49 mmol) with iron powder (2.01 g, 36.00 mmol) and acetic acid (5.14 mL, 89.80 mmol), in 300 mL of ethanol (95%), after 8.5 hours.



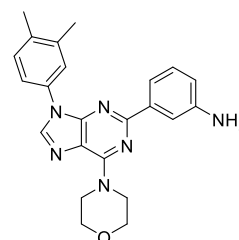
3-(6-morpholino-9-(p-tolyl)-9H-purin-2-yl)aniline (3)

Compound **3** (0.54 g, 1.40 mmol, 46%) was obtained as a white solid from the reaction of compound **29b** (1.26 g, 3.02 mmol) with iron powder (1.35 g, 24.19 mmol) and acetic acid (3.46 mL, 60.50 mmol), in 180 mL of ethanol (95%), after 8.5 hours.



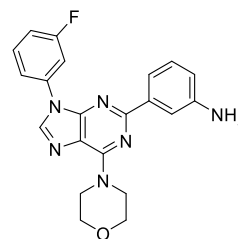
3-(9-(3,4-dimethylphenyl)-6-morpholino-9H-purin-2-yl)aniline (5)

Compound **5** (1.13 g, 2.82 mmol, 86%) was obtained as a white solid from the reaction of compound **29c** (1.42 g, 3.31 mmol) with iron powder (1.48 g, 26.50 mmol) and acetic acid (3.79 mL, 66.20 mmol), in 150 mL of ethanol (95%), after 6 hours.

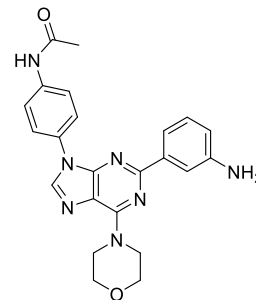


3-(9-(3-fluorophenyl)-6-morpholino-9H-purin-2-yl)aniline (7)

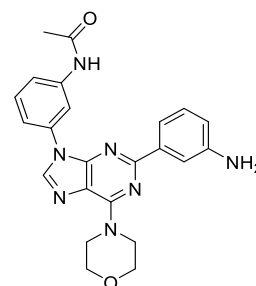
Compound **7** (0.55 g, 1.42 mmol, 87%) was obtained as a light yellow solid from the reaction of compound **29d** (0.68 g, 1.63 mmol) with iron powder (0.73 g, 13.00 mmol) and acetic acid (1.86 mL, 32.50 mmol), in 100 mL of ethanol (95%), after 8.5 hours.

**N-(4-(2-(3-aminophenyl)-6-morpholino-9H-purin-9-yl)phenyl)acetamide (8)**

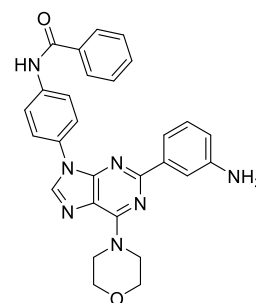
Compound **8** (0.54 g, 1.25 mmol, 91%) was obtained as an off white solid from the reaction of compound **29i** (0.63 g, 1.37 mmol) with iron powder (0.61 g, 10.99 mmol) and acetic acid (1.57 mL, 27.47 mmol), in 150 mL of ethanol (95%), after 7 hours.

**N-(3-(2-(3-aminophenyl)-6-morpholino-9H-purin-9-yl)phenyl)acetamide (9)**

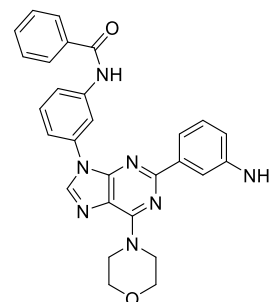
Compound **9** (0.55 g, 1.27 mmol, 99%) was obtained as an off white solid from the reaction of compound **29j** (0.59 g, 1.27 mmol) with iron powder (0.57 g, 10.20 mmol) and acetic acid (1.46 mL, 25.48 mmol), in 200 mL of ethanol (95%), after 7.5 hours.

**N-(4-(2-(3-aminophenyl)-6-morpholino-9H-purin-9-yl)phenyl)benzamide (10)**

Compound **10** (0.51 g, 1.04 mmol, 97%) was obtained as an off white solid from the reaction of compound **29k** (0.56 g, 1.06 mmol) with iron powder (0.48 g, 8.52 mmol) and acetic acid (1.22 mL, 21.29 mmol), in 150 mL of ethanol (95%), after 7 hours.

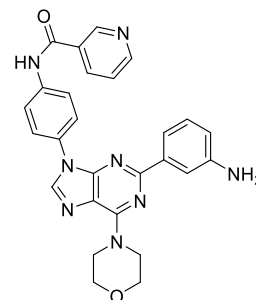
**N-(3-(2-(3-aminophenyl)-6-morpholino-9H-purin-9-yl)phenyl)benzamide (11)**

Compound **11** (52.5 mg, 0.11 mmol, 49%) was obtained as a white solid from the reaction of compound **29l** (114.0 mg, 0.22 mmol) with iron powder (0.15 g, 2.63 mmol) and acetic acid (0.25 mL, 4.37 mmol), in 45 mL of ethanol (90%), after 5.5 hours.

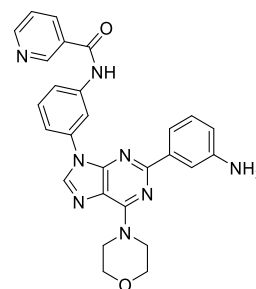


***N*-(4-(2-(3-aminophenyl)-6-morpholino-9*H*-purin-9-yl)phenyl)nicotinamide (12)**

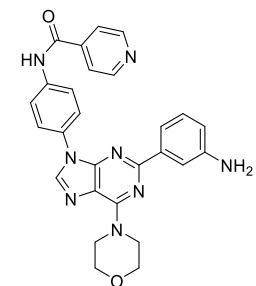
Compound **12** (91.3 mg, 0.18 mmol, 69%) was obtained as an off white solid from the reaction of compound **29m** (0.14 g, 0.27 mmol) with iron powder (0.12 g, 2.14 mmol) and acetic acid (0.95 mL, 5.34 mmol), in 50 mL of ethanol (95%), after 9 hours.

***N*-(3-(2-(3-aminophenyl)-6-morpholino-9*H*-purin-9-yl)phenyl)nicotinamide (13)**

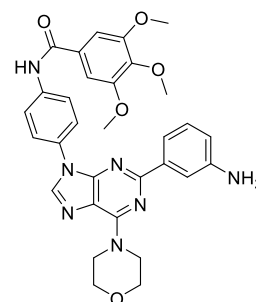
Compound **13** (0.26 g, 0.59 mmol, 62%) was obtained as an off white solid from the reaction of compound **29n** (0.50 g, 0.95 mmol) with iron powder (0.43 g, 7.62 mmol) and acetic acid (1.09 mL, 19.05 mmol), in 150 mL of ethanol (95%), after 9 hours.

***N*-(4-(2-(3-aminophenyl)-6-morpholino-9*H*-purin-9-yl)phenyl)isonicotinamide (14)**

Compound **14** (0.20 g, 0.40 mmol, 69%) was obtained as an off white solid from the reaction of compound **29o** (0.31 g, 0.59 mmol) with iron powder (0.26 g, 4.68 mmol) and acetic acid (0.67 mL, 11.70 mmol), in 100 mL of ethanol (95%), after 8 hours.

***N*-(4-(2-(3-aminophenyl)-6-morpholino-9*H*-purin-9-yl)phenyl)-3,4,5-dimethoxybenzamide (18)**

Compound **18** (1.06 g, 1.82 mmol, 99%) was obtained as a white solid from the reaction of compound **29q** (1.13 g, 1.85 mmol) with iron powder (0.83 g, 14.81 mmol) and acetic acid (2.12 mL, 37.02 mmol), in 150 mL of ethanol (95%), after 9 hours.



5.3.2. Final Products

In this section are described only the experimental procedures of new compounds. Hence, the compounds previously synthesized **2.1f**, **7.1f** and **7.1b** were obtained following the experimental protocols reported in [93].

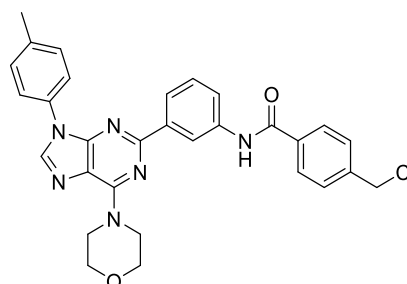
5.3.2.1. General procedure for the acylation of 2-(3-aminophenyl)-purine derivatives

Method A: Under anhydrous conditions, the 2-(3-aminophenyl)-purine derivatives (**1-23**) was solubilized in dry THF. To the respective solution, K_2CO_3 (1.2 – 1.5 eq.) and the respective acylation agent **32** (1.2 – 1.5 eq.) were added. The suspension was left to react in a closed vial, at room temperature, under efficient magnetic stirring and was carefully monitored by TLC. When the absence of limiting reagent was confirmed, water was added to the reaction mixture. The resulting suspension was cooled using an ice bath, and the solid was filtered and then washed with water, cold ethanol and diethyl ether. The solid obtained was isolated and identified as the pure desired product.

Method B: Under anhydrous conditions, the 2-(3-aminophenyl)-purine derivatives (**1-23**) was solubilized in dry dioxane. To the respective solution, $NaHCO_3$ (1.3 eq.) and the respective acylation agent **32f** (1.3 eq.) were added. The suspension was left to react in a closed vial, at room temperature, under efficient magnetic stirring and was carefully monitored by TLC. When the absence of limiting reagent was confirmed, water was added to the reaction mixture. The resulting suspension was cooled using an ice bath, and the solid was filtered and then washed with water, cold ethanol and diethyl ether. The solid obtained was isolated and identified as the pure desired product.

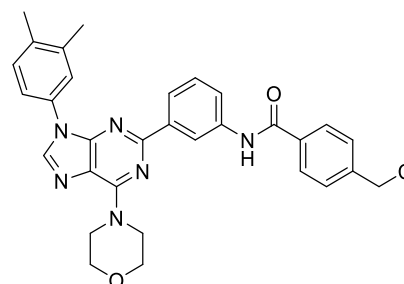
4-(chloromethyl)-*N*-(3-(6-morpholino-9-(*p*-tolyl)-9*H*-purin-2-yl)phenyl) benzamide (**3.1f**)

(Method A) Compound **3.1f** (0.39 g, 0.73 mmol, 99%) was obtained as a white solid from the reaction of compound **3** (0.28 g, 0.73 mmol) with **32a** (0.19 g, 0.98 mmol, 1.3 eq.) and K_2CO_3 (0.14 g, 0.98 mmol, 1.3 eq.), in 3 mL of dry THF, after 1 hour.



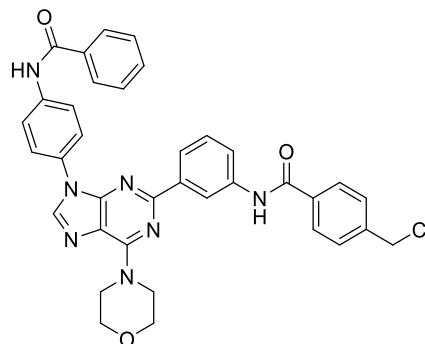
4-(chloromethyl)-*N*-(3-(9-(3,4-dimethylphenyl)-6-morpholino-9*H*-purin-2-yl)phenyl)benzamide (**5.1f**)

(Method A) Compound **5.1f** (1.08 g, 1.96 mmol, 97%) was obtained as an off- white solid from the reaction of compound **5** (0.80 g, 2.01 mmol) with **32a** (0.47 g, 2.51 mmol, 1.25 eq.) and K_2CO_3 (0.35 g, 2.51 mmol, 1.25 eq.), in 10 mL of dry THF, after 2.5 hours.

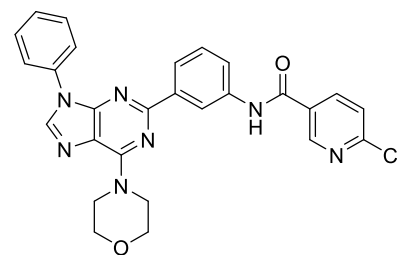


***N*-(3-(9-(4-benzamidophenyl)-6-morpholino-9*H*-purin-2-yl)phenyl)-4-(chloromethyl)benzamide (10.1f)**

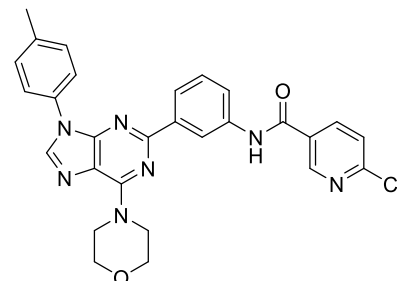
(Method A) Compound **10.1f** (0.21 g, 0.33 mmol, 98%) was obtained as a light brown solid from the reaction of compound **10** (0.17 g, 0.34 mmol) with **32a** (0.09 g, 0.45 mmol, 1.3 eq.) and K₂CO₃ (0.06 g, 0.45 mmol, 1.3 eq.), in 6 mL of dry THF, after 1 hour.

**6-chloro-*N*-(3-(6-morpholino-9-phenyl-9*H*-purin-2-yl)phenyl)nicotinamide (2.3f)**

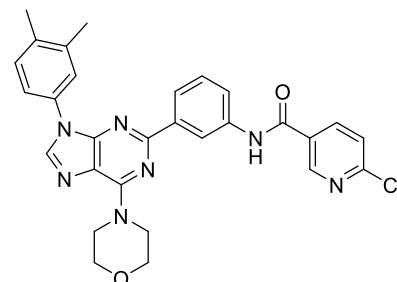
(Method A) Compound **2.3f** (0.54 g, 1.06 mmol, 76%) was obtained as an off-white solid from the reaction of compound **2** (0.42 g, 1.14 mmol) with **32b** (0.26 g, 1.48 mmol, 1.3 eq.) and K₂CO₃ (0.21 g, 1.48 mmol, 1.3 eq.), in 4 mL of dry THF, after 2 hours.

**6-chloro-*N*-(3-(6-morpholino-9-(*p*-tolyl)-9*H*-purin-2-yl)phenyl)nicotinamide (3.3f)**

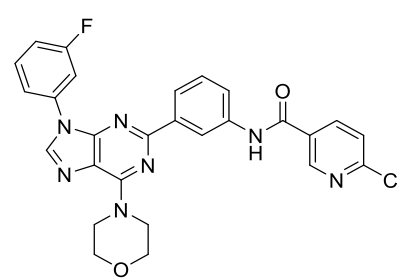
(Method A) Compound **3.3f** (0.41 g, 0.78 mmol, 85%) was obtained as a white solid from the reaction of compound **3** (0.35 g, 0.91 mmol) with **32b** (0.21 g, 1.19 mmol, 1.3 eq.) and K₂CO₃ (0.16 g, 1.19 mmol, 1.3 eq.), in 4 mL of dry THF, after 2 hours.

**6-chloro-*N*-(3-(9-(3,4-dimethylphenyl)-6-morpholino-9*H*-purin-2-yl)phenyl)nicotinamide (5.3f)**

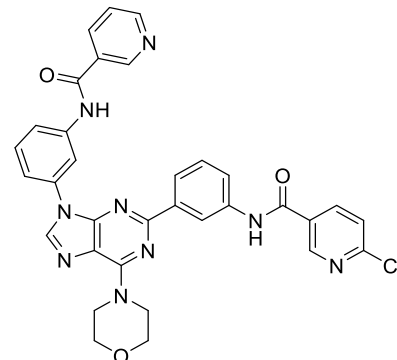
(Method A) Compound **5.3f** (0.26 g, 0.47 mmol, 94%) was obtained as an off-white solid from the reaction of compound **5** (0.20 g, 0.51 mmol) with **32b** (0.12 g, 0.66 mmol, 1.3 eq.) and K₂CO₃ (0.09 g, 0.66 mmol, 1.3 eq.), in 4 mL of dry THF, after 2.5 hours.

**6-chloro-*N*-(3-(9-(3-fluorophenyl)-6-morpholino-9*H*-purin-2-yl)phenyl)nicotinamide (7.3f)**

(Method A) Compound **7.3f** (0.32 g, 0.61 mmol, 84%) was obtained as a white solid from the reaction of compound **7** (0.28 g, 0.73 mmol) with **32b** (0.17 g, 0.95 mmol, 1.3 eq.) and K₂CO₃ (0.13 g, 0.95 mmol, 1.3 eq.), in 4 mL of dry THF, after 2 hours.

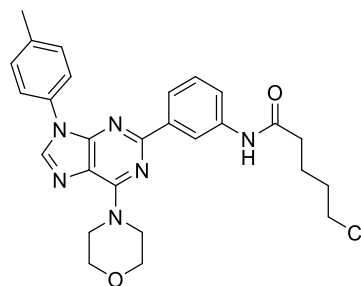
**6-chloro-*N*-(3-(6-morpholino-9-(3-(nicotinamido)phenyl)-9*H*-purin-2-yl)phenyl)nicotinamide (13.3f)**

(Method A) Compound **13.3f** (0.20 g, 0.31 mmol, 86%) was obtained as an off-white solid from the reaction of compound **13** (0.18 g, 0.37 mmol) with **32b** (0.08 g, 0.48 mmol, 1.3 eq.) and K₂CO₃ (0.07 g, 0.48 mmol, 1.3 eq.), in 15 mL of dry THF, after 3.5 hours.

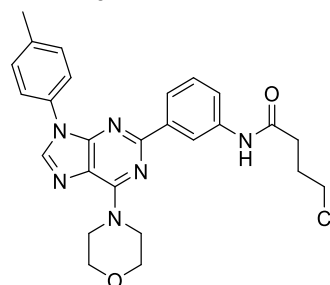


5-chloro-N(3-(6-morpholino-9-(p-tolyl)-9H-purin-2-yl)phenyl) pentanamide (3.5f)

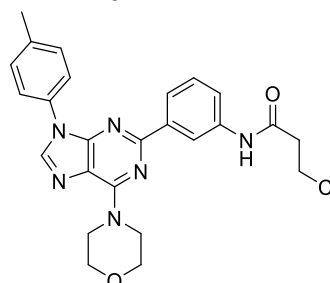
(Method A) Compound **3.5f** (0.24 g, 0.47 mmol, 85%) was obtained as a white solid from the reaction of compound **3** (0.21 g, 0.55 mmol) with **32c** (106.3 μ L, 0.82 mmol, 1.5 eq.) and K_2CO_3 (0.11 g, 0.82 mmol, 1.5 eq.), in 4 mL of dry THF, after 2.5 hours.

**4-chloro-N(3-(6-morpholino-9-(p-tolyl)-9H-purin-2-yl)phenyl) butanamide (3.6f)**

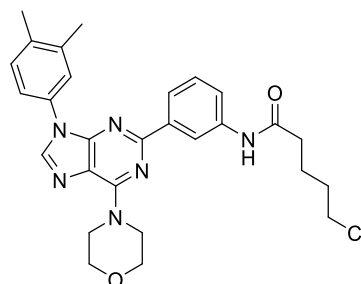
(Method A) Compound **3.6f** (0.23 g, 0.46 mmol, 82%) was obtained as an off- white solid from the reaction of compound **3** (0.22 g, 0.57 mmol) with **32d** (95.5 μ L, 0.85 mmol, 1.5 eq.) and K_2CO_3 (0.12 g, 0.85 mmol, 1.5 eq.), in 3 mL of dry THF, after 2.5 hours.

**3-chloro-N(3-(6-morpholino-9-(p-tolyl)-9H-purin-2-yl)phenyl) propanamide (3.7f)**

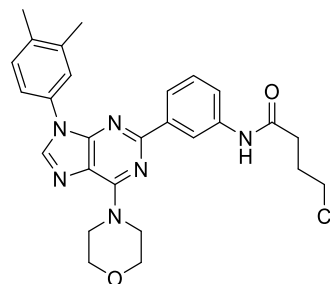
(Method A) Compound **3.7f** (0.32 g, 0.68 mmol, 88%) was obtained as an off- white solid from the reaction of compound **3** (0.30 g, 0.77 mmol) with **32e** (113.4 μ L, 1.18 mmol, 1.5 eq.) and K_2CO_3 (0.16 g, 1.15 mmol, 1.5 eq.), in 3 mL of dry THF, after 2.5 hours.

**5-chloro-N(3-(9-(3,4-dimethylphenyl)-6-morpholino-9H-purin-2-yl) phenyl)pentanamide (5.5f)**

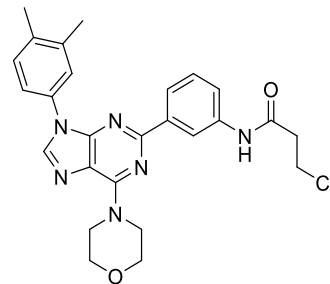
(Method A) Compound **5.5f** (0.26 g, 0.50 mmol, 97%) was obtained as a white solid from the reaction of compound **5** (0.21 g, 0.51 mmol) with **32c** (86.1 μ L, 0.67 mmol, 1.3 eq.) and K_2CO_3 (0.09 g, 0.67 mmol, 1.3 eq.), in 4 mL of dry THF, after 3.5 hours.

**4-chloro-N(3-(9-(3,4-dimethylphenyl)-6-morpholino-9H-purin-2-yl) phenyl)butanamide (5.6f)**

(Method A) Compound **5.6f** (0.25 g, 0.50 mmol, 93%) was obtained as an off- white solid from the reaction of compound **5** (0.21 g, 0.53 mmol) with **32d** (77.7 μ L, 0.69 mmol, 1.3 eq.) and K_2CO_3 (0.10 g, 0.69 mmol, 1.3 eq.), in 4 mL of dry THF, after 3.5 hours.

**3-chloro-N(3-(9-(3,4-dimethylphenyl)-6-morpholino-9H-purin-2-yl) phenyl)propanamide (5.7f)**

(Method A) Compound **5.7f** (0.26 g, 0.52 mmol, 97%) was obtained as a white solid from the reaction of compound **5** (0.21 g, 0.54 mmol) with **32e** (69.0 μ L, 0.72 mmol, 1.3 eq.) and K_2CO_3 (0.10 g, 0.72 mmol, 1.3 eq.), in 4 mL of dry THF, after 2.5 hours.



2-chloroethyl (3-(6-morpholino-9-phenyl-9H-purin-2-yl)phenyl) carbamate (2.8f)

(Method B) Compound **2.8f** (0.29 g, 0.61 mmol, 79%) was obtained as a white solid from the reaction of compound **2** (0.29 g, 0.77 mmol) with **32f** (108 μ L, 1.04 mmol, 1.3 eq.) and NaHCO₃ (0.16 g, 1.93 mmol, 2.5 eq.), in 3 mL of dry dioxane, after 1 hour.

2-chloroethyl (3-(9-(3,4-dimethylphenyl)-6-morpholino-9H-purin-2-yl) phenyl)carbamate (5.8f)

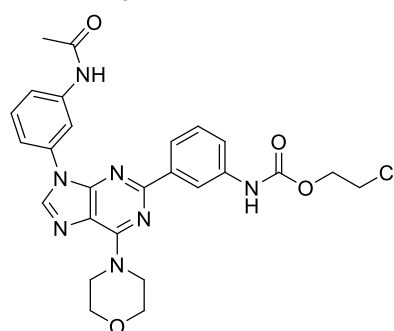
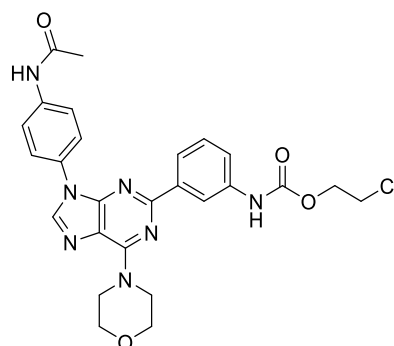
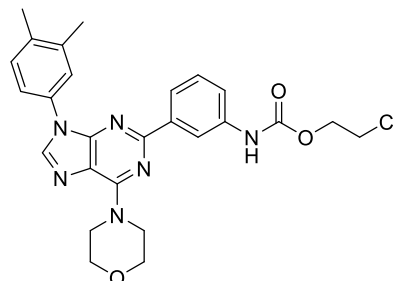
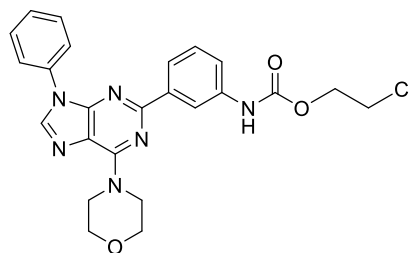
(Method B) Compound **5.8f** (0.23 g, 0.45 mmol, 96%) was obtained as an off-white solid from the reaction of compound **5** (0.19 g, 0.47 mmol) with **32f** (65.1 μ L, 0.63 mmol, 1.3 eq.) and NaHCO₃ (0.10 g, 1.10 mmol, 2.5 eq.), in 3 mL of dry dioxane, after 2 hours.

2-chloroethyl (3-(9-(4-acetamidophenyl)-6-morpholino-9H-purin-2-yl) phenyl)carbamate (8.8f)

(Method B) Compound **8.8f** (0.23 g, 0.43 mmol, 80%) was obtained as an off-white solid from the reaction of compound **8** (0.23 g, 0.55 mmol) with **32f** (76.0 μ L, 0.73 mmol, 1.3 eq.) and NaHCO₃ (0.11 g, 1.37 mmol, 2.5 eq.), in 4 mL of dry dioxane, after 1 hour.

2-chloroethyl (3-(9-(3-acetamidophenyl)-6-morpholino-9H-purin-2-yl) phenyl)carbamate (9.8f)

(Method B) Compound **9.8f** (0.25 g, 0.46 mmol, 72%) was obtained as an off-white solid from the reaction of compound **9** (0.28 g, 0.64 mmol) with **32f** (89.3 μ L, 0.86 mmol, 1.3 eq.) and NaHCO₃ (0.13 g, 1.60 mmol, 2.5 eq.), in 2 mL of dry dioxane, after 1 hour.

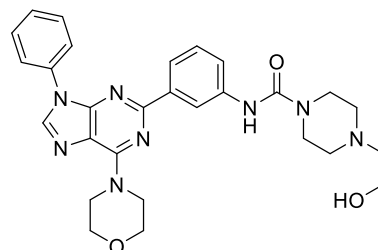
**5.3.2.2. General procedure for the one pot synthesis of ureas from 2-(3-aminophenyl)-purine derivatives**

Under anhydrous conditions, the 2-(3-aminophenyl)-purine derivatives (**1-23**) were solubilized in dry dioxane. To the respective solution, NaHCO₃ (2.5 eq.) and phenyl chloroformate **33** (1.25 eq.) were added. The suspension was left to react in a closed vial, at room temperature, under efficient magnetic stirring and was carefully monitored by TLC. When the absence of limiting reagent was confirmed, Et₃N (3 eq.) and an excess of amine **34** (1.25 eq.) were added to the reaction mixture. The suspension was kept in a closed vial and was heated up to 80°C under efficient magnetic stirring. It was again carefully monitored by TLC. When the absence of the reaction intermediate was confirmed, the

reaction was allowed to cool down to room temperature. Then, distilled water was added. The resulting suspension was cooled down in an ice bath, and the solid was filtered off and washed successively with water, cold ethanol and cold diethyl ether. Analytical pure samples were obtained by recrystallization of the solids from acetone.

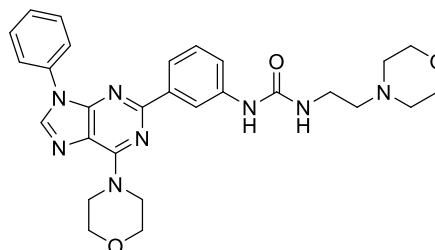
4-(2-hydroxyethyl)-N-(3-(6-morpholino-9-phenyl-9H-purin-2-yl)phenyl)piperazine-1-carboxamide (2.4h)

Compound **2.4h** (0.08 g, 0.15 mmol, 38%) was obtained as a white solid from the one-pot reaction of compound **2** (0.15 g, 0.41 mmol) with **33** (63.9 μ L, 0.51 mmol, 1.25 eq.) and NaHCO₃ (0.09 g, 1.02 mmol, 2.5 eq.), in 2 mL of dry dioxane, after 1 hour, and later reaction with Et₃N (170 μ L, 1.22 mmol, 3 eq.) and **34a** (74.8 μ L, 0.61 mmol, 1.5 eq.) after 2.5 hours.



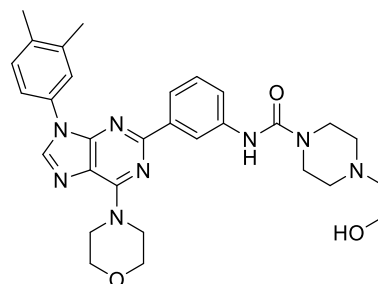
1-(3-(6-morpholino-9-phenyl-9H-purin-2-yl)phenyl)-3-(2-morpholinoethyl)urea (2.9c)

Compound **2.9c** (0.16 g, 0.30 mmol, 83%) was obtained as a white solid from the one-pot reaction of compound **2** (0.13 g, 0.36 mmol) with **33** (56.4 μ L, 0.45 mmol, 1.25 eq.) and NaHCO₃ (0.08 g, 0.90 mmol, 2.5 eq.), in 2 mL of dry dioxane, after 1 hour, and later reaction with Et₃N (150 μ L, 1.07 mmol, 3 eq.) and **34b** (70.0 μ L, 0.54 mmol, 1.5 eq.) after 2.5 hours.



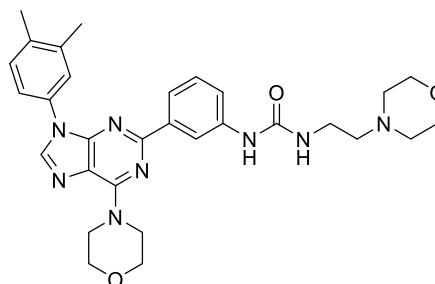
N-(3-(9-(3,4-dimethylphenyl)-6-morpholino-9H-purin-2-yl)phenyl)-4-(2-hydroxyethyl)piperazine-1-carboxamide (5.4h)

Compound **5.4h** (0.12 g, 0.22 mmol, 83%) was obtained as a white solid from the one-pot reaction of compound **5** (0.10 g, 0.26 mmol) with **33** (41.1 μ L, 0.33 mmol, 1.25 eq.) and NaHCO₃ (0.06 g, 0.65 mmol, 2.5 eq.), in 2 mL of dry dioxane, after 1 hour, and later reaction with Et₃N (109 μ L, 0.78 mmol, 3 eq.) and **34a** (39.0 μ L, 0.31 mmol, 1.25 eq.) after 2.5 hours.



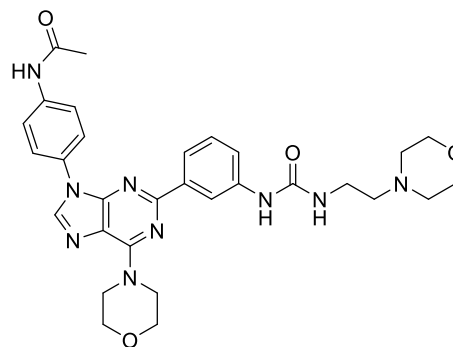
1-(3-(9-(3,4-dimethylphenyl)-6-morpholino-9H-purin-2-yl)phenyl)-3-(2-morpholinoethyl)urea (5.9c)

Compound **5.9c** (0.13 g, 0.23 mmol, 85%) was obtained as a white solid from the one-pot reaction of compound **5** (0.11 g, 0.27 mmol) with **33** (42.8 μ L, 0.34 mmol, 1.25 eq.) and NaHCO₃ (0.06 g, 0.68 mmol, 2.5 eq.), in 2 mL of dry dioxane, after 1 hour, and later reaction with Et₃N (114 μ L, 0.82 mmol, 3 eq.) and **34b** (44.6 μ L, 0.34 mmol, 1.25 eq.) after 3 hours.

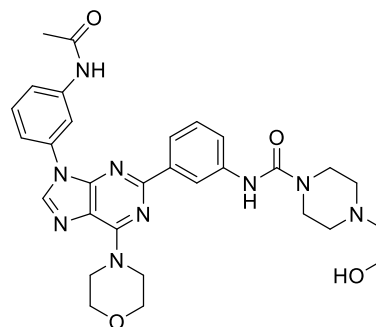


***N*-(4-(6-morpholino-2-(3-(3-(2-morpholinoethyl)ureido)phenyl)-9H-purin-9-yl)phenyl)acetamide (8.9c)**

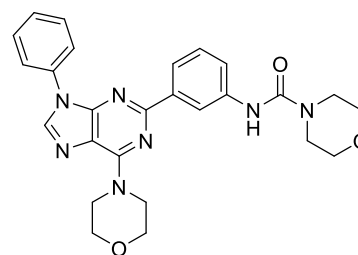
Compound **8.9c** (0.07 g, 0.11 mmol, 40%) was obtained as an off-white solid from the one-pot reaction of compound **8** (0.12 g, 0.29 mmol) with **33** (45.2 μ L, 0.36 mmol, 1.25 eq.) and NaHCO₃ (0.06 g, 0.72 mmol, 2.5 eq.), in 4 mL of dry dioxane, after 1 hour, and later reaction with Et₃N (120 μ L, 0.86 mmol, 3 eq.) and **34b** (56.5 μ L, 0.43 mmol, 1.5 eq.) after 3 hours.

***N*-(3-(9-(3-acetamidophenyl)-6-morpholino-9H-purin-2-yl)phenyl)-4-(2-hydroxyethyl)piperazine-1-carboxamide (9.4h)**

Compound **9.4h** (0.12 g, 0.20 mmol, 52%) was obtained as an off-white solid from the one-pot reaction of compound **9** (0.16 g, 0.38 mmol) with **33** (59.3 μ L, 0.47 mmol, 1.25 eq.) and NaHCO₃ (0.08 g, 0.94 mmol, 2.5 eq.), in 3 mL of dry dioxane, after 1 hour, and later reaction with Et₃N (158 μ L, 1.13 mmol, 3 eq.) and **34a** (69.5 μ L, 0.57 mmol, 1.5 eq.) after 3 hours.

**Synthesis of *N*-(3-(6-morpholino-9-phenyl-9H-purin-2-yl)phenyl) morpholine-4-carboxamide (38)**

Under anhydrous conditions, **2** (0.10 g, 0.28 mmol) was solubilized in dry dioxane (2 mL). To the respective solution, NaHCO₃ (0.06g, 0.70 mmol, 2.5 eq.) and phenyl chloroformate **33** (44.0 μ L, 0.35 mmol, 1.25 eq.) were added. The suspension was left to react in a closed vial, at room temperature, under efficient magnetic stirring and was carefully monitored by TLC. The absence of starting material was confirmed after 1 hour. Then, an excess of morpholine (122 μ L, 1.40 mmol, 5 eq.) was added to the reaction mixture. The suspension was kept in a closed vial and was heated up to 80°C under efficient magnetic stirring. It was again carefully monitored by TLC. When the absence of the reaction intermediate was confirmed, after 3 hours, the reaction was allowed to cool down to room temperature. Then, distilled water was added. The resulting suspension was cooled down in an ice bath, and the solid was filtered off and washed successively with water, cold ethanol and cold diethyl ether. After recrystallization from acetone, the solid was identified as **38** (0.10 g, 0.20 mmol, 73%).



5.3.2.3. Reaction of the acylated 2-(3-aminophenyl)-purine derivatives with nitrogen nucleophiles

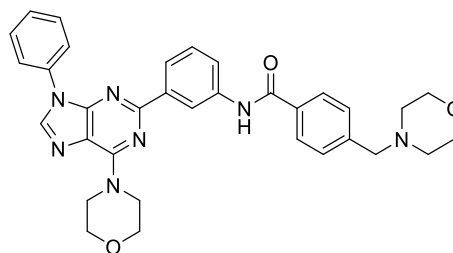
Method A: A nitrogen nucleophile (5 eq.) was added to a suspension of acylated 2-(3-aminophenyl)-purine derivatives in dioxane. The mixture was stirred in a closed vial, at 110°C, until all the starting material was consumed (evidence by TLC). Then, the reaction was allowed to cool down to room temperature and distilled water was added. The resulting suspension was cooled down in an ice bath, and the solid was filtered off and washed successively with water, cold ethanol and cold diethyl ether.

Method A1: A nitrogen nucleophile (5 eq.) was added to a suspension of acylated 2-(3-aminophenyl)-purine derivatives in dioxane. The mixture was stirred in a closed vial, at 110°C, until all the starting material was consumed (evidence by TLC). Then, the reaction was allowed to cool down to room temperature and diethyl ether was added. The resulting suspension was cooled down in an ice bath, and the solid was filtered off and washed with cold diethyl ether.

Method B: Sodium azide (5 - 6 eq.) was added to a solution of an acylated 2-(3-aminophenyl)-purine derivative in DMSO. The mixture was stirred in a closed vial, at 110°C, until all the starting material was consumed (evidence by TLC). Then, the reaction was allowed to cool down to room temperature and distilled water was added. The resulting suspension was cooled down in an ice bath, and the solid was filtered off and washed successively with water, cold ethanol and cold diethyl ether.

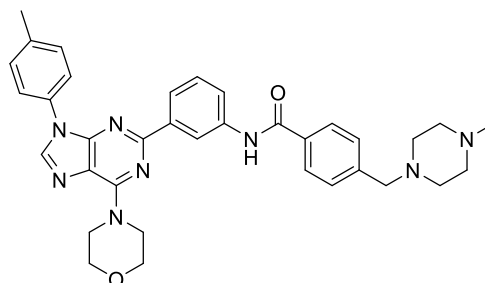
***N*-(3-(6-morpholino-9-phenyl-9H-purin-2-yl)phenyl)-4-(morpholinomethyl)benzamide (2.1c)**

(Method A) Compound **2.1c** (0.14 g, 0.24 mmol, 83%), was obtained as a white solid from the reaction of **2.1f** (0.15 g, 0.29 mmol) with morpholine **34c** (127 μ L, 1.46 mmol, 5 eq.) in dioxane (1 mL) after 13 hours.



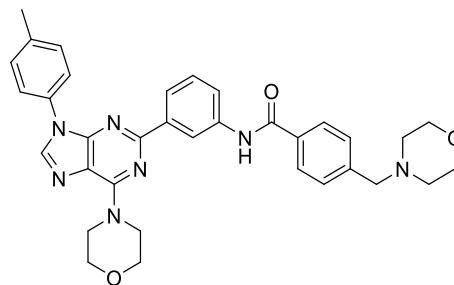
4-((4-methylpiperazin-1-yl)methyl)-*N*-(3-(6-morpholino-9-(*p*-tolyl)-9H-purin-2-yl)phenyl)benzamide (3.1b)

(Method A) Compound **3.1b** (0.07 g, 0.12 mmol, 78%), was obtained as a white solid from the reaction of **3.1f** (0.08 g, 0.15 mmol) with *N*-methyl-piperazine **34d** (82.3 μ L, 0.74 mmol, 5 eq.) in dioxane (0.5 mL) after 5 hours.

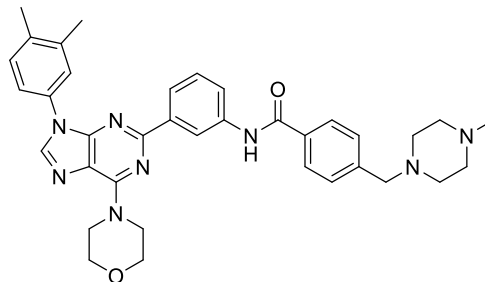


***N*-(3-(6-morpholino-9-(*p*-tolyl)-9*H*-purin-2-yl)phenyl)-4-(morpholinomethyl)benzamide (3.1c)**

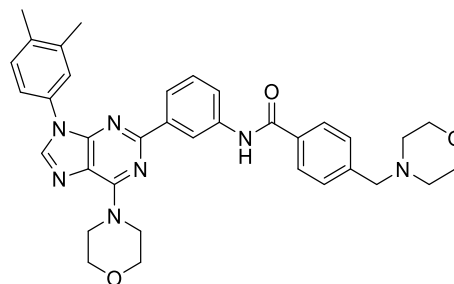
(Method A) Compound **3.1c** (0.09 g, 0.16 mmol, 75%), was obtained as a white solid from the reaction of **3.1f** (0.11 g, 0.21 mmol) with morpholine **34c** (90.8 μ L, 1.04 mmol, 5 eq.) in dioxane (0.5 mL) after 8 hours.

***N*-(3-(9-(3,4-dimethylphenyl)-6-morpholino-9*H*-purin-2-yl) phenyl)-4-((4-methylpiperazin-1-yl)methyl) benzamide (5.1b)**

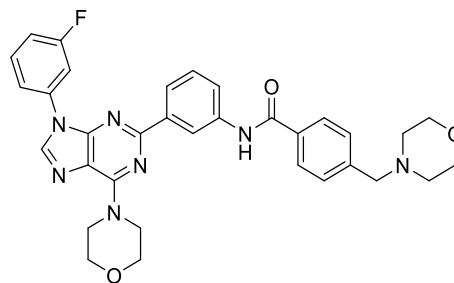
(Method A) Compound **5.1b** (0.15 g, 0.24 mmol, 77%), was obtained as an off-white solid from the reaction of **5.1f** (0.17 g, 0.32 mmol) with *N*-methyl-piperazine **34d** (176 μ L, 1.58 mmol, 5 eq.) in dioxane (2 mL) after 14 hours.

***N*-(3-(9-(3,4-dimethylphenyl)-6-morpholino-9*H*-purin-2-yl) phenyl)-4-(morpholinomethyl)benzamide (5.1c)**

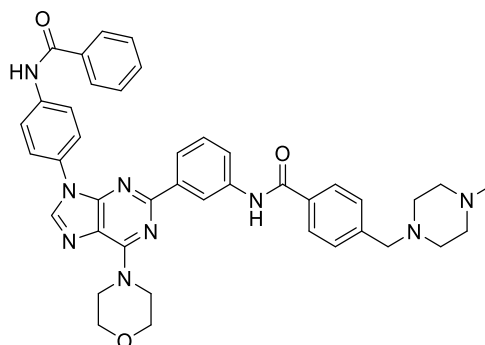
(Method A) Compound **5.1c** (0.13 g, 0.21 mmol, 73%), was obtained as a white solid from the reaction of **5.1f** (0.15 g, 0.29 mmol) with morpholine **34c** (127 μ L, 1.46 mmol, 5 eq.) in dioxane (2 mL) after 14 hours.

***N*-(3-(9-(3-fluorophenyl)-6-morpholino-9*H*-purin-2-yl) phenyl)-4-(morpholinomethyl)benzamide (7.1c)**

(Method A) Compound **7.1c** (0.13 g, 0.22 mmol, 86%), was obtained as a white solid from the reaction of **7.1f** (0.14 g, 0.26 mmol) with morpholine **34c** (114 μ L, 1.30 mmol, 5 eq.) in dioxane (0.5 mL) after 14.5 hours.

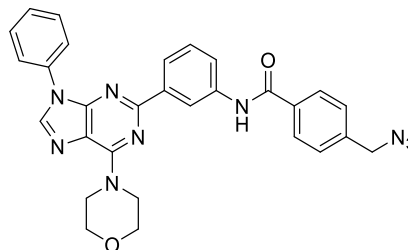
***N*-(3-(9-(4-benzamidophenyl)-6-morpholino-9*H*-purin-2-yl) phenyl)-4-((4-methylpiperazin-1-yl)methyl) benzamide (10.1b)**

(Method A1) Compound **10.1b** (0.05 g, 0.07 mmol, 36%), was obtained as an off-white solid from the reaction of **10.1f** (0.13 g, 0.20 mmol) with *N*-methyl-piperazine **34d** (109 μ L, 0.98 mmol, 5 eq.) in dioxane (1 mL) after 31 hours.

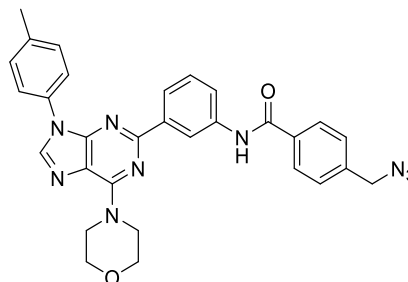


4-(azidomethyl)-*N*-(3-(6-morpholino-9-phenyl-9*H*-purin-2-yl)phenyl)benzamide (2.1g)

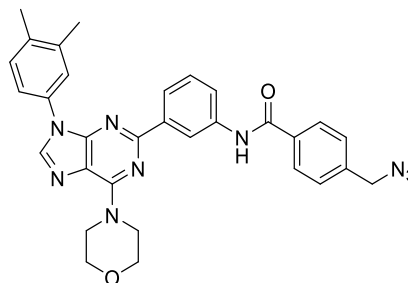
(Method B) Compound **2.1g** (0.17 g, 0.32 mmol, 81%), was obtained as a white solid from the reaction of **2.1f** (0.21 g, 0.40 mmol) with sodium azide **35** (0.16 g, 2.40 mmol, 6 eq.) in DMSO (1 mL) after 12 hours.

**4-(azidomethyl)-*N*-(3-(6-morpholino-9-(*p*-tolyl)-9*H*-purin-2-yl)phenyl)benzamide (3.1g)**

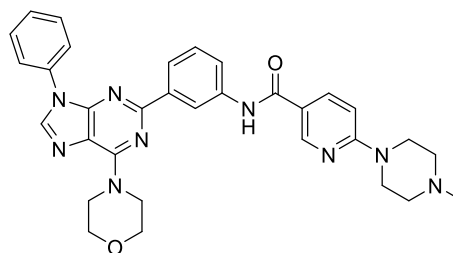
(Method B) Compound **3.1g** (0.13 g, 0.24 mmol, 86%), was obtained as a white solid from the reaction of **3.1f** (0.15 g, 0.28 mmol) with sodium azide **35** (0.09 g, 1.41 mmol, 5 eq.) in DMSO (1 mL) after 1 hour.

**4-(azidomethyl)-*N*-(3-(9-(3,4-dimethylphenyl)-6-morpholino-9*H*-purin-2-yl)phenyl)benzamide (5.1g)**

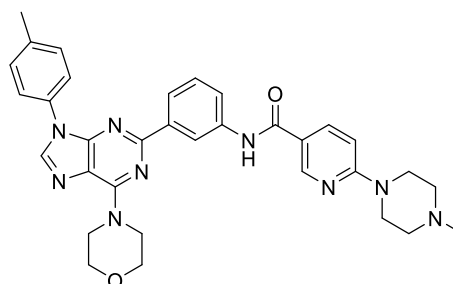
(Method B) Compound **5.1g** (0.20 g, 0.38 mmol, 99%), was obtained as a white solid from the reaction of **5.1f** (0.20 g, 0.38 mmol) with sodium azide **35** (0.15 g, 2.29 mmol, 6 eq.) in DMSO (2 mL) after 14 hours.

**6-(4-methylpiperazin-1-yl)-*N*-(3-(6-morpholino-9-phenyl-9*H*-purin-2-yl)phenyl)nicotinamide (2.3b)**

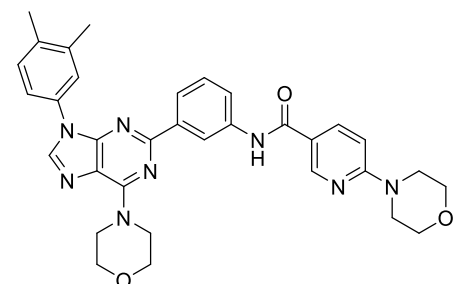
(Method A) Compound **2.3b** (0.12 g, 0.21 mmol, 72%), was obtained as a white solid from the reaction of **2.3f** (0.15 g, 0.29 mmol) with *N*-methyl-piperazine **34d** (163 μ L, 1.50 mmol, 5 eq.) in dioxane (0.4 mL) after 20 hours.

**6-(4-methylpiperazin-1-yl)-*N*-(3-(6-morpholino-9-(*p*-tolyl)-9*H*-purin-2-yl)phenyl)nicotinamide (3.3b)**

(Method A) Compound **3.3b** (0.16 g, 0.27 mmol, 80%), was obtained as an off-white solid from the reaction of **3.3f** (0.18 g, 0.33 mmol) with *N*-methyl-piperazine **34d** (185 μ L, 1.67 mmol, 5 eq.) in dioxane (0.5 mL) after 12 hours.

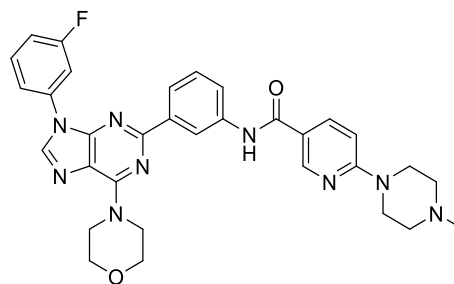
***N*-(3-(9-(3,4-dimethylphenyl)-6-morpholino-9*H*-purin-2-yl)phenyl)-6-morpholinonicotinamide (5.3c)**

(Method A) Compound **5.3c** (0.08 g, 0.14 mmol, 87%), was obtained as an off-white solid from the reaction of **5.3f** (0.09 g, 0.17 mmol) with morpholine **34c** (72.0 μ L, 0.83 mmol, 5 eq.) in dioxane (0.5 mL) after 24 hours.

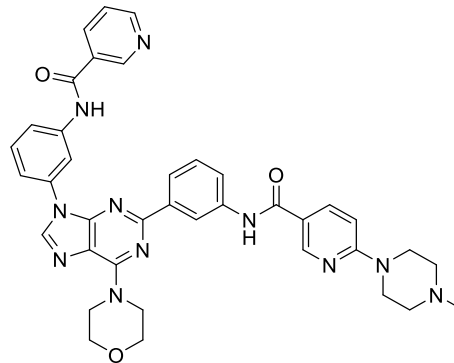


***N*-(3-(9-(3-fluorophenyl)-6-morpholino-9*H*-purin-2-yl)phenyl)-6-(4-methylpiperazin-1-yl)nicotinamide (7.3b)**

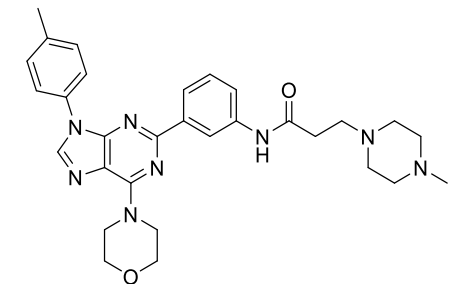
(Method A) Compound **7.3b** (0.11 g, 0.18 mmol, 70%), was obtained as an off-white solid from the reaction of **7.3f** (0.14 g, 0.26 mmol) with *N*-methyl-piperazine **34d** (145 μ L, 1.31 mmol, 5 eq.) in dioxane (0.5 mL) after 16 hours.

**6-(4-methylpiperazin-1-yl)-*N*-(3-(6-morpholino-9-(3-(nicotinamido)phenyl)-9*H*-purin-2-yl)phenyl)nicotinamide (13.3b)**

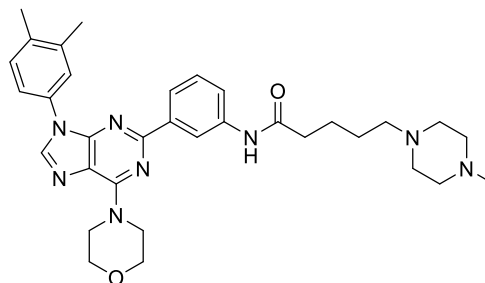
(Method A1) Compound **13.3b** (0.04 g, 0.06 mmol, 39%), was obtained as an off-white solid from the reaction of **13.3f** (0.10 g, 0.15 mmol) with *N*-methyl-piperazine **34d** (85.0 μ L, 0.76 mmol, 5 eq.) in dioxane (0.3 mL) after 16 hours.

**3-(4-methylpiperazin-1-yl)-*N*-(3-(6-morpholino-9-(*p*-tolyl)-9*H*-purin-2-yl)phenyl)propanamide (3.7b)**

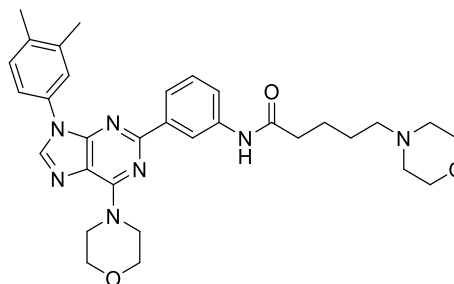
(Method A1) Compound **3.7b** (0.06 g, 0.11 mmol, 42%), was obtained as an off-white solid from the reaction of **3.7f** (0.12 g, 0.26 mmol) with *N*-methyl-piperazine **34d** (142 μ L, 1.27 mmol, 5 eq.) in dioxane (0.5 mL) after 3.5 hours.

***N*-(3-(9-(3,4-dimethylphenyl)-6-morpholino-9*H*-purin-2-yl)phenyl)-5-(4-methylpiperazin-1-yl)pentanamide (5.5b)**

(Method A) Compound **5.5b** (0.05 g, 0.08 mmol, 38%), was obtained as an off-white solid from the reaction of **5.5f** (0.11 g, 0.22 mmol) with *N*-methyl-piperazine **34d** (123 μ L, 1.11 mmol, 5 eq.) in dioxane (0.5 mL) after 3.5 hours.

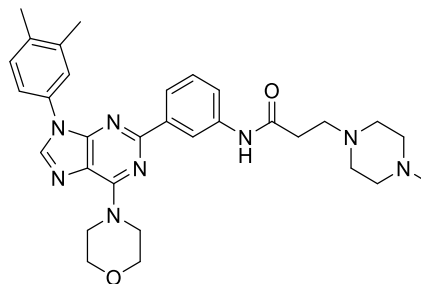
***N*-(3-(9-(3,4-dimethylphenyl)-6-morpholino-9*H*-purin-2-yl)phenyl)-5-morpholinopentanamide (5.5c)**

(Method A) Compound **5.5c** (0.06 g, 0.11 mmol, 66%), was obtained as an off-white solid from the reaction of **5.5f** (0.08 g, 0.16 mmol) with morpholine **34c** (70.8 μ L, 0.81 mmol, 5 eq.) in dioxane (0.5 mL) after 6 hours.

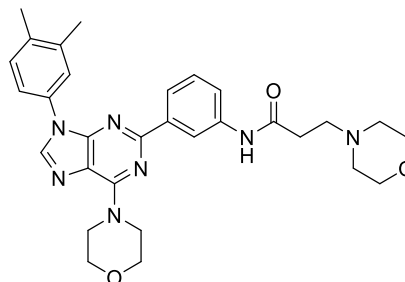


***N*-(3-(9-(3,4-dimethylphenyl)-6-morpholino-9*H*-purin-2-yl) phenyl)-3-(4-methylpiperazin-1-yl)propanamide (5.7b)**

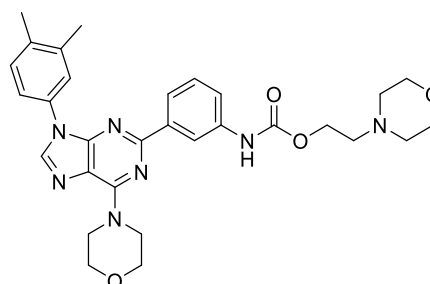
(Method A) Compound **5.7b** (0.07 g, 0.13 mmol, 67%), was obtained as an off-white solid from the reaction of **5.7f** (0.09 g, 0.19 mmol) with *N*-methyl-piperazine **34d** (106 μ L, 0.95 mmol, 5 eq.) in dioxane (0.5 mL) after 3.5 hours.

***N*-(3-(9-(3,4-dimethylphenyl)-6-morpholino-9*H*-purin-2-yl) phenyl)-3-morpholinopropanamide (5.7c)**

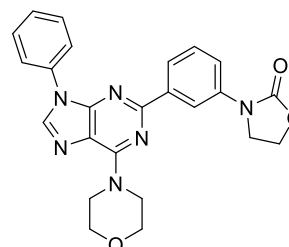
(Method A) Compound **5.7c** (0.05 g, 0.10 mmol, 58%), was obtained as a white solid from the reaction of **5.7f** (0.08 g, 0.17 mmol) with morpholine **34c** (73.0 μ L, 0.84 mmol, 5 eq.) in dioxane (0.5 mL) after 6 hours.

**2-morpholinoethyl (3-(9-(3,4-dimethylphenyl)-6-morpholino-9*H*-purin-2-yl)phenyl)carbamate (5.8c)**

Morpholine (86.1 μ L, 0.99 mmol, 10 eq.) was added to a suspension of **5.8f** (0.05 g, 0.10 mmol) in acetonitrile (0.25 mL). The suspension was left to react in a closed vial, at 80°C, under efficient magnetic stirring and was carefully monitored by TLC. The absence of starting material was confirmed after 22 hours. Then, the reaction was allowed to cool down to room temperature, and water was added to the reaction mixture. The resulting suspension was cooled down in an ice bath, and the solid was filtered off and washed with distilled water. After recrystallization from ethanol, the white solid was identified as **5.8c** (0.04 g, 0.07 mmol, 75%).

**3-(3-(6-morpholino-9-phenyl-9*H*-purin-2-yl)phenyl)oxazolidin-2-one (37)**

Morpholine (140 μ L, 1.61 mmol, 5 eq.) was added to a suspension of **2.8f** (0.15 g, 0.32 mmol) in DMSO (0.5 mL). The suspension was left to react in a closed vial, at 80 °C, under efficient magnetic stirring and was carefully monitored by TLC. The absence of starting material was confirmed after 16 hours. Then, the reaction was allowed to cool down to room temperature and distilled water was added. The resulting suspension was cooled down in an ice bath, and the solid was filtered off and washed with distilled water and diethyl ether. The solid (0.13 g) was identified as a mixture of compounds. The solid was recrystallized from acetone and compound **37** was isolated as a white solid (0.02 g, 0.04 mmol, 12%).



Chapter 6

REFERENCES

- [1] C. Tomasetti, L. Li, and B. Vogelstein, 'Stem cell divisions, somatic mutations, cancer etiology, and cancer prevention', *Science*, vol. 355, pp. 1330–1334, 2017.
- [2] V. Asati, D. K. Mahapatra, and S. K. Bharti, 'PI3K / Akt / mTOR and Ras / Raf / MEK / ERK signaling pathways inhibitors as anticancer agents : Structural and pharmacological perspectives', *Eur. J. Med. Chem.*, vol. 109, pp. 314–341, 2016.
- [3] S. H. Hassanpour and M. Dehghani, 'Review of cancer from perspective of molecular', *J. Cancer Res. Pract.*, vol. 4, pp. 127–129, 2017.
- [4] A. Umar, B. K. Dunn, and P. Greenwald, 'Future directions in cancer prevention', *Nat. Rev. Cancer*, vol. 12, pp. 835–848, 2012.
- [5] National Cancer Institute, 'Cancer Statistics', 2021. [Online]. Available: <https://www.cancer.gov/about-cancer/understanding/statistics>. [Accessed: 23-Jan-2021].
- [6] Gco.iarc.fr, 'Cancer today', 2021. [Online]. Available: <https://gco.iarc.fr/today/online-analysis-pie>. [Accessed: 23-Jan-2021].
- [7] N. Cancer, 'The global challenge of cancer', vol. 1, no. January, pp. 1–2, 2020.
- [8] X. Jin *et al.*, 'A metastasis map of human cancer cell lines', *Nature*, vol. 588, no. 7837, pp. 331–336, 2020.
- [9] National Cancer Institute, 'Cancer Treatment', 2021. [Online]. Available: <https://www.cancer.gov/about-cancer/treatment>. [Accessed: 08-Feb-2021].
- [10] Y. T. Lee, Y. J. Tan, and C. E. Oon, 'Author's Accepted Manuscript Molecular targeted therapy : treating cancer with', *Eur. J. Pharmacol.*, 2018.
- [11] M. J. Duffy and J. Crown, 'Drugging "undruggable" genes for cancer treatment: Are we making progress?', *Int. J. Cancer*, vol. 148, no. 1, pp. 8–17, 2021.
- [12] C. V Dang, E. P. Reddy, K. M. Shokat, and L. Soucek, 'targets', *Nat. Publ. Gr.*, 2017.
- [13] C. Sawyers, 'Targeted cancer therapy', *Nature*, vol. 432, pp. 294–297, 2004.
- [14] J. Jin *et al.*, 'Identification of Genetic Mutations in Cancer : Challenge and Opportunity in the New Era of Targeted Therapy', vol. 9, no. April, pp. 1–7, 2019.
- [15] D. Uprety and A. A. Adjei, 'KRAS: From undruggable to a druggable Cancer Target', *Cancer Treat. Rev.*, vol. 89, no. July, pp. 102–170, 2020.
- [16] A. B. Gurung and A. Bhattacharjee, 'Significance of Ras Signaling in Cancer and Strategies for its Control', *Oncol. Hematol. Rev.*, vol. 11, no. 02, p. 147, 2015.
- [17] I. A. Prior, F. E. Hood, and J. L. Hartley, 'The frequency of ras mutations in cancer', *Cancer Res.*, vol. 80, no. 14, pp. 2669–2974, 2020.
- [18] B. Papke and C. J. Der, 'Drugging RAS: Know the enemy', *Science*, vol. 355, no. 6330, pp. 1158–1163, 2017.
- [19] M. B. Ryan and R. B. Corcoran, 'Therapeutic strategies to target RAS-mutant cancers', *Nat. Rev. Clin. Oncol.*, vol. 15, no. 11, pp. 709–720, 2018.
- [20] L. Buscail, B. Bournet, and P. Cordelier, 'Role of oncogenic KRAS in the diagnosis, prognosis and treatment of pancreatic cancer', *Nat. Rev. Gastroenterol. Hepatol.*, vol. 17, no. 3, pp. 153–168, 2020.
- [21] K. M. Mann, H. Ying, J. Juan, N. A. Jenkins, and N. G. Copeland, 'KRAS-related proteins in pancreatic cancer', *Pharmacol. Ther.*, vol. 168, pp. 29–42, 2016.
- [22] F. McCormick, 'KRAS as a therapeutic target', *Clin. Cancer Res.*, vol. 21, no. 8, pp. 1797–1801, 2015.
- [23] J. Downward, 'Targeting RAS signalling pathways in cancer therapy', *Nat. Rev. Cancer*, vol. 3, no. 1, pp. 11–22, 2003.

Chapter 6 – References

- [24] A. Bahrami *et al.*, 'Targeting RAS signaling pathway as a potential therapeutic target in the treatment of colorectal cancer', *J. Cell. Physiol.*, vol. 233, no. 3, pp. 2058–2066, 2018.
- [25] M. W. and J. H. Ufuk Degirmenci, 'Targeting Aberrant RAS/RAF/MEK/ERK Signaling for Cancer Therapy', *Cells*, vol. 9, no. 198, pp. 1–33, 2020.
- [26] F. M. Elmenier, D. S. Lasheen, and K. A. M. Abouzid, 'Phosphatidylinositol 3 kinase (PI3K) inhibitors as new weapon to combat cancer', *Eur. J. Med. Chem.*, vol. 183, p. 111718, 2019.
- [27] A. Esposito, G. Viale, and G. Curigliano, 'Safety, Tolerability, and Management of Toxic Effects of Phosphatidylinositol 3-Kinase Inhibitor Treatment in Patients with Cancer: A Review', *JAMA Oncol.*, vol. 5, no. 9, pp. 1347–1354, 2019.
- [28] S. Hariri, B. Rasti, M. Mirpour, G. Vaghar-Lahijani, F. Attar, and F. Shiri, 'Structural insights into the origin of phosphoinositide 3-kinase inhibition', *Struct. Chem.*, vol. 31, no. 4, pp. 1505–1522, 2020.
- [29] F. Xu, L. Na, Y. Li, and L. Chen, 'Roles of the PI3K/AKT/mTOR signalling pathways in neurodegenerative diseases and tumours', *Cell Biosci.*, vol. 10, no. 1, pp. 1–12, 2020.
- [30] D. A. Fruman, H. Chiu, B. D. Hopkins, S. Bagrodia, L. C. Cantley, and R. T. Abraham, 'The PI3K Pathway in Human Disease', *Cell*, vol. 170, no. 4, pp. 605–635, 2017.
- [31] L. C. Cantley, 'The phosphoinositide 3-kinase pathway', *Science*, vol. 296, no. 5573, pp. 1655–1657, 2002.
- [32] F. Janku, T. A. Yap, and F. Meric-Bernstam, 'Targeting the PI3K pathway in cancer: Are we making headway?', *Nat. Rev. Clin. Oncol.*, vol. 15, no. 5, pp. 273–291, 2018.
- [33] A. Eisenreich and U. Rauch, 'PI3K Inhibitors in Cardiovascular Disease', *Cardiovasc. Ther.*, vol. 29, no. 1, pp. 29–36, 2011.
- [34] M. K. Rathinaswamy and J. E. Burke, 'Class I phosphoinositide 3-kinase (PI3K) regulatory subunits and their roles in signaling and disease', *Adv. Biol. Regul.*, vol. 75, no. September 2019, p. 100657, 2020.
- [35] T. N. Durrant and I. Hers, 'PI3K inhibitors in thrombosis and cardiovascular disease', *Clin. Transl. Med.*, vol. 9, no. 1, 2020.
- [36] B. Yu, J. Zhang, Y. Zeng, · Li, L. Xiangdong, and W. Editors, *Single-cell Sequencing and Methylation Methods and Clinical Applications*. 2020.
- [37] T. Crabbe, M. J. Welham, and S. G. Ward, 'The PI3K inhibitor arsenal: choose your weapon!', *Trends Biochem. Sci.*, vol. 32, no. 10, pp. 450–456, 2007.
- [38] C. Cintas and J. Guillermet-Guibert, 'Heterogeneity of phosphatidylinositol-3-kinase (PI3K)/AKT/mammalian target of rapamycin activation in cancer: Is PI3k isoform specificity important?', *Front. Oncol.*, vol. 7, no. JAN, pp. 1–4, 2018.
- [39] R. R. Madsen and B. Vanhaesebroeck, 'Cracking the context-specific PI3K signaling code', *Sci. Signal.*, vol. 13, no. 613, pp. 1–14, 2020.
- [40] A. A. Helwa, N. M. El-Dydamony, R. A. Radwan, S. M. Abdelraouf, and R. M. Abdelnaby, 'Novel antiproliferative agents bearing morpholinopyrimidine scaffold as PI3K inhibitors and apoptosis inducers; design, synthesis and molecular docking', *Bioorg. Chem.*, vol. 102, no. May, p. 104051, 2020.
- [41] E. C. Lien, C. C. Dibble, and A. Toker, 'PI3K signaling in cancer: beyond AKT', *Curr. Opin. Cell Biol.*, vol. 45, no. March, pp. 62–71, 2017.
- [42] R. Liu *et al.*, 'PI3K/AKT pathway as a key link modulates the multidrug resistance of cancers', *Cell Death Dis.*, vol. 11, no. 9, pp. 2–12, 2020.
- [43] W. Zhao, Y. Qiu, and D. Kong, 'Class I phosphatidylinositol 3-kinase inhibitors for cancer therapy', *Acta Pharm. Sin. B*, vol. 7, no. 1, pp. 27–37, 2017.

- [44] M. C. De Santis, F. Gulluni, C. C. Campa, M. Martini, and E. Hirsch, 'Targeting PI3K signaling in cancer: Challenges and advances', *Biochim. Biophys. Acta - Rev. Cancer*, vol. 1871, no. 2, pp. 361–366, 2019.
- [45] R. Dienstmann, J. Rodon, V. Serra, and J. Tabernero, 'Picking the point of inhibition: A comparative review of PI3K/AKT/mTOR pathway inhibitors', *Mol. Cancer Ther.*, vol. 13, no. 5, pp. 1021–1031, 2014.
- [46] K. E. Anderson and S. P. Jackson, 'Class I phosphoinositide 3-kinases', *Int. J. Biochem. Cell Biol.*, vol. 35, no. 7, pp. 1028–1033, 2003.
- [47] R. Baer, C. Cintas, N. Therville, and J. Guillermet-Guibert, 'Implication of PI3K/Akt pathway in pancreatic cancer: When PI3K isoforms matter?', *Adv. Biol. Regul.*, vol. 59, pp. 19–35, 2015.
- [48] D. Papadatos-Pastos, R. Rabbie, P. Ross, and D. Sarker, 'The role of the PI3K pathway in colorectal cancer', *Crit. Rev. Oncol. Hematol.*, vol. 94, no. 1, pp. 18–30, 2015.
- [49] X. Wang, J. Ding, and L. H. Meng, 'PI3K isoform-selective inhibitors: Next-generation targeted cancer therapies', *Acta Pharmacol. Sin.*, vol. 36, no. 10, pp. 1170–1176, 2015.
- [50] M. Zhang, H. Jang, R. Nussinov, and R. Nussinov, 'PI3K inhibitors: Review and new strategies', *Chem. Sci.*, vol. 11, no. 23, pp. 5855–5865, 2020.
- [51] S. Xie *et al.*, 'Divergent Roles of PI3K Isoforms in PTEN-Deficient Glioblastomas', *Cell Rep.*, vol. 32, no. 13, p. 108196, 2020.
- [52] F. Adefemi, D. A. Fruman, and A. J. Marshall, 'A Case for Phosphoinositide 3-Kinase-Targeted Therapy for Infectious Disease', *J. Immunol.*, vol. 205, no. 12, pp. 3237–3245, 2020.
- [53] R. Mishra, H. Patel, S. Alanazi, M. K. Kilroy, and J. T. Garrett, 'PI3K inhibitors in cancer: Clinical implications and adverse effects', *Int. J. Mol. Sci.*, vol. 22, no. 7, 2021.
- [54] F. Janku, 'Phosphoinositide 3-kinase (PI3K) pathway inhibitors in solid tumors: From laboratory to patients', *Cancer Treat. Rev.*, vol. 59, pp. 93–101, 2017.
- [55] S. L. Drew *et al.*, 'Discovery of Potent and Selective PI3K γ Inhibitors', *J. Med. Chem.*, vol. 63, no. 19, pp. 11235–11257, 2020.
- [56] G. A. Hobbs *et al.*, 'Atypical KRASG12R mutant is impaired in PI3K signaling and macropinocytosis in pancreatic cancer', *Cancer Discov.*, vol. 10, no. 1, pp. 104–123, 2020.
- [57] J. Zhu *et al.*, 'Targeting phosphatidylinositol 3-kinase gamma (PI3K γ): Discovery and development of its selective inhibitors', *Med. Res. Rev.*, vol. 41, no. 3, pp. 1599–1621, 2021.
- [58] J. Chang *et al.*, 'Targeting PIK3CG in combination with paclitaxel as a potential therapeutic regimen in claudin-low breast cancer', *Cancer Manag. Res.*, vol. 12, pp. 2641–2651, 2020.
- [59] C. N. Cavasotto and M. G. Aucar, 'High-Throughput Docking Using Quantum Mechanical Scoring', *Front. Chem.*, vol. 8, no. April, pp. 1–10, 2020.
- [60] C. N. Cavasotto, N. S. Adler, and M. G. Aucar, 'Quantum chemical approaches in structure-based virtual screening and lead optimization', *Front. Chem.*, vol. 6, no. MAY, pp. 1–7, 2018.
- [61] A. A. Adeniyi and M. E. S. Soliman, 'Implementing QM in docking calculations: is it a waste of computational time?', *Drug Discov. Today*, vol. 22, no. 8, pp. 1216–1223, 2017.
- [62] P. A. Ravindranath, S. Forli, D. S. Goodsell, A. J. Olson, and M. F. Sanner, 'AutoDockFR: Advances in Protein-Ligand Docking with Explicitly Specified Binding Site Flexibility', *PLoS Comput. Biol.*, vol. 11, no. 12, pp. 1–28, 2015.
- [63] A. Allouche, 'Software News and Updates Gabedit – A Graphical User Interface for Computational Chemistry Softwares', *J. Comput. Chem.*, vol. 32, pp. 174–182, 2012.
- [64] A. E. Cho, J. Y. Chung, M. Kim, and K. Park, 'Quantum mechanical scoring for protein docking', *J. Chem. Phys.*,

Chapter 6 – References

- vol. 131, no. 13, 2009.
- [65] E. Yuriev, M. Agostino, and P. A. Ramsland, 'Challenges and advances in computational docking: 2009 in review', *J. Mol. Recognit.*, vol. 24, no. 2, pp. 149–164, 2011.
- [66] N. D. Yilmazer and M. Korth, 'Comparison of molecular mechanics, semi-empirical quantum mechanical, and density functional theory methods for scoring protein-ligand interactions', *J. Phys. Chem. B*, vol. 117, no. 27, pp. 8075–8084, 2013.
- [67] A. E. Cho, V. Guallar, B. J. Berne, and R. Friesner, 'Importance of accurate charges in molecular docking: Quantum Mechanical/Molecular Mechanical (QM/MM) approach', *J. Comput. Chem.*, vol. 26, no. 9, pp. 915–931, 2005.
- [68] N. S. Pagadala, K. Syed, and J. Tuszynski, 'Software for molecular docking: a review', *Biophys. Rev.*, vol. 9, no. 2, pp. 91–102, 2017.
- [69] Y. Chen, L. Zhang, H. Wang, and W. Weinan, 'Ground State Energy Functional with Hartree-Fock Efficiency and Chemical Accuracy', *J. Phys. Chem. A*, vol. 124, no. 35, pp. 7155–7165, 2020.
- [70] W. Thiel, 'Semiempirical quantum-chemical methods', *Wiley Interdiscip. Rev. Comput. Mol. Sci.*, vol. 4, no. 2, pp. 145–157, 2014.
- [71] A. M. Venkatesan *et al.*, 'Novel imidazolopyrimidines as dual PI3-Kinase/mTOR inhibitors', *Bioorganic Med. Chem. Lett.*, vol. 20, no. 2, pp. 653–656, 2010.
- [72] 'Categorical Principal Components Analysis (CATPCA)'. [Online]. Available: <https://www.ibm.com/docs/en/spss-statistics/24.0.0?topic=option-categorical-principal-components-analysis-catpca>.
- [73] M. F. Ward, *Heterocyclic chemistry*, vol. 41, no. 95. 1999.
- [74] R. G. Alves, M.J., Carvalho, M.A., Proença, M.F.J., Booth, B.L. and Pritchard, 'Synthesis of 6-cyanopurines and the isolation and X-ray structure of novel 2H-pyrroles.', *J. Heterocycl. Chem.*, vol. 34, pp. 739–743, 1997.
- [75] M. F. J. R. P. Alves, M. J., Booth, B. L., Freitas, A. P., & Proença, '(Z)-N3-(2-amino-1,2-dicyanovinyl)formamidrazone: A precursor in the synthesis of 1,5-diaminoimidazoles and 6-carbamoyl-1,2-dihydropurines', *J. Chem. Soc. Perkin Trans. 1*, vol. 1, no. 7, pp. 913–917, 1992.
- [76] C. Correia, M. A. Carvalho, and M. F. Proença, 'Synthesis and in vitro activity of 6-amino-2,9-diarylpurines for Mycobacterium tuberculosis', *Tetrahedron*, vol. 65, no. 34, pp. 6903–6911, 2009.
- [77] Merck, 'IR Spectrum Table & Chart'. [Online]. Available: <https://www.sigmaaldrich.com/PT/en/technical-documents/technical-article/analytical-chemistry/photometry-and-reflectometry/ir-spectrum-table>. [Accessed: 29-Dec-2021].
- [78] MichelLegraverend, 'Recent advances in the synthesis of purine derivatives and their precursors', *Tetrahedron*, vol. 64, no. 37, pp. 8585–8603, 2008.
- [79] M. A. C. Ashly Rocha, M. F. Proença, 'Synthesis of 2-(Aminophenyl)adenine Derivatives: a Simple Protocol using the Classical Iron Powder/Acetic Acid Reduction Methodology', *Can. J. Chem.*, vol. 98, no. 3, pp. 145–150, 2020.
- [80] M. I. Lavrov, V. L. Lapteva, V. V. Grigor'Ev, V. A. Palyulin, S. O. Bachurin, and N. S. Zefirov, 'Search for new drugs: Synthesis and ampa-receptor modulating activity of benzodioxanecarboxylic and piperonylic acid derivatives', *Pharm. Chem. J.*, vol. 46, no. 2, pp. 92–95, 2012.
- [81] D. R. Joshi and N. Adhikari, 'An Overview on Common Organic Solvents and Their Toxicity', *J. Pharm. Res. Int.*, vol. 28, no. 3, pp. 1–18, 2019.
- [82] M. P. Huestis *et al.*, 'Targeting KRAS Mutant Cancers via Combination Treatment: Discovery of a 5-Fluoro-4-(3 H)-quinazolinone Aryl Urea pan-RAF Kinase Inhibitor', *J. Med. Chem.*, vol. 64, no. 7, pp. 3940–3955, 2021.

- [83] Q. Zhang, K. Zhao, L. Zhang, X. Jiao, Y. Zhang, and C. Tang, 'Synthesis and biological evaluation of diaryl urea derivatives as FLT3 inhibitors', *Bioorganic Med. Chem. Lett.*, vol. 30, no. 23, p. 127525, 2020.
- [84] F. Laduron, V. Tamborowski, L. Moens, A. Horváth, D. De Smaele, and S. Leurs, 'Efficient and scalable method for the selective alkylation and acylation of secondary amines in the presence of primary amines', *Org. Process Res. Dev.*, vol. 9, no. 1, pp. 102–104, 2005.
- [85] M. Pittelkow, R. Lewinsky, and J. B. Christensen, 'Selective synthesis of carbamate protected polyamines using alkyl phenyl carbonates', *Synthesis (Stuttg.)*, vol. 2, no. 15, pp. 2195–2202, 2002.
- [86] K. J. Padiya *et al.*, 'Unprecedented "in water" imidazole carbonylation: Paradigm shift for preparation of urea and carbamate', *Org. Lett.*, vol. 14, no. 11, pp. 2814–2817, 2012.
- [87] Y. Qin, S. Qiang, S. Ji, Z. Liu, C. Hu, and S. Ma, 'Synthesis and antibacterial activity of novel 3-O-arylalkylcarbonyl-3-O-descladinosyl-9-O-(2-chlorobenzyl)oxime clarithromycin derivatives', *Bioorganic Med. Chem. Lett.*, vol. 28, no. 20, pp. 3324–3328, 2018.
- [88] K. Takahashi *et al.*, 'Practical synthesis of precursor of [*N*-methyl-¹¹C]vorozole, an efficient PET tracer targeting aromatase in the brain', *Bioorganic Med. Chem.*, vol. 19, no. 4, pp. 1464–1470, 2011.
- [89] W. Lin, X. Zhang, Z. He, Y. Jin, L. Gong, and A. Mi, 'Reduction of azides to amines or amides with zinc and ammonium chloride as reducing agent', *Synth. Commun.*, vol. 32, no. 21, pp. 3279–3284, 2002.
- [90] K. Suthagar and A. J. Fairbanks, 'A new way to do an old reaction: highly efficient reduction of organic azides by sodium iodide in the presence of acidic ion exchange resin', *Chem. Commun.*, vol. 53, no. 4, pp. 713–715, 2017.
- [91] Y. G. Gololobov and L. F. Kasukhin, 'Recent advances in the staudinger reaction', *Tetrahedron*, vol. 48, no. 8, pp. 1353–1406, 1992.
- [92] D. C. Batesky, M. J. Goldfogel, and D. J. Weix, 'Removal of triphenylphosphine oxide by precipitation with zinc chloride in polar solvents', *J. Org. Chem.*, vol. 82, no. 19, pp. 9931–9936, 2017.
- [93] M.A.C.- Unpublished results.
- [94] M. S. Gibson and R. W. Bradshaw, 'The Gabriel Synthesis of Primary Amines', *Angew. Chemie Int. Ed. English*, vol. 7, no. 12, pp. 919–930, 1968.
- [95] 'RCSB PDB'. [Online]. Available: <https://www.rcsb.org/>.
- [96] X. Fradera *et al.*, 'Design of selective PI3K δ inhibitors using an iterative scaffold-hopping workflow', *Bioorganic Med. Chem. Lett.*, vol. 29, no. 18, pp. 2575–2580, 2019.
- [97] V. Certal *et al.*, 'Discovery and optimization of pyrimidone indoline amide PI3K β inhibitors for the treatment of phosphatase and tensin homologue (PTEN)-deficient cancers', *J. Med. Chem.*, vol. 57, no. 3, pp. 903–920, 2014.
- [98] B. S. Safina *et al.*, 'Design of Selective Benzoxazepin PI3K δ Inhibitors Through Control of Dihedral Angles', *ACS Med. Chem. Lett.*, vol. 8, no. 9, pp. 936–940, 2017.
- [99] Z. A. Henley *et al.*, 'Optimization of Orally Bioavailable PI3K δ inhibitors and Identification of Vps34 as a Key Selectivity Target', *J. Med. Chem.*, vol. 63, no. 2, pp. 638–655, 2020.
- [100] G. Studer, C. Rempfer, A. M. Waterhouse, R. Gumienny, J. Haas, and T. Schwede, 'QMEANDisCo—distance constraints applied on model quality estimation', *Bioinformatics*, vol. 36, no. 6, pp. 1765–1771, 2020.
- [101] S. Bienert *et al.*, 'The SWISS-MODEL Repository-new features and functionality', *Nucleic Acids Res.*, vol. 45, no. D1, pp. D313–D319, 2017.
- [102] M. Bertoni, F. Kiefer, M. Biasini, L. Bordoli, and T. Schwede, 'Modeling protein quaternary structure of homo- and hetero-oligomers beyond binary interactions by homology', *Sci. Rep.*, vol. 7, no. 1, pp. 1–15, 2017.

Chapter 6 – References

- [103] N. Guex, M. C. Peitsch, and T. Schwede, 'Automated comparative protein structure modeling with SWISS-MODEL and Swiss-PdbViewer: A historical perspective', *Electrophoresis*, vol. 30, no. SUPPL. 1, pp. 162–173, 2009.
- [104] A. Waterhouse *et al.*, 'SWISS-MODEL: Homology modelling of protein structures and complexes', *Nucleic Acids Res.*, vol. 46, no. W1, pp. W296–W303, 2018.
- [105] W. Schrödinger, L., & DeLano, 'PyMOL', 2020. [Online]. Available: <http://www.pymol.org/pymol>.
- [106] A. J. Morris, G. M., Huey, R., Lindstrom, W., Sanner, M. F., Belew, R. K., Goodsell, D. S. and Olson, 'Autodock4 and AutoDockTools4: automated docking with selective receptor flexibility.', *J. Comput. Chem.*, vol. 30, no. 16, pp. 2785–91, 2009.
- [107] U. Ryde and P. Söderhjelm, 'Ligand-Binding Affinity Estimates Supported by Quantum-Mechanical Methods', *Chem. Rev.*, vol. 116, no. 9, pp. 5520–5566, 2016.
- [108] L. A. Curtiss, P. C. Redfern, and K. Raghavachari, 'Gaussian-4 theory', *J. Chem. Phys.*, vol. 126, no. 8, 2007.
- [109] S. Yockel, B. Mintz, and A. K. Wilson, 'Accurate energetics of small molecules containing third-row atoms Ga-Kr: A comparison of advanced ab initio and density functional theory', *J. Chem. Phys.*, vol. 121, no. 1, pp. 60–77, 2004.
- [110] D. J. F. M. J. Frisch, G. W. Trucks, H. B. Schlegel, G. E. Scuseria, M. A. Robb, J. R. Cheeseman, G. Scalmani, V. Barone, B. Mennucci, G. A. Petersson, H. Nakatsuji, M. Caricato, X. Li, H. P. Hratchian, A. F. Izmaylov, J. Bloino, G. Zheng, J. L. Sonnenberg, M. Had, 'Gaussian 09 (Gaussian, Inc., Wallingford CT)'. 2009.
- [111] N. M. O'Boyle, M. Banck, C. A. James, C. Morley, T. Vandermeersch, and G. R. Hutchison, 'Open Babel', *J. Cheminform.*, vol. 3, no. 33, pp. 1–14, 2011.
- [112] A. J. Trott, O., & Olson, 'AutoDock Vina: Improving the Speed and Accuracy of Docking with a New Scoring Function, Efficient Optimization, and Multithreading', *J. Comput. Chem.*, vol. 31, no. 2, pp. 455–461, 2010.
- [113] IBM Corp., 'IBM SPSS Statistics for Windows'. Armonk, NY: IBM Corp.
- [114] I. T. Jolliffe and J. Cadima, 'Principal component analysis: A review and recent developments', *Philos. Trans. R. Soc. A Math. Phys. Eng. Sci.*, vol. 374, no. 2065, 2016.
- [115] Y. J. Liu, T. Tran, G. Postma, L. M. C. Buydens, and J. Jansen, 'Estimating the number of components and detecting outliers using Angle Distribution of Loading Subspaces (ADLS) in PCA analysis', *Anal. Chim. Acta*, vol. 1020, pp. 17–29, 2018.

Appendix

Table 1 PDB code selection of the targets chosen for the Virtual Screening based on resolution, publication date and publisher, expression organism and structure size of the original ligand.

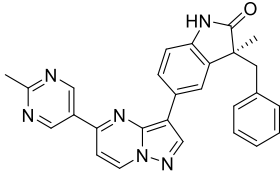
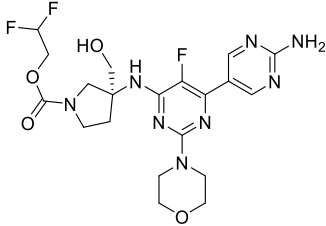
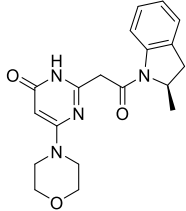
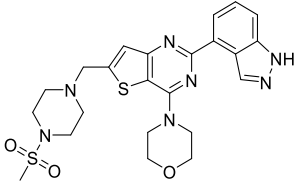
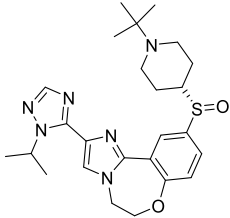
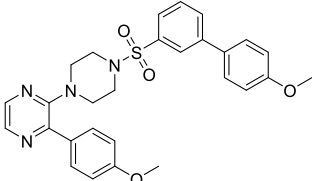
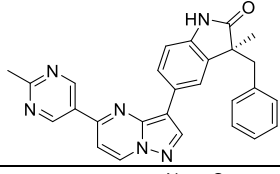
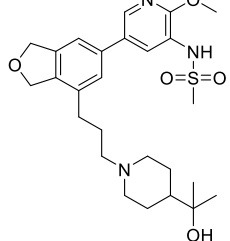
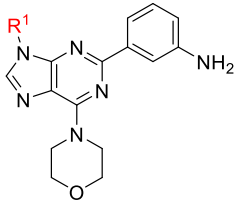
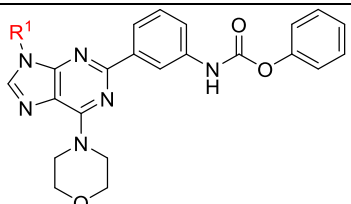
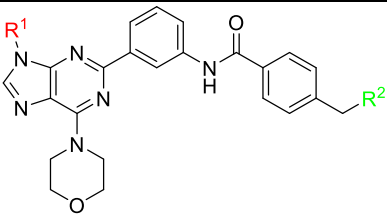
Protein	PDB code	Resolution (Å)	Date	Publisher	Organism(s)	Ligand Structure
PI3K α	6PYS	2.19	2019	Bioorg Med Chem Lett	Homo sapiens	
	7K6M	2.41	2021	J Med Chem	Homo sapiens	
PI3K β	4BFR	2.80	2014	J Med Chem	Mus musculus	
	2Y3A	3.30	2011	Mol Cell	Mus musculus	
PI3K γ	6AUD	2.015	2017	ACS Med Chem Lett	Homo sapiens	
	4ANV	2.13	2012	J Med Chem	Homo sapiens	
PI3K δ	6PYR	2.21	2019	Bioorg Med Chem Lett	Homo sapiens	
	6TNR	1.90	2020	J Med Chem	Mus musculus	

Table 2 Description of the ligands under study (**1-23**) and presentation of their physicochemical properties and affinity values for the 4 targets.


R ¹	Physicochemical and structural properties						$\Delta G_{\text{binding}}$ (kcal/mol)			
	Charge	HBA	HBD	Log P	M _w	R _f	PI3K α	PI3K β	PI3K γ	PI3K δ
1	0	7	3	1.80	296.33	95.51	-8.6	-8.4	-8.3	-8.0
2	0	7	2	3.69	372.43	130.51	-10.0	-8.3	-9.1	-8.8
3	0	7	2	4.19	386.46	135.55	-10.0	-8.5	-9.3	-8.7
4	0	7	2	4.19	386.46	135.55	-10.3	-8.7	-9.6	-8.9
5	0	7	2	4.69	400.49	140.59	-10.4	-8.7	-9.8	-8.9
6	0	7	2	3.84	390.42	130.72	-9.8	-8.4	-9.2	-9.2
7	0	7	2	3.84	390.42	130.72	-10.2	-8.5	-9.3	-9.2
8	0	9	3	3.02	429.48	145.37	-10.1	-8.4	-9.8	-9.4
9	0	9	3	3.02	429.48	145.37	-10.0	-8.8	-9.7	-9.0
10	0	9	3	4.75	491.56	166.04	-10.8	-9.4	-10.4	-8.8
11	0	9	3	4.75	491.56	166.04	-9.8	-9.1	-11.0	-10.1
12	0	10	3	3.52	492.54	163.88	-10.6	-8.9	-10.0	-9.0
13	0	10	3	3.52	492.54	163.88	-9.6	-9.1	-10.2	-9.7
14	0	10	3	3.52	492.54	163.88	-10.5	-8.7	-9.6	-8.5
15	0	10	3	3.52	492.54	163.88	-9.7	-9.1	-10.3	-9.7
16	0	13	3	4.44	535.56	171.81	-10.4	-9.9	-10.7	-9.5
17	0	13	3	4.44	535.56	171.81	-10.3	-9.6	-11.1	-10.8
18	0	15	3	4.16	581.63	185.43	-9.6	-8.3	-8.7	-9.1
19	0	15	3	4.16	581.63	185.43	-10.4	-8.4	-9.6	-8.5
20	-1	12	2	5.13	516.60	167.10	-10.0	-8.8	-9.1	-9.9
21	-1	12	2	5.13	516.60	167.10	-10.1	-9.0	-10.3	-9.1
22	+1	9	3	4.29	499.62	167.13	-9.7	-8.5	-9.2	-8.7
23	+1	9	3	4.29	499.62	167.13	-9.9	-8.4	-9.9	-9.5

Table 3 Description of the **Class 0** ligands under study and presentation of their physicochemical properties and affinity values for the 4 targets.


R ¹	Physicochemical and structural properties						$\Delta G_{\text{binding}}$ (kcal/mol)			
	Charge	HBA	HBD	Log P	M _w	R _f	PI3K α	PI3K β	PI3K γ	PI3K δ
1	0	9	2	4.17	416.44	127.08	-9.4	-9.5	-9.8	-8.8
2	0	9	1	6.06	492.54	162.07	-10.8	-10.3	-10.8	-9.4
3	0	9	1	6.56	506.57	167.11	-11.8	-10.4	-11.1	-9.6
4	0	9	1	6.56	506.57	167.11	-11.3	-10.5	-11.4	-9.6
5	0	9	1	7.06	520.59	172.15	-12.0	-10.6	-11.6	-9.8
6	0	9	1	6.21	510.53	162.29	-11.7	-10.3	-10.6	-10.1
7	0	9	1	6.21	510.53	162.29	-10.9	-10.4	-11.0	-9.7
8	0	11	2	5.39	549.59	176.93	-12.1	-10.2	-10.6	-9.6
9	0	11	2	5.39	549.59	176.93	-10.5	-10.7	-11.4	-9.8
10	0	11	2	7.12	611.66	197.60	-12.1	-10.5	-11.5	-10.3
11	0	11	2	7.12	611.66	197.60	-10.6	-10.9	-11.9	-10.4
12	0	12	2	5.89	612.65	195.45	-12.0	-10.6	-11.2	-10.4
13	0	12	2	5.89	612.65	195.45	-11.9	-10.8	-11.1	-10.3
14	0	12	2	5.89	612.65	195.45	-12.0	-10.5	-11.6	-9.6
15	0	12	2	5.89	612.65	195.45	-11.9	-10.9	-11.6	-10.2
16	0	15	2	6.81	655.67	203.37	-12.5	-11.3	-11.7	-9.2
17	0	15	2	6.81	655.67	203.37	-12.5	-11.3	-11.7	-10.9
18	0	17	2	6.53	701.74	216.99	-11.3	-9.6	-11.3	-9.7
19	0	17	2	6.53	701.74	216.99	-10.7	-9.9	-11.1	-9.3
20	-1	14	1	7.50	636.71	198.67	-12.2	-10.7	-10.8	-10.0
21	-1	14	1	7.50	636.71	198.67	-11.7	-10.2	-11.4	-10.2
22	+1	11	2	6.66	619.73	198.70	-11.2	-10.1	-10.7	-10.0
23	+1	11	2	6.66	619.73	198.70	-10.4	-10.0	-10.9	-9.3

Table 4 Description of the **Class 1** ligands under study and presentation of their physicochemical properties and affinity values for the 4 targets.


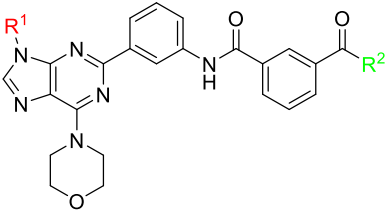
R ¹	R ²	Physicochemical and structural properties						$\Delta G_{\text{binding}}$ (kcal/mol)			
		Charge	HBA	HBD	Log P	M _w	R _f	PI3K α	PI3K β	PI3K γ	PI3K δ
1	a	+1	8	5	2.33	429.48	134.82	-9.2	-9.2	-10.9	-9.5
	b	+1	9	3	3.40	512.62	160.94	-9.7	-9.8	-11.4	-9.6
	c	0	11	2	3.28	499.58	153.96	-9.8	-9.4	-11.4	-9.5
	d	0	9	3	4.93	505.58	161.15	-10.2	-10.7	-11.9	-9.8
	e	0	10	3	4.38	533.59	164.93	-10.4	-10.7	-10.8	-10.3
2	a	+1	8	4	4.66	505.58	169.81	-10.3	-10.1	-10.0	-9.5
	b	+1	9	2	5.29	588.72	195.93	-11.0	-8.4	-10.5	-9.3
	c	0	11	1	5.17	575.67	188.96	-11.1	-8.4	-10.3	-10.2
	d	0	9	2	6.81	581.68	196.15	-10.8	-10.0	-11.2	-10.1
	e	0	10	2	6.27	609.69	199.93	-11.4	-8.1	-10.5	-9.9
3	a	+1	8	4	5.16	519.61	174.85	-10.3	-10.3	-11.5	-9.7
	b	+1	9	2	5.79	602.74	200.97	-11.1	-9.8	-10.5	-9.7
	c	0	11	1	5.67	589.70	194.00	-11.1	-9.3	-10.5	-10.1
	d	0	9	2	7.31	595.71	201.19	-11.4	-9.8	-11.1	-10.0
	e	0	10	2	6.77	623.72	204.97	-11.1	-9.4	-10.6	-9.8
4	a	+1	8	4	5.16	519.61	174.85	-10.9	-10.4	-11.8	-9.8
	b	+1	9	2	5.79	602.74	200.97	-11.0	-10.0	-10.6	-9.9
	c	0	11	1	5.67	589.70	194.00	-11.1	-10.1	-10.6	-9.5
	d	0	9	2	7.31	595.71	201.19	-11.7	-10.4	-10.1	-9.0
	e	0	10	2	6.77	623.72	204.97	-11.7	-9.7	-10.7	-8.4
5	a	+1	8	4	5.66	533.64	179.90	-10.6	-10.5	-12.0	-10.0
	b	+1	9	2	6.29	616.77	206.02	-10.8	-9.9	-10.9	-9.8
	c	0	11	1	6.17	603.73	199.04	-10.9	-10.0	-10.7	-9.9
	d	0	9	2	7.81	609.73	206.23	-11.8	-10.7	-10.8	-10.1
	e	0	10	2	7.27	637.74	210.01	-11.1	-9.8	-10.8	-10.2
6	a	+1	8	4	4.81	523.57	170.03	-10.3	-10.3	-11.3	-10.1
	b	+1	9	2	5.44	606.71	196.15	-10.6	-9.9	-10.7	-9.5
	c	0	11	1	5.32	593.66	189.17	-11.0	-8.9	-10.5	-10.5
	d	0	9	2	6.96	599.67	196.36	-11.0	-10.3	-10.3	-9.7
	e	0	10	2	6.42	627.68	200.14	-11.5	-9.5	-10.7	-10.4
7	a	+1	8	4	4.81	523.57	170.03	-10.5	-10.3	-11.5	-9.8
	b	+1	9	2	5.44	606.71	196.15	-11.1	-9.1	-10.7	-9.3
	c	0	11	1	5.32	593.66	189.17	-11.3	-9.3	-10.6	-9.3
	d	0	9	2	6.96	599.67	196.36	-11.8	-10.3	-10.3	-10.3
	e	0	10	2	6.42	627.68	200.14	-11.7	-9.6	-10.7	-10.1
8	a	+1	10	5	3.99	562.63	184.68	-10.3	-10.1	-10.0	-9.6
	b	+1	11	3	4.62	645.77	210.80	-10.9	-9.9	-10.8	-10.2
	c	0	13	2	4.50	632.73	203.82	-10.8	-9.7	-10.6	-10.0
	d	0	11	3	6.14	638.73	211.01	-11.3	-10.6	-11.4	-9.8
	e	0	12	3	5.60	666.74	214.79	-11.2	-9.4	-10.7	-10.1
9	a	+1	10	5	3.99	562.63	184.68	-11.3	-10.6	-10.6	-10.4
	b	+1	11	3	4.62	645.77	210.80	-10.6	-9.5	-11.0	-9.4
	c	0	13	2	4.50	632.73	203.82	-10.7	-9.5	-10.4	-9.7
	d	0	11	3	6.14	638.73	211.01	-11.1	-10.4	-10.6	-9.7
	e	0	12	3	5.60	666.74	214.79	-11.2	-9.9	-10.9	-11.1

Table 4 Description of the **Class 1** ligands under study and presentation of their physicochemical properties and affinity values for the 4 targets. (continuation)

R ¹	R ²	Physicochemical and structural properties						$\Delta G_{\text{binding}}$ (kcal/mol)			
		Charge	HBA	HBD	Log P	M _w	R _f	PI3K α	PI3K β	PI3K γ	PI3K δ
10	a	+1	10	5	5.72	624.71	205.35	-11.5	-10.1	-11.5	-9.9
	b	+1	11	3	6.35	707.84	231.47	-11.0	-9.5	-10.9	-10.0
	c	0	13	2	6.23	694.80	224.49	-10.8	-9.9	-10.5	-9.8
	d	0	11	3	7.87	700.80	231.68	-10.4	-10.4	-11.0	-10.2
	e	0	12	3	7.33	728.81	235.46	-11.0	-10.8	-11.1	-10.4
11	a	+1	10	5	5.72	624.71	205.35	-11.3	-10.0	-11.3	-9.8
	b	+1	11	3	6.35	707.84	231.47	-11.8	-10.4	-10.7	-11.0
	c	0	13	2	6.23	694.80	224.49	-11.8	-10.6	-10.5	-10.7
	d	0	11	3	7.87	700.80	231.68	-11.8	-10.5	-10.8	-9.9
	e	0	12	3	7.33	728.81	235.46	-12.4	-11.1	-11.1	-10.8
12	a	+1	11	5	4.49	625.69	203.19	-11.3	-10.1	-10.1	-9.8
	b	+1	12	3	5.12	708.83	229.31	-10.7	-10.2	-10.8	-9.6
	c	0	14	2	5.00	695.78	222.33	-10.5	-10.1	-10.4	-10.0
	d	0	12	3	6.64	701.79	229.52	-10.2	-10.9	-10.7	-10.0
	e	0	13	3	6.10	729.80	233.30	-10.5	-10.9	-11.2	-10.5
13	a	+1	11	5	4.49	625.69	203.19	-11.1	-10.2	-11.8	-10.6
	b	+1	12	3	5.12	708.83	229.31	-11.4	-9.8	-10.5	-9.8
	c	0	14	2	5.00	695.78	222.33	-11.5	-10.7	-10.6	-10.4
	d	0	12	3	6.64	701.79	229.52	-11.6	-10.7	-10.8	-10.3
	e	0	13	3	6.10	729.80	233.30	-12.3	-10.6	-11.1	-10.5
14	a	+1	11	5	4.49	625.69	203.19	-11.3	-10.1	-10.1	-9.8
	b	+1	12	3	5.12	708.83	229.31	-10.6	-8.4	-10.4	-10.4
	c	0	14	2	5.00	695.78	222.33	-10.4	-10.0	-10.4	-9.8
	d	0	12	3	6.64	701.79	229.52	-10.3	-9.8	-10.6	-9.7
	e	0	13	3	6.10	729.80	233.30	-10.8	-10.8	-10.9	-10.3
15	a	+1	11	5	4.49	625.69	203.19	-11.4	-9.4	-10.3	-10.6
	b	+1	12	3	5.12	708.83	229.31	-11.6	-10.6	-10.5	-10.7
	c	0	14	2	5.00	695.78	222.33	-11.5	-10.5	-10.6	-9.8
	d	0	12	3	6.64	701.79	229.52	-11.6	-11.2	-10.8	-9.6
	e	0	13	3	6.10	729.80	233.30	-12.2	-10.5	-11.2	-10.8
16	a	+1	14	5	5.41	668.71	211.11	-11.0	-10.5	-10.8	-11.0
	b	+1	15	3	6.04	751.85	237.23	-11.8	-10.5	-10.8	-10.1
	c	0	17	2	5.92	738.81	230.26	-11.6	-10.3	-10.4	-10.4
	d	0	15	3	7.56	744.81	237.45	-11.4	-11.1	-11.9	-10.2
	e	0	16	3	7.02	772.82	241.23	-11.7	-10.4	-11.1	-10.6
17	a	+1	14	5	5.41	668.71	211.11	-11.7	-10.7	-10.6	-11.3
	b	+1	15	3	6.04	751.85	237.23	-12.0	-10.4	-11.7	-10.4
	c	0	17	2	5.92	738.81	230.26	-11.8	-11.2	-10.9	-10.8
	d	0	15	3	7.56	744.81	237.45	-12.0	-10.8	-11.2	-12.0
	e	0	16	3	7.02	772.82	241.23	-12.7	-10.9	-11.9	-10.5
18	a	+1	16	5	5.14	714.78	224.74	-10.2	-9.5	-10.3	-9.7
	b	+1	17	3	5.76	797.92	250.86	-10.9	-8.2	-10.3	-9.1
	c	0	19	2	5.64	784.87	243.88	-10.9	-9.6	-10.1	-8.9
	d	0	17	3	7.29	790.89	251.07	-10.7	-10.4	-9.4	-9.0
	e	0	18	3	6.74	818.89	254.85	-11.1	-10.3	-10.8	-9.7
19	a	+1	16	5	5.14	714.78	224.74	-10.8	-9.8	-10.6	-10.1
	b	+1	17	3	5.76	797.92	250.86	-10.9	-9.1	-11.1	-8.9
	c	0	19	2	5.64	784.87	243.88	-10.8	-9.0	-11.0	-9.1
	d	0	17	3	7.29	790.89	251.07	-11.5	-9.6	-10.8	-8.8
	e	0	18	3	6.74	818.89	254.85	-11.5	-10.5	-11.3	-10.7

Table 4 Description of the **Class 1** ligands under study and presentation of their physicochemical properties and affinity values for the 4 targets. (continuation)

R ¹	R ²	Physicochemical and structural properties						$\Delta G_{\text{binding}}$ (kcal/mol)			
		Charge	HBA	HBD	Log P	M _w	R _f	PI3K α	PI3K β	PI3K γ	PI3K δ
20	a	0	13	4	3.93	649.75	206.41	-10.2	-10.6	-11.1	-10.1
	b	0	14	2	4.63	732.88	232.53	-9.8	-10.1	-10.8	-10.2
	c	-1	16	1	5.38	719.84	225.55	-10.3	-10.6	-9.7	-10.2
	d	-1	14	2	8.12	725.85	232.74	-11.8	-11.3	-11.5	-10.1
	e	-1	15	2	7.71	753.86	236.53	-11.4	-10.7	-11.3	-11.5
21	a	0	13	4	3.93	649.75	206.41	-10.9	-10.4	-11.2	-10.6
	b	0	14	2	4.63	732.88	232.53	-10.7	-9.5	-10.2	-9.7
	c	-1	16	1	5.38	719.84	225.55	-11.4	-9.1	-10.1	-11.0
	d	-1	14	2	8.12	725.85	232.74	-12.0	-8.5	-10.8	-11.1
	e	-1	15	2	7.71	753.86	236.53	-11.7	-9.0	-10.9	-12.0
22	a	+2	10	5	5.26	632.77	206.44	-10.1	-10.0	-11.2	-9.8
	b	+2	11	3	5.89	715.90	232.56	-10.3	-8.7	-10.6	-9.2
	c	+1	13	2	5.77	702.86	225.58	-10.0	-10.1	-10.5	-9.0
	d	+1	11	3	7.41	708.87	232.77	-10.2	-10.4	-10.5	-9.3
	e	+1	12	3	6.87	736.88	236.55	-10.7	-10.4	-9.8	-9.9
23	a	+2	10	5	5.26	632.77	206.44	-10.5	-9.8	-10.9	-10.1
	b	+2	11	3	5.89	715.90	232.56	-10.1	-9.5	-10.1	-9.8
	c	+1	13	2	5.77	702.86	225.58	-10.3	-9.4	-9.9	-10.0
	d	+1	11	3	7.41	708.87	232.77	-10.4	-9.3	-10.1	-9.5
	e	+1	12	3	6.87	736.88	236.55	-11.0	-10.0	-11.1	-9.0

Table 5 Description of the **Class 2** ligands under study and presentation of their physicochemical properties and affinity values for the 4 targets.


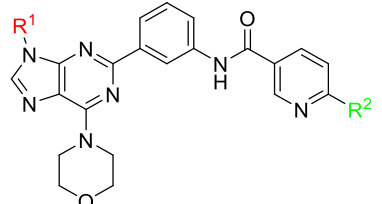
R ¹	R ²	Physicochemical and structural properties						$\Delta G_{\text{binding}}$ (kcal/mol)			
		Charge	HBA	HBD	Log P	M _w	R _f	PI3K α	PI3K β	PI3K γ	PI3K δ
1	a	0	10	4	2.42	443.47	135.43	-10.7	-10.5	-11.2	-10.1
	b	0	11	2	2.72	526.60	161.27	-11.8	-10.9	-9.9	-10.1
	c	0	12	2	2.60	513.21	154.29	-11.6	-10.8	-10.1	-9.3
	d	0	10	3	4.70	519.57	161.88	-9.7	-11.1	-10.8	-11.3
	e	0	12	3	4.16	547.58	165.66	-11.8	-11.1	-11.3	-11.0
2	a	0	10	3	4.31	519.57	170.42	-11.3	-10.4	-11.0	-10.3
	b	0	11	1	4.61	602.70	196.26	-10.5	-9.9	-11.5	-9.2
	c	0	12	1	4.49	589.66	189.29	-12.2	-9.7	-11.4	-10.6
	d	0	10	2	6.59	595.66	196.87	-11.3	-11.3	-11.3	-10.4
	e	0	12	2	6.05	623.67	200.65	-11.8	-9.2	-11.5	-10.0
3	a	0	10	3	4.81	533.59	175.46	-11.8	-10.6	-10.6	-10.6
	b	0	11	1	5.11	616.73	201.30	-11.2	-10.5	-11.4	-10.1
	c	0	12	1	4.99	603.68	194.33	-11.4	-10.3	-11.2	-10.5
	d	0	10	2	7.09	609.69	201.91	-11.9	-11.4	-11.9	-11.0
	e	0	12	2	6.55	637.70	205.70	-11.5	-10.6	-11.6	-10.3
4	a	0	10	3	4.81	533.59	175.46	-11.8	-10.7	-11.6	-10.4
	b	0	11	1	5.11	616.73	201.30	-11.0	-10.1	-11.7	-10.1
	c	0	12	1	4.99	603.68	194.33	-12.1	-9.9	-11.7	-10.9
	d	0	10	2	7.09	609.69	201.91	-11.3	-11.5	-11.4	-10.4
	e	0	12	2	6.55	637.70	205.70	-12.0	-10.3	-11.7	-10.3
5	a	0	10	3	5.31	547.62	180.50	-11.2	-10.8	-10.9	-10.6
	b	0	11	1	5.61	630.75	206.34	-11.6	-10.3	-11.7	-10.3
	c	0	12	1	5.49	617.71	199.37	-12.3	-10.1	-11.5	-10.7
	d	0	10	2	7.59	623.72	206.96	-11.1	-11.6	-11.4	-9.5
	e	0	12	2	7.05	651.73	210.74	-12.1	-10.2	-11.8	-9.9
6	a	0	10	3	4.46	537.56	170.63	-11.8	-10.5	-11.2	-10.7
	b	0	11	1	4.75	620.69	196.48	-11.1	-10.1	-11.5	-9.8
	c	0	12	1	4.63	607.65	189.50	-12.1	-9.5	-11.4	-10.9
	d	0	10	2	6.74	613.65	197.09	-11.5	-11.3	-11.3	-9.9
	e	0	12	2	6.20	641.66	200.87	-12.0	-9.1	-11.7	-10.0
7	a	0	10	3	4.46	537.56	170.63	-11.5	-10.6	-11.2	-10.6
	b	0	11	1	4.75	620.69	196.48	-10.7	-9.8	-11.6	-12.6
	c	0	12	1	4.63	607.65	189.50	-12.5	-9.6	-11.5	-10.6
	d	0	10	2	6.74	613.65	197.09	-11.4	-11.4	-11.4	-10.6
	e	0	12	2	6.20	641.66	200.87	-12.0	-10.2	-11.7	-10.8
8	a	0	12	4	3.64	576.62	185.28	-12.0	-10.3	-11.2	-10.5
	b	0	13	2	3.94	659.75	211.13	-10.6	-9.5	-11.4	-10.6
	c	0	14	2	3.82	646.71	204.15	-11.6	-10.5	-11.3	-10.5
	d	0	12	3	5.92	652.72	211.74	-11.5	-9.5	-10.9	-11.2
	e	0	14	3	5.38	680.73	215.52	-11.0	-10.3	-11.7	-10.0
9	a	0	12	4	3.64	576.62	185.28	-11.4	-11.0	-11.2	-10.4
	b	0	13	2	3.94	659.75	211.13	-11.6	-10.7	-11.8	-10.8
	c	0	14	2	3.82	646.71	204.15	-11.5	-11.3	-10.9	-11.8
	d	0	12	3	5.92	652.72	211.74	-11.0	-11.4	-11.7	-10.7
	e	0	14	3	5.38	680.73	215.52	-11.9	-11.4	-12.5	-10.0

Table 5 Description of the **Class 2** ligands under study and presentation of their physicochemical properties and affinity values for the 4 targets. (continuation)

R ¹	R ²	Physicochemical and structural properties						$\Delta G_{\text{binding}}$ (kcal/mol)			
		Charge	HBA	HBD	Log P	M _w	R _f	PI3K α	PI3K β	PI3K γ	PI3K δ
10	a	0	12	4	5.37	638.69	205.95	-12.0	-10.2	-11.4	-11.1
	b	0	13	2	5.67	721.82	231.80	-11.2	-10.4	-10.9	-10.9
	c	0	14	2	5.55	708.78	224.82	-11.1	-11.3	-10.9	-10.8
	d	0	12	3	7.65	714.79	232.41	-11.5	-11.2	-10.9	-11.2
	e	0	14	3	7.11	742.80	236.19	-11.5	-10.9	-12.1	-9.9
11	a	0	12	4	5.37	638.69	205.95	-11.3	-10.4	-11.0	-10.9
	b	0	13	2	5.67	721.82	231.80	-12.6	-10.6	-11.7	-10.0
	c	0	14	2	5.55	708.78	224.82	-12.3	-12.2	-11.6	-10.6
	d	0	12	3	7.65	714.79	232.41	-11.9	-11.2	-11.6	-11.3
	e	0	14	3	7.11	742.80	236.19	-12.8	-11.5	-11.8	-11.5
12	a	0	13	4	4.14	639.68	203.80	-11.9	-10.2	-10.5	-11.2
	b	0	14	2	4.43	722.81	229.64	-10.7	-10.6	-11.0	-10.6
	c	0	15	2	4.31	709.77	222.66	-10.7	-11.4	-10.9	-10.3
	d	0	13	3	6.42	715.77	230.25	-12.0	-11.1	-11.1	-10.1
	e	0	15	3	5.87	743.78	234.03	-12.4	-11.1	-11.5	-11.3
13	a	0	13	4	4.14	639.68	203.80	-11.8	-11.3	-10.9	-10.8
	b	0	14	2	4.43	722.81	229.64	-12.3	-11.1	-11.5	-12.4
	c	0	15	2	4.31	709.77	222.66	-12.0	-12.3	-11.6	-10.2
	d	0	13	3	6.42	715.77	230.25	-11.7	-11.5	-11.4	-11.8
	e	0	15	3	5.87	743.78	234.03	-12.6	-11.0	-11.7	-11.7
14	a	0	13	4	4.14	639.68	203.80	-12.0	-10.2	-10.5	-11.0
	b	0	14	2	4.43	722.81	229.64	-10.7	-10.5	-11.0	-11.8
	c	0	15	2	4.31	709.77	222.66	-10.7	-10.4	-10.9	-10.1
	d	0	13	3	6.42	715.77	230.25	-11.8	-11.1	-11.0	-11.1
	e	0	15	3	5.87	743.78	234.03	-12.1	-11.0	-11.7	-11.7
15	a	0	13	4	4.14	639.68	203.80	-11.6	-11.0	-11.0	-11.0
	b	0	14	2	4.43	722.81	229.64	-12.5	-11.0	-11.6	-10.0
	c	0	15	2	4.31	709.77	222.66	-12.1	-12.1	-11.5	-10.6
	d	0	13	3	6.42	715.77	230.25	-11.7	-11.4	-11.5	-10.7
	e	0	15	3	5.87	743.78	234.03	-12.5	-11.0	-11.8	-11.7
16	a	0	16	4	5.06	682.70	211.72	-12.6	-10.5	-11.0	-11.4
	b	0	17	2	5.35	765.83	237.56	-12.0	-10.4	-11.1	-10.6
	c	0	18	2	5.23	752.79	230.59	-12.0	-11.2	-11.0	-10.4
	d	0	16	3	7.34	758.80	238.17	-11.7	-11.4	-10.8	-11.3
	e	0	18	3	6.79	786.81	241.96	-12.1	-10.9	-12.2	-12.2
17	a	0	16	4	5.06	682.70	211.72	-12.2	-11.2	-11.3	-9.9
	b	0	17	2	5.35	765.83	237.56	-12.9	-11.9	-11.9	-10.4
	c	0	18	2	5.23	752.79	230.59	-12.4	-12.8	-11.8	-11.2
	d	0	16	3	7.34	758.80	238.17	-12.2	-12.2	-11.8	-11.0
	e	0	18	3	6.79	786.81	241.96	-13.1	-10.1	-11.9	-11.9
18	a	0	18	4	4.78	728.77	225.34	-11.5	-9.6	-10.6	-10.6
	b	0	19	2	5.08	811.90	251.19	-11.3	-9.6	-10.4	-9.4
	c	0	20	2	4.96	798.86	244.21	-11.2	-9.6	-10.3	-9.3
	d	0	18	3	7.06	804.86	251.80	-11.2	-10.4	-10.1	-10.1
	e	0	20	3	6.52	832.87	255.58	-11.3	-10.8	-10.6	-10.7
19	a	0	18	4	4.78	728.77	225.34	-10.9	-10.0	-11.4	-10.3
	b	0	19	2	5.08	811.90	251.19	-11.8	-9.4	-11.7	-10.4
	c	0	20	2	4.96	798.86	244.21	-11.6	-9.9	-11.6	-10.5
	d	0	18	3	7.06	804.86	251.80	-11.1	-10.9	-10.4	-11.2
	e	0	20	3	6.52	832.87	255.58	-11.8	-10.6	-12.2	-11.0

Table 5 Description of the **Class 2** ligands under study and presentation of their physicochemical properties and affinity values for the 4 targets. (continuation)

R ¹	R ²	Physicochemical and structural properties						$\Delta G_{\text{binding}}$ (kcal/mol)			
		Charge	HBA	HBD	Log P	M _w	R _f	PI3K α	PI3K β	PI3K γ	PI3K δ
20	a	-1	15	3	5.75	663.73	207.02	-11.2	-10.7	-11.3	-10.9
	b	-1	16	1	6.05	746.87	232.86	-10.3	-10.6	-10.8	-10.0
	c	-1	17	1	5.93	733.82	225.88	-10.2	-11.7	-10.9	-9.8
	d	-1	15	2	8.03	739.83	233.47	-11.7	-11.5	-11.0	-11.2
	e	-1	17	2	7.49	767.84	237.25	-11.9	-11.4	-11.8	-11.5
21	a	-1	15	3	5.75	663.73	207.02	-12.1	-11.0	-11.9	-10.2
	b	-1	16	1	6.05	746.87	232.86	-10.3	-9.9	-10.9	-9.9
	c	-1	17	1	5.93	733.82	225.88	-10.2	-11.0	-10.6	-10.8
	d	-1	15	2	8.03	739.83	233.47	-11.2	-10.8	-11.9	-10.2
	e	-1	17	2	7.49	767.84	237.25	-12.1	-11.0	-12.1	-11.4
22	a	+1	12	4	4.91	646.75	207.04	-10.3	-10.1	-10.7	-10.5
	b	+1	13	2	5.21	729.89	232.89	-10.9	-10.0	-10.7	-8.7
	c	+1	14	2	5.09	716.84	225.91	-10.6	-10.6	-10.6	-10.2
	d	+1	12	3	7.19	722.85	233.50	-11.0	-10.9	-10.8	-10.7
	e	+1	14	3	6.65	750.86	237.28	-11.0	-9.5	-11.1	-10.6
23	a	+1	12	4	4.91	646.75	207.04	-10.6	-10.2	-11.0	-9.2
	b	+1	13	2	5.21	729.89	232.89	-11.1	-9.8	-10.9	-10.0
	c	+1	14	2	5.09	716.84	225.91	-10.8	-11.3	-10.4	-10.3
	d	+1	12	3	7.19	722.85	233.50	-10.6	-10.5	-11.5	-10.1
	e	+1	14	3	6.65	750.86	237.28	-11.3	-9.9	-10.9	-10.4

Table 6 Description of the **Class 3** ligands under study and presentation of their physicochemical properties and affinity values for the 4 targets.


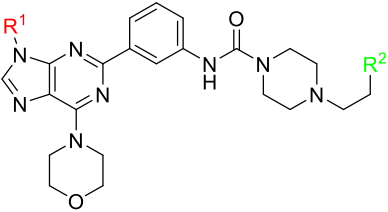
R ¹	R ²	Physicochemical and structural properties						$\Delta G_{\text{binding}}$ (kcal/mol)			
		Charge	HBA	HBD	Log P	M _w	R _f	PI3K α	PI3K β	PI3K γ	PI3K δ
1	a	0	10	4	2.26	416.45	129.20	-9.3	-10.0	-9.6	-9.6
	b	0	11	3	3.07	499.58	154.98	-10.3	-10.2	-9.6	-9.7
	c	0	12	2	2.95	486.54	148.01	-10.4	-10.6	-9.7	-9.4
	d	0	10	3	4.34	492.54	152.99	-10.9	-10.6	-11.4	-10.1
	e	0	11	3	4.10	520.55	160.04	-10.8	-9.6	-9.7	-9.8
2	a	0	10	3	4.14	492.54	164.20	-10.8	-10.6	-11.4	-10.2
	b	0	11	1	4.95	575.68	189.98	-10.3	-9.2	-9.9	-10.6
	c	0	12	1	4.83	562.63	183.00	-11.5	-10.9	-10.6	-10.5
	d	0	10	2	6.22	568.64	187.98	-11.8	-10.4	-10.1	-10.5
	e	0	11	2	5.98	596.65	195.03	-10.4	-8.7	-10.5	-11.1
3	a	0	10	3	4.64	506.57	169.24	-10.9	-10.7	-10.2	-10.4
	b	0	11	1	5.45	589.70	195.02	-11.2	-9.1	-10.5	-10.3
	c	0	12	1	5.33	576.66	188.04	-12.0	-9.2	-10.8	-10.5
	d	0	10	2	6.72	582.67	193.02	-11.5	-8.5	-10.2	-9.7
	e	0	11	2	6.48	610.68	200.07	-11.5	-10.5	-10.3	-10.7
4	a	0	10	3	4.64	506.57	169.24	-11.5	-10.9	-11.9	-10.5
	b	0	11	1	5.45	589.70	195.02	-10.3	-10.1	-10.1	-10.1
	c	0	12	1	5.33	576.66	188.04	-11.0	-9.8	-10.1	-10.3
	d	0	10	2	6.72	582.67	193.02	-12.1	-9.4	-10.3	-10.1
	e	0	11	2	6.48	610.68	200.07	-11.2	-10.2	-11.2	-10.4
5	a	0	10	3	5.14	520.60	174.28	-11.2	-11.0	-12.2	-10.7
	b	0	11	1	5.95	603.73	200.06	-11.0	-9.2	-10.7	-9.5
	c	0	12	1	5.83	590.69	193.08	-11.4	-9.1	-10.5	-9.9
	d	0	10	2	7.22	596.70	198.07	-12.3	-9.4	-10.8	-10.8
	e	0	11	2	6.98	624.71	205.11	-11.2	-10.8	-10.4	-9.2
6	a	0	10	3	4.29	510.53	164.41	-11.4	-10.7	-11.4	-10.4
	b	0	11	1	5.10	593.67	190.19	-11.0	-9.1	-10.5	-9.4
	c	0	12	1	4.98	580.62	183.22	-11.0	-9.0	-10.5	-9.3
	d	0	10	2	6.37	586.63	188.20	-12.1	-9.3	-10.3	-10.8
	e	0	11	2	6.13	614.64	195.25	-11.4	-10.5	-11.1	-10.8
7	a	0	10	3	4.29	510.53	164.41	-11.0	-10.8	-11.6	-10.6
	b	0	11	1	5.10	593.67	190.19	-11.1	-9.1	-10.5	-10.0
	c	0	12	1	4.98	580.62	183.22	-11.0	-10.6	-9.8	-10.4
	d	0	10	2	6.37	586.63	188.20	-12.1	-10.5	-10.3	-10.3
	e	0	11	2	6.13	614.64	195.25	-11.0	-10.9	-10.9	-10.2
8	a	0	12	4	3.47	549.60	179.06	-11.7	-10.5	-11.1	-10.3
	b	0	13	2	4.28	632.73	204.84	-10.8	-9.3	-10.7	-10.2
	c	0	14	2	4.16	619.69	197.86	-11.2	-10.1	-10.5	-9.2
	d	0	12	3	5.55	625.69	202.85	-11.3	-9.7	-10.9	-9.3
	e	0	13	3	5.31	653.70	209.89	-11.6	-9.5	-10.5	-10.6
9	a	0	12	4	3.47	549.60	179.06	-11.9	-11.1	-10.8	-10.3
	b	0	13	2	4.28	632.73	204.84	-10.7	-9.7	-10.6	-9.2
	c	0	14	2	4.16	619.69	197.86	-10.7	-10.7	-10.5	-10.3
	d	0	12	3	5.55	625.69	202.85	-11.6	-9.6	-10.7	-10.2
	e	0	13	3	5.31	653.70	209.89	-10.6	-9.2	-11.2	-10.0

Table 6 Description of the **Class 3** ligands under study and presentation of their physicochemical properties and affinity values for the 4 targets. (continuation)

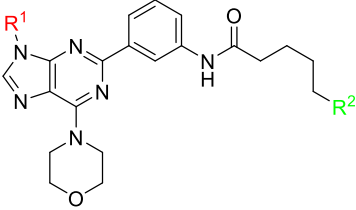
R ¹	R ²	Physicochemical and structural properties						$\Delta G_{\text{binding}}$ (kcal/mol)			
		Charge	HBA	HBD	Log P	M _w	R _f	PI3K α	PI3K β	PI3K γ	PI3K δ
10	a	0	12	4	5.20	611.67	199.73	-11.9	-10.4	-11.5	-10.7
	b	0	13	2	6.01	694.80	225.51	-10.8	-9.6	-10.8	-10.2
	c	0	14	2	5.89	681.76	218.53	-11.6	-10.6	-10.8	-10.0
	d	0	12	3	7.28	687.76	223.52	-11.1	-10.8	-10.7	-9.6
	e	0	13	3	7.04	715.77	230.56	-11.4	-9.9	-11.3	-9.8
11	a	0	12	4	5.20	611.67	199.73	-11.7	-10.0	-10.8	-10.6
	b	0	13	2	6.01	694.80	225.51	-11.9	-10.0	-10.9	-10.7
	c	0	14	2	5.89	681.76	218.53	-11.4	-11.8	-10.8	-10.5
	d	0	12	3	7.28	687.76	223.52	-12.6	-11.7	-10.8	-9.7
	e	0	13	3	7.04	715.77	230.56	-11.8	-10.7	-10.6	-10.7
12	a	0	13	4	3.97	612.65	197.57	-11.8	-10.4	-11.0	-10.6
	b	0	14	2	4.78	695.79	223.35	-10.5	-9.3	-10.4	-10.7
	c	0	15	2	4.66	682.75	216.38	-11.3	-10.8	-10.3	-9.7
	d	0	13	3	6.05	688.75	221.36	-10.8	-9.3	-10.7	-9.3
	e	0	14	3	5.81	716.76	228.41	-11.1	-9.4	-9.8	-10.4
13	a	0	13	4	3.97	612.65	197.57	-11.8	-10.4	-10.7	-10.4
	b	0	14	2	4.78	695.79	223.35	-11.9	-9.4	-10.8	-9.9
	c	0	15	2	4.66	682.75	216.38	-11.4	-11.9	-11.5	-9.9
	d	0	13	3	6.05	688.75	221.36	-12.4	-11.8	-10.3	-10.5
	e	0	14	3	5.81	716.76	228.41	-11.6	-10.0	-10.7	-11.7
14	a	0	13	4	3.97	612.65	197.57	-11.7	-10.4	-10.9	-11.2
	b	0	14	2	4.78	695.79	223.35	-10.4	-9.5	-10.4	-10.4
	c	0	15	2	4.66	682.75	216.38	-11.4	-10.7	-10.7	-9.3
	d	0	13	3	6.05	688.75	221.36	-10.1	-10.1	-10.3	-9.4
	e	0	14	3	5.81	716.76	228.41	-10.9	-9.8	-9.7	-9.7
15	a	0	13	4	3.97	612.65	197.57	-12.0	-9.8	-10.7	-10.7
	b	0	14	2	4.78	695.79	223.35	-11.8	-9.4	-10.9	-10.5
	c	0	15	2	4.66	682.75	216.38	-11.7	-11.7	-11.4	-10.8
	d	0	13	3	6.05	688.75	221.36	-12.4	-11.5	-11.1	-10.4
	e	0	14	3	5.81	716.76	228.41	-11.6	-10.0	-10.5	-11.0
16	a	0	16	4	4.89	655.68	205.50	-11.3	-10.5	-10.7	-10.6
	b	0	17	2	5.70	738.81	231.28	-12.2	-9.4	-11.0	-10.6
	c	0	18	2	5.58	725.77	224.30	-12.8	-9.9	-10.9	-10.0
	d	0	16	3	6.97	731.77	229.28	-12.3	-10.9	-11.0	-10.4
	e	0	17	3	6.73	759.78	236.33	-12.1	-10.1	-10.5	-11.2
17	a	0	16	4	4.89	655.68	205.50	-12.4	-10.2	-10.9	-11.4
	b	0	17	2	5.70	738.81	231.28	-12.7	-10.3	-11.3	-11.0
	c	0	18	2	5.58	725.77	224.30	-12.7	-12.0	-11.2	-10.5
	d	0	16	3	6.97	731.77	229.28	-12.9	-12.0	-11.0	-11.0
	e	0	17	3	6.73	759.78	236.33	-13.1	-11.4	-11.4	-10.9
18	a	0	18	4	4.62	701.74	219.12	-10.9	-9.8	-9.9	-10.2
	b	0	19	2	5.43	784.88	244.90	-10.8	-8.7	-9.7	-9.4
	c	0	20	2	5.31	771.84	237.92	-10.8	-8.8	-10.0	-9.5
	d	0	18	3	6.70	777.84	242.91	-11.1	-9.2	-9.6	-9.6
	e	0	19	3	6.46	805.85	249.95	-10.9	-9.3	-10.0	-9.0
19	a	0	18	4	4.62	701.74	219.12	-11.4	-9.9	-10.9	-10.2
	b	0	19	2	5.43	784.88	244.90	-11.5	-8.6	-10.9	-9.2
	c	0	20	2	5.31	771.84	237.92	-11.0	-11.3	-10.6	-9.8
	d	0	18	3	6.70	777.84	242.91	-11.8	-9.9	-10.7	-10.3
	e	0	19	3	6.46	805.85	249.95	-11.9	-10.2	-11.5	-10.6

Table 6 Description of the **Class 3** ligands under study and presentation of their physicochemical properties and affinity values for the 4 targets. (continuation)

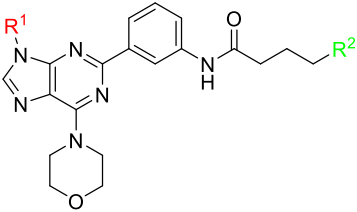
R ¹	R ²	Physicochemical and structural properties						$\Delta G_{\text{binding}}$ (kcal/mol)			
		Charge	HBA	HBD	Log P	M _w	R _f	PI3K α	PI3K β	PI3K γ	PI3K δ
20	a	-1	15	3	5.58	636.71	200.79	-10.9	-11.0	-11.2	-10.7
	b	-1	16	1	6.39	719.84	226.57	-11.1	-9.0	-9.8	-10.4
	c	-1	17	1	6.27	706.80	219.60	-11.0	-10.6	-9.6	-10.2
	d	-1	15	2	7.66	712.81	224.58	-11.2	-10.6	-10.5	-10.9
	e	-1	16	2	7.42	740.82	231.63	-11.8	-9.2	-11.2	-10.4
21	a	-1	15	3	5.58	636.71	200.79	-10.9	-10.7	-12.1	-10.4
	b	-1	16	1	6.39	719.84	226.57	-10.3	-9.1	-10.9	-11.6
	c	-1	17	1	6.27	706.80	219.60	-11.3	-9.5	-10.8	-11.2
	d	-1	15	2	7.66	712.81	224.58	-11.8	-8.6	-12.1	-11.1
	e	-1	16	2	7.42	740.82	231.63	-11.8	-9.2	-11.6	-10.1
22	a	+1	12	4	4.74	619.73	200.82	-10.4	-10.3	-11.1	-10.3
	b	+1	13	2	5.55	702.86	226.60	-10.2	-8.2	-10.4	-9.8
	c	+1	14	2	5.43	689.82	219.62	-10.5	-10.1	-10.4	-9.1
	d	+1	12	3	6.82	695.83	224.61	-11.0	-9.8	-10.8	-9.7
	e	+1	13	3	6.58	723.84	231.65	-11.3	-9.1	-10.2	-9.4
23	a	+1	12	4	4.74	619.73	200.82	-10.9	-10.3	-11.4	-10.0
	b	+1	13	2	5.55	702.86	226.60	-10.6	-9.7	-10.6	-9.9
	c	+1	14	2	5.43	689.82	219.62	-10.7	-10.8	-10.8	-9.8
	d	+1	12	3	6.82	695.83	224.61	-10.5	-9.8	-10.9	-10.7
	e	+1	13	3	6.58	723.84	231.65	-11.7	-9.2	-11.1	-10.0

Table 7 Description of the **Class 4** ligands under study and presentation of their physicochemical properties and affinity values for the 4 targets.


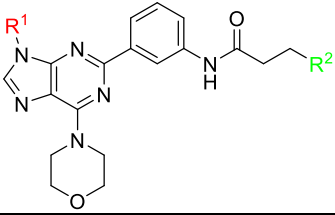
R ¹	R ²	Physicochemical and structural properties						$\Delta G_{\text{binding}}$ (kcal/mol)			
		Charge	HBA	HBD	Log P	M _w	R _f	PI3K α	PI3K β	PI3K γ	PI3K δ
1	a	+1	9	5	1.14	451.54	138.15	-9.4	-9.2	-9.0	-8.3
	b	+1	10	3	1.77	534.67	164.27	-10.0	-10.1	-9.2	-9.2
	c	0	12	2	1.65	521.63	157.29	-10.2	-9.9	-9.1	-8.8
	d	0	10	3	3.29	527.63	164.48	-10.1	-9.7	-10.2	-9.0
	e	0	11	3	2.75	555.64	168.26	-10.3	-9.7	-10.5	-9.7
2	a	+1	9	4	3.03	527.63	173.14	-10.4	-8.7	-9.3	-9.1
	b	+1	10	2	3.66	610.77	199.26	-9.9	-9.3	-9.6	-10.3
	c	0	12	1	3.54	597.72	192.28	-10.4	-9.2	-9.8	-9.9
	d	0	10	2	5.18	603.73	199.47	-10.5	-9.8	-9.9	-10.3
	e	0	11	2	4.64	631.74	203.25	-10.0	-8.8	-10.6	-10.4
3	a	+1	9	4	3.53	541.66	178.18	-10.0	-8.8	-9.6	-9.4
	b	+1	10	2	4.16	624.79	204.30	-10.1	-9.4	-9.6	-10.1
	c	0	12	1	4.04	611.75	197.32	-10.6	-9.4	-9.6	-10.1
	d	0	10	2	5.68	617.76	204.51	-10.1	-10.0	-9.8	-10.3
	e	0	11	2	5.14	645.77	208.30	-10.4	-10.4	-10.9	-9.8
4	a	+1	9	4	3.53	541.66	178.18	-10.8	-8.8	-9.6	-9.5
	b	+1	10	2	4.16	624.79	204.30	-10.7	-9.3	-10.1	-9.2
	c	0	12	1	4.04	611.75	197.32	-11.1	-9.1	-10.8	-10.1
	d	0	10	2	5.68	617.76	204.51	-11.0	-9.3	-10.2	-9.9
	e	0	11	2	5.14	645.77	208.30	-11.3	-10.3	-10.6	-10.6
5	a	+1	9	4	4.03	555.69	183.22	-10.5	-9.0	-9.9	-8.8
	b	+1	10	2	4.66	638.82	209.34	-10.7	-9.4	-10.1	-9.7
	c	0	12	1	4.54	625.78	202.37	-11.3	-9.4	-10.1	-9.5
	d	0	10	2	6.18	631.79	209.56	-10.7	-9.7	-10.2	-10.4
	e	0	11	2	5.64	659.80	213.34	-11.4	-10.4	-10.7	-10.8
6	a	+1	9	4	3.18	545.62	173.36	-10.3	-8.7	-9.5	-9.3
	b	+1	10	2	3.81	628.76	199.48	-10.1	-9.2	-10.0	-9.9
	c	0	12	1	3.69	615.71	192.50	-10.9	-9.2	-9.9	-9.6
	d	0	10	2	5.33	621.72	199.69	-10.7	-9.9	-9.9	-10.2
	e	0	11	2	4.79	649.73	203.47	-11.5	-9.8	-10.5	-10.9
7	a	+1	9	4	3.18	545.62	173.36	-10.6	-8.8	-9.6	-9.5
	b	+1	10	2	3.81	628.76	199.48	-10.4	-9.3	-9.9	-10.0
	c	0	12	1	3.69	615.71	192.50	-11.2	-9.3	-9.9	-9.9
	d	0	10	2	5.33	621.72	199.69	-10.9	-9.9	-10.1	-10.1
	e	0	11	2	4.79	649.73	203.47	-11.4	-10.2	-10.3	-10.6
8	a	+1	11	5	2.36	584.69	188.00	-10.2	-8.7	-10.0	-9.0
	b	+1	12	3	2.99	667.82	214.12	-10.0	-9.2	-9.9	-9.9
	c	0	14	2	2.87	654.78	207.15	-9.9	-9.1	-9.9	-9.2
	d	0	12	3	4.51	660.78	214.34	-10.3	-9.3	-9.5	-9.5
	e	0	13	3	3.97	688.79	218.12	-11.6	-10.0	-10.5	-10.2
9	a	+1	11	5	2.36	584.69	188.00	-10.8	-9.2	-9.6	-8.9
	b	+1	12	3	2.99	667.82	214.12	-11.1	-9.7	-9.9	-10.0
	c	0	14	2	2.87	654.78	207.15	-11.3	-9.5	-9.9	-9.7
	d	0	12	3	4.51	660.78	214.34	-11.5	-10.3	-10.5	-9.2
	e	0	13	3	3.97	688.79	218.12	-11.6	-9.9	-10.3	-10.8

Table 8 Description of the **Class 5** ligands under study and presentation of their physicochemical properties and affinity values for the 4 targets.


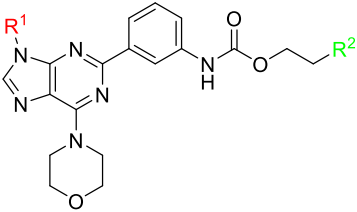
R ¹	R ²	Physicochemical and structural properties						$\Delta G_{\text{binding}}$ (kcal/mol)			
		Charge	HBA	HBD	Log P	M _w	R _f	PI3K α	PI3K β	PI3K γ	PI3K δ
1	a	+1	8	5	1.89	395.47	123.09	-8.3	-8.9	-9.0	-7.6
	b	+1	9	3	2.52	478.60	149.21	-9.3	-9.4	-9.2	-8.3
	c	0	11	2	2.40	465.56	142.23	-9.2	-9.2	-9.2	-8.3
	d	0	9	3	4.04	471.57	149.42	-9.3	-9.8	-9.5	-8.6
	e	0	10	3	3.50	499.58	153.21	-10.1	-9.6	-10.3	-8.9
2	a	+1	8	4	3.78	471.57	158.08	-10.2	-8.7	-9.5	-8.4
	b	+1	9	2	4.41	554.70	184.20	-10.7	-8.7	-9.1	-9.1
	c	0	11	1	4.29	541.66	177.23	-10.2	-9.7	-9.2	-9.3
	d	0	9	2	5.93	547.66	184.42	-10.7	-9.6	-8.3	-9.6
	e	0	10	2	5.38	575.67	188.20	-11.0	-9.8	-10.2	-9.7
3	a	+1	8	4	4.28	485.59	163.13	-9.8	-8.7	-9.7	-8.6
	b	+1	9	2	4.90	568.73	189.25	-10.4	-8.7	-9.2	-9.0
	c	0	11	1	4.78	555.68	182.27	-9.9	-9.1	-9.3	-9.4
	d	0	9	2	6.43	561.69	189.46	-10.1	-9.7	-8.4	-8.9
	e	0	10	2	5.88	589.70	193.24	-10.4	-10.1	-8.8	-8.6
4	a	+1	8	4	4.28	485.59	163.13	-9.6	-8.9	-10.1	-8.7
	b	+1	9	2	4.90	568.73	189.25	-10.7	-9.9	-9.3	-9.4
	c	0	11	1	4.78	555.68	182.27	-10.1	-10.0	-9.2	-9.4
	d	0	9	2	6.43	561.69	189.46	-10.4	-10.5	-8.5	-7.8
	e	0	10	2	5.88	589.70	193.24	-10.5	-10.6	-10.9	-9.2
5	a	+1	8	4	4.78	499.62	168.17	-9.4	-9.0	-10.1	-8.8
	b	+1	9	2	5.40	582.75	194.29	-10.0	-9.6	-9.3	-9.3
	c	0	11	1	5.28	569.71	187.31	-10.5	-9.3	-9.4	-9.4
	d	0	9	2	6.93	575.72	194.50	-10.0	-9.8	-8.4	-9.4
	e	0	10	2	6.38	603.73	198.28	-10.4	-10.3	-9.0	-9.6
6	a	+1	8	4	3.92	489.56	158.30	-10.2	-8.8	-9.5	-8.8
	b	+1	9	2	4.55	572.69	184.42	-10.6	-9.1	-9.0	-9.1
	c	0	11	1	4.43	559.65	177.44	-10.0	-9.1	-9.3	-9.7
	d	0	9	2	6.08	565.65	184.63	-10.4	-10.3	-9.5	-10.0
	e	0	10	2	5.53	593.66	188.42	-10.5	-10.2	-10.2	-9.7
7	a	+1	8	4	3.92	489.56	158.30	-10.4	-8.6	-9.7	-8.6
	b	+1	9	2	4.55	572.69	184.42	-10.8	-8.7	-9.1	-9.7
	c	0	11	1	4.43	559.65	177.44	-10.4	-9.6	-9.2	-9.4
	d	0	9	2	6.08	565.65	184.63	-10.9	-10.4	-8.4	-9.4
	e	0	10	2	5.53	593.66	188.42	-11.3	-10.5	-10.5	-9.6
8	a	+1	10	5	3.11	528.62	172.95	-10.0	-8.7	-9.3	-8.6
	b	+1	11	3	3.74	611.75	199.07	-10.3	-8.6	-8.9	-9.4
	c	0	13	2	3.62	598.71	192.09	-10.4	-9.6	-9.2	-9.1
	d	0	11	3	5.26	604.72	199.28	-10.3	-10.0	-9.2	-9.3
	e	0	12	3	4.71	632.73	203.06	-10.1	-10.2	-10.1	-9.2
9	a	+1	10	5	3.11	528.62	172.95	-9.9	-9.1	-9.6	-8.6
	b	+1	11	3	3.74	611.75	199.07	-10.2	-9.0	-9.5	-9.3
	c	0	13	2	3.62	598.71	192.09	-10.2	-9.5	-9.7	-9.2
	d	0	11	3	5.26	604.72	199.28	-10.6	-10.0	-8.7	-9.1
	e	0	12	3	4.71	632.73	203.06	-10.9	-10.4	-11.1	-9.6

Table 9 Description of the **Class 6** ligands under study and presentation of their physicochemical properties and affinity values for the 4 targets.


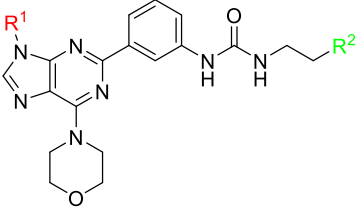
R ¹	R ²	Physicochemical and structural properties						$\Delta G_{\text{binding}}$ (kcal/mol)			
		Charge	HBA	HBD	Log P	M _w	R _f	PI3K α	PI3K β	PI3K γ	PI3K δ
1	a	+1	8	5	1.47	381.44	118.49	-8.3	-8.5	-8.8	-7.7
	b	+1	9	3	2.10	464.57	144.61	-9.2	-9.6	-9.4	-8.5
	c	0	10	3	1.98	451.53	137.63	-9.2	-9.3	-9.3	-8.3
	d	0	9	3	3.62	457.54	144.82	-9.6	-10.1	-9.5	-9.2
	e	0	10	3	3.08	485.55	148.60	-9.5	-10.1	-10.1	-9.6
2	a	+1	8	4	3.36	457.54	153.48	-10.4	-8.5	-9.7	-8.7
	b	+1	9	2	3.98	540.67	179.60	-10.2	-8.9	-9.5	-9.4
	c	0	11	1	3.86	527.63	172.63	-10.3	-9.2	-9.9	-9.5
	d	0	9	2	5.51	533.64	179.82	-10.7	-9.9	-9.3	-8.7
	e	0	10	2	4.96	561.65	183.60	-11.1	-10.0	-9.5	-10.1
3	a	+1	8	4	3.86	471.57	158.52	-10.0	-8.7	-9.5	-8.3
	b	+1	9	2	4.48	554.70	184.64	-10.7	-9.0	-9.8	-9.2
	c	0	11	1	4.36	541.66	177.67	-10.3	-9.3	-10.0	-9.2
	d	0	9	2	6.01	547.66	184.86	-10.5	-10.0	-8.6	-8.2
	e	0	10	2	5.46	575.67	188.64	-11.0	-10.2	-9.0	-10.1
4	a	+1	8	4	3.86	471.57	158.52	-9.8	-8.8	-10.1	-9.0
	b	+1	9	2	4.48	554.70	184.64	-10.0	-9.0	-9.3	-9.5
	c	0	11	1	4.36	541.66	177.67	-10.4	-9.3	-10.0	-9.3
	d	0	9	2	6.01	547.66	184.86	-10.8	-10.7	-10.1	-8.6
	e	0	10	2	5.46	575.67	188.64	-11.0	-10.4	-10.3	-9.9
5	a	+1	8	4	4.36	485.59	163.57	-9.6	-8.9	-10.4	-8.8
	b	+1	9	2	4.98	568.73	189.69	-10.3	-9.2	-9.8	-9.4
	c	0	11	1	4.86	555.68	182.71	-10.5	-9.5	-9.3	-9.4
	d	0	9	2	6.51	561.69	189.90	-10.0	-10.3	-8.7	-9.9
	e	0	10	2	5.96	589.70	193.68	-10.5	-10.5	-9.9	-9.8
6	a	+1	8	4	3.50	475.53	153.70	-10.5	-8.6	-9.7	-9.0
	b	+1	9	2	4.13	558.66	179.82	-10.4	-9.0	-9.6	-9.5
	c	0	11	1	4.01	545.62	172.84	-10.1	-9.3	-9.8	-9.8
	d	0	9	2	5.65	551.63	180.03	-10.5	-10.0	-9.9	-8.8
	e	0	10	2	5.11	579.64	183.81	-10.9	-10.3	-10.2	-9.0
7	a	+1	8	4	3.50	475.53	153.70	-10.6	-8.7	-9.9	-8.4
	b	+1	9	2	4.13	558.66	179.82	-10.2	-9.0	-9.5	-9.5
	c	0	11	1	4.01	545.62	172.84	-10.5	-9.3	-10.0	-10.1
	d	0	9	2	5.65	551.63	180.03	-11.1	-10.1	-9.4	-10.5
	e	0	10	2	5.11	579.64	183.81	-11.7	-10.2	-10.2	-9.8
8	a	+1	10	5	2.69	514.59	168.35	-10.1	-8.6	-9.6	-8.6
	b	+1	11	3	3.31	597.72	194.47	-10.4	-8.9	-9.8	-9.2
	c	0	13	2	3.20	584.68	187.49	-10.5	-9.1	-9.8	-9.7
	d	0	11	3	4.84	590.69	194.68	-10.3	-9.9	-9.5	-9.4
	e	0	12	3	4.29	618.70	198.46	-10.7	-10.2	-9.1	-9.9
9	a	+1	10	5	2.69	514.59	168.35	-10.2	-9.1	-9.6	-8.6
	b	+1	11	3	3.31	597.72	194.47	-10.4	-9.3	-9.7	-9.5
	c	0	13	2	3.20	584.68	187.49	-10.3	-9.3	-9.8	-9.2
	d	0	11	3	4.84	590.69	194.68	-11.0	-10.4	-10.2	-8.4
	e	0	12	3	4.29	618.70	198.46	-11.0	-10.6	-10.5	-9.2

Table 10 Description of the **Class 7** ligands under study and presentation of their physicochemical properties and affinity values for the 4 targets.


R ¹	R ²	Physicochemical and structural properties						$\Delta G_{\text{binding}}$ (kcal/mol)			
		Charge	HBA	HBD	Log P	M _w	R _f	PI3K α	PI3K β	PI3K γ	PI3K δ
1	a	+1	8	5	1.20	367.41	113.74	-8.6	-8.6	-8.8	-7.8
	b	+1	9	3	1.82	450.55	139.85	-9.5	-9.5	-9.2	-8.6
	c	0	11	2	1.70	437.50	132.88	-9.4	-9.4	-9.4	-8.5
	d	0	9	3	3.35	443.51	140.07	-9.7	-10.2	-9.5	-9.0
	e	0	10	3	2.80	471.52	143.85	-9.7	-9.9	-10.1	-9.6
2	a	+1	8	4	3.08	443.51	148.73	-10.3	-8.2	-9.5	-8.8
	b	+1	9	2	3.71	526.65	174.85	-10.4	-9.1	-9.6	-9.3
	c	0	11	1	3.59	513.60	167.87	-10.4	-9.4	-10.0	-9.4
	d	0	9	2	5.23	519.61	175.06	-11.0	-10.1	-10.0	-8.5
	e	0	10	2	4.69	547.62	178.84	-11.5	-10.4	-10.1	-9.7
3	a	+1	8	4	3.58	457.54	153.77	-9.7	-8.3	-9.7	-9.0
	b	+1	9	2	4.21	540.67	179.89	-10.6	-9.3	-10.4	-9.1
	c	0	11	1	4.09	527.63	172.91	-10.8	-9.5	-10.1	-8.6
	d	0	9	2	5.73	533.64	180.10	-10.7	-10.3	-9.2	-8.7
	e	0	10	2	5.19	561.65	183.88	-10.9	-10.5	-10.3	-9.7
4	a	+1	8	4	3.58	457.54	153.77	-9.9	-9.0	-10.0	-8.9
	b	+1	9	2	4.21	540.67	179.89	-10.7	-9.3	-10.6	-9.2
	c	0	11	1	4.09	527.63	172.91	-10.8	-9.6	-10.4	-9.1
	d	0	9	2	5.73	533.64	180.10	-11.1	-10.2	-10.4	-8.3
	e	0	10	2	5.19	561.65	183.88	-11.5	-10.7	-10.8	-9.9
5	a	+1	8	4	4.08	471.57	158.81	-10.0	-8.6	-10.2	-9.0
	b	+1	9	2	4.71	554.70	184.93	-10.7	-9.5	-10.5	-9.5
	c	0	11	1	4.59	541.66	177.95	-11.1	-9.7	-9.6	-8.8
	d	0	9	2	6.23	547.66	185.14	-10.4	-10.5	-9.9	-9.4
	e	0	10	2	5.69	575.67	188.93	-11.6	-10.9	-10.8	-10.2
6	a	+1	8	4	3.23	461.50	148.95	-10.4	-8.3	-9.8	-8.9
	b	+1	9	2	3.86	544.64	175.06	-10.3	-9.3	-9.9	-9.6
	c	0	11	1	3.74	531.59	168.09	-10.1	-9.5	-10.0	-9.4
	d	0	9	2	5.38	537.60	175.28	-10.7	-10.2	-9.7	-9.7
	e	0	10	2	4.84	565.61	179.06	-11.5	-10.3	-10.6	-9.2
7	a	+1	8	4	3.23	461.50	148.95	-10.4	-8.4	-9.7	-8.8
	b	+1	9	2	3.86	544.64	175.06	-10.5	-9.3	-9.8	-9.1
	c	0	11	1	3.74	531.59	168.09	-10.6	-9.6	-10.5	-9.3
	d	0	9	2	5.38	537.60	175.28	-11.2	-10.2	-10.2	-8.6
	e	0	10	2	4.84	565.61	179.06	-12.0	-10.6	-10.3	-9.3
8	a	+1	10	5	2.41	500.56	163.59	-10.0	-8.6	-9.8	-8.9
	b	+1	11	3	3.04	583.70	189.71	-10.3	-9.2	-9.8	-9.4
	c	0	13	2	2.92	570.65	182.74	-11.1	-9.4	-10.2	-9.2
	d	0	11	3	4.56	576.66	189.92	-10.5	-10.0	-10.0	-9.2
	e	0	12	3	4.02	604.67	193.71	-11.0	-10.5	-10.6	-10.0
9	a	+1	10	5	2.41	500.56	163.59	-10.3	-8.8	-9.9	-8.9
	b	+1	11	3	3.04	583.70	189.71	-10.6	-9.7	-9.9	-8.8
	c	0	13	2	2.92	570.65	182.74	-11.1	-9.9	-10.3	-9.6
	d	0	11	3	4.56	576.66	189.92	-11.3	-10.5	-9.9	-9.2
	e	0	12	3	4.02	604.67	193.71	-10.7	-10.9	-11.0	-9.7

Table 11 Description of the **Class 8** ligands under study and presentation of their physicochemical properties and affinity values for the 4 targets.


R ¹	R ²	Physicochemical and structural properties						$\Delta G_{\text{binding}}$ (kcal/mol)			
		Charge	HBA	HBD	Log P	M _w	R _f	PI3K α	PI3K β	PI3K γ	PI3K δ
1	a	+1	9	5	1.72	383.41	115.25	-8.6	-8.3	-8.6	-7.7
	b	+1	10	3	2.35	466.55	141.37	-9.0	-8.9	-9.3	-8.5
	c	0	12	2	2.23	453.50	134.39	-9.0	-9.4	-9.2	-8.4
	d	0	10	3	3.87	459.51	141.58	-8.9	-10.1	-9.1	-8.9
	e	0	11	3	3.33	487.52	145.36	-9.6	-10.5	-9.8	-8.5
2	a	+1	9	4	3.61	459.51	150.24	-10.1	-8.2	-9.2	-8.7
	b	+1	10	2	4.24	542.64	176.36	-10.0	-8.8	-9.1	-9.1
	c	0	12	1	4.12	529.60	169.39	-10.1	-9.0	-9.5	-9.2
	d	0	10	2	5.76	535.61	176.58	-10.7	-9.9	-9.2	-8.8
	e	0	11	2	5.22	563.62	180.36	-11.1	-10.0	-10.3	-9.8
3	a	+1	9	4	4.11	473.54	155.28	-9.4	-8.3	-9.4	-8.2
	b	+1	10	2	4.74	556.67	181.40	-10.5	-9.2	-9.6	-9.3
	c	0	12	1	4.62	543.63	174.43	-10.4	-9.2	-9.9	-9.2
	d	0	10	2	6.26	549.64	181.62	-10.5	-10.0	-8.3	-8.5
	e	0	11	2	5.72	577.65	185.40	-10.5	-10.1	-8.9	-8.4
4	a	+1	9	4	4.11	473.54	155.28	-9.7	-8.5	-9.6	-8.5
	b	+1	10	2	4.74	556.67	181.40	-10.0	-9.0	-9.7	-8.7
	c	0	12	1	4.62	543.63	174.43	-10.3	-9.3	-9.7	-9.2
	d	0	10	2	6.26	549.64	181.62	-10.7	-10.1	-10.2	-8.9
	e	0	11	2	5.72	577.65	185.40	-11.1	-10.4	-10.5	-9.5
5	a	+1	9	4	4.61	487.56	160.33	-9.6	-8.6	-9.8	-8.5
	b	+1	10	2	5.24	570.70	186.44	-10.5	-9.1	-9.9	-8.8
	c	0	12	1	5.12	557.66	179.47	-10.3	-9.3	10.3	-8.8
	d	0	10	2	6.76	563.66	186.66	-10.4	-10.2	-9.8	-9.1
	e	0	11	2	6.22	591.67	190.44	-10.5	-10.5	-10.2	-8.5
6	a	+1	9	4	3.76	477.50	150.46	-10.3	-8.3	-9.2	-9.0
	b	+1	10	2	4.38	560.63	176.58	-10.1	-8.9	-9.3	-9.6
	c	0	12	1	4.26	547.59	169.60	-9.8	-9.0	-9.8	-9.0
	d	0	10	2	5.91	553.60	176.79	-10.5	-9.9	-9.6	-9.1
	e	0	11	2	5.36	581.61	180.57	-11.0	-10.2	-10.5	-10.2
7	a	+1	9	4	3.76	477.50	150.46	-10.3	-8.4	-9.4	-8.5
	b	+1	10	2	4.38	560.63	176.58	-10.1	-9.0	-9.4	-9.4
	c	0	12	1	4.26	547.59	169.60	-10.5	-9.2	-9.9	-9.6
	d	0	10	2	5.91	553.60	176.79	-10.9	-10.0	-9.4	-9.7
	e	0	11	2	5.36	581.61	180.57	-11.5	-10.2	-10.4	-9.9
8	a	+1	11	5	2.94	516.56	165.11	-9.9	-8.6	-9.2	-8.4
	b	+1	12	3	3.57	599.70	191.23	-10.0	-8.9	-9.3	-9.2
	c	0	14	2	3.45	586.65	184.25	-10.4	-9.1	-9.6	-8.9
	d	0	12	3	5.09	592.66	191.44	-10.4	-9.9	-8.6	-9.3
	e	0	13	3	4.55	620.67	195.22	-10.5	-10.2	-8.6	-9.8
9	a	+1	11	5	2.94	516.56	165.11	-10.1	-8.8	-9.8	-8.4
	b	+1	12	3	3.57	599.70	191.23	-10.1	-9.3	-9.1	-8.6
	c	0	14	2	3.45	586.65	184.25	-10.3	-9.5	-9.8	-8.8
	d	0	12	3	5.09	592.66	191.44	-10.9	-10.1	-10.0	-9.2
	e	0	13	3	4.55	620.67	195.22	-10.9	-10.4	-10.6	-9.2

Table 12 Description of the **Class 9** ligands under study and presentation of their physicochemical properties and affinity values for the 4 targets.


R ¹	R ²	Physicochemical and structural properties						$\Delta G_{\text{binding}}$ (kcal/mol)			
		Charge	HBA	HBD	Log P	M _w	R _f	PI3K α	PI3K β	PI3K γ	PI3K δ
1	a	+1	8	6	1.08	382.43	117.20	-9.0	-8.7	-9.0	-8.7
	b	+1	9	4	1.71	465.56	143.32	-9.8	-9.4	-9.1	-9.3
	c	0	11	3	1.59	452.52	136.34	-9.6	-9.3	-9.8	-9.3
	d	0	9	4	3.23	458.53	143.53	-9.1	-10.6	-9.9	-9.4
	e	0	10	4	2.69	486.54	147.31	-9.9	-10.1	-10.5	-9.9
2	a	+1	8	5	2.97	458.53	152.19	-10.5	-8.4	-9.5	-8.9
	b	+1	9	3	3.60	541.66	178.31	-11.1	-9.1	-9.8	-10.0
	c	0	11	2	3.48	528.62	171.34	-10.7	-9.3	-9.4	-9.2
	d	0	9	3	5.12	534.62	178.53	-11.3	-10.1	-9.8	-8.7
	e	0	10	3	4.58	562.63	182.31	-11.4	-10.3	-9.0	-8.6
3	a	+1	8	5	3.47	472.55	157.23	-10.2	-8.8	-9.8	-9.2
	b	+1	9	3	4.10	555.69	183.35	-10.7	-9.4	-9.9	-9.7
	c	0	11	2	3.98	542.64	176.38	-10.6	-9.2	-10.2	-9.7
	d	0	9	3	5.62	548.65	183.57	-10.8	-10.2	-9.8	-9.1
	e	0	10	3	5.07	576.66	187.35	-10.3	-10.5	-9.2	-9.7
4	a	+1	8	5	3.47	472.55	157.23	-10.0	-8.6	-10.1	-9.2
	b	+1	9	3	4.10	555.69	183.35	-11.2	-9.3	-10.4	-9.2
	c	0	11	2	3.98	542.64	176.38	-10.9	-9.6	-10.3	-9.9
	d	0	9	3	5.62	548.65	183.57	-11.2	-10.2	-10.1	-8.9
	e	0	10	3	5.07	576.66	187.35	-11.2	-11.0	-10.6	-10.4
5	a	+1	8	5	3.97	486.58	162.28	-9.9	-8.8	-10.3	-8.8
	b	+1	9	3	4.59	569.71	188.39	-10.7	-9.5	-10.4	-9.9
	c	0	11	2	4.48	556.67	181.42	-10.8	-9.9	-10.4	-10.2
	d	0	9	3	6.12	562.68	188.61	-10.7	-10.4	-10.5	-10.0
	e	0	10	3	5.57	590.69	192.39	-10.6	-11.1	-10.6	-9.5
6	a	+1	8	5	3.12	476.52	152.41	-10.5	-8.5	-9.6	-8.5
	b	+1	9	3	3.74	559.65	178.53	-11.1	-9.0	-9.8	-10.1
	c	0	11	2	3.62	546.61	171.55	-10.3	-9.6	-9.3	-9.4
	d	0	9	3	5.27	552.61	178.74	-11.0	-10.1	-9.9	-8.8
	e	0	10	3	4.72	580.62	182.52	-11.3	-10.8	-10.4	-10.4
7	a	+1	8	5	3.12	476.52	152.41	-10.6	-8.6	-9.8	-8.6
	b	+1	9	3	3.74	559.65	178.53	-11.2	-9.6	-9.9	-10.3
	c	0	11	2	3.62	546.61	171.55	-10.8	-9.6	-10.0	-9.1
	d	0	9	3	5.27	552.61	178.74	-11.6	-10.1	-10.1	-9.2
	e	0	10	3	4.72	580.62	182.52	-11.8	-10.9	-9.6	-9.3
8	a	+1	10	6	2.30	515.58	167.06	-10.5	-9.4	-9.6	-8.7
	b	+1	11	4	2.93	598.71	193.18	-10.6	-9.0	-9.5	-9.5
	c	0	13	3	2.81	585.67	186.20	-10.7	-9.7	-10.3	-9.5
	d	0	11	4	4.45	591.68	193.39	-10.8	-10.0	-10.2	-8.9
	e	0	12	4	3.91	619.69	197.17	-10.8	-10.7	-10.1	-8.9
9	a	+1	10	6	2.30	515.58	167.06	-10.3	-9.0	-9.7	-8.9
	b	+1	11	4	2.93	598.71	193.18	-10.6	-9.5	-9.8	-9.1
	c	0	13	3	2.81	585.67	186.20	-11.1	-9.9	-9.8	-9.3
	d	0	11	4	4.45	591.68	193.39	-11.4	-10.4	-10.4	-9.4
	e	0	12	4	3.91	619.69	197.17	-10.8	-11.0	-11.0	-9.8

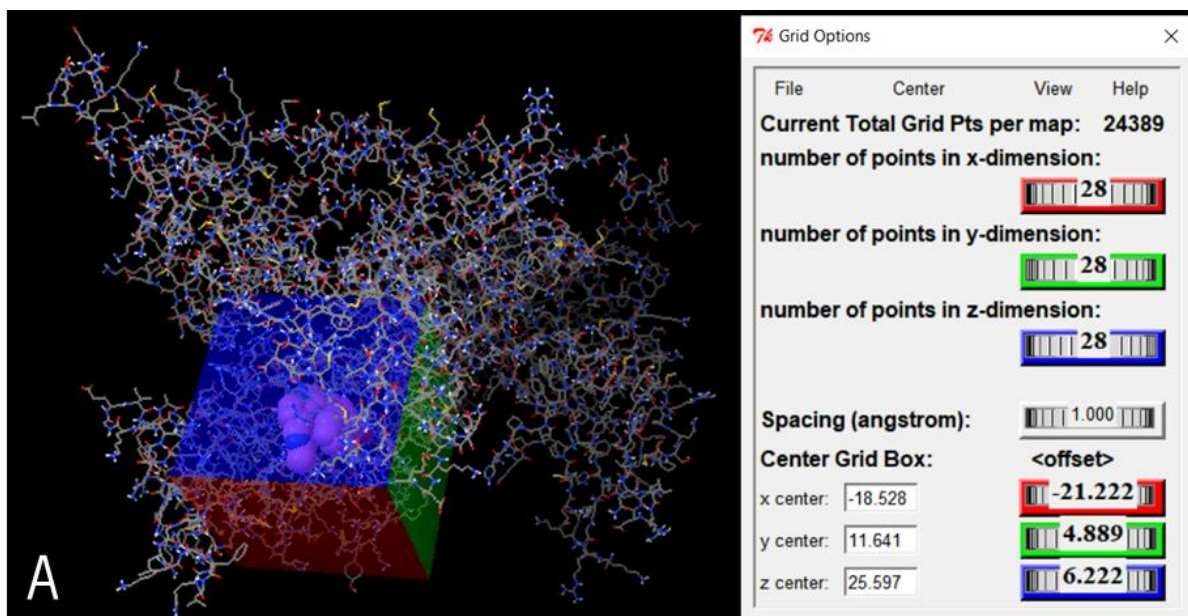


Figure 1 Spatial coordinates relative to the centre of the Grid Box and dimension values (x,y,z) of the Grid Box for **PI3K α** .

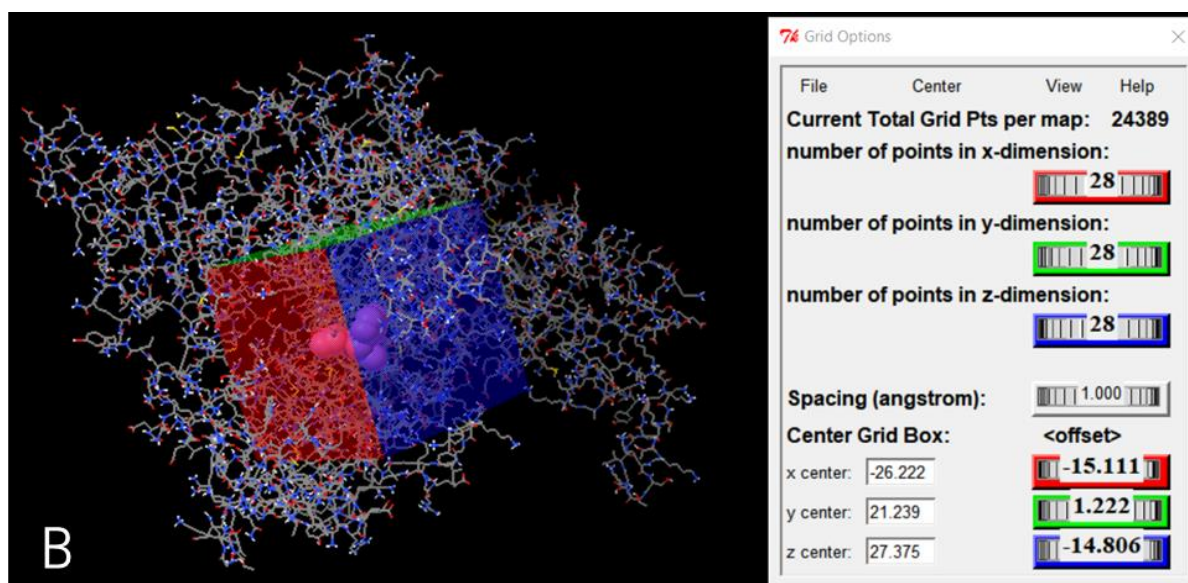


Figure 2 Spatial coordinates relative to the centre of the Grid Box and dimension values (x,y,z) of the Grid Box for **PI3K β** .

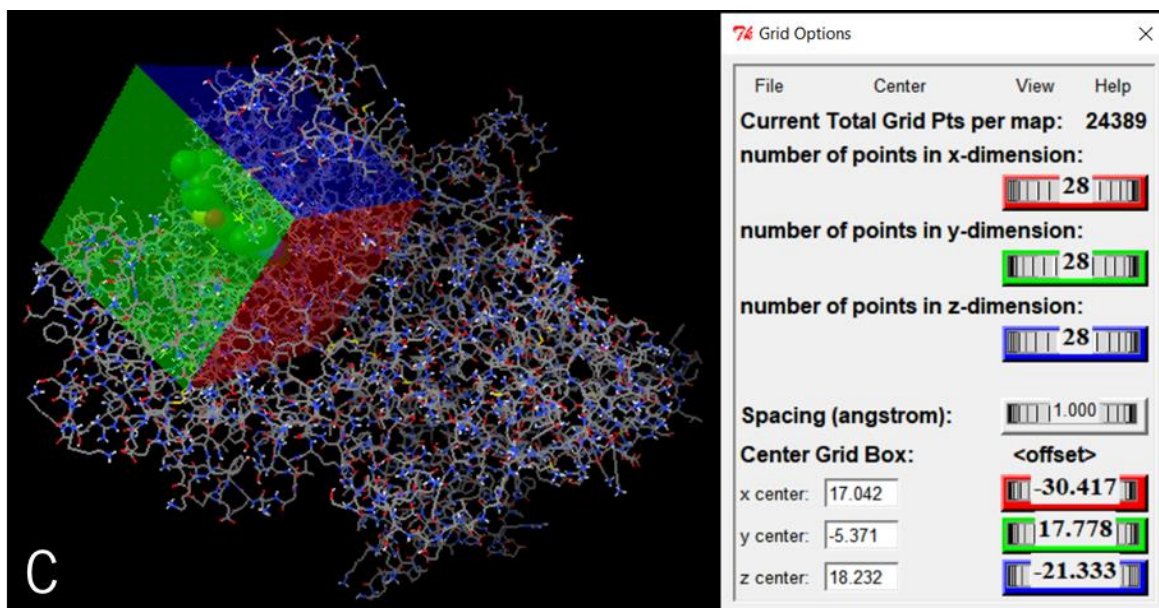


Figure 3 Spatial coordinates relative to the centre of the Grid Box and dimension values (x,y,z) of the Grid Box for PI3K γ .

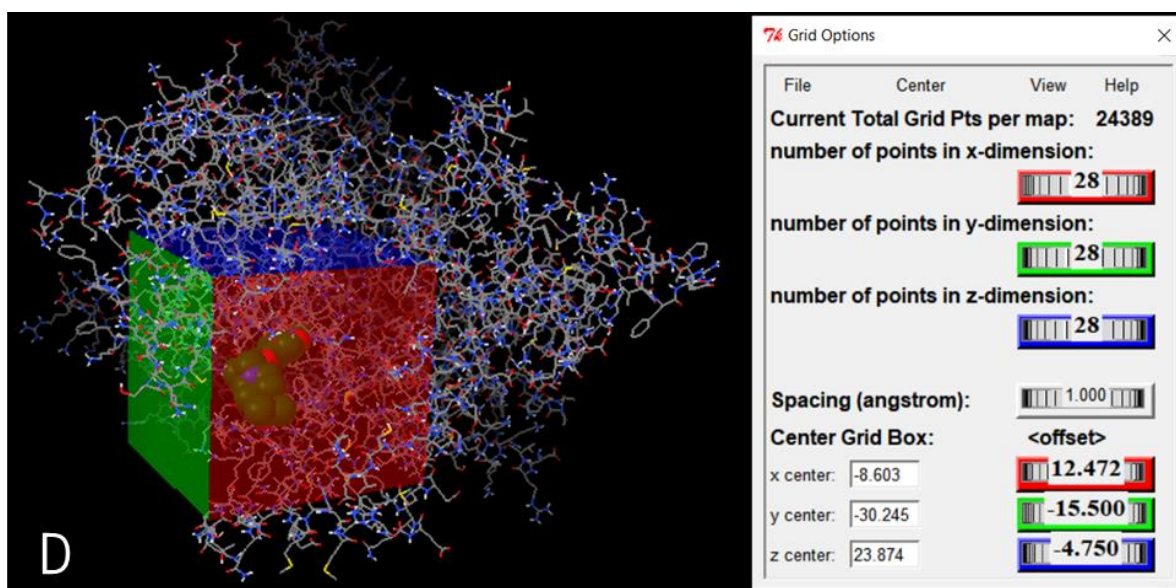


Figure 4 Spatial coordinates relative to the centre of the Grid Box and dimension values (x,y,z) of the Grid Box for PI3K δ .